

**TOWARDS A DESIGN ENVIRONMENT FOR BUILDING-  
INTEGRATED ENERGY SYSTEMS: THE INTEGRATION  
OF ELECTRICAL POWER FLOW MODELLING WITH  
BUILDING SIMULATION**

**Nicolas James Kelly B.Eng., M.Sc.**

**A thesis submitted for the  
Degree of Doctor of Philosophy**

**Department of Mechanical Engineering  
Energy Systems Research Unit  
University of Strathclyde, Glasgow, UK.**

**October 1998**

**to my family**

© The Copyright of this thesis belongs to the author under the terms of the United Kingdom Copyright Acts as qualified by the University of Strathclyde Regulation 3.49. Due acknowledgement must always be made to the use of any material contained in or derived from this thesis.

# Table of Contents

<b>Acknowledgements .....</b>	<b>x</b>
<b>Abstract.....</b>	<b>xi</b>
<b>Chapter 1 - Buildings Energy and Environment .....</b>	<b>1</b>
1.1 Energy Use within Buildings .....	1
1.1.1 Environmental Implications .....	2
1.1.2 Economic Implications .....	3
1.2 The Means of Reducing Energy Consumption .....	4
1.2.1 Energy End-Use Reduction.....	4
1.2.2 Reducing High-Grade Energy Usage .....	5
1.2.3 Electrical Energy Displacement .....	7
1.2.4 The Advantages of Building-Integrated Power Generation.....	8
1.3 Designing for Building-Integrated Energy Systems .....	9
1.3.1 Towards an Integrated Design Tool .....	10
1.4 Objectives .....	10
1.5 Larger-Scale Energy Systems .....	12
1.6 Summary .....	12
1.7 References .....	13
<b>Chapter 2 - Modelling the Building.....</b>	<b>15</b>
2.1 The ESP-r System .....	15
2.2 Control Volumes .....	16
2.2.1 The Control Volume Applied to a Zone .....	18
2.2.2 Application of a Mass Balance to the Fluid Volume.....	23
2.2.3 Application of Energy Mass and Momentum Balances (CFD) .....	25
2.2.4 The Control Volume Applied to the Building Fabric .....	28
2.2.5 The Control Volume Applied to Plant Components.....	35
2.3 Treatment and Solution of the Finite Volume Equation Sets .....	40
2.3.1 Zonal Energy Equations .....	40
2.3.2 The Plant Energy Equations.....	45

2.3.3 Treatment of Time-Varying and Non-Linear Processes .....	46
2.3.4 The Fluid Flow Equations.....	47
2.4 Simultaneous Solution.....	50
2.4.1 Benefits of the Modular Approach and Application to Other Subsystems .....	52
2.4.2 Variable Frequency Processing.....	52
2.5 Example Application of the Control Volume Modelling Technique .....	53
2.6 Summary .....	57
2.7 References .....	59
2.8 Bibliography .....	60
<b>Chapter 3 - Modelling the Electrical Network.....</b>	<b>61</b>
3.1 A Brief Overview of the Electrical System .....	61
3.2 Developing a Model of the Electrical System .....	63
3.2.1 The Control Volume Applied in an Electrical Context .....	63
3.2.2 Developing an Electrical Network .....	66
3.2.3 Extracting the Equation Set .....	68
3.2.4 Translation to Power Flow.....	70
3.3 Solution of the Equation Set .....	75
3.3.1 Requirements for the Network Solution .....	85
3.4 Application to Typical Building Electrical Systems .....	86
3.4.1 Alternating Current and Phasor System Variables .....	87
3.4.2 Three Phase and Single Phase a.c. Systems .....	88
3.4.3 d.c. Systems .....	98
3.5 Application of the Technique to an Exemplar .....	101
3.5.1 Developing the Network Model.....	103
3.5.2 Forming the Matrix Equation for the Network .....	104
3.6 Modelling Larger Electrical Systems.....	106
3.7 Summary .....	106
3.8 References .....	107
3.9 Bibliography .....	107
<b>Chapter 4 - Integration of Power Flow Modelling into ESP-r.....</b>	<b>109</b>
4.1 Coupling the Electrical Network to the Integrated Model.....	109

4.2 Coupling the Electrical Solver into ESP-r's Integrated Solution Process .....	111
4.2.1 Positioning of the Electrical Solver in the Solution Process .....	113
4.3 The Structure of the Electrical Solver .....	116
4.3.1 Obtaining Initial Values for the Iterative Solution .....	117
4.3.2 Forming the Elements of the Jacobian Matrix .....	117
4.3.3 Convergence .....	118
4.4 More Complex Couplings: the 'Onion' Approach.....	119
4.5 Summary .....	120
4.6 References .....	123
 <b>Chapter 5 - Component Models for Building-Integrated Energy Systems Simulation .....</b>	<b>124</b>
5.1 Components of the Electrical Network .....	124
5.1.1 Conductors .....	125
5.1.2 Transformers .....	138
5.2 Hybrid Components .....	148
5.2.1 Hybrid Load Components.....	148
5.2.2 Fans and Pumps.....	152
5.3 Hybrid Electrical Power Generation Components .....	155
5.3.1 Small-Scale Combined Heat and Power (CHP).....	155
5.3.2 Photovoltaics.....	169
5.4 Control in Integrated Simulations .....	180
5.4.1 The Action of the Control Loop on the Electrical Network.....	180
5.4.2 The Addition of an Electrical Control Loop .....	181
5.4.3 A Generator Voltage Control Law .....	181
5.4.4 Global Control.....	182
5.5 Summary .....	184
5.6 References .....	186
 <b>Chapter 6 - Verification of the Electrical Network Solver and Hybrid Model Calibration</b>	<b>189</b>
6.1 Verification of the Electrical Solver.....	189
6.1.1 Testing for Robustness .....	190
6.1.2 The Verification Process.....	190
6.1.3 Inter-model Comparison.....	192

6.1.4 Inter-algorithmic Comparison and Testing for Robustness .....	195
6.2 Calibration of the Hybrid Power Generating Component Models .....	196
6.2.1 Calibration of the CHP Engine Model with Test Data .....	196
6.2.2 Calibration of the PV model .....	198
6.2.3 Calibration of the Heat Exchanger Components .....	200
6.3 Summary .....	202
6.4 References .....	204
<b>Chapter 7 - Modelling and Simulation of Building-Integrated Energy Systems: Examples</b>	<b>206</b>
7.1 Modelling Integrated Systems in ESP-r .....	206
7.1.1 The Definition of Integrated Models in ESP-r .....	207
7.1.2 Simulation of Integrated Models .....	210
7.2 Example 1: Combined Heat and Power in a Sport Centre.....	211
7.2.1 The Form and Function of the Model.....	211
7.2.2 Simulations with the Model .....	218
7.2.3 Typical Output from the Simulation.....	219
7.3 A Photovoltaic Facade on a Factory Building .....	221
7.3.1 The Form and Function of the Model.....	222
7.3.2 Simulation.....	226
7.3.3 Typical Results Output from the Simulation .....	227
7.4 Summary .....	229
7.5 References .....	230
7.6 Bibliography .....	230
<b>Chapter 8 - Review and Conclusions.....</b>	<b>231</b>
8.1 Review.....	231
8.2 The Integration of Electrical Power Flow Modelling into ESP-r .....	233
8.2.1 Description of the Electrical System .....	233
8.2.2 Solution of the Electrical Power Flows .....	233
8.2.3 Integration into ESP-r.....	234
8.2.4 Electrical Conductor Component Models.....	234
8.2.5 'Hybrid' Component Model Development .....	234
8.2.6 Verification .....	235

8.2.7 Demonstration.....	235
8.3 Suggestions for Future Work.....	236
8.3.1 Improvements to ESP-r and the Power Flow Solver .....	236
8.3.2 Uses for Integrated Thermal/Electrical Modelling.....	237
8.4 Perspective.....	240
8.5 References .....	242
<b>Appendix 1 - Photovoltaic Technology Review.....</b>	<b>244</b>
A.1 Solar Cells.....	244
A.1.1 Solar Cell Physics.....	246
A.1.2 The p-n Junction.....	247
A.1.3 Cell Characteristics.....	254
A.2 Photovoltaic Panels .....	255
A.2.1 Power Conditioning.....	256
A.3 The Integration of PV into Buildings .....	257
A.3.1 Integration into the Building Fabric .....	257
A.3.2 Grid Connection of Building-Integrated PV .....	258
A.3.3 Heat Recovery from PV Facades .....	259
A.4 References.....	261
A.5 Bibliography .....	261
<b>Appendix B - Small-Scale Combined Heat and Power Technology Review .....</b>	<b>263</b>
B.1 The Components of a CHP System.....	264
B.1.1 The Engine .....	264
B.1.2 The Generator.....	265
B.1.3 Heat Recovery System.....	266
B.2 Control of CHP Systems.....	267
B.2.1 Temperature Control.....	267
B.2.2 Control of Power Output.....	267
B.3 Connecting the CHP system into the Building Services.....	270
B.4 The Viability of CHP.....	270
B.4.1 Efficiency and Savings.....	271
B.4.2 Measures of Efficiency .....	271



B.4.3 Financial Savings from CHP.....	272
B.5 References.....	274
B.6 Bibliography.....	274

# Acknowledgements

This thesis would never have been completed without the following people and institutions.

I wish to express my gratitude to Professor Joe Clarke for his enthusiastic guidance and support throughout the course of this project.

Thanks to the Staff and Students of ESRU (past and present) for their help and many useful discussions: Essam Aasem, Tin Tai Chow, Robert Dannecker, Mark Evans, Jon Hand, Dr. Jan Hensen, Cameron Johnstone, Iain Macdonald, Dr. John MacQueen, Craig McLean, Dr. Abdullatif Nahki, Dr. Cezar Negrao and Dr. Paul Strachan.

Thanks also go to Dave Cronin and Dr. Elizabeth Silver at the Building Research Establishment for reading and commenting on some sections of the text.

I very gratefully acknowledge the support of the Carnegie Scholarship for the Universities of Scotland, who funded my study.

Finally, I wish to thank my family for their never-faltering support and patience throughout all my long years in education. This thesis is dedicated to them.

# Abstract

Building-integrated energy systems, providing heat *and* power (photovoltaic building facades and small-scale combined heat and power), are becoming a common feature in building design. However, because of the interdependency of thermal and electrical flows in such systems, building simulation tools cannot model them adequately due to their lack of a power flow modelling capacity. This thesis describes the integration of power flow modelling with a building simulation program, ESP-r, to facilitate the modelling of building-integrated energy systems.

ESP-r uses a control volume approach to model a building. This has been expanded to describe the power system, providing a means for its integration into the building model. The electrical system is represented by a network (consistent with the representation of other building subsystems in ESP-r).

An electrical network solver has been developed and coupled into ESP-r's simulation engine, enabling the integrated solution of thermal and electrical flows in the building. The electrical network solution requires that boundary conditions (power flows) are supplied from the thermal domain of the building, done by coupling 'hybrid' components to the network.

Hybrid components models straddle the thermal and electrical 'worlds', linking the thermal and electrical energy flows. Models have been developed for electrical loads: fans, pumps, lights and small power loads. The hybrid concept has also been used in the development of two power generating component models: a combined heat and power unit and a facade-integrated photovoltaic module. The power generating component models and the electrical solver have been verified using a practical testing methodology.

Finally, two exemplars are presented, showing how the model of the building, the electrical network and hybrid components are coupled together to form a complete model of a building-integrated energy system. The thesis concludes with recommendations as to the uses of this work and ideas for its further development.

# Chapter 1 - Buildings Energy and Environment

## 1. Introduction

Buildings are a dominant feature in modern society. We work, eat, sleep and enjoy much of our leisure time inside them. Up to 80% of an individual's life is spent indoors [1].

The function of the building has evolved from a simple shelter to an advanced, self-contained and tightly controlled environment which provides a wide variety of services to its occupants: environmental conditioning, vertical transportation, sanitation, artificial lighting, communications and security. To perform this range of functions the building must consume energy.

### 1.1 Energy Use within Buildings

All energy used within buildings can be classed under two main categories: high-grade and low-grade [2]; the grade of energy is determined by its ability to perform work. The prime example of high-grade energy is electricity, which can be efficiently converted to work via an electric motor. An example of low-grade energy encountered in buildings is the heat energy used to maintain conditions suitable for human comfort.

Although the majority of the energy consumed within buildings is low-grade (figure 1.1), it is the high-grade electrical energy which is the more important. Electricity performs a greater variety of functions and is required in the transportation of low-grade energy from the point of production to the point of use, e.g. the transportation of conditioned air through a ducting system using a fan.

Figure 1.1 shows the breakdown of energy usage in a typical air-conditioned office building [3]; high-grade energy uses are denoted by a \*.

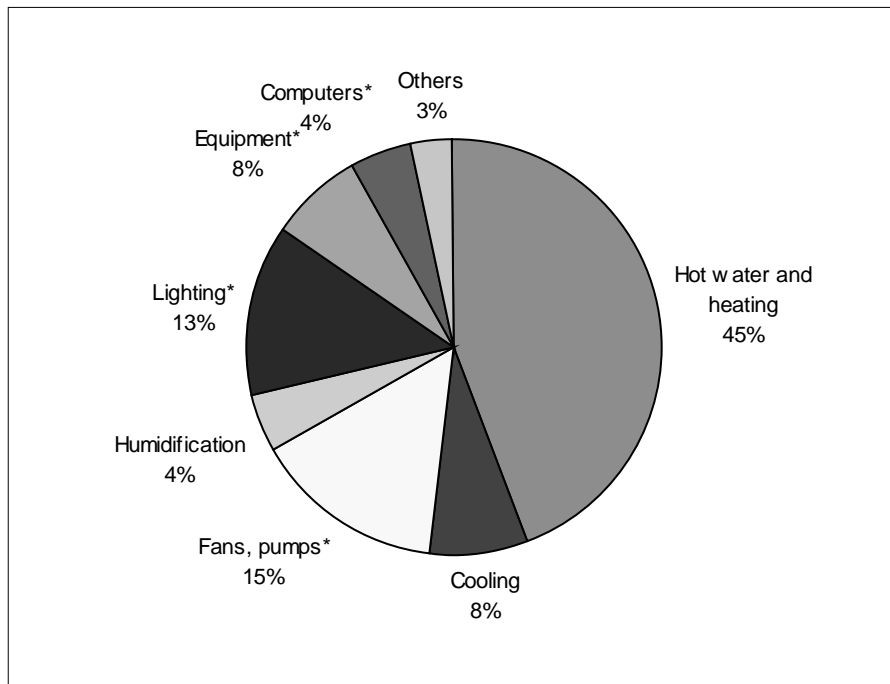


Figure 1.1 The energy usage in a typical office building.

It is a well quoted fact that the built environment consumes up to 50% of delivered energy [4]. A US survey [5] revealed that much of this energy is used inefficiently: in buildings over 10 years old 30-40% of the energy consumed is wasted due to the poor condition of the building envelope and plant. In the UK, buildings over 10 years old account for 90% of the building stock [5]. Assuming a worst case scenario from these figures, it is possible that 18% of all delivered energy is wasted due to the poor quality of the older building stock. This waste of energy has two major implications: environmental, and perhaps more importantly for the building owner, economic.

### 1.1.1 Environmental Implications

It has been clear for many years that the inefficient consumption of both high and low-grade energy, derived from fossil fuel sources, has a detrimental effect on the natural environment. The environmental damage from particulate pollution, acid rain, and climate change has been described extensively in many other publications (e.g. [6]) and does not require to be discussed

further here. The need, however, to reduce the environmental impact of buildings is clear, particularly through reducing their wastage of energy.

### 1.1.2 Economic Implications

The economics of the inefficient use of energy in the built environment have, perhaps, been over-shadowed by the environmental implications. However, in this area too, the argument for a reduction in energy wastage is compelling: the loss of up to 40% of the energy delivered to the building represents an enormous financial cost to the building owner. This energy wastage is especially inexcusable when it is considered that many energy saving measures are relatively cheap to implement: it is estimated that an extra 1% spent on the capital cost of a building can reduce its energy consumption by 30-40% [4]. A small outlay on the maintenance of fabric and plant would have a similar beneficial effect.

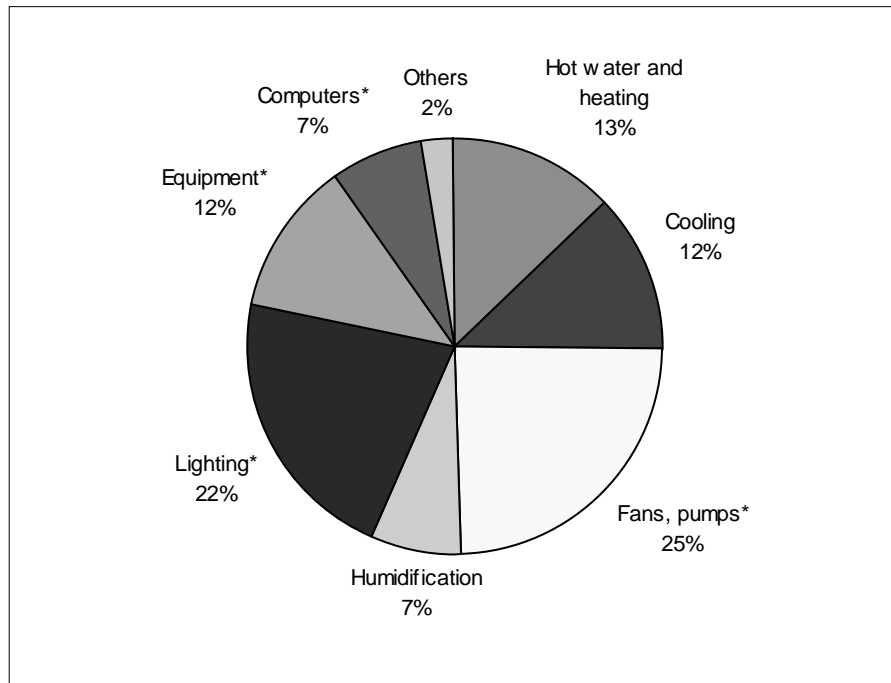


Figure 1.2 The expenditure on energy within a typical office building [3].

A further economic argument for reducing a building's use of energy is that the reduction usually results from improvements in the building fabric, plant and environmental control. These improvements lead to more comfortable conditions, which have a beneficial effect on occupant productivity. Given that the largest portion of a commercial building's running costs are the wages of the employees [9], a fairly small rise in productivity will help energy saving scheme pay for itself.

## 1.2 The Means of Reducing Energy Consumption

The need to improve the energy efficiency of buildings is clear and is primarily a question of good energy conscious building design, both in the construction of new buildings and in the retrofitting of energy saving features to the existing building stock.

### 1.2.1 Energy End-Use Reduction

To date, the means of improving the energy efficiency of buildings has focused on the reduction of energy consumption at the point of use, through the reduction in the heating and/or cooling requirements. Examples are given in table 1.1.

Area	Measure	Saving in energy consumption
fabric	improved envelope insulation	49%
	advanced glazing	20%
plant	duct insulation	15%
	hot water supply temperature control	10-15%

control	boiler sequencing control	3-10%
---------	---------------------------	-------

Table 1.1 Low-grade energy saving measures [7].

The energy saving measures listed in table 1.1 are simple and inexpensive, and can result in significant improvements in the overall energy efficiency of the building, especially in the case of improved insulation.

### 1.2.2 Reducing High-Grade Energy Usage

Significant financial savings can result from the implementation of high-grade energy saving schemes, especially when it is considered that high-grade energy costs between 3-10 times as much per kWh, as the equivalent unit of low-grade energy [10]. Also note that high-grade electrical uses (indicated by a \* in figure 1.1) account for only 40% of energy consumption but figure 1.2 shows that these high-grade energy end-uses account for 66% of energy expenditure.

In environmental terms, the high-grade energy consumed within buildings is far more damaging than its low-grade equivalent: for each kWh of electricity consumed between 3-4 kWh of fossil fuel is required. Only 1.2kWh of fossil fuel is required to produce 1kWh of heat energy.

Clearly, reducing the high-grade energy use in a building provides great scope for financial savings and the reduction of its impact on the environment.

A reduction in electrical energy consumption at the point of consumption is achievable by numerous means: installing energy efficient lighting and appliances, improved control and monitoring of electrical equipment, load shedding<sup>1</sup> (shutting down non-essential equipment at

---

<sup>1</sup> Load shedding is done more for financial reasons (i.e. reduction in peak electricity charges) rather than for its energy saving benefits.



times of peak loading), daylight and occupancy responsive controls for lighting. Some high-grade energy saving options are shown in table 1.2.

Area	Description	Saving in energy consumption
HVAC <sup>2</sup>	high efficiency motors	3%
	variable speed motors	31%
	regulation of circulation pumps	20-40%
	high efficiency fans	4%
lighting <sup>3</sup>	improved luminaires	16%
	high efficiency lighting	5%
	lighting control	30-70%
power demand	demand control	12%
	power factor correction	9%

---

<sup>2</sup> The saving for HVAC is relative to the energy consumption of the system, not the entire building.

<sup>3</sup> See previous footnote.

	peak lopping	6-8%
--	--------------	------

Table 1.2 High-grade energy saving measures [7, 8, 9, and 11].

### 1.2.3 Electrical Energy Displacement

Advances in both construction and plant technology have opened up another possibility for improving the electrical efficiency of buildings: electrical energy displacement. Displacement is a means of reducing both the costs and environmental impact of electrical energy consumption: inefficiently produced electricity from a central power station is replaced with power produced locally from more efficient and cleaner sources. This localised power production, using a *building-integrated energy system*, is a major area of interest in modern energy-conscious building design. Three examples of this system are:

- *Solar electricity production by means of photovoltaic (PV) materials*: these are integrated into the building façade and are a clean method of producing power. Though the efficiency of conversion is low (4-18%), it can be boosted by recovering heat from the façade [12] in the form of warm air. This warm air can be passed into the building and used for heating purposes.
- *Small-scale combined heat and power systems (CHP)*: this involves the generation of both the heat and power using an engine integrated into the building's hot water services; in buildings this is often a gas powered internal combustion engine. Other types of engine (e.g. gas turbines) are mentioned in appendix 2. The engine drives an electrical generator and hot water is recovered from both the cooling water and exhaust gases. The efficiency of these units can be as high as 80-90%, compared to the normal efficiency of conversion found in power stations of only 30% [13]: the efficiency is defined as the ratio of useful heat and work output to fuel energy consumption.
- *Production of electricity using small ducted wind turbines*: like PV power production, this involves the integration of power producing components into the building construction, in

this case small wind turbines [14]. This is a novel application of wind power that is, as yet, restricted to only the most futuristic of building designs. The technology is embryonic and its viability has yet to be tested.

#### **1.2.4 The Advantages of Building-Integrated Power Generation**

The deregulation of the UK electricity market in 1998 increases the attractiveness of incorporating a building-integrated energy system into a building design. Small power producers can now export directly to the grid, while consumers can choose whom to buy their power from; this allows the owner the possibility of actually generating income from an energy saving scheme through selling surplus power. The benefits of building-integrated energy systems are therefore two-fold:

- money is saved through efficient production of power and possibly heat, with surplus electricity being sold to the grid, generating revenue;
- the environmental impact of the building's energy consumption is reduced.

It is this ability to generate income, while at the same time saving energy and reducing environmental impact that makes building-integrated energy systems an increasingly attractive option to energy conscious building designers. Note however that the practicality of exporting surplus power to the grid is strongly influenced by the price paid for this electricity. In many cases this is a fraction of the price paid for power drawn from the grid. Grid connection is discussed further in appendix 1

An indication of the increasing popularity of building-integrated energy systems can be gauged from the rapid increase in the number of schemes: 100 PV systems are being installed in schools as part of the UK Solar program [15]; the UK government's target for installed CHP is 5000MW by the year 2000 [16] (the potential is estimated at 10 to 17 GW [16]) and structurally-integrated wind turbines are being included in a low-energy building in Glasgow [17].

### 1.3 Designing for Building-Integrated Energy Systems

Clearly, the building-integrated energy system may well become an important feature of buildings in future years. However, to achieve the potential energy benefits of such systems they must be properly designed as an integrated part of the building. However, compared to simpler energy end-use reduction schemes, the design of these systems is a complicated task:

- A building-integrated energy system affects all constituents of the building: fabric, heating, lighting, occupants, plant and control. For the effective design of a building-integrated energy scheme, its effect on all these disparate elements of the building must be evaluated.
- The systems incorporate complex electro-mechanical devices and advanced materials: controls, engines, PV materials, etc.
- Building-integrated energy systems straddle both electrical and thermal energy flows, the interaction and coupling between these two flow-paths must be considered.
- The electrical and thermal loads of the building must be estimated and any designed scheme should be optimised to meet these loads.
- The transient effects of the external climate, building occupation and control action will affect the operation of the system, and must be accounted for in the design process.

An appropriate means by which the complexity of a building-integrated energy system can be analysed is through computer simulation using an integrated energy model, incorporating both the building-integrated energy system and the building it serves. The creation of such an integrated model entails the representation of the whole building (fabric, occupants, plant, air flow, electrical system, etc.) as a single mathematical entity. Solution of this model with real weather data allows the performance of the building with its integrated energy system to be analysed, optimised and tested in a realistic context.

### **1.3.1 Towards an Integrated Design Tool**

Tools to model and simulate building designs have been available for many years (e.g. ESP-r<sup>4</sup>, Tas<sup>5</sup>, CLIM2000<sup>6</sup>). The areas where such tools are used in the design process include: heating and cooling strategies, natural ventilation schemes, active solar systems, thermal comfort and overheating analysis. These uses have dictated that, in the current generation of simulation programs, the ability to model the building's thermal performance has been of paramount importance.

The maturity and the increasing awareness of simulation tools by designers means that thermal modelling is slowly gaining acceptance as a necessary part of the building design process. Unfortunately, when more complex systems are considered, i.e. those which incorporate an electrical energy generation system, problems are encountered: this is due to the fact that, in building energy simulation, the area of electrical systems modelling has been overlooked. The reasons for this are unclear. However, the absence of an electrical modelling capability means that systems with strongly coupled thermal and electrical energy flows, such as those encountered in building-integrated energy systems, cannot be modelled adequately. To facilitate the modelling of these systems there is a clear need to augment the thermal modelling capability of simulation tools with the ability to model electrical energy flows.

## **1.4 Objectives**

The objective of this thesis is therefore to integrate the modelling of electrical systems into thermal simulation tools. The means by which this will be achieved is by extending the capabilities of the ESP-r [18] simulation program to encompass the field of electrical systems modelling. ESP-r is widely used in simulation modelling research and, as will be explained in the next chapter, is well suited to the integration of power flow modelling.

---

4 Developed by the Energy Simulation Research Unit, University of Strathclyde.

5 Developed by Environmental Design Solutions Ltd.

6 Developed by Électricité de France.

The steps involved in the integration process will be:

- The development of a means to model electrical systems and solve the associated electrical energy flows.
- Integration of both the electrical model and solver into the ESP-r simulation package, enabling, for the first time, the simulation of both the high and low grade energy flows in the context of an integrated, whole-building, simulation.
- Creation of models for use in the simulation process: photovoltaic panels, CHP engines, generators, transmission lines, heat exchangers etc.
- Testing of the electrical system solution method and component models.
- The development of example system models, which illustrate the capabilities of the integrated tool.

The integration of electrical modelling with thermal modelling will enable the evaluation of all the important energy flows occurring within a building, allowing a greater breadth of building energy systems (such as the aforementioned building-integrated energy systems) and scenarios of energy usage to be modelled.

Other commonplace phenomena occurring in the electrical domain, such as those shown in table 1.2 can also be modelled using an energy simulation tool augmented with electrical modelling capabilities.

Modelling of the building electrical system will allow the power flows and demand of the building to be determined in the same way as simulation tools are currently used to determine heating and cooling loads. This enables a complete picture of the building's energy performance to be obtained from a single simulation.

## **1.5 Larger-Scale Energy Systems**

This chapter has focused on the concept of modelling the building as a complete energy system, where the energy system includes the thermal and electrical energy flows. However, the notion of the energy system need not be confined to a single building: its definition can be enlarged to encompass groups of buildings and multiple sources of power generation. It is hoped that the integrated modelling method that emerges from this thesis will prove flexible enough to adapt to the modelling of any type of energy system: from the single building to community-sized systems.

## **1.6 Summary**

This chapter has outlined the reasons behind the choice of subject for this thesis: the emergence of new building-integrated energy system technologies in the built environment and the need for a simulation tool to aid in their design.

The lack of the ability to model electrical energy flows in current simulation tools was identified as a major impediment to their use in modelling building-integrated energy systems. The primary objective of this thesis was therefore defined as the integration of electrical power flow modelling into building energy simulation tools.

The program to be used as the vehicle to achieve this objective was the ESP-r energy simulation tool. The principles behind ESP-r and their relevance to the integration of power flow modelling into thermal simulation are examined in the next chapter.

## 1.7 References

1. Peng X, *Modelling of indoor thermal conditions for comfort control in buildings*, PhD Thesis, Delft University of Technology, 1996.
2. Twidell J and Weir T, *Renewable energy resources*, E. & F. Spon Ltd., London, 1986.
3. DETR, *Energy consumption guide 19 - energy use in offices*, Energy Efficiency Office, Best Practice Programme, 1998.
4. Johnston S, *Greener buildings – the environmental impact of property*, MacMillan Press, Basingstoke, 1993.
5. The Ove Arup Partnership, *Building design for energy economy*, The Construction Press, Lancaster, 1980.
6. The World Commission on Environment and Development, *Our common future*, The Oxford University Press, Oxford, 1987.
7. *Buildings and Environment: proceedings of the first international conference*, Building Research Establishment, Garston, 1994.
8. Holtz M, *Electrical energy savings in office buildings*, Swedish Council for Building Research, Stockholm, 1990.
9. Sherrat A F C, *Air conditioning and energy conservation*, The Architectural Press, London, 1980.
10. Dept. of Trade and Industry, *Digest of United Kingdom energy statistics*, HMSO, 1992.



11. *Energy for buildings: microprocessor technology*, OECD/IEA, Paris, 1986.
12. Strachan P A, Johnston C M, Kelly N J, Bloem J J and Ossenbrink H, *Results of thermal and power modelling of the PV facade on the ELSA buildings, Ispra*, Proc 14<sup>th</sup> European Photovoltaic Solar Energy Conference, Barcelona, July 1997.
13. Evans R D, *Environmental and economic implications of small-scale CHP*, Energy and Environment Paper No. 3, ETSU, 1990.
14. Dannecker R, *The ducted wind turbine module and its integration in a conventional building*, Report to: Joule Grant Holders Conference, University College Cork, 1<sup>st</sup>-6<sup>th</sup> April, 1998.
15. Building Services Journal, March 1997.
16. Department of the Environment press release, DETR 414/ENV 1997.
17. The Observer, February 21<sup>st</sup> 1998.
18. Clarke J A, *Energy Simulation in Building Design*, Adam Hilger, Bristol, 1985.

# **Chapter 2 - Modelling the Building**

## **2. Introduction**

The modern building comprises many different elements and is a many-faceted, synergistic energy system that evolves dynamically with time due to environmental excitation, human occupation, plant and controls interaction. The problem of attempting to describe and model such a complex system is not a new one. Many techniques have been developed which attempt to obtain a solution as to how the building will respond, over time, to differing control, occupancy and climatic scenarios. Solution strategies vary from the simplest, steady state hand calculations, to the current state-of-the-art use of dynamic computer simulation.

The availability of low-cost, high-power computers has lead to a proliferation of computer tools utilising numerical methods in the analysis of the building (some examples are given in section 1.3.1). These tools have the ability to model (in varying levels of detail): heat transfer, fluid flow, climatic effects, plant and controls, as part of an integrated building model. Note, however that these ‘integrated’ models do not yet have the ability to model the electrical system.

### **2.1 The ESP-r System**

The ESP-r system is of particular interest as it applies the same basic modelling principle to all aspects of the building and is flexible enough to be applied later in the modelling of the electrical system. In ESP-r the model of the building is broken down into many small control volumes: a control volume being a region of space, represented by a node, to which the principles of conservation of mass, energy and momentum can be applied. Buildings modelled using this technique may require the use of many thousands of control volumes to describe its fundamental characteristics: opaque and transparent structure, plant components, fluid volumes, etc. Clarke [1] summarises this approach to modelling the building as follows.

*“...ESP-r will accept some building/plant description in terms of three-dimensional geometry, construction, usage and control. This continuous system is then made discrete by division into many small, but finite volumes of space. These finite volumes then represent the various regions of the building within and between which energy can flow.”*

The discretisation technique used within ESP-r is termed a ‘control volume flux-balance’ approach [2].

An equation can be derived for each control volume using the laws governing the conservation of mass, energy or momentum. This derived equation describes the fundamental physical process occurring within the volume, e.g. heat conduction and storage, air flow, moisture flow, convection, etc. Sets of these equations can be extracted from the building model and grouped according to physical process. Solution of the equation sets, with real climate data and user defined control objectives as boundary conditions, allows the determination and quantification of the transient energy and fluid flow processes occurring within the building. In effect, a picture is obtained of the environmental performance of the building during a simulated period.

The attraction of this modelling technique is that it can be extended from the modelling of low-grade heat transfer and fluid flow processes, to the area of high-grade electrical energy flows. This is the subject of chapter 3. This chapter describes the principles behind the control volume technique and its application to the modelling of the thermal and fluid flow processes encountered within the building.

## **2.2 Control Volumes**

ESP-r’s model of the building consists of a number of coupled polyhedral zones that describe the geometry and fabric. Augmenting these zones are a series of networks, each of which describes an energy sub-system: heating and air conditioning plant, air, fluid and moisture flow. The combination of the thermal zones and associated networks, together with occupancy characteristics, user defined control strategies and climate data forms a complete model of the building. The physical elements of the model: zones and networks are described using control volumes.

A control volume is created by defining a fictitious boundary around a region of space. The characteristics of this control volume can vary greatly: homogeneous or non-homogeneous, solid or fluid, size and shape. Despite the variety of the characteristics, the conservation of mass, energy and momentum can always be applied.

The flexibility of control volumes allows them to be used in the modelling of any part of the building and a multiplicity of physical processes (figure 2.1).

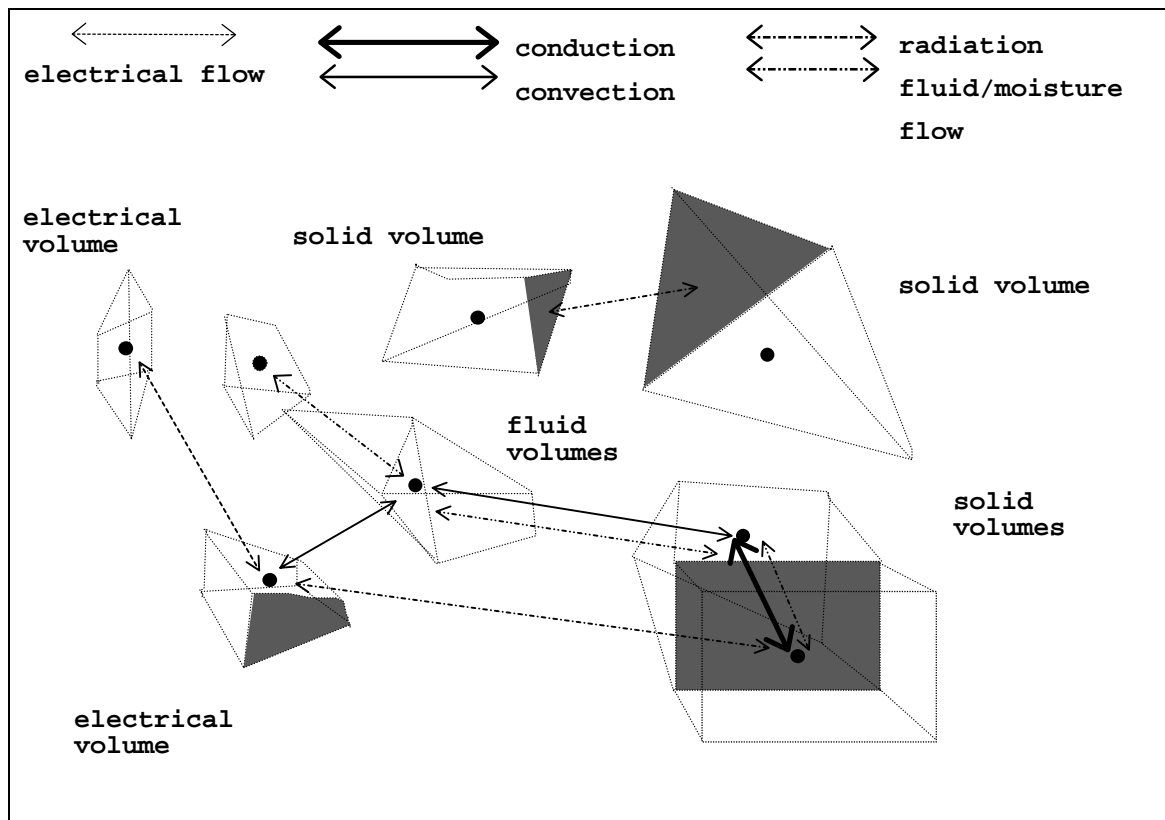


Figure 2.1 Finite volumes as used in ESP-r.

As mentioned previously, characteristic equations are defined for each control volume based on one or more of the conservation equations: energy, mass or momentum. These characteristic equations encapsulate the physical characteristics and phenomena associated with the control volume and also implicitly link the volume to its neighbours. The linkage takes the form of an energy or mass exchange with adjacent volumes.

The following paragraphs demonstrate applications of the control volume principle in ESP-r. Knowledge of the application of control volumes in a thermal context is crucial to the understanding of their application in modelling the electrical energy subsystem. This also gives an insight into how thermal and electrical systems can be modelled in a truly integrated fashion, by using the same modelling technique for both.

Note that the derivations of the control volume characteristic equations that follow are only intended to introduce the reader to this approach to modelling the building. A more complete and rigorous treatment of the theory behind control volumes and ESP-r is given by Clarke [1].

### **2.2.1 The Control Volume Applied to a Zone**

This section deals with the application of the control volumes to the most important element of a building model: the enclosed air (fluid) volumes that constitute the thermal zones of the building. They are also perhaps the most thermodynamically interesting areas of the building, as the modeller can successively apply energy, mass and momentum balances to a volume of fluid, depending on the rigour of analysis required. In addition, the zones of the building are subject to many varied energy exchanges: heat and vapour gains from occupants, plant interaction, solar energy transmitted through glazing, infiltration, air exchange with other spaces etc. Finally, and as a link to chapter 3, a coupling between this control volume and the electrical ‘world’ is the heat gain to the building interior from lights and other electrical appliances. Other thermal/electrical couplings are explored later.

The flexibility of the control volumes in analysing physical problems at varying levels of complexity will be shown in this section, as the control volume technique will be applied with increasing rigour to the zone. Subsequent sections will demonstrate the application of the control volume technique to the fluid volume’s bounding and peripheral elements: fabric and conditioning plant.

At the most basic level of detail a single control volume, represented by a single node, can be used to describe the volume of fluid that constitutes the zone. This volume is bounded by solid constructions and is subject to heat transfer by convection, fluid exchange with its neighbouring

volumes, infiltration from the exterior, heat and vapour gains from occupants, plant interaction, etc. The fundamental equation governing these exchanges is an energy balance of the form

$$\rho_i V_i c_i \frac{\partial \theta_i}{\partial t} = \sum_{j=1}^n q_{ij} . \quad (2.1)$$

$V_i$  is the volume ( $\text{m}^3$ ) of the fluid volume  $i$ ,  $\rho_i$  is its average density ( $\text{kg}/\text{m}^3$ ),  $c_i$  is its average specific heat ( $\text{J}/\text{kgK}$ ) and  $\theta_i$  is its average temperature ( $^{\circ}\text{C}$ ). The left-hand side of the equation represents the thermal capacitance of the fluid volume, while the  $\sum_{j=1}^n q_{ij}$  term is the sum of the energy fluxes (W) that interact with the control volume. These are of three types: surface to fluid heat transfer, fluid flow from other fluid volumes and sensible energy gains from sources inside the zone.

The general form of the equation describing the convective heat transfer (W) between a surface  $s$  and the fluid volume  $i$  is

$$q_{is} = h_{cs} A_s (\theta_s - \theta_i) . \quad (2.2)$$

$\theta_s$  is the surface temperature,  $A_s$  is the contact area ( $\text{m}^2$ ) with the fluid volume and  $h_{cs}$  is the heat transfer coefficient ( $\text{W}/\text{m}^2\text{K}$ ). Note that in this equation, a linear convective heat transfer coefficient is used to describe the non-linear process of convective heat transfer. This is done to preserve the overall linearity of the equation, eventually enabling fast, efficient solution methods to be applied in the solution of the equation sets that describe the zonal energy flows (this is discussed in section 2.3.1). ESP-r's treatment of non-linear processes using linear coefficients is explained in section 2.3.3.

The form of the equation describing the energy exchange (W) due to fluid flow between two fluid volumes  $i$  and  $k$  is

$$q_{ij} = \dot{m}_{ij} c_j (\theta_j - \theta_i) \quad (2.3)$$

$\dot{m}_{ij}$  is the pressure/temperature driven mass flow rate (kg/s) between the two volumes, calculation of this value is dealt with in the next section.  $c_j$  is the specific heat of the fluid transferred from the neighbouring volume and  $\theta_j$  is its temperature.

The gains from sources inside the zone (W) can be lumped together into a single term,  $q_i$ , which includes such phenomena as sensible heat gains from the lighting, small power loads and the sensible heat gain from occupants.

The basic equations for the control volume energy balance can be applied to the fluid volume shown in figure 2.2.

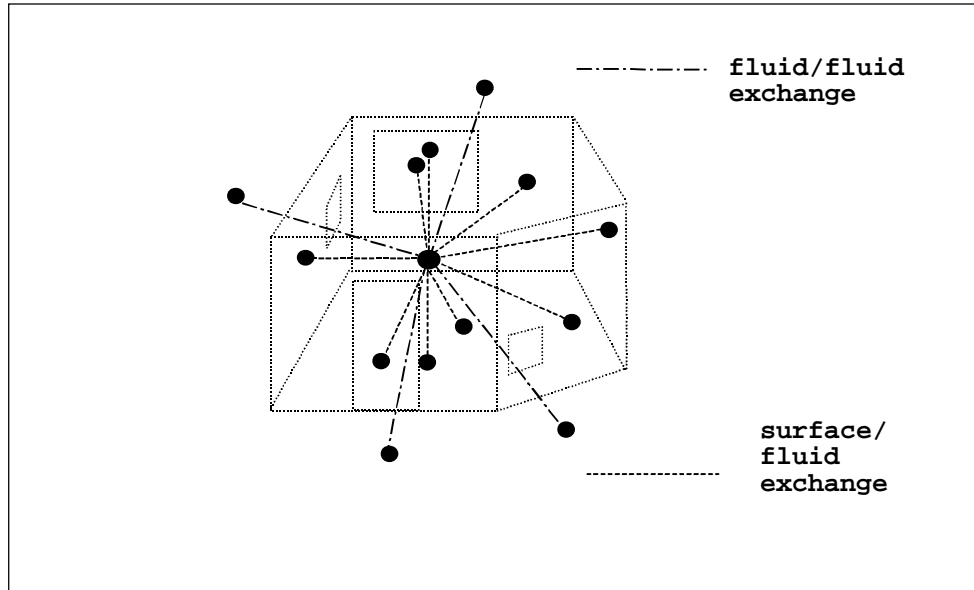


Figure 2.2 Energy exchanges associated with a zone fluid volume

The volume is bounded by nine different surfaces, each of which exchange energy by convection with the air volume. There are also four fluid exchanges with surrounding fluid volumes (some of which may be exchanges with the external environment). Applying the previously defined equations to the fluid volume of figure 2.2 gives the following expression

$$\rho_i V_i c_i \frac{\partial \theta_i}{\partial t} = \sum_{j=1}^9 h_{cij} A_{sj} (\theta_{sj} - \theta_i) + \sum_{k=1}^4 \dot{m}_{ik} c_k (\theta_k - \theta_i) + q_i . \quad (2.4)$$

Applying a backward difference scheme to the partial derivative term, over some finite time interval,  $\Delta t$  (s), the following expression emerges.

$$\frac{\rho_i V_i c_i (\theta_i^{t+\Delta t} - \theta_i^t)}{\Delta t} = \sum_{j=1}^9 h_{cij}^t A_{sj} (\theta_{sj}^t - \theta_i^t) + \sum_{k=1}^4 \dot{m}_{ik}^t c_k (\theta_k^t - \theta_i^t) + q_i^t. \quad (2.5)$$

Dividing by the volume  $V_i$ :

$$\frac{\rho_i c_i (\theta_i^{t+\Delta t} - \theta_i^t)}{\Delta t} = \frac{\sum_{j=1}^9 h_{cij}^t A_{sj} (\theta_{sj}^t - \theta_i^t)}{V_i} + \frac{\sum_{k=1}^4 \dot{m}_{ik}^t c_k (\theta_k^t - \theta_i^t)}{V_i} + \frac{q_i^t}{V_i} \quad (2.6)$$

For reasons of numerical stability during the solution process, ESP-r uses a mixed implicit/explicit form of the heat balance equation [3]. The implicit form is given by

$$\begin{aligned} \frac{\rho_i c_i (\theta_i^{t+\Delta t} - \theta_i^t)}{\Delta t} &= \frac{\sum_{j=1}^9 h_{cij}^{t+\Delta t} A_{sj} (\theta_{sj}^{t+\Delta t} - \theta_i^{t+\Delta t})}{V_i} + \frac{\sum_{k=1}^4 \dot{m}_{ik}^{t+\Delta t} c_k (\theta_k^{t+\Delta t} - \theta_i^{t+\Delta t})}{V_i} \\ &+ \frac{q_i^{t+\Delta t}}{V_i}. \end{aligned} \quad (2.7)$$

Adding equations 2.6 and 2.7 together, re-arranging and grouping the future time step terms on the right hand side gives the mixed expression for the energy balance at fluid node  $i$ .



$$\begin{aligned}
& \left( \frac{2\rho_i c_i}{\Delta t} + \frac{\sum_{j=1}^9 h_c^{t+\Delta t} A_{s,j}}{V_i} + \frac{\sum_{k=1}^4 \dot{m}_{ik}^{t+\Delta t} c_k}{V_i} \right) \theta_i^{t+\Delta t} \\
& + \frac{\sum_{j=1}^9 h_c^{t+\Delta t} A_{s,j} \theta_{sj}^{t+\Delta t}}{V_i} + \frac{\sum_{k=1}^4 \dot{m}_{ik}^{t+\Delta t} c_k \theta_k^{t+\Delta t}}{V_i} + \frac{q_i^{t+\Delta t}}{V_i} \\
& = \left( \frac{2\rho_i V_i c_i}{\Delta t} + \frac{\sum_{j=1}^9 h_{c,ij}^t A_{s,j}}{V_i} + \frac{\sum_{k=1}^4 \dot{m}_{ik}^t c_k}{V_i} \right) \theta_i^t - \frac{\sum_{j=1}^9 h_{c,ij}^t A_{s,j} \theta_{sj}^t}{V_i} - \frac{\sum_{k=1}^4 \dot{m}_{ik}^t c_k \theta_k^t}{V_i} - \frac{q_i^t}{V_i}.
\end{aligned} \tag{2.8}$$

This is the basic equation used by ESP-r in the calculation of a fluid volume's temperature. The bracketed term in front of the nodal temperature  $\theta_i^{t+\Delta t}$  is known as the self-coupling coefficient. The terms in front of the other future time step nodal temperatures are the cross coupling coefficients. These provide the link to the other nodes which exchange energy with node  $i$ . The right hand side of the equation can be regarded as a single coefficient comprising calculated present time step terms and known boundary conditions.

The above equation describes the one-dimensional heat flow associated with the air volume. ESP-r deals with three-dimensional heat flow in the air volume using integrated computational fluid dynamics (CFD). This is discussed in the section 2.2.3. ESP-r can also deal with two and three dimensional heat flow calculations in solid elements. The use of control volumes in modelling the solid structure of the building is discussed later.

For the sake of clarity in the derived equations 2.1-8 the nodal thermophysical properties  $\rho$ ,  $k$  and  $c$ , are shown as time-invariant. However, these properties can vary with temperature and hence become functions of the, as yet unknown, future time step temperature  $\theta_i^{t+\Delta t}$ . ESP-r can deal with these time-varying thermophysical properties using the techniques outlined in section 2.3.3.

Note that the derived balance equations contains terms relating to bulk air (fluid) flow ( $\dot{m}$ ); the principles of the control volume can be extended to model this phenomena as well.

Also note that the derived characteristic equation gives equal weighting to the implicit and explicit terms, the so-called Crank-Nicholson formulation of the equation. It should be kept in mind when reading the derivations that follow, that ESP-r allows the user to change the weighting between the implicit and explicit components of the characteristic equations.

### 2.2.2 Application of a Mass Balance to the Fluid Volume

As with the plant and zonal energy equations, the fluid flow equations for a control volume are derived from a basic balance equation; this assumes that the sum of the connected mass flow rates is zero and that no mass is stored:

$$\sum_{j=1}^n \dot{m}_{ij} = 0. \quad (2.9)$$

$\dot{m}_{ij}$  is the mass flow rate between nodes  $i$  and  $j$  (kg/s) and  $n$  is the number of connected fluid volumes that exchange mass with node  $i$ . Consider the following room, described in the previous section, connected to four other volumes  $i+1 \dots i+4$  by various openings.

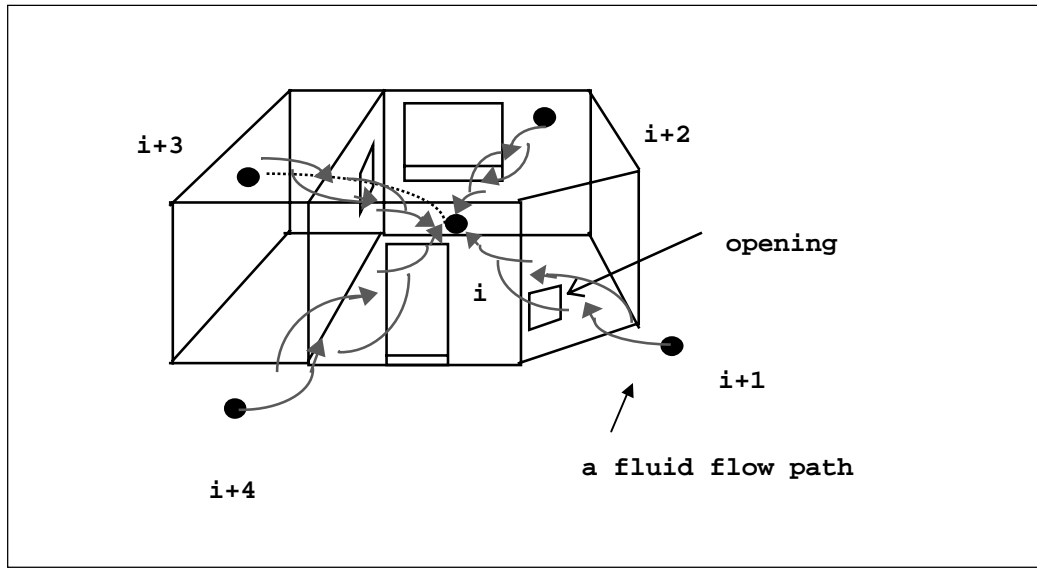


Figure 2.3 The control volume representation of a fluid volume.

Flow between volumes is generally governed by a non-linear function of the pressure difference across the opening separating them:

$$\dot{m}_{x,y} = f(p_x, p_y) = f(\Delta p_{x,y}). \quad (2.10)$$

Here  $p_n$  is the pressure of the node (Pa). The total pressure difference across an opening is a combination of static pressure difference and pressure differences caused by height and density variations between the two connected fluid volumes (i.e. buoyancy effects).

The general form of the balance equation for the node  $i$  is

$$f(\Delta p_{i,i+1}) + f(\Delta p_{i,i+2}) + f(\Delta p_{i,i+3}) + f(\Delta p_{i,i+4}) = 0. \quad (2.11)$$

If all the openings into the zone are small cracks (i.e. through small window openings and under doors) then the non-linear equations governing the flow are of the general form

$$\dot{m} = \rho_x \kappa_{x,y} (\Delta p_{x,y})^n, \quad (2.12)$$

where  $n$  and  $\kappa$  are empirically derived values dependant upon the opening characteristics (area, hydraulic perimeter, length, etc.). The balance equation is therefore

$$\begin{aligned} &\rho_{i+1}\kappa_{i,i+1}(\Delta p_{i,i+1})^a + \rho_{i+2}\kappa_{i,i+2}(\Delta p_{i,i+2})^b + \rho_{i+3}\kappa_{i,i+3}(\Delta p_{i,i+3})^c \\ &+ \rho_{i+4}\kappa_{i,i+4}(\Delta p_{i,i+4})^d = 0. \end{aligned} \quad (2.13)$$

Equation 2.13 is a non-linear function of the inter-nodal pressure differences, which describes the flow balance at node  $i$ . Note that the governing equations of mass flow through an opening need not be the same as equation 2.13, but can be any function of the pressure difference across it.

Many researchers (e.g. Cockroft [4]) have developed expressions of the form of equation 2.10 that describe the flow of fluids across building components (doors, cracks, ducts piping, etc.)

### 2.2.3 Application of Energy Mass and Momentum Balances (CFD)

The representation of a zone using a single control volume as described previously is easy for the modeller to conceptualise, computationally efficient and simple to implement in simulation tools. This single control volume model of the zone provides the modeller with information regarding the bulk temperature and air flows within the room. However, the implicit assumption behind the use of the single air volume is that the air is well mixed; this is sometimes not the case as temperature stratification, stagnant areas, thermal plumes and cold down draughts usually exist in heated rooms. If these phenomena are to be modelled, and more detailed design information is required, such as room air velocities or room temperature distribution, then a more detailed approach to modelling the zone air volume must be taken.

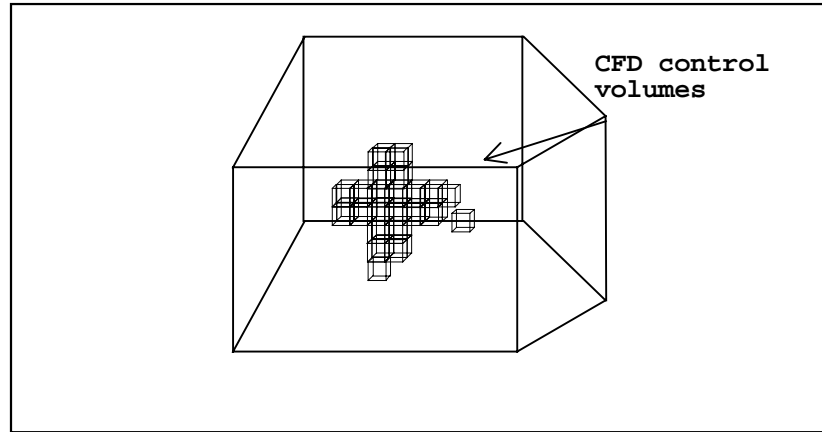


Figure 2.4 The zone subdivided into smaller control volumes.

Subdivision of the zone into many smaller control volumes and the addition of a momentum balance and perhaps a concentration balance (e.g. the quantity of water or contaminant in each volume) to each, introduces the prospect of integration of computational fluid dynamics (CFD) into the building simulation. The use of CFD to model the zone allows not only the determination of bulk fluid energy flows, but also the airflow patterns and temperature distribution as well. However, it should be noted that increasing detail is achieved at the expense of increasing computational and data input overhead. The advantages, disadvantages and applicability of integrating CFD into a simulation must be carefully considered by the modeller.

The equations for each CFD control volume (or cell) involve the conservation of mass momentum, energy and concentration. These equations have the following general form:

$$\frac{\partial}{\partial t} \rho \phi = \frac{\partial}{\partial x_i} \left( \Gamma_{\phi} \frac{\partial \phi}{\partial x_i} \right)_i + S_{\phi} . \quad (2.14)$$

Here  $\phi$  is a transport variable,  $\Gamma_{\phi}$  is a diffusion coefficient and  $S_{\phi}$  is a source term.

Indoor air flows are complex, chaotic phenomena that can be simulated using turbulent transport models. In these models the fundamental equations are time-averaged and are augmented by a

further two equations representing local turbulent energy,  $k$  (J), and its dissipation,  $\varepsilon$  (J/s); these equations form the  $k$ - $\varepsilon$  turbulence model.

Substituting the terms shown in the table below into equation 2.14 gives the time-averaged conservation equations for mass, energy, momentum and concentration, plus the equations for turbulent energy and its dissipation rate.

Equation type	$\phi$	$\Gamma_\phi$	$S_\phi$
Continuity (mass)	1	-	-
Momentum	$V_i$	$\mu_{ef}$	$-\frac{\partial P}{\partial x_i} + \frac{\partial}{\partial x_i} \left[ \mu_{ef} \left( \frac{\partial V_j}{\partial x_i} \right) + \left( \frac{\partial V_i}{\partial x_j} \right) \right] - \rho g_i$
Energy	$T$	$\Gamma_T$	$\frac{q'''}{c_p}$
Concentration	$C$	$\Gamma_C$	$\dot{m}'''$
Turbulent energy	$k$	$\frac{\mu_{ef}}{\sigma_k}$	$G - C_D \rho \varepsilon - G_b$
Energy dissipation	$\varepsilon$	$\frac{\mu_{ef}}{\sigma_\varepsilon}$	$C_1 \frac{\varepsilon}{k} G - C_2 \rho \frac{\varepsilon^2}{k} - C_3 \frac{\varepsilon}{k} G_b$
$\Gamma_T = \frac{\mu}{Pr} + \frac{\mu_t}{\sigma_T}; \Gamma_C = \frac{\mu}{S_C} + \frac{\mu_t}{\sigma_C}; \mu_{ef} = \mu_t + \mu; \rho = \rho(T, C)$ $G_b = g \left( \beta_T \frac{\mu_T}{\sigma_T} \frac{\partial T}{\partial x_i} + \beta_C \frac{\mu_t}{\sigma_C} \frac{\partial C}{\partial x_i} \right); G = \mu_t \left( \frac{\partial V_i}{\partial x_j} + \frac{\partial V_j}{\partial x_i} \right) \frac{\partial V_i}{\partial x_j}$ $C_D=1.0; C_D=1.44; C_2=1.92; \sigma_k = 1.0; \sigma_\varepsilon = 1.3; \sigma_T = 0.9; \sigma_C = 0.9$			

Table 2.1 Diffusion coefficients and source terms for the  $k$ - $\varepsilon$  model.

The  $V$  terms in the equations represents time-averaged velocity components (m/s), while  $T$  and  $P$  represent time-averaged temperature (K) and pressure (Pa) respectively;  $\mu_t$  is the eddy-viscosity (kg/ms) of the flow, while  $q'''$  and  $m'''$  are the per-unit volume rates of heat (W/m<sup>3</sup>) and mass generation (kg/m<sup>3</sup>); Pr is the Prandtl number. The other symbols used in the equations represent their usual thermophysical properties.

The equations of the  $k$ - $\varepsilon$  model are solved iteratively to yield the temperature and velocity distributions within the space described by the CFD control volumes. However, the  $k$ - $\varepsilon$  turbulence model is valid only for high Reynolds Numbers. At low Reynolds Numbers, typically

encountered at wall surfaces due to viscous effects, log-law wall functions are required to describe the velocity and temperature distributions.

Negrao [5] describes the basic theory behind CFD modelling and how it is applied within the context of a building simulation. Clarke and Beausoleil-Morrison [6] describe how CFD has been fully integrated into the ESP-r system: a graded approach is taken, in which the CFD and building model can interact at varying levels of complexity. At the simplest level of integration the CFD model is run to provide the surface convective heat transfer coefficients (the  $h_c$  term of equation 2.2) for the thermal model. At the most complex level of integration, the CFD model is fully coupled with both the thermal zones *and* the fluid flow network (which provides mass flow and velocity boundary conditions). The CFD solution then provides air temperature and velocity distributions within the zone, as well as air flow information to the fluid flow network.

The surface convective heat transfer coefficients calculated using the CFD model can be used directly with the group of control volumes described in the next section: those which describe the bounding multi-layered construction of the zone fluid volumes.

The integration of CFD into ESP-r illustrates the trend towards increased rigour and complexity in building energy modelling. This trend is driven by the desire to model the physical processes occurring within the building in a more realistic fashion. A result of this move towards integration is that once separate modelling tasks such as CFD, lighting analysis and building thermal simulation are now performed simultaneously within an integrated model. The addition of electrical power flow modelling to building simulation is another step in this direction.

#### **2.2.4 The Control Volume Applied to the Building Fabric**

In ESP-r multi-layered constructions are used to represent the solid elements which make up the building fabric and provide the physical boundaries to the zones. Consider now the application of the control volume principle to the fundamental heat transfer process occurring in these solid elements: conduction, convection and radiation.

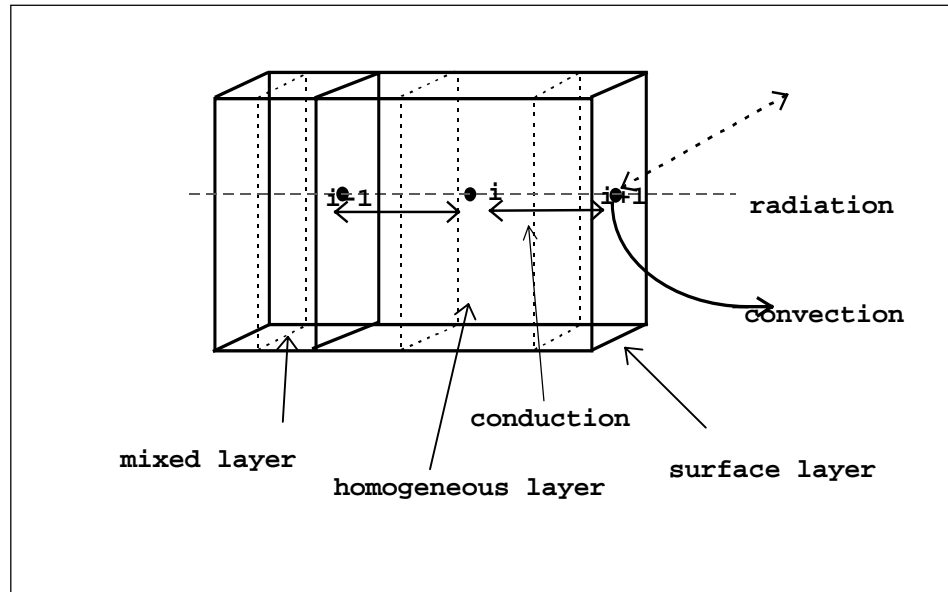


Figure 2.5 Heat transfer in a multi-layered construction.

It is possible to represent the surface layer of the construction shown in figure 2.5 using three control volumes: a homogeneous material volume, a surface volume and a mixed property volume located at the boundary with the next layer of material. Each is of dimensions  $\Delta x_n, \Delta y_n, \Delta z_n$ , (m), where  $\Delta x_n$  is the thickness,  $\Delta y_n$  the breadth and  $\Delta z_n$  the height of element  $n$ . Consider firstly the application to the homogeneous volume, represented by node  $i$ :

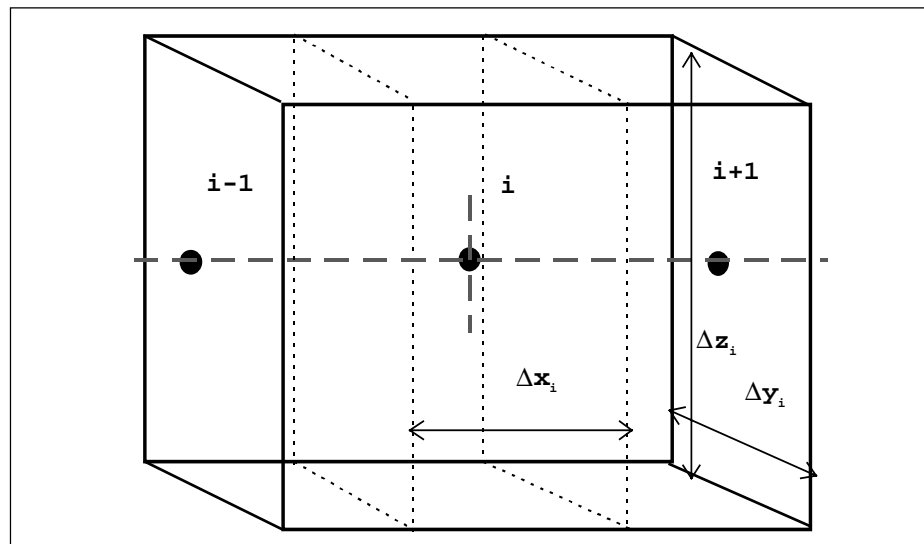


Figure 2.6 A control volume representation of a layer of homogeneous material.



The following is the basic heat balance equation for one dimensional heat flow along the x-axis in this element.

$$\rho_i c_i V_i \frac{\partial \theta_i}{\partial t} = \sum_{j=1}^n q_{ij} \quad (2.15)$$

Note that the basic equation for the solid control volumes is identical to that applied to the fluid volume (equation 2.1).

Again, applying a backwards difference scheme to the partial derivative term over some finite time interval  $\Delta t$  (s), and considering the heat fluxes shown in figure 2.5 the following expression emerges.

$$\frac{\rho_i c_i V_i (\theta_i^{t+\Delta t} - \theta_i^t)}{\Delta t} = q_{i,i+1}^t + q_{i,i-1}^t + q_{i_e}^t. \quad (2.16)$$

$\theta^t$  represents the temperature at the current time  $t$  and  $\theta^{t+\Delta t}$  the temperature at some future time  $t+\Delta t$ . The  $q_{i_e}^t$  (W) term included in the equation is a general heat generation term that can be adapted to suit various temperature independent phenomena, e.g. plant heat input or solar absorption. The conductive heat transfers with adjacent nodes (W),  $q_{i,i+1}$ , and  $q_{i,i-1}$ , can also be expressed in discrete form:

$$q_{i,i+1}^t = \frac{k_{i,i+1} \Delta z_i \Delta y_i (\theta_{i+1}^t - \theta_i^t)}{\Delta x_i}, \quad (2.17)$$

similarly,

$$q_{i,i-1}^t = \frac{k_{i,i-1} \Delta z_i \Delta y_i (\theta_{i-1}^t - \theta_i^t)}{\Delta x_i}. \quad (2.18)$$

Where  $k_{m,n}$  represents the conductivity (W/mK) of the material between the two nodes  $m$  and  $n$ . Substituting equations 2.17 and 2.18 back into equation 2.16 gives

$$\frac{\rho_i c_i V_i (\theta_i^{t+\Delta t} - \theta_i^t)}{\Delta t} = \frac{k_{i,i+1} \Delta z_i \Delta y_i (\theta_{i+1}^t - \theta_i^t)}{\Delta x_i} + \frac{k_{i,i-1} \Delta z_i \Delta y_i (\theta_{i-1}^t - \theta_i^t)}{\Delta x_i} + q_{ie}^t. \quad (2.19)$$

This is the explicit form of the heat balance equation for the control volume represented by node  $i$ . The implicit form of the equation is given by

$$\begin{aligned} \frac{\rho_i c_i V_i (\theta_i^{t+\Delta t} - \theta_i^t)}{\Delta t} &= \frac{k_{i,i+1} \Delta z_i \Delta y_i (\theta_{i+1}^{t+\Delta t} - \theta_i^{t+\Delta t})}{\Delta x_i} + \frac{k_{i,i-1} \Delta z_i \Delta y_i (\theta_{i-1}^{t+\Delta t} - \theta_i^{t+\Delta t})}{\Delta x_i} \\ &+ q_{ie}^{t+\Delta t} \end{aligned} \quad (2.20)$$

Adding 2.19 and 2.20 together gives the following mixed expression.

$$\begin{aligned} 2 \frac{\rho_i c_i V_i (\theta_i^{t+\Delta t} - \theta_i^t)}{\Delta t} &= \frac{k_{i,i+1} \Delta z_i \Delta y_i (\theta_{i+1}^{t+\Delta t} - \theta_i^{t+\Delta t})}{\Delta x_i} + \frac{k_{i,i-1} \Delta z_i \Delta y_i (\theta_{i-1}^{t+\Delta t} - \theta_i^{t+\Delta t})}{\Delta x_i} + \\ &\frac{k_{i,i+1} \Delta z_i \Delta y_i (\theta_{i+1}^{t+\Delta t} - \theta_i^{t+\Delta t})}{\Delta x_i} + \frac{k_{i,i-1} \Delta z_i \Delta y_i (\theta_{i-1}^{t+\Delta t} - \theta_i^{t+\Delta t})}{\Delta x_i} + q_{ie}^t + q_{ie}^{t+\Delta t}. \end{aligned} \quad (2.21)$$

Dividing by the volume  $V_i = (\Delta x \Delta y \Delta z)_i$  and grouping the future time row terms  $(t+\Delta t)$  on the left hand side of the equation gives

$$\begin{aligned} &\left( \frac{2\rho_i c_i}{\Delta t} + \frac{k_{i,i+1} + k_{i,i-1}}{\Delta x_i^2} \right) \theta_i^{t+\Delta t} - \frac{k_{i,i+1}}{\Delta x_i^2} \theta_{i+1}^{t+\Delta t} - \frac{k_{i,i-1}}{\Delta x_i^2} \theta_{i-1}^{t+\Delta t} - \frac{q_{ie}^{t+\Delta t}}{(\Delta x \Delta y \Delta z)_i} \\ &= \left( \frac{2\rho_i c_i}{\Delta t} + \frac{k_{i,i+1} + k_{i,i-1}}{\Delta x_i^2} \right) \theta_i^t + \frac{k_{i,i+1}}{\Delta x_i^2} \theta_{i+1}^t + \frac{k_{i,i-1}}{\Delta x_i^2} \theta_{i-1}^t + \frac{q_{ie}^t}{(\Delta x \Delta y \Delta z)_i}. \end{aligned} \quad (2.22)$$

This is the basic energy balance equation used by ESP-r in the calculation of nodal temperatures in a homogeneous layer of material. Note the similarity between this equation and the energy balance derived for the fluid volume (equation 2.8).

Similar equations can be constructed for the control volume at the surface layer of a material, represented by node  $i+1$ , and the mixed property element, node  $i-1$ , located at the boundary with another layer.

A control volume as shown in figure 2.7 represents the surface layer of the construction, shown in figure 2.5

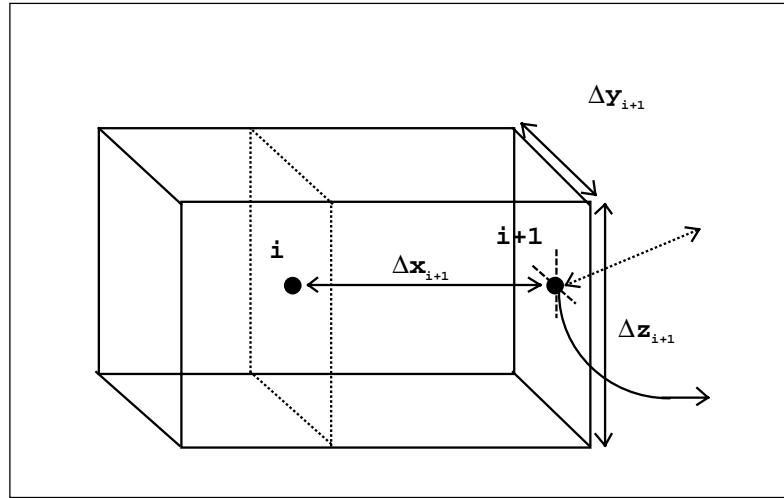


Figure 2.7 A control volume representation of the surface layer of a material.

Considering only one-dimensional conduction and applying the same procedures as were used with the homogeneous element, the following equation for the energy balance in the control volume emerges.

$$\begin{aligned}
& \left( \frac{2\rho_{i+1}}{\Delta t} \frac{c_{i+1}}{\Delta x_{i+1}^2} + \sum_{s=1}^n \frac{h_{r,s,i+1}}{\Delta x_{i+1}} + \frac{h_{c,i+1}}{\Delta x_{i+1}} \right) \theta_{i+1}^{t+\Delta t} - \frac{k_{i,i+1}}{\Delta x_{i+1}^2} \theta_i^{t+\Delta t} - \sum_{s=1}^n \frac{h_{r,s,i+1} \theta_s^{t+\Delta t}}{\Delta t} \\
& - \frac{h_{c,i+1}}{\Delta x_{i+1}} \theta_a^{t+\Delta t} - \frac{q_{ri+1}^{t+\Delta t}}{(\Delta x \Delta y \Delta z)_{i+1}} \\
& = \left( \frac{2\rho_{i+1}}{\Delta t} \frac{c_{i+1}}{\Delta x_{i+1}^2} + \sum_{s=1}^n \frac{h_{r,s,i+1}}{\Delta x_{i+1}} + \frac{h_{c,i+1}}{\Delta x_{i+1}} \right) \theta_{i+1}^t + \frac{k_{i,i+1}}{\Delta x_{i+1}^2} \theta_i^t + \sum_{s=1}^n \frac{h_{r,s,i+1} \theta_s^t}{\Delta t} \\
& + \frac{h_{c,i+1}}{\Delta x_{i+1}} \theta_a^t + \frac{q_{ri+1}^t}{(\Delta x \Delta y \Delta z)_{i+1}}.
\end{aligned} \tag{2.23}$$

Again, the self-coupling coefficient, cross coupling coefficients and right hand side coefficient are evident in the equation structure. However additional terms are included to account for physical phenomena occurring at the surface of a material.  $h_c$  is the convective heat transfer coefficient, described in section 2.2.1.  $\theta_a$  is the temperature of the adjacent air volume.

$\sum_{s=1}^n h_{r,s,i+1}$  are the radiative heat transfer coefficients (W) that characterise the long wave radiant heat transfer between this and the  $n$  other surfaces in the zone. The term  $q_r$  represents solar and other radiant gains (W) to the surface (e.g. from plant and occupants).

The final type of element shown in figure 2.5 is the mixed property control volume, represented by node  $i-1$ , this is shown in more detail in figure 2.8.

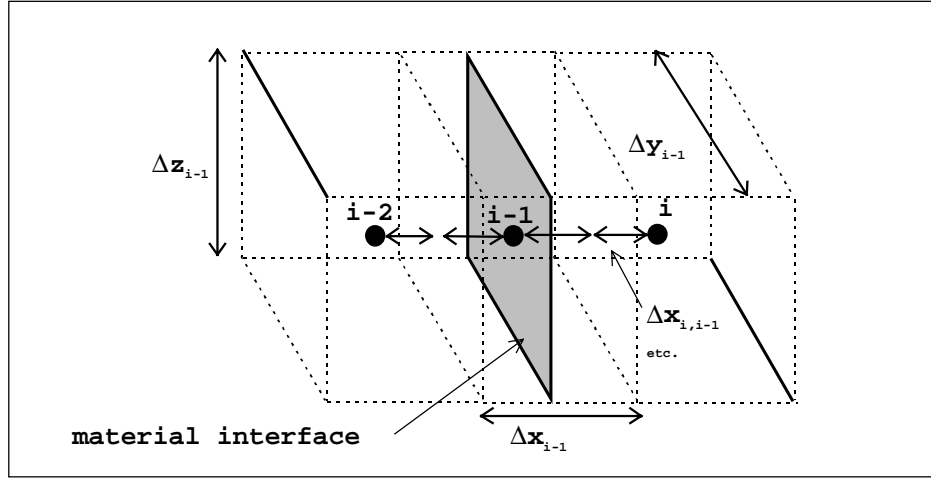


Figure 2.8 The control volume representation of a mixed property region.

In a similar fashion to the homogeneous and surface regions, the following equation describing the energy balance in the finite volume can be derived.

$$\begin{aligned}
 & \left( \frac{2\rho_{i-1}c_{i-1}}{\Delta t} + \frac{k_{i,i-1}R + 2\Delta x_{i-1}}{\Delta x_{i-1}(\Delta x_{i,i-1} + \Delta x_{i-2,i-1})R} + \frac{k_{i-2,i-1}R + 2\Delta x_{i-1}}{\Delta x_{i-1}(\Delta x_{i,i-1} + \Delta x_{i-2,i-1})R} \right) \theta_{i-1}^{t+\Delta t} - \\
 & \left( \frac{k_{i,i-1}R + 2\Delta x_{i-1}}{\Delta x_{i-1}(\Delta x_{i,i-1} + \Delta x_{i-2,i-1})R} \right) \theta_i^{t+\Delta t} - \left( \frac{k_{i-2,i-1}R + 2\Delta x_{i-1}}{\Delta x_{i-1}(\Delta x_{i,i-1} + \Delta x_{i-2,i-1})R} \right) \theta_{i-2}^{t+\Delta t} \\
 & - \frac{q_{i-1e}^{t+\Delta t}}{(\Delta x \Delta y \Delta z)_{i-1}} \\
 & = \left( \frac{2\rho_{i-1}c_{i-1}}{\Delta t} + \frac{k_{i,i-1}R + 2\Delta x_{i-1}}{\Delta x_{i-1}(\Delta x_{i,i-1} + \Delta x_{i-2,i-1})R} + \frac{k_{i-2,i-1}R + 2\Delta x_{i-1}}{\Delta x_{i-1}(\Delta x_{i,i-1} + \Delta x_{i-2,i-1})R} \right) \theta_{i-1}^t + \\
 & \left( \frac{k_{i,i-1}R + 2\Delta x_{i-1}}{\Delta x_{i-1}(\Delta x_{i,i-1} + \Delta x_{i-2,i-1})R} \right) \theta_i^t + \left( \frac{k_{i-2,i-1}R + 2\Delta x_{i-1}}{\Delta x_{i-1}(\Delta x_{i,i-1} + \Delta x_{i-2,i-1})R} \right) \theta_{i-2}^t \\
 & + \frac{q_{i-1e}^t}{(\Delta x \Delta y \Delta z)_{i-1}}
 \end{aligned} \tag{2.24}$$

Note that the density  $\rho_{i-1}$  and the specific heat  $c_{p\ i-1}$  of this control volume are a volume weighted average of its two constituent materials.  $R$  represents an added resistance ( $\text{m}^2\text{K/W}$ ) at the material interface.

Also note that the equations shown here deal only with one-dimensional heat conduction. As was noted earlier, ESP-r can also model two or three-dimensional heat flow in elements of the building structure. Clarke [2] outlines how the control volume method is extended to deal with this.

The previous sections illustrated the control volume technique applied to the characteristic elements of the zone: the fluid volume and its bounding constructions. Equations describing the energy flow in those elements were derived. Clarke [2] uses the same methods to develop equations for other constituents of a thermal zone: transparent constructions, air gaps etc.

### **2.2.5 The Control Volume Applied to Plant Components**

As with the zones that make up the building model, the control volume technique can also be used to derive the equation sets describing a building's plant network. In ESP-r the plant network consists of a coupled group of plant component models, each of these models being described by one or more control volumes. Consider the application of the technique to a typical plant component; an air/water heat exchanger. The component can be described using three control volumes: one for the fluid, one for the air and one for the solid elements of the component. More or less control volumes can be used, depending on the level of detail required by the modeller. This representation of the plant component is shown in figure 2.9.

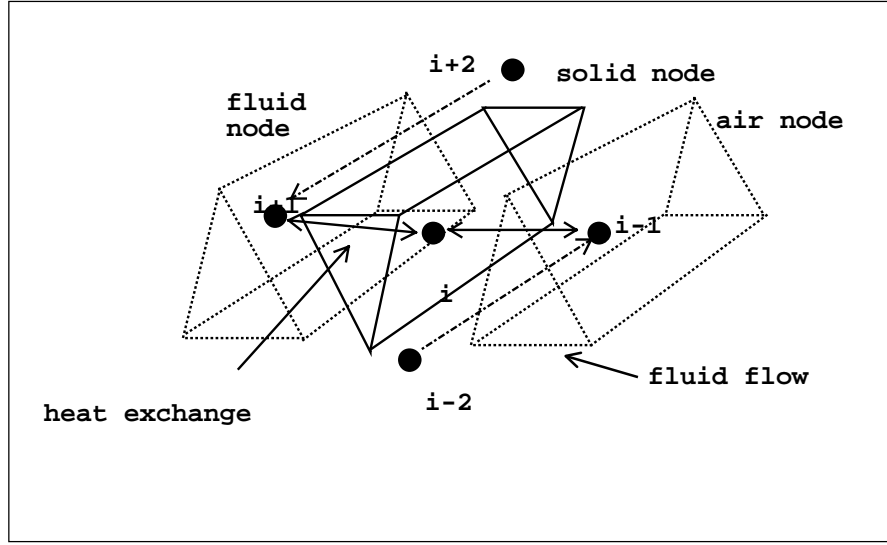


Figure 2.9 The control volume representation of an air/water heat exchanger.

The energy balance equation 2.1 can also be applied to the control volumes of the plant component. Discretising this equation for the solid node,  $i$ , of the plant component gives

$$\rho_i c_i V_i \frac{(\theta_i^{t+\Delta t} - \theta_i^t)}{\Delta t} = q_{i,i+1} + q_{i,i-1} + q_{i,\infty}. \quad (2.25)$$

Where  $q_{i,i+1}$ ,  $q_{i,i-1}$  are the heat exchanges (W) with the neighbouring fluid and air volumes of the heat exchanger,  $q_{i,\infty}$  is the heat exchange (W) with the environment surrounding the plant component.  $q_{i,i+1}$ , and  $q_{i,i-1}$  can be expressed as a function of temperature:

$$q_{i,i+1} = h_{i,i+1} A_{i,i+1} (\theta_{i+1} - \theta_i); \quad (2.26)$$

similarly,

$$q_{i,i-1} = h_{i,i-1} A_{i,i-1} (\theta_{i-1} - \theta_i). \quad (2.27)$$

$A_{i,n}$  are the contact areas ( $\text{m}^2$ ) between the volume represented by node  $i$  and connected volumes: in this case the contact area of the neighbouring air and fluid streams with the solid casing.  $h_{i,n}$  are the heat transfer coefficients between the fluid streams and the casing ( $\text{W}/\text{m}^2\text{K}$ ). As with the

building equations, linear coefficients are used in the representation of non-linear heat transfer exchanges between the fluids and the casing. Again, refer to section 2.3.3 for an explanation of how ESP-r deals with these non-linear processes.

The exchange between the plant component and the environment can be expressed in a similar form to equations 2.26 and 2.27

$$q_{i,\infty} = h_{i,\infty} (\theta_{\infty} - \theta_i). \quad (2.28)$$

Where  $h_{i,\infty}$  is the heat transfer coefficient between the control volume and the environment at a temperature  $\theta_{\infty}$ .

Substituting 2.26-8 into equation 2.25 at some time  $t$ , gives the implicit form of the control volume energy balance equation for node  $i$ .

$$\rho_i c_i V_i \frac{(\theta_i^{t+\Delta t} - \theta_i^t)}{\Delta t} = h_{i,i+1} A_{i,i+1} (\theta_{i+1}^t - \theta_i^t) + h_{i,i-1} A_{i,i-1} (\theta_{i-1}^t - \theta_i^t) + h_{i,\infty} A_{i,\infty} (\theta_{\infty}^t - \theta_i^t). \quad (2.29)$$

As with the building equation sets, ESP-r uses a mixed implicit/explicit expression as the characteristic equation. The implicit form of equation 2.29 is

$$\begin{aligned} \rho_i c_i V_i \frac{(\theta_i^{t+\Delta t} - \theta_i^t)}{\Delta t} &= h_{i,i+1} A_{i,i+1} (\theta_{i+1}^{t+\Delta t} - \theta_i^{t+\Delta t}) + h_{i,i-1} A_{i,i-1} (\theta_{i-1}^{t+\Delta t} - \theta_i^{t+\Delta t}) \\ &+ h_{i,\infty} A_{i,\infty} (\theta_{\infty}^{t+\Delta t} - \theta_i^{t+\Delta t}). \end{aligned} \quad (2.30)$$

Adding the implicit and explicit expressions and grouping future time step terms on the left-hand side of the equation gives



$$\begin{aligned}
& \left( \frac{2\rho_i c_i V_i + h_{i,i+1} A_{i,i+1} + h_{i,i-1} A_{i,i-1} + h_{i,\infty} A_{i,\infty}}{\Delta t} \right) \theta_i^{t+\Delta t} - h_{i,i+1} A_{i,i+1} \theta_{i+1}^{t+\Delta t} - h_{i,i-1} A_{i,i-1} \theta_{i-1}^{t+\Delta t} \\
& - h_{i,\infty} A_{i,\infty} \theta_{\infty}^{t+\Delta t} \\
& = \left( \frac{2\rho_i c_i V_i + h_{i,i+1} A_{i,i+1} + h_{i,i-1} A_{i,i-1} + h_{i,\infty} A_{i,\infty}}{\Delta t} \right) \theta_i^t + h_{i,i+1} A_{i,i+1} \theta_{i+1}^t + h_{i,i-1} A_{i,i-1} \theta_{i-1}^t \\
& + h_{i,\infty} A_{i,\infty} \theta_{\infty}^t.
\end{aligned} \tag{2.31}$$

The plant control volume characteristic equation has an identical structure to those derived for the multi-layered construction, with a self-coupling coefficient, cross coupling coefficients linking adjacent control volumes and a right hand side containing previously calculated and known values.

Turning to the other two control volumes in the heat exchanger and applying the same basic energy balance as was as used with node  $i$ , two characteristic equations can be derived. Note, that in these two cases energy is exchanged by fluid transfers with adjacent volumes where the heat exchange ( $W$ ) between two nodes  $x$  and  $y$ , coupled by fluid flow is given by

$$q_{x,y} = \dot{m}_{x,y} c_y (\theta_x - \theta_y). \tag{2.32}$$

The air in the heat exchanger is a binary mixture, consisting of both dry air and water vapour, hence in equation 2.33 subscript  $v$  refers to vapour properties and  $a$  refers to dry air properties,  $\dot{m}$  refers to a mass flow rate of air or vapour (kg/s). The heat exchange with nodes coupled by fluid flow is given by

$$q_{x,y} = \dot{m}_{v x,y} c_{v y} (\theta_x - \theta_y) + \dot{m}_{a x,y} c_{p a y} (\theta_x - \theta_y). \tag{2.33}$$

The air and vapour are assumed to be at the same temperature.

For the air volume node  $i-1$ , the energy balance equation is therefore

$$\begin{aligned}
& \left( 2 \frac{[\rho_{v,i-1} c_{v,i-1} V_{v,i-1} + \rho_{a,i-1} c_{a,i-1} V_{a,i-1}]}{\Delta t} + \dot{m}_{v,i-1,i-2}^{t+\Delta t} c_{v,i-2} + \dot{m}_{a,i-1,i-2}^{t+\Delta t} c_{a,i-2} + h_{i,i-1} A_{i,i-1} \right) \theta_{i-1}^{t+\Delta t} \\
& - \dot{m}_{v,i-1,i-2}^{t+\Delta t} c_{v,i-2} \theta_{i-2}^{t+\Delta t} - \dot{m}_{a,i-1,i-2}^{t+\Delta t} c_{a,i-2} \theta_{i-2}^{t+\Delta t} - h_{i,i-1} A_{i,i-1} \theta_i^{t+\Delta t} \\
& = \left( 2 \frac{[\rho_{v,i-1} c_{v,i-1} V_{v,i-1} + \rho_{a,i-1} c_{a,i-1} V_{a,i-1}]}{\Delta t} + \dot{m}_{v,i-1,i-2}^t c_{v,i-2} + \dot{m}_{a,i-1,i-2}^t c_{a,i-2} + h_{i,i-1} A_{i,i-1} \right) \theta_{i-1}^t \\
& + \dot{m}_{v,i-1,i-2}^t c_{v,i-2} \theta_{i-2}^t + \dot{m}_{a,i-1,i-2}^t c_{a,i-2} \theta_{i-2}^t + h_{i,i-1} A_{i,i-1} \theta_i^t.
\end{aligned} \tag{2.34}$$

For the fluid volume represented by node  $i+1$ , the energy balance equation is

$$\begin{aligned}
& \left( 2 \frac{[\rho_{i+1} c_{i+1} V_{i+1}]}{\Delta t} + \dot{m}_{v,i+1,i+2}^{t+\Delta t} c_{v,i-2} + h_{i,i+1} A_{i,i+1} \right) \theta_{i+1}^{t+\Delta t} \\
& - \dot{m}_{i+1,i+2}^{t+\Delta t} c_{i+2} \theta_{i+2}^{t+\Delta t} - h_{i,i+1} A_{i,i+1} \theta_i^{t+\Delta t} \\
& = \left( 2 \frac{[\rho_{i-1} c_{i-1} V_{i-1}]}{\Delta t} + \dot{m}_{i+1,i+2}^t c_{i+2} + h_{i,i-1} A_{i,i-1} \right) \theta_{i-1}^t \\
& + \dot{m}_{v,i+1,i+2}^t c_{i+2} \theta_{i+2}^t + h_{i,i+1} A_{i,i+1} \theta_i^t.
\end{aligned} \tag{2.35}$$

Note that, as with the equations for the zonal fluid volume, the energy equations contain terms relating to fluid flow. Again these would be evaluated using a mass balance technique applied to a fluid control volume.

Clarke [2], Tang [7], Aasem [8] and Hensen [9] apply the control volume modelling technique to a variety of plant components, while Mclean [10] applies it to solar energy systems. The resulting library of developed component models allows the simulation of air conditioning systems, hot water heating systems and mixed air/hot water systems as a plant network in ESP-r. Chow [11] has extended the principle of the control volumes in plant modelling by identifying

27 fundamental ‘primitive parts’, which are essentially characteristic control volumes describing the basic thermodynamic processes occurring in air conditioning systems. The aim of this work is that any plant component can be described and modelled from coupled groups of these primitive parts.

## **2.3 Treatment and Solution of the Finite Volume Equation Sets**

The previous sections demonstrate the applicability of the control volume to different aspects of the building and how for each, a characteristic equation can be extracted. Having derived these equations, it is necessary to arrange them in a form suitable for solution within the context of a transient energy simulation.

Two different types of equation were derived in sections 2.2.1-2.2.5: the linearised zonal and plant equations and the non-linear, fluid flow equations. Grouping each set of equations according to subsystem and type allows them to be processed in the most appropriate manner: direct methods for the linearised plant and building equations and iterative techniques for the non-linear fluid flow equations. Note that the processing method is determined by the linearity or non-linearity of the system’s characteristic equations, rather than the linearity or non-linearity of the system itself (i.e. air flow is a linear system modelled using non-linear equations, the reverse is true for the building and plant energy flows).

All of the derived equations contain terms relating to other coupled volumes, so a simultaneous solution is required. The following sections describe the methods of solution for the building, plant and fluid flow equation sets. Section 2.4 shows how they are solved simultaneously by a process of iterative handshaking.

### **2.3.1 Zonal Energy Equations**

The equations which describe the energy flows in the thermal zones of the model have the general form

$$\begin{aligned}
a_1 \theta_1^{t+\Delta t} + \sum_{j=1}^n b_{1j} \theta_j^{t+\Delta t} + c_1 q_1^{t+\Delta t} &= a_1 \theta_1^t + \sum_{j=1}^n b_{1j} \theta_j^t + c_1 q_n^t + d_1 \\
&\vdots
\end{aligned} \tag{2.36}$$

$$a_n \theta_n^{t+\Delta t} + \sum_{j=1}^n b_{nj} \theta_j^{t+\Delta t} + c_n q_n^{t+\Delta t} = a_n \theta_n^t + \sum_{j=1}^n b_{nj} \theta_j^t + c_n q_n^t + d_n.$$

For any node  $i$ ,  $\theta_i$  is a nodal temperature,  $a_i$  the self-coupling coefficient,  $\sum_{j=1}^n b_{ij}$  are the cross coupling coefficients to connected nodes,  $c_i$  is the coefficient for the heat generation term,  $q_i$  and  $d_i$  are any ‘known’ boundary condition (e.g. climate parameters). The terms on the right-hand-side represent the unknown future time step of the simulation,  $t + \Delta t$ , while the left-hand-side terms contains the present time step and known boundary terms.

In matrix form, the set of zonal equations can be written as

$$\mathbf{A} \mathbf{x}^{t+\Delta t} = (\mathbf{B} \mathbf{x}^t + \mathbf{C}) = \mathbf{Z}. \tag{2.37}$$

Where  $\mathbf{A}$  is the matrix of future time step nodal self and cross-coupling coefficients,  $\mathbf{B}$  is the matrix of present time step coefficients and  $\mathbf{C}$  is the matrix of known terms and boundary conditions.  $\mathbf{Z}$  is the combined matrix of solved present time step and known terms,  $\mathbf{x}^{t+\Delta t}$  and  $\mathbf{x}^t$  are column matrices of nodal temperatures and heat injections at the present and future time steps respectively.

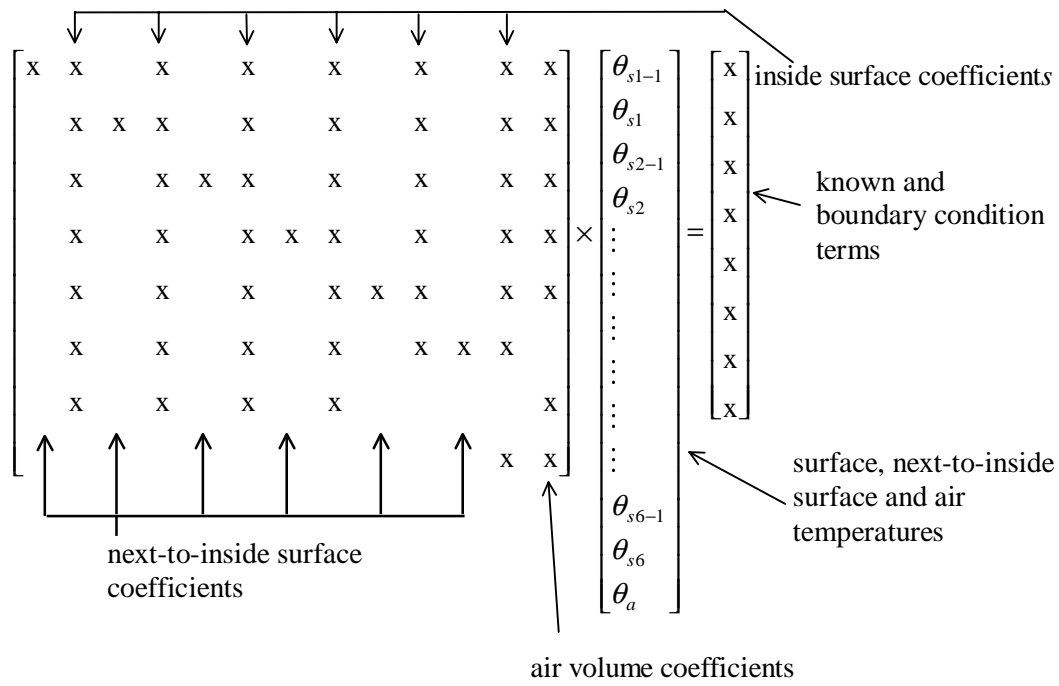
Solution of equation 2.37 can be achieved by multiplication of both sides by the inverse of  $\mathbf{A}$ , to give the unknown temperatures and heat injections. Unfortunately, the  $\mathbf{A}$  matrix is characterised by its size and sparsity (in the typical building model the  $\mathbf{A}$  matrix will contain thousands of entries, most of them zero). Inversion of this type of matrix at each time step in a simulation is both a computationally expensive and time-consuming process. This solution method is therefore unacceptable for use in a simulation tool. ESP-r uses a more efficient, customised solution process. Instead of forming one large matrix equation for the whole building, smaller

equation sets are derived on a zonal basis: one for each multi-layered construction and one for the fluid volume enclosed by them. The equation sets can still be grouped in matrix form similar to equation 2.37. The multi-layered construction equation sets contain all the nodal equations for the structure, except those of the surface node bounding the fluid volume, which is included in the fluid volume equation set. The form of a solid construction equation set is shown below, with one point of plant interaction. Note that even with this smaller matrix, many of the coefficients will be zero (an x represents a non-zero coefficient entry).

$$\begin{bmatrix}
 \boxed{x} & \boxed{x} & \boxed{x} \\
 & x & x & x \\
 & & x & x & x \\
 & & & x & x & x \\
 & & & & \boxed{x} & \boxed{x} & \boxed{x} \\
 & & & & & x
 \end{bmatrix}
 \begin{bmatrix}
 \theta_0 \\
 \theta_1 \\
 \theta_2 \\
 \theta_3 \\
 \theta_4 \\
 \theta_5 \\
 \theta_s \\
 q_p
 \end{bmatrix}
 =
 \begin{bmatrix}
 x \\
 x \\
 x \\
 x \\
 x \\
 x
 \end{bmatrix}$$

outside surface  
 known and boundary condition terms  
 plant injection coefficient  
 next-to-inside surface  
 nodal temperatures and plant injections  
 surface coefficient held for reduction process (see Clarke [2]).  
 matrix of self and cross-coupling coefficients

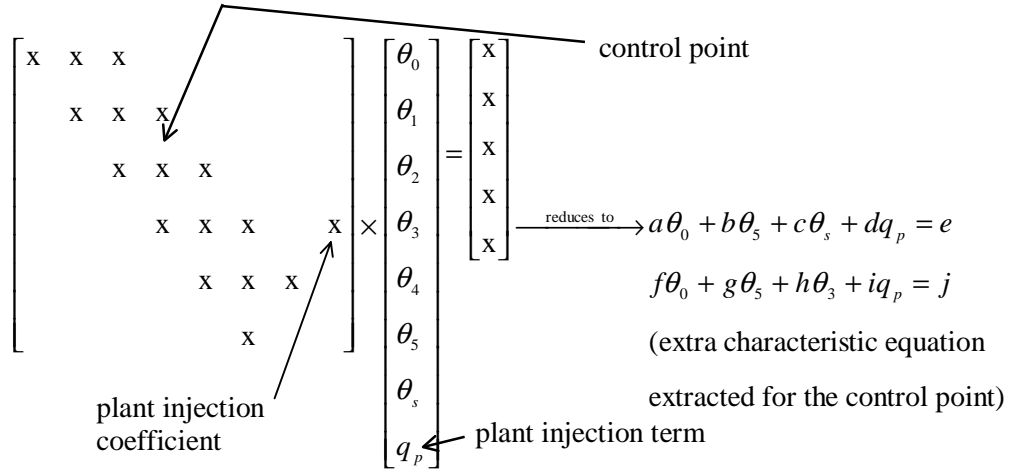
For a zone with one air node and six enclosing surfaces a typical form of the air and surface nodal matrix equation is as follows.



Subscript  $sn$  refers to a surface node,  $sn-1$  refers to the next-to-inside surface node and  $\theta_a$  is the temperature of the zone air node. The aim of the solution method is to process the zonal equation sets, taking into account the interaction of other factors, such as plant input and control objectives, on the eventual solution. The control objectives are central to the processing of the equation sets and require some explanation.

The basis of control in ESP-r is the control loop, through which a property of a node is sensed and an appropriate action taken at an actuation point, which may be the same or another node in the model. The aim of the actuation is to bring the sensed nodal variable to a desired value. As an example: it is possible to change the temperature of air delivered to a room by altering the flow of hot water to a heating coil located in an air handling unit in another part of the building. The operation of control in ESP-r is discussed at length by Clarke [2].

Returning to the solution process, this proceeds using a forward reduction technique, in which the equation set of each multi-layered construction is processed so that one characteristic equation is derived:



Where  $a \dots j$  are the modified coefficients emerging from the reduction process. The characteristic equation contains the essential properties of its associated equation set. Note that if one of the nodes in a particular construction is a sensed node then an extra characteristic equation is derived from the construction's equation set. This extra equation incorporates the temperature of the sensed node  $\theta_c$ , as shown above, where the sensed node is 3. This control temperature will be used in the final solution of the zonal energy equation.

The extracted equations are added, arithmetically, to the air volume equation set, which is in turn forward reduced to a final characteristic equation for the entire zone:

$$\sum_{i=1}^n a_i \theta_n + b\theta_c + cq_p = d . \quad (2.38)$$

Again,  $b$ ,  $c$  and  $d$  are the modified nodal coefficients emerging from the final reduction process,

while  $\sum_{i=1}^n a_i$  are the modified coefficients relating to the bounding temperatures of the zone,  $\theta_i$ ,

e.g. the temperatures of other connected zones or an external temperature.  $q_p$  represents the energy input from plant, while  $\theta_c$  is the temperature of the sensed node in the zone. If previous

time step values<sup>7</sup> are used for the as yet unknown zonal bounding temperatures, the equation can be solved in one of two ways: if the control temperature,  $\theta_c$  is known, then  $q_p$  can be calculated, alternatively if  $q_p$  is known then the temperature of the controlled node can be determined. Both methods are required in the simultaneous solution scheme outlined in section 2.4.

All the other nodal temperatures in the zone are found by a process of back-substitution from this single solved temperature. The solution process outlined here is described in more detail by Clarke [2] and can be applied to all other the zones in a building model.

### 2.3.2 The Plant Energy Equations

The plant equations derived in section 2.2.5 are of a similar form to the building equations and can be solved using direct methods. Unlike the building solution method, partitioning is not required, due to the fact that a far smaller number of equations are used in the description of the plant network.

The general form of the plant energy equations was

$$a_i \theta_i^{t+\Delta t} + \sum_{j=1}^n b_{ij} \theta_j^{t+\Delta t} = a_i \theta_i^t + \sum_{j=1}^n b_{ij} \theta_j^t + c. \quad (2.39)$$

Note the similarity to the zonal equations. Again,  $a_i$  is the self coupling coefficient,  $\sum_{j=1}^n b_{ij}$  are

cross coupling coefficients,  $\theta^{t+\Delta t}$  and  $\theta^t$  are the self nodal temperatures at the future and present time steps respectively. The coefficient  $c$  holds known and boundary data such as: fuel flow rates, external temperatures, heat injection terms, connected zone temperatures, etc.

---

<sup>7</sup> At hourly or sub-hourly simulation time steps the error introduced by this assumption is small.



As with the building equations, the set of plant equations can be written in matrix form:

$$\mathbf{A}\theta^{t+\Delta t} = \mathbf{B}\theta^t + \mathbf{C}. \quad (2.40)$$

Where the symbols have the same meaning as in equation 2.37. Solution for the future time step nodal temperatures can be achieved by a direct method such as Gaussian elimination.

As with the building, the solution of the plant matrix is dictated by control interaction, where the state of the system components is adjusted to bring about a desired control objective. The sensed node for the plant control may be another plant component or another node in the building model, e.g. the flow rate of cold water into a chiller coil may be controlled based on the relative humidity in a thermal zone. Control is calculated for the plant network prior to solution of the plant equations, hence the solution incorporates the effects of control action. The control action is calculated based in the previous time step calculated values, i.e. one time step in arrears.

### 2.3.3 Treatment of Time-Varying and Non-Linear Processes

The equations derived for both building and plant are in linear-algebraic form, which allows their solution using the efficient, direct methods outlined in sections 2.3.1 and 2.3.2. This solution technique can be easily adapted to cope with the time-dependency of thermophysical properties and/or non-linear heat transfer processes.

All the equations derived for the zones and plant contain terms relating to thermophysical properties such as: density, specific heat capacity, conductivity etc. If these are considered time-variant, e.g. as a function of temperature, then the value of the coefficients on the left-hand-side (future time step) of the control volume energy equations cannot be determined, as the future time step temperature is unknown. ESP-r's solution to this problem is to calculate the material properties based on the previously calculated time step temperatures. This has the advantage of maintaining the linear form of the zonal and plant energy equations. If a great degree of accuracy is required, or where certain processes or material properties are highly non-linear, then an iterative solution mechanism can be employed, whereby the equation sets are solved assuming the previous time step temperatures and processed to give the future time step solution. If the

difference between the assumed and calculated temperatures is too great then the solution is repeated for that time step until convergence is obtained.

The same solution can be applied where non-linear heat transfer processes occur, e.g. long wave radiant or convective heat transfer. In the zonal and plant equation sets these phenomena are represented by linear coefficients<sup>8</sup>, whose values are calculated based on previous time step temperature. Again, if a great degree of accuracy is required then the iterative mechanism can be employed. In practice though, the assumption of previous time step temperatures proves acceptable in hourly or sub-hourly building simulations.

### 2.3.4 The Fluid Flow Equations

The equations which govern the fluid flows (air and water) associated with the building are non-linear. Hence, to achieve a solution of the fluid network equation set, an iterative solution technique must be employed. Recall that the basic mass balance equation for each node in the network was

$$\sum_{j=1}^n \dot{m}_{ij} = 0.$$

Each flow associated with node  $i$  can be expressed as a function of pressure difference:

$$\dot{m}_{ij} = f(p_i, p_j) = f(\Delta p_{ij}).$$

---

<sup>8</sup> Note that the calculation leading to the determination of the heat transfer coefficient may be a complicated process e.g. where coefficient can be calculated from a highly non-linear equation. This is particularly true in the case of explicitly calculated radiative heat transfer coefficients for zones (see Clarke[2]).

The sum of mass flows at a node  $i$  can therefore be expressed as a function of all the pressure differences between it and all connected nodes:

$$\sum_{j=1}^n \dot{m} = f(\Delta p_{i,1}, \Delta p_{i,2}, \dots, \Delta p_{i,n-1}, \Delta p_{i,n}) = f_i(\Delta \mathbf{p}) = 0. \quad (2.41)$$

Expansion of the function about some known set of nodal pressures differences  $\Delta \mathbf{p}^k$  by Taylor's series gives the following expression for an unknown set of nodal pressures  $\Delta \mathbf{p}^{k+1}$ .

$$\begin{aligned} f_i(\Delta \mathbf{p}^{k+1}) = & f_i(\Delta \mathbf{p}^k) + \frac{\partial f_i(\Delta \mathbf{p}^k)}{\partial \Delta p_{i,1}} \Delta(\Delta p_{i,1}) + \frac{\partial f_i(\Delta \mathbf{p}^k)}{\partial \Delta p_{i,2}} \Delta(\Delta p_{i,2}) + \dots + \frac{\partial f_i(\Delta \mathbf{p}^k)}{\partial \Delta p_{i,n}} \Delta(\Delta p_{i,n}) + \\ & \frac{\partial^2 f_i(\Delta \mathbf{p}^k)}{\partial \Delta p_{i,1}^2} (\Delta(\Delta p_{i,1}))^2 + \frac{\partial^2 f_i(\Delta \mathbf{p}^k)}{\partial \Delta p_{i,2}^2} (\Delta(\Delta p_{i,2}))^2 + \dots + \frac{\partial^2 f_i(\Delta \mathbf{p}^k)}{\partial \Delta p_{i,n}^2} (\Delta(\Delta p_{i,n}))^2 + \dots \end{aligned} \quad (2.42)$$

Truncating terms above first order and rearranging gives

$$f_i(\Delta \mathbf{p}^{k+1}) - f_i(\Delta \mathbf{p}^k) = \left[ \frac{\partial f_i(\Delta \mathbf{p}^k)}{\partial \Delta p_{i,1}} \Delta(\Delta p_{i,1}) + \frac{\partial f_i(\Delta \mathbf{p}^k)}{\partial \Delta p_{i,2}} \Delta(\Delta p_{i,2}) + \dots + \frac{\partial f_i(\Delta \mathbf{p}^k)}{\partial \Delta p_{i,n}} \Delta(\Delta p_{i,n}) \right]. \quad (2.43)$$

Applying this equation to all  $n$  nodes, and noting that at each node  $f_i(\Delta \mathbf{p}^k)$  should be equal to zero and  $\Delta(\Delta p_{i,j}) = \Delta p_i - \Delta p_j$ , the following matrix equation emerges.

$$\begin{bmatrix} f_1(\Delta \mathbf{p}^k) \\ f_2(\Delta \mathbf{p}^k) \\ \vdots \\ f_{n-1}(\Delta \mathbf{p}^k) \\ f_n(\Delta \mathbf{p}^k) \end{bmatrix} = - \begin{bmatrix} \sum_{j=1}^m \frac{\partial f_1(\Delta \mathbf{p}^k)}{\partial \Delta p_{1,1}} & -\frac{\partial f_1(\Delta \mathbf{p}^k)}{\partial \Delta p_{1,2}} & \dots & -\frac{\partial f_1(\Delta \mathbf{p}^k)}{\partial \Delta p_{1,n-1}} & -\frac{\partial f_1(\Delta \mathbf{p}^k)}{\partial \Delta p_{1,n}} \\ -\frac{\partial f_2(\Delta \mathbf{p}^k)}{\partial \Delta p_{2,1}} & \sum_{j=1}^m \frac{\partial f_2(\Delta \mathbf{p}^k)}{\partial \Delta p_{2,2}} & \dots & -\frac{\partial f_2(\Delta \mathbf{p}^k)}{\partial \Delta p_{2,n-1}} & -\frac{\partial f_2(\Delta \mathbf{p}^k)}{\partial \Delta p_{2,n}} \\ \vdots & \vdots & \ddots & \vdots & \vdots \\ -\frac{\partial f_{n-1}(\Delta \mathbf{p}^k)}{\partial \Delta p_{n-1,1}} & -\frac{\partial f_{n-1}(\Delta \mathbf{p}^k)}{\partial \Delta p_{n-1,2}} & \dots & \sum_{j=1}^m \frac{\partial f_{n-1}(\Delta \mathbf{p}^k)}{\partial \Delta p_{n-1,n-1}} & -\frac{\partial f_{n-1}(\Delta \mathbf{p}^k)}{\partial \Delta p_{n-1,n}} \\ -\frac{\partial f_n(\Delta \mathbf{p}^k)}{\partial \Delta p_{n,1}} & -\frac{\partial f_n(\Delta \mathbf{p}^k)}{\partial \Delta p_{n,2}} & \dots & -\frac{\partial f_n(\Delta \mathbf{p}^k)}{\partial \Delta p_{n,n-1}} & \sum_{j=1}^m \frac{\partial f_n(\Delta \mathbf{p}^k)}{\partial \Delta p_{n,n}} \end{bmatrix} \times \begin{bmatrix} \Delta p_1 \\ \Delta p_2 \\ \vdots \\ \Delta p_{n-1} \\ \Delta p_n \end{bmatrix} \quad (2.44)$$

The diagonal terms of the matrix of equation 2.44 represent the rate of change of the mass balance at node  $i$  with respect to pressure. The off-diagonal terms represent the rates of change of the flows in the branches connected to node  $i$ . Equation 2.44 forms the basis for an iterative solution for the fluid flow network and can be condensed to the following form

$$\mathbf{R} = \mathbf{J}[\Delta \mathbf{P}], \quad (2.45)$$

Where  $\mathbf{J}$  is the matrix of partial derivative terms, known as the Jacobian.  $\Delta \mathbf{P}$  is the matrix of nodal pressure changes between iterations  $k$  and  $k+1$ .  $\mathbf{R}$  is the matrix of mass flow residuals at the previous calculation of nodal pressures,  $P^k$ . At each node  $i$  in the network,  $\mathbf{R}$  is given by

$$R_i = \sum_{j=1}^n m_{ij} \quad \text{and} \quad \mathbf{R} = \begin{bmatrix} R_1 \\ R_2 \\ \vdots \\ R_n \end{bmatrix},$$

as the ideal solution of equation 2.44 is reached  $\mathbf{R} \approx 0$ .

An iterative solution of the nodal pressures can be set up using the previously defined equations, where at each successive iteration,  $k+1$ , the nodal pressures are calculated from

$$\mathbf{p}^{k+1} = \mathbf{p}^k + \Delta \mathbf{p}, \quad (2.46)$$

where  $\Delta \mathbf{p}$  is found by solution of the matrix equation 2.44 using LU decomposition with pivoting (explained in more detail by Hensen [9]).

At each time step of the simulation, equation 2.44 is solved iteratively until user defined convergence criteria have been reached and  $\mathbf{R} \rightarrow 0$ . Walton [12] has refined the described solution mechanism to cope with cases of slow convergence due to oscillating pressure corrections. The implementation of the fluid flow solution technique in ESP-r is described by Clarke and Hensen [13]. Hensen [9] has extended the capabilities of the flow solver so it can also deal with the fluid flows in a plant network.

To successfully solve the fluid flow network, at least one nodal pressure must be known. This pressure acts as reference datum for the iterative solution. One method of providing these known pressures is to calculate wind-induced driving pressures at the building envelope, using climate data and the building's geometry. In a closed plant network (i.e. a hot water heating system) the boundary condition could be an arbitrary reference pressure defined by the modeller. In chapter 3 the same iterative technique will be applied in the solution of equations derived from the electrical network. Solution of building air flows with computational fluid dynamics used in conjunction with the air flow network is described by Negrao [5].

## 2.4 Simultaneous Solution

Sections 2.3.1 to 2.3.4 have demonstrated how the different control volume equation sets from the energy-related subsystems can be solved in an efficient manner: direct methods for the zonal and plant equation sets, and an iterative method for the fluid flow equations. However, as stated previously, the requirements for a whole building solution necessitate a simultaneous solution of the entire model; this entails the application of a unified solution technique incorporating all the solvers of the subsystem equation sets. The technique employed to link the various solution methods into a simultaneous solution involves a process of iterative handshaking at coupled variables. Examples of these coupled variables occur in all the equations derived in the previous sections: zonal and plant equations contain flow terms, while the some flow properties are

strongly linked to temperatures, e.g. buoyancy driven flow. The handshaking involves solving the subsystem equation sets separately, based on assumed (i.e. previous time step) values of the coupled variables and then iterating to a solution. Figure 2.10 shows the handshaking between the zonal, fluid flow and plant solutions.

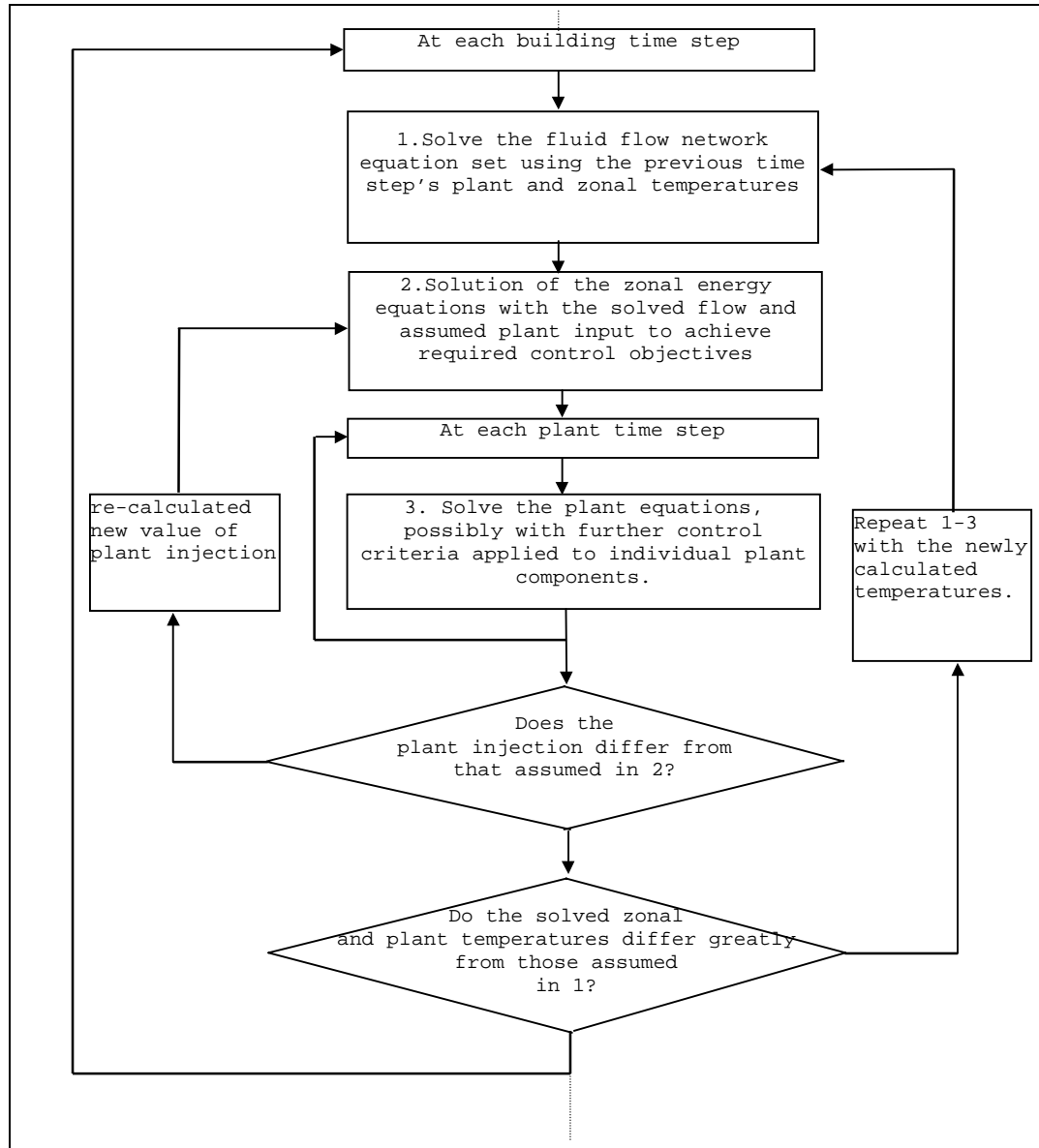


Figure 2.10 A building, plant and flow solution process as used in ESP-r (after Clarke [2])

This solution process shown above has been described by its author as modular simultaneous, and is discussed at more length in chapter 5.

#### **2.4.1 Benefits of the Modular Approach and Application to Other Subsystems**

One of the great benefits of the modular solution method is that it is extensible to other energy related subsystems such as moisture flow networks [14], integrated CFD (see section 2.2.3), and, more importantly for this project, electrical network modelling. Chapter 4 deals with how the solution method is extended to encompass electrical energy flows.

The modular approach also allows flexibility in the simulation of the building. This allows the modeller to decide on the number and combination of subsystems to use in a model. The greater the number of subsystems, the greater the detail and complexity of the model. The modeller also has a choice of focusing on one particular subsystem and modelling it in great detail, while other areas are modelled in a more simplistic fashion. However, for a true integrated approach to modelling the building, it is desirable that all the important subsystems, such as zones, plant, flow and power are included. This type of model will be shown later in the integrated models of chapter 7.

#### **2.4.2 Variable Frequency Processing**

The various equation sets for the building model represent systems with very different time constants: in the fabric of the building, temperatures change slowly over a period of hours, while in the plant system temperatures and flow change rapidly, within minutes. A feature of the modular solution process is the ability to vary the solution frequency of each equation set, enabling the solution to capture the thermal dynamics of a particular system. The zonal energy equations can be processed at hourly or sub hourly intervals, while the plant and flow equations sets can be processed at a higher frequency, to suit their much smaller time constants. The means of achieving this mixed frequency processing in ESP-r to solve the plant and flow equations  $n$  times for each building time step. The advantage of this process is that plant and flow can be rigorously simulated without adding to the computational overhead of solving the much larger

number of building equations at an unnecessarily high frequency. Variable frequency processing will be used in the simulation of the building's electrical system. This is discussed in chapter 4.

## **2.5 Example Application of the Control Volume Modelling Technique**

The following example demonstrates the use of the control volume techniques, outlined in this chapter, in the modelling of a multi-zone building with a flow and plant network. This example will be expanded in the next chapter to include the electrical network. Note that this is purely an illustrative example of how the control volume technique is applied, no attempt is made to explicitly formulate or solve the equation sets. For more exhaustive examples refer to Clarke [2].

The model consists of two thermal zones (an office and a factory area). A simple mechanical ventilation system serves the office building and also heats the incoming air, the amount of heating being controlled on the office air temperature. The building is modelled using two thermal zones, a plant and flow network as shown in figure 2.11



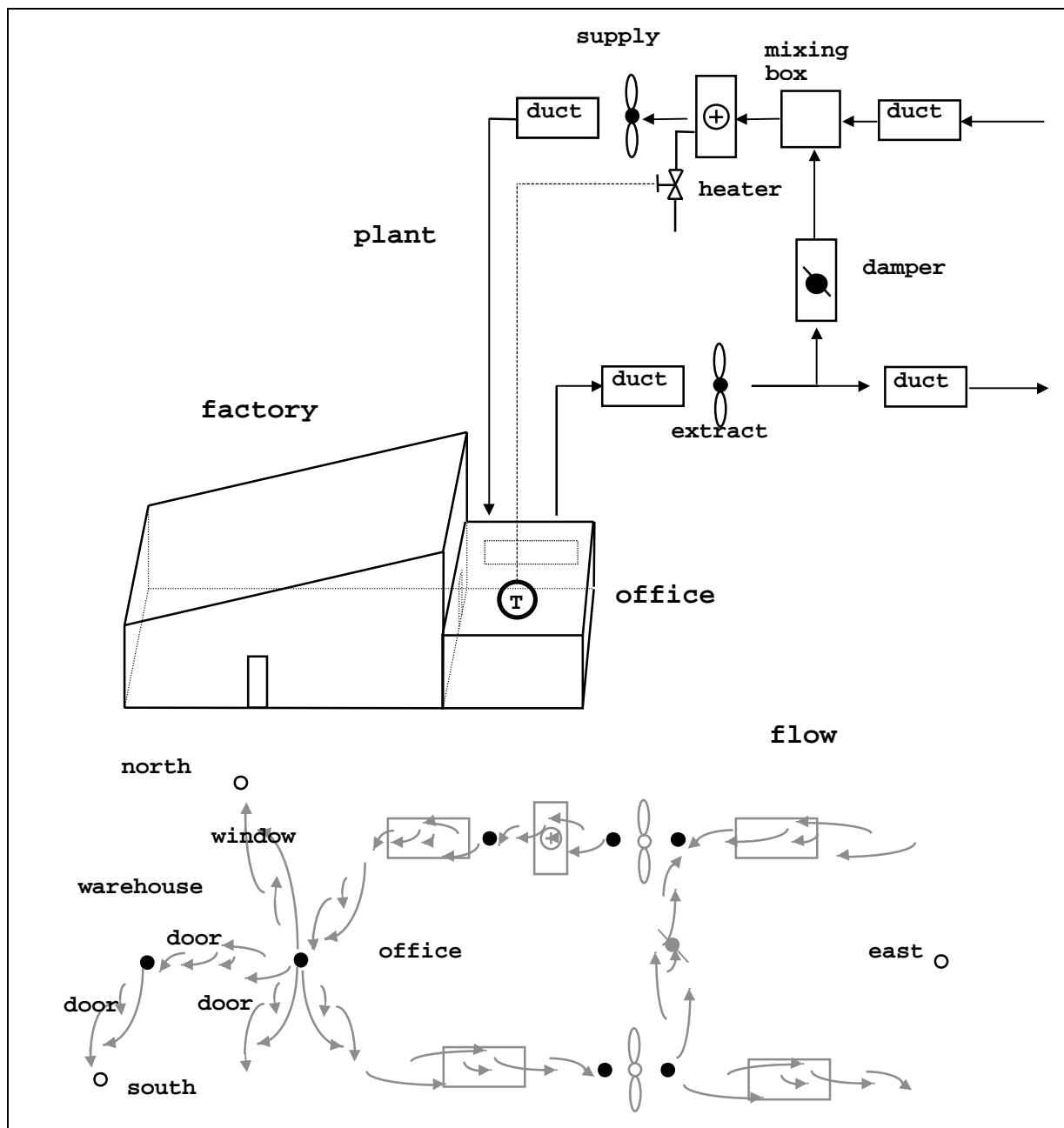


Figure 2.11 A two zone building model with an air flow and plant network.

The zones and the networks are discretised into a system of coupled control volumes. The nodal representation of the building is shown in figure 2.12.

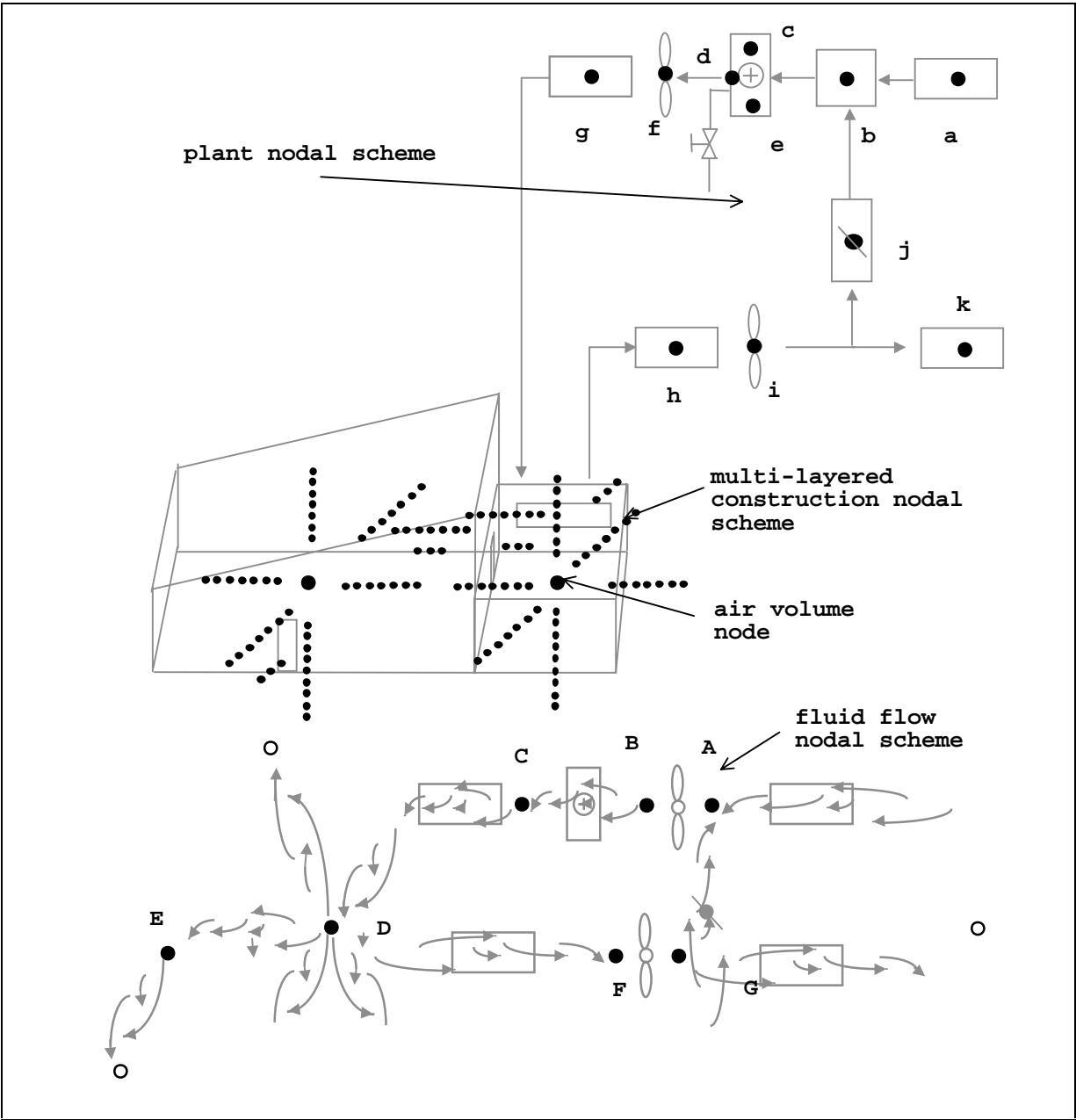


Figure 2.12 The nodal representation of the zones and associated networks.

The derived plant matrix is of the form shown below, where an x indicates a non-zero entry.

The form of the derived fluid flow matrix would be as shown over, again an x represents a non-zero term in the Jacobian matrix.

$$\begin{bmatrix}
 x & x & & & & x \\
 x & x & x & & & \\
 & x & x & x & & \\
 & & x & x & x & x \\
 & & & x & x & \\
 & & & x & & x & x \\
 x & & & & & x & x
 \end{bmatrix}
 \times
 \begin{bmatrix}
 R_A^k \\
 R_B^k \\
 \vdots \\
 \vdots \\
 \vdots \\
 R_G^k \\
 R_H^k
 \end{bmatrix}
 =
 \begin{bmatrix}
 \Delta P_A \\
 \Delta P_B \\
 \vdots \\
 \vdots \\
 \vdots \\
 \Delta P_G \\
 \Delta P_H
 \end{bmatrix}$$

Partial derivative terms
Mass flow rate residuals for each fluid flow node at iteration k

Nodal pressure correction terms

The sets of equations extracted from this model would be solved in the manner indicated in the preceding sections, with climatic and occupancy data used as the boundary conditions. Solution of the equation sets will give the transient nodal state variables (temperature and pressure) as well as the energy and fluid flows, over the simulation period.

## 2.6 Summary

This chapter has demonstrated how the concept of the control volume can be applied in the modelling of the various constituents of the building: fabric, fluid volumes, etc. Characteristic equations were derived for each volume, which were based on basic energy or mass balance equations. These were grouped according to their energy subsystem (plant, fluid flow, fabric, etc.). A modular solution technique was applied, whereby each equation set was solved simultaneously (by the an efficient method) with the other subsystem equation sets. This solution gave the transient energy and flows occurring in the building.

A major attraction of the control volume technique is that it is flexible enough to be consistently applied to all the constituents of the building model. According to Tang [7]:

*“... this technique has not only the ability to model complex boundary conditions, time-varying parameters, multi-dimensional problems, but also has the potential of applying the methods of modern control theory , leading to a higher level of modelling and development.”*

In the next chapter the flexibility of the modelling techniques outlined in this chapter will be demonstrated by their application to electrical networks.

## 2.7 References

1. Clarke J A, *Development of a prototypical component-based energy modelling system*, Final Report for Grant GR/D/26610.
2. Clarke J A, *Energy simulation in building design*, Adam Hilger, Bristol, 1985.
3. Mitchell A R, *Computational methods in partial differential equations*, Wiley, New York, 1969.
4. Cockroft J P, *Heat transfer and air flow in buildings*, PhD thesis, University of Glasgow, 1979.
5. Negrao C O R, *Conflation of Computational fluid dynamics with building energy simulation*, PhD Thesis, University of Strathclyde, Glasgow, 1995.
6. Clarke J A and Beausoleil-Morrison I, *The integration of Computational Fluid Dynamics into building simulation*, IBPSA News, Vol. 9, No. 2, Dec 1997.
7. Tang D, *Modelling of heating and air-conditioning system*, PhD Thesis, University of Strathclyde, 1985.
8. Aasem E O, *Practical simulation of buildings and air-conditioning systems in the transient domain*, PhD Thesis, University of Strathclyde, Glasgow 1993.
9. Hensen J L M, *ESPmfs, a building and plant mass flow network solver*, Collaborative FAGO/ESRU report 90.14K, 1990.
10. McLean D, *Simulation of solar energy systems*, PhD Thesis, University of Strathclyde, 1982.

11. Chow TT, Clarke J A and Dunn A, *Primitive parts: an approach to air-conditioning component modelling*, Energy and Buildings No. 26, 1997.
12. Walton G, *A computer algorithm for predicting infiltration and inter-room air flows*, ASHRAE Transactions, 1990, Part 1.
13. Clarke J A and Hensen J L M, *Implementation of a new air flow equation solver in ESP*, ESRU Technical Report, University of Strathclyde, 1988.
14. Nakhi A E, *Adaptive construction modelling within whole building dynamic simulation*, PhD Thesis, University of Strathclyde, Glasgow, 1995.

## **2.8 Bibliography**

Clarke J A, *Energy Simulation in Building Design*, Adam Hilger, Bristol, 1985.

Hensen J L M, *On the thermal interaction of building structure and heating and ventilation system*, PhD. Thesis, Eindhoven University of Technology, 1991.

## **Chapter 3 - Modelling the Electrical Network**

### **3. Introduction**

In the previous chapter the concept of modelling the building using characteristic control volumes was introduced. These were used to model the building fabric and associated networks (plant, fluid flow etc.). However, one critical constituent of the building was not included: the electrical energy subsystem. The ability to model this element of the building is vital if simulation tools are to be used in the design, evaluation and optimisation of the building-integrated energy systems outlined in chapter 1.

This chapter sets out to develop a means of modelling and simulating the electrical energy subsystem as a component of an integrated building model, which incorporates all the important energy and mass transport phenomena: heat transfer and storage in the fabric, infiltration, air and vapour flows, heat transfer and fluid flows in the plant system, heat gains from occupants and lighting, moisture migration and storage and electrical energy flows.

Addition of electrical energy flows to the building model requires that the concept of the control volume, as described in chapter 2, is extended to the modelling of the building's electrical system. As with plant, fluid and moisture flow, the power system is modelled as a network, constructed from a coupled set of electrical control volumes.

However, before describing the principles behind the modelling of the electrical system, it is important to understand its key characteristics and function.

#### **3.1 A Brief Overview of the Electrical System**

Any electrical power system has three main constituents: loads, sources and a distribution system. The loads are the end-points of the power system, consuming the electrical energy supplied by the sources, which are either local generators or points where the power system



draws energy from a larger network such as the electricity supply grid. Transmitting the electrical energy between these two are the cables, transmission lines and transformers which make up the distribution system.

Thinking in terms of a building, the main electrical loads would consist of electric heaters, lights, office equipment and the motors driving fans and pumps. Normally, a building will be powered by a connection to the local grid, which can be considered as a source of electrical energy. When considering building-integrated energy systems, the connection to the local electricity supply is augmented or replaced by the building-integrated sources of power discussed in chapter 1: façade-integrated photovoltaic arrays (PV) or small scale combined heat and power (CHP). The cabling connecting the generators, local supply and the loads make up the building's distribution system.

The loads in a power system can be considered as the points of interaction between the thermal and the electrical energy subsystems: electrical loads release heat into the building through the degradation of the high grade electrical energy, also the electrically-powered motors in fans and pumps circulate air and water throughout the building. In effect, the loads couple the thermal to the electrical systems through the conversion of electrical to thermal energy, or by assisting in the transport of thermal energy to the point of use.

In addition to interactions at the loads, the thermal and electrical energy subsystems can interact at the points of energy production, e.g. a combined heat and power unit (CHP) will supply power to the building's electrical system, while at the same time providing hot water to the building plant.

The modelling of the loads and sources that draw or provide electrical energy to this network is the subject of chapter 5. This chapter is concerned with the modelling and solution of the distribution system and its associated electrical energy flows.

### 3.2 Developing a Model of the Electrical System

Any model of a building's electrical system must incorporate the fundamental characteristics outlined in the previous paragraphs and also allow its simulation, in an integrated fashion, with the rest of the building model. Towards this end, the same modelling techniques applied in chapter 2 will be used here in the development of the electrical system model.

- The control volume principle will be extended to electrical systems, along with the development of a corresponding characteristic equation.
- The concept of linking the control volumes to form a network, introduced in chapter 2, will be used as the means of describing the electrical system.
- An equation set will be extracted from the control volumes for use in the solution of the network.
- A solution technique will be introduced, suitable for integration into the modular simultaneous solution process used by ESP-r.

#### 3.2.1 The Control Volume Applied in an Electrical Context

The fundamental basis behind all the equations derived for the control volumes of chapter 2 was the application of the laws of conservation of mass, energy and momentum. In the context of the electrical energy subsystem, only one conservation law is relevant: the conservation of electrical energy. This is achieved by the application of Kirchhoff's current law, which stipulates that the sum of phasor<sup>9</sup> currents at any point in an electrical system is always zero. The application of

---

<sup>9</sup> The concept of the phasor is explained in section 3.4.1.

this law in terms of a control volume<sup>10</sup> is shown in figure 3.1 in which a fictitious boundary is drawn around a point in an electrical system.

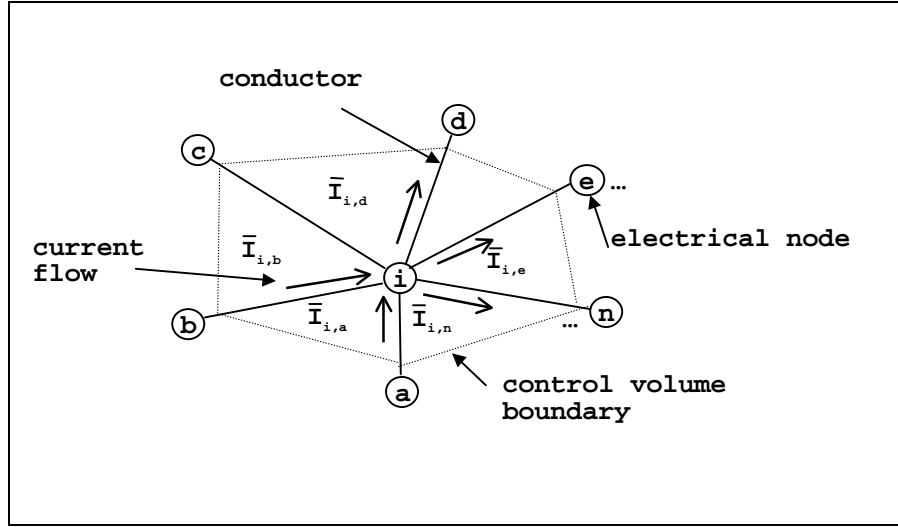


Figure 3.1 An electrical control volume.

For the control volume shown in figure 3.1 the basic balance equation is as follows

$$\sum_{j=1}^n \bar{I}_{i,j} = 0. \quad (3.1)$$

---

<sup>10</sup> This chapter's definition of the electrical control volume is intended to be as generic as possible: the control volume modelling technique can be applied to both alternating current (a.c.) and direct current (d.c.). The following examples illustrate the application to a.c. systems but section 3.4.3 details how it can be applied to d.c. systems.

$n$  is the number of current flows associated with node  $i$ .  $\bar{I}_{i,j}$  is the phasor of the current (A) flowing between the control volume node  $i$  and some other connected node  $j$ . Note that the current phasor is represented by a complex number of the form  $\bar{I} = x + iy$ : the bar above the  $I$  indicates a complex term.

Equation 3.1 can be further refined by classing each current associated with a control volume into three categories [1]:

1. the current which is transmitted to other nodes;
2. the current which is absorbed by a load connected to the node;
3. the current which is injected into the node from a connected source.

The reason for the distinction is that currents flowing to loads and from sources are assumed to be external to the network, and can therefore be regarded as boundary conditions. In order to achieve a solution for the equations derived in this section these boundary conditions must be known; this is discussed in section 3.3.1.

Equation 3.1 can therefore be re-written as

$$\sum_{a=1}^{nT} \bar{I}_{Ti,a} + \sum_{b=1}^{nG} \bar{I}_{Gi^b} - \sum_{c=1}^{nL} \bar{I}_{Li^c} = 0. \quad (3.2)$$

$\sum_{a=1}^{nT} \bar{I}_{Ti,a}$  is the sum of currents transmitted to other nodes,  $\sum_{b=1}^{nG} \bar{I}_{Gi^b}$  is the sum of currents injected into the node from a connected electrical energy source and  $-\sum_{c=1}^{nL} \bar{I}_{Li^c}$  is the sum of currents absorbed by connected loads. Current flowing from the node is arbitrarily considered as

negative; this is the same convention as used ESP-r with the thermal and fluid flow subsystems. Referring to equation 3.1, the number of transmitted, injected and absorbed currents is the same as the  $n$  currents associated with the node:  $nT + nG + nL = n$ .

Equation 3.2 is the basic balance equation, derived by the application of Kirchhoff's current law, for the electrical control volume.

### 3.2.2 Developing an Electrical Network

To illustrate the use of the electrical control volume in modelling an electrical system, consider the following example; this consists of a series of electrical loads and sources connected by a distribution system.

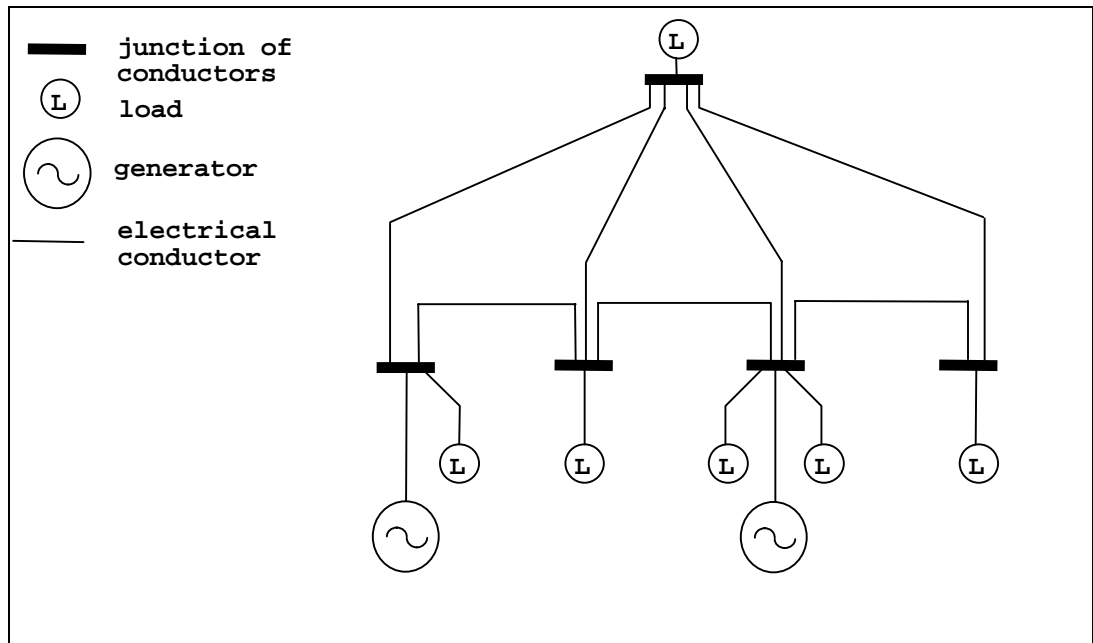


Figure 3.2 A simple electrical system.

To develop an electrical network model, electrical control volumes (represented by nodes) are placed at critical points in the system. The critical points are the junctions of the electrical conductors, as shown in figure 3.2. The connections between the nodes and loads are represented

by complex impedances ( $\Omega$ ), giving the network shown in figure 3.3. This network is an equivalent circuit representation of the power system of figure 3.2.

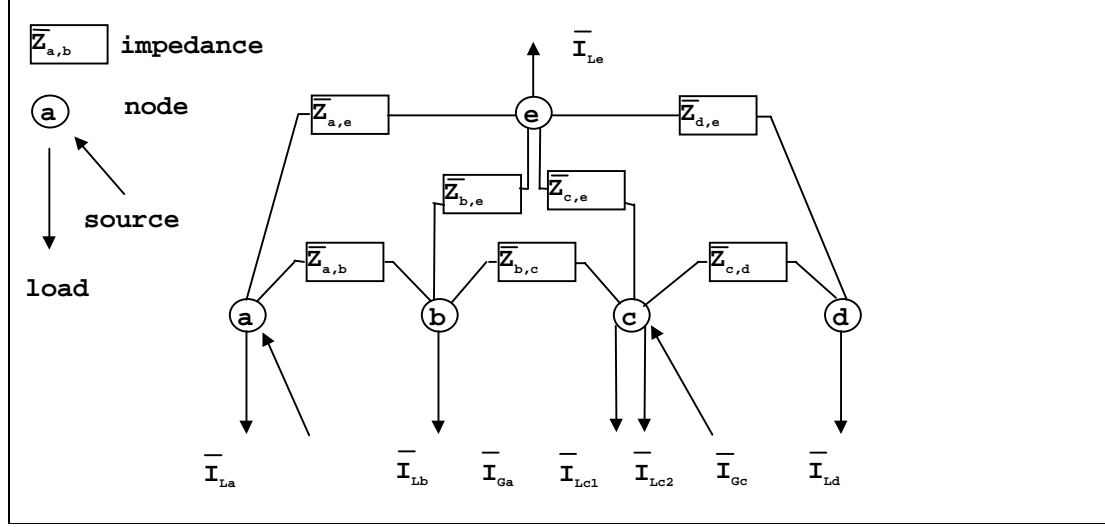


Figure 3.3 The network representation of equation of a simple power system.

If the basic current balance equation 3.2 is applied to node  $a$  in the network the following equation emerges.

$$\bar{I}_{T_{a,b}} + \bar{I}_{T_{a,e}} + \bar{I}_{G_a} - \bar{I}_{L_a} = 0. \quad (3.3)$$

Placing the boundary terms (loads and generated currents) on the right hand side gives

$$\bar{I}_{T_{a,b}} + \bar{I}_{T_{a,e}} = -\bar{I}_{G_a} + \bar{I}_{L_a}. \quad (3.4a)$$

Doing likewise for the other nodes in the network gives the following.

$$\bar{I}_{T_{b,a}} + \bar{I}_{T_{b,c}} + \bar{I}_{T_{b,e}} = \bar{I}_{L_b}; \quad (3.3b)$$

$$\bar{I}_{T_{c,b}} + \bar{I}_{T_{c,d}} + \bar{I}_{T_{c,e}} = -\bar{I}_{G_c} + \bar{I}_{L_c^1} + \bar{I}_{L_c^2} ; \quad (3.3c)$$

$$\bar{I}_{T_{d,c}} + \bar{I}_{T_{d,e}} = \bar{I}_{L_d} ; \quad (3.3d)$$

$$\bar{I}_{T_{e,a}} + \bar{I}_{T_{e,b}} + \bar{I}_{T_{e,c}} + \bar{I}_{T_{e,d}} = \bar{I}_{L_e} . \quad (3.3e)$$

### 3.2.3 Extracting the Equation Set

Equations 3.3a-e are the basic control volume current balance equations of the simple power system of figure 3.2. Like the equations derived in chapter 2, they are based on the balance of a flow variable such as heat flux, air or fluid flow. In this case the flow variable is electric current. However, to solve the derived equations it will be necessary to convert them to the form seen in all the characteristic equations of chapter 2 (e.g. equations 2.8, 2.13, 2.22 etc.). These equations contain three types of variables: driving variables (e.g. temperature or pressure), resistance or conductance (e.g. thermal resistance) and known boundary condition terms. The equations were then solved for the driving variable: in an electrical network this is the voltage.

Equations 3.3a-e already contain the boundary terms in the form of the generated and load currents. However, they will require some manipulation to introduce voltage and resistance terms. This is achieved using Ohm's law to replace the transmitted currents:

$$\bar{I}_{i,j} = \frac{\bar{V}_i - \bar{V}_j}{\bar{Z}_{i,j}} . \quad (3.5)$$

$\bar{V}_i$  and  $\bar{V}_j$  are the voltages (V) at nodes  $i$  and  $j$  respectively,  $\bar{Z}_{i,j}$  is the impedance ( $\Omega$ ) of the connection between them. The  $\bar{Z}_{i,j}$  term is derived from a small equivalent circuit model of a line, cable or transformer which connects the two points  $i$  and  $j$ . The formulation of these circuit models is described in chapter 5.

Substituting equation 3.5 into 3.4a gives an expression for the electrical energy balance at node  $a$  in terms of a driving variable (the voltage), resistance (i.e. the impedance) and the boundary variables  $\bar{I}_{G_a}$  and  $\bar{I}_{L_a}$ :

$$\frac{\bar{V}_a - \bar{V}_b}{\bar{Z}_{a,b}} + \frac{\bar{V}_a - \bar{V}_e}{\bar{Z}_{a,e}} = -\bar{I}_{G_a} + \bar{I}_{L_a}. \quad (3.6)$$

Rearranging the equation for  $\bar{V}_a$  gives

$$(\bar{Y}_{a,b} + \bar{Y}_{a,e})\bar{V}_a - \bar{Y}_{a,b}\bar{V}_b - \bar{Y}_{a,e}\bar{V}_e = -\bar{I}_{G_a} + \bar{I}_{L_a}. \quad (3.7)$$

The symbol  $\bar{Y}$  is used in place of  $1/\bar{Z}$ , where  $\bar{Y}$  is the inverse of impedance, termed the admittance ( $\Omega^{-1}$ ).

Similar equations can be derived for all the other nodes in the network:

$$-\bar{Y}_{a,b}\bar{V}_a + (\bar{Y}_{a,b} + \bar{Y}_{b,c} + \bar{Y}_{b,e})\bar{V}_b - \bar{Y}_{b,c}\bar{V}_c - \bar{Y}_{b,e}\bar{V}_e = \bar{I}_{L_b}; \quad (3.6b)$$

$$-\bar{Y}_{b,c}\bar{V}_b + (\bar{Y}_{b,c} + \bar{Y}_{c,d} + \bar{Y}_{c,e})\bar{V}_c - \bar{Y}_{c,d}\bar{V}_d - \bar{Y}_{c,e}\bar{V}_e = -\bar{I}_{G_c} + \bar{I}_{L_c^1} + \bar{I}_{L_c^2}; \quad (3.6c)$$

$$-\bar{Y}_{c,d}\bar{V}_d + (\bar{Y}_{c,d} + \bar{Y}_{d,e})\bar{V}_d - \bar{Y}_{d,e}\bar{V}_e = \bar{I}_{L_e}; \quad (3.6d)$$

$$-\bar{Y}_{a,e}\bar{V}_a - \bar{Y}_{b,e}\bar{V}_b - \bar{Y}_{c,e}\bar{V}_c - \bar{Y}_{d,e}\bar{V}_d + (\bar{Y}_{a,e} + \bar{Y}_{b,e} + \bar{Y}_{c,e} + \bar{Y}_{d,e})\bar{V}_e = \bar{I}_{L_e}. \quad (3.6e)$$

The equations are now in a form similar to those developed in chapter 2: defined in terms of a driving variable ( $\bar{V}_i$ ), conductance ( $\bar{Y}_{i,j}$ ) and boundary condition variables  $\bar{I}_G$  and  $\bar{I}_L$ .



The general form of equations 3.6a-e is

$$\left( \sum_{y=1}^z \bar{Y}_{x,y} \right) \bar{V}_x - \sum_{y=1}^z \bar{Y}_{x,y} \bar{V}_y = - \sum_{t=1}^u I_{G_x^t} + \sum_{v=1}^w \bar{I}_{L_x^v}, \quad (3.8)$$

where  $z$  is the number of nodes in the network,  $u$  is the number of coupled electrical sources and  $w$  is the number of coupled loads.

Hence, from the simple current balance associated with each electrical control volume, a set of characteristic equations have been derived in terms of voltage, impedance (admittance) and current flow. The equation set is linear and can be solved by direct methods for the set of complex nodal voltages  $\bar{\mathbf{V}}$ :

$$\bar{\mathbf{V}} = \begin{bmatrix} V_1 \\ V_2 \\ \vdots \\ V_{n-1} \\ V_n \end{bmatrix}.$$

### 3.2.4 Translation to Power Flow

While the derived set of equations offer a suitable means of determining the nodal voltages of the network shown in figure 3.2, their solution is only achievable if the boundary conditions (the electrical energy which is injected and drawn from the network) are defined in terms of current. However, in the field of energy simulation, loads are typically defined in terms of a power demand (W or VA). Similarly, the output of electrical sources would also be defined in terms of power. It is therefore more appropriate to define the electrical network boundary conditions in terms of power flow. Fortunately, the characteristic equations 3.6a-e are easily modified to enable this is explained below.

Consider again the basic control volume current balance for node  $i$  (equation 3.2):

$$\sum_{a=1}^{nT} \bar{I}_{T_{i,a}} + \sum_{b=1}^{nG} \bar{I}_{G_{i^l}} - \sum_{c=1}^{nL} \bar{I}_{L_{i^m}} = 0.$$

Now a complex (or apparent) power can be expressed in terms of voltage and current by the following equation

$$\bar{S} = \bar{V}\bar{I}', \quad (3.9)$$

where  $\bar{S}$  is the complex power (VA) and  $\bar{I}'^{11}$  is the conjugate ( $a-ib$ ) of the complex current.

Taking the conjugate of equation 3.2 and multiplying by the nodal voltage  $\bar{V}_i$  gives

$$\bar{V}_i \left( \sum_{m=1}^{nT} \bar{I}_{T_{i,a}} + \sum_{b=1}^{nG} \bar{I}_{G_{i^l}} - \sum_{c=1}^{nL} \bar{I}_{L_{i^m}} \right)' = 0, \quad (3.10)$$

which can be re-arranged to

$$\sum_{p=1}^{nT} \bar{V}_i \bar{I}'_{T_{i,p}} + \sum_{q=1}^{nG} \bar{V}_i \bar{I}'_{G_{i^q}} - \sum_{r=1}^{nL} \bar{V}_i \bar{I}'_{L_{i^r}} = 0. \quad (3.11)$$

Hence, substituting equation (3.9):

$$\sum_{p=1}^{nT} \bar{S}_{T_{i,p}} + \sum_{q=1}^{nG} \bar{S}_{G_{i^q}} - \sum_{r=1}^{nL} \bar{S}_{L_{i^r}} = 0. \quad (3.12)$$

---

<sup>11</sup> In all the following equations  $\bar{A}'$  indicates the complex conjugate of  $\bar{A}$ .

$\sum_{p=1}^{nT} \bar{S}_{Ta,b}$  is the complex power transmitted between the node  $i$  and connected nodes,  $\sum_{q=1}^{nG} \bar{S}_{Gi^q}$  is the complex power injected at node  $i$  and  $\sum_{r=1}^{nL} \bar{S}_{Li^r}$  is the complex power drawn from the node by a load.

Further, complex power can be decomposed into its real and imaginary parts such that

$$\bar{S} = P + iQ, \quad (3.13)$$

where  $P$  is the real power part (W) and  $Q$  is the imaginary power part (VAR). Splitting equation 3.12 into real and imaginary parts gives

$$\sum_{p=1}^{nT} P_{Ti,p} + \sum_{q=1}^{nG} P_{Gi^q} - \sum_{r=1}^{nL} P_{Li^r} = 0; \quad (3.14a)$$

and

$$\sum_{p=1}^{nT} Q_{Ti,p} + \sum_{q=1}^{nG} Q_{Gi^q} - \sum_{r=1}^{nL} Q_{Li^r} = 0. \quad (3.14b)$$

The subscripts have the same meaning as before.

Hence, from the current balance equation 3.2, three power balance equations have been derived: one each for complex, real and reactive power.

Returning to the network of figure 3.3, its characteristic equations can be re-written with the boundary variables expressed in terms of complex power. Consider again the current balance equation for node  $a$ ,

$$\bar{I}_{T_{a,b}} + \bar{I}_{T_{a,e}} = -\bar{I}_{G_a} + \bar{I}_{L_a}.$$

Taking its conjugate and multiplying by the nodal voltage:

$$\bar{V}_a (\bar{I}_{T_{a,b}} + \bar{I}_{T_{a,e}})' = \bar{V}_a (-\bar{I}_{G_a} + \bar{I}_{L_a})'. \quad (3.15)$$

Using Ohm's law the transmitted currents can be expressed in terms of nodal voltages and impedance (see equation 3.5).

$$\bar{V}_a \left( \frac{\bar{V}_a - \bar{V}_b}{\bar{Z}_{a,b}} + \frac{\bar{V}_a - \bar{V}_e}{\bar{Z}_{a,e}} \right)' = \bar{V}_a (-\bar{I}_{G_a} + \bar{I}_{L_a})'. \quad (3.16)$$

Writing the right-hand-side of the equation in terms of power flow and replacing the impedance terms with admittance gives

$$\bar{V}_a ((\bar{V}_a - \bar{V}_b)\bar{Y}_{a,b} + (\bar{V}_a - \bar{V}_e)\bar{Y}_{a,e})' = -\bar{S}_{G_a} + \bar{S}_{L_a}. \quad (3.17)$$

Re-arranging the equation for  $\bar{V}_a$ :

$$(\bar{V}_a' \bar{Y}_{a,b}' + \bar{V}_a' \bar{Y}_{a,e}') \bar{V}_a - (\bar{V}_b' \bar{Y}_{a,b}' + \bar{V}_e' \bar{Y}_{a,e}') \bar{V}_a = -\bar{S}_{G_a} + \bar{S}_{L_a}. \quad (3.18a)$$

This is the basic form of the power balance at node  $a$ . The left hand side of the equation represents the power transmitted to connected nodes in terms of the voltage and impedance (admittance). The right hand side of the equation contains the boundary terms expressed as complex power flows. Note that as a result of the conversion from current flow to power flow the balance equation is now non-linear and will have to be solved iteratively. This is discussed in section 3.3.

Equations of a similar form can be derived for all the other nodes in the network:

$$(\bar{V}_b'Y_{a,b}' + \bar{V}_b'Y_{b,c}' + \bar{V}_b'Y_{b,e}')\bar{V}_b - (\bar{V}_a'Y_{a,b}' + \bar{V}_c'Y_{b,c}' + \bar{V}_e'Y_{b,e}')\bar{V}_b = \bar{S}_{Lb}; \quad (3.18b)$$

$$(\bar{V}_c'Y_{b,c}' + \bar{V}_c'Y_{c,d}' + \bar{V}_c'Y_{c,e}')\bar{V}_c - (\bar{V}_b'Y_{b,c}' + \bar{V}_d'Y_{c,d}' + \bar{V}_e'Y_{c,e}')\bar{V}_c = -\bar{S}_{Gc} + \bar{S}_{Lc}^1 + \bar{S}_{Lc}^2; \quad (3.18c)$$

$$(\bar{V}_d'Y_{c,d}' + \bar{V}_d'Y_{d,e}')\bar{V}_d - (\bar{V}_c'Y_{c,d}' + \bar{V}_e'Y_{d,e}')\bar{V}_d = \bar{S}_{Ld}; \quad (3.18d)$$

$$(\bar{V}_e'Y_{a,e}' + \bar{V}_e'Y_{b,e}' + \bar{V}_e'Y_{c,e}' + \bar{V}_e'Y_{d,e}')\bar{V}_e - (\bar{V}_a'Y_{a,e}' + \bar{V}_b'Y_{b,e}' + \bar{V}_c'Y_{c,e}' + \bar{V}_d'Y_{d,e}')\bar{V}_e = \bar{S}_{Le}. \quad (3.18e)$$

The general form of the power balance equation at any node  $i$  can be written as

$$\left[ \left( \sum_{p=1}^n \bar{V}_i' \bar{Y}_{i,p}' \right) - \left( \sum_{p=1, p \neq i}^x \bar{V}_p' \bar{Y}_{i,p}' \right) \right] \bar{V}_i = - \sum_{q=1}^y \bar{S}_{G_i}^q + \sum_{r=1}^z \bar{S}_{L_i}^r, \quad (3.19)$$

where  $n$  is the number of nodes in the network,  $y$  is the number of connected sources and  $z$  is the number of connected loads.

Equation 3.19 can be simplified by adding the bracketed summation terms on the left-hand-side of the equation such that

$$\left( \sum_{p=1}^n \bar{V}_p' \bar{Y}_{i,p}' \right) \bar{V}_i = - \sum_{q=1}^y \bar{S}_{G_i}^q + \sum_{r=1}^z \bar{S}_{L_i}^r \quad (3.20)$$

where  $\bar{Y}_{i,i} = \sum_{p=1}^n \bar{Y}_{i,p}'$  and  $\bar{Y}_{i,p_{p \neq i}} = -\bar{Y}_{i,p}'$ .

$\bar{Y}_{i,i}$  is the short circuit driving port admittance of node  $i$  and  $\bar{Y}_{i,p}$  is a transfer admittance between node  $i$  and some node  $p$  [2].

Equation 3.20 is the basic power balance equation for any node in an electrical network. Notice its similarity with the fluid flow equations of section 2.3.4 in that it is a non-linear equation expressed in terms of a driving variable  $\bar{V}$ . The electrical network equation set consists of the variants of equation 3.20 derived for each node.

### 3.3 Solution of the Equation Set

As with the fluid flow equations, a Newton-Raphson iterative technique is employed, which solves for the voltages at each node. Once the nodal voltages are solved all other network unknowns (such as current and transmitted power) can be derived. The solution of the electrical network equation set, using the Newton-Raphson technique and power terms as boundary conditions, is described as a ‘load flow solution’ by Stagg and El-Abiad [2]. Gross [1] describes the same solution technique but using a compact polar notation; this is adopted in the description which follows.

The first step in the solution process requires that the general nodal equation 3.20 is split into its real and reactive parts. To achieve this, the complex variables on the left-hand side of the equation are expressed in polar form, e.g. for  $\bar{V}$  :

$$\bar{V} = V(\cos \theta + i \sin \theta), \quad (3.21a)$$

and

$$\bar{V}' = V(\cos \theta - i \sin \theta). \quad (3.21b)$$

where  $V$  is the modulus of  $\bar{V}$  and  $\theta$  is its argument. Applying De Moivre's theorem<sup>12</sup>, equation 3.20 can be decomposed into the following real and imaginary components.

$$\sum_{p=1}^n V_i V_p Y_{i,p} \cos(\theta_i - \theta_p - \alpha_{i,p}) = -\sum_{q=1}^y P_{G_i^q} + \sum_{r=1}^z P_{L_i^r}, \quad (3.22a)$$

and for the imaginary terms (dividing through by  $i$ ):

$$\sum_{p=1}^n V_i V_p Y_{i,p} \sin(\theta_i - \theta_p - \alpha_{i,p}) = -\sum_{q=1}^y Q_{G_i^q} + \sum_{r=1}^z Q_{L_i^r}. \quad (3.22b)$$

In the previous equations  $\bar{V}_i = V_i(\cos \theta_i + i \sin \theta_i)$ ,  $\bar{V}_p' = V_p(\cos \theta_p - i \sin \theta_p)$  and  $\bar{Y}_{i,p}' = Y_{i,p}(\cos \alpha_{i,p} - i \sin \alpha_{i,p})$ . Also,  $\bar{S}_{G_i} = P_{G_i} + iQ_{G_i}$ , and  $\bar{S}_{L_i} = P_{L_i} + iQ_{L_i}$ .

With equation 3.20 now split into real and reactive components each node  $i$  in an electrical network has two non-linear characteristic equations: one describing the real power balance, the other describing the reactive power balance. There are also two unknowns:  $V_i$  and  $\theta_i$ . Hence, an  $n$  node electrical network would create  $2n$  non-linear characteristic equations in  $2n$  unknowns.

The Newton-Raphson solution method used with the fluid flow network is now applied in the solution of the electrical network. Recall that the basis for the fluid flow solution was a Taylor's series expansion of a function  $f_i(x_1, x_2, \dots, x_i, \dots, x_n) = 0$  about some known set of values  $x^k$ ,

where  $x^k = (x_1, x_2, \dots, x_n)^k$ . In the case of the fluid flow equations, the function described the

---

<sup>12</sup> De Moivre's theorem (from [3]):

$$(\cos \theta_1 + i \sin \theta_1)(\cos \theta_2 + i \sin \theta_2) \dots (\cos \theta_n + i \sin \theta_n) = \cos(\theta_1 + \theta_2 + \dots + \theta_n) + i \sin(\theta_1 + \theta_2 + \dots + \theta_n)$$

flow balance equation at each node  $i$  in the network and the function unknowns were the nodal pressures differences  $\Delta p_{ij}$ . Two functions of a similar form can be derived at each node  $i$  in the electrical network; this is achieved by re-arranging equations 3.21a and 3.21b, and moving the known terms to the left-hand side as follows.

$$\sum_{p=1}^n V_i V_p Y_{s,p} \cos(\theta_i - \theta_p - \alpha_{i,p}) + \sum_{q=1}^y P_{G_i^q} - \sum_{r=1}^z P_{L_i^r} = 0 \quad (3.23a)$$

and

$$\sum_{p=1}^n V_i V_p Y_{s,p} \sin(\theta_i - \theta_p - \alpha_{i,p}) + \sum_{q=1}^y Q_{G_i^q} - \sum_{r=1}^z Q_{L_i^r} = 0. \quad (3.23b)$$

These two equations can be characterised by the functions which follow.

The real power balance:

$$f_i(V_1, V_2, \dots, V_i, \dots, V_n, \theta_1, \theta_2, \dots, \theta_i, \dots, \theta_n) = 0, \quad (3.24a)$$

and the reactive power balance equation:

$$g_i(V_1, V_2, \dots, V_i, \dots, V_n, \theta_1, \theta_2, \dots, \theta_i, \dots, \theta_n) = 0. \quad (3.24b)$$

In the following equations these functions will be abbreviated to  $f_i(V, \theta)$  and  $g_i(V, \theta)$ , where  $V = (V_1, V_2, \dots, V_n)$  and  $\theta = (\theta_1, \theta_2, \dots, \theta_n)$ . Note that the function for the fluid flow equations involved only one type of variable (the nodal pressures  $P_n$ ), while both the electrical power balance equations are functions with two types of variables:  $V_i$  and  $\theta_i$ . Taylor's series can be extended to deal with this. Consider the expansion for the function  $f_i(V, \theta)$  for an unknown set of values  $V^{k+1}$  and  $\theta^{k+1}$  about the known set of values  $V^k$  and  $\theta^k$ .



$$f_i(V^{k+1}, \theta^{k+1}) =$$

$$\begin{aligned}
& f_i(V^k, \theta^k) + \frac{\partial f_i(V^k, \theta^k)}{\partial \mathcal{V}_1} \Delta V_i + \frac{\partial f_i(V^k, \theta^k)}{\partial \mathcal{V}_2} \Delta V_i + \dots + \frac{\partial f_i(V^k, \theta^k)}{\partial \mathcal{V}_{n-1}} \Delta V_i + \frac{\partial f_i(V^k, \theta^k)}{\partial \mathcal{V}_n} \Delta V_i \\
& + \frac{\partial^2 f_i(V^k, \theta^k)}{\partial \mathcal{V}_1^2} \Delta V_i^2 + \frac{\partial^2 f_i(V^k, \theta^k)}{\partial \mathcal{V}_2^2} \Delta V_i^2 + \dots + \frac{\partial^2 f_i(V^k, \theta^k)}{\partial \mathcal{V}_{n-1}^2} \Delta V_i^2 + \frac{\partial^2 f_i(V^k, \theta^k)}{\partial \mathcal{V}_n^2} \Delta V_i^2 \\
& + \frac{\partial^3 f_i(V^k, \theta^k)}{\partial \mathcal{V}_1^3} \Delta V_i^3 + \frac{\partial^3 f_i(V^k, \theta^k)}{\partial \mathcal{V}_2^3} \Delta V_i^3 + \dots + \frac{\partial^3 f_i(V^k, \theta^k)}{\partial \mathcal{V}_{n-1}^3} \Delta V_i^3 + \frac{\partial^3 f_i(V^k, \theta^k)}{\partial \mathcal{V}_n^3} \Delta V_i^3 + \dots \\
& \vdots \\
& \dots + \frac{\partial f_i(V^k, \theta^k)}{\partial \theta_1} \Delta \theta_i + \frac{\partial f_i(V^k, \theta^k)}{\partial \theta_2} \Delta \theta_i + \dots + \frac{\partial f_i(V^k, \theta^k)}{\partial \theta_{n-1}} \Delta \theta_i + \frac{\partial f_i(V^k, \theta^k)}{\partial \theta_n} \Delta \theta_i \\
& + \frac{\partial^2 f_i(V^k, \theta^k)}{\partial \theta_1^2} \Delta \theta_i^2 + \frac{\partial^2 f_i(V^k, \theta^k)}{\partial \theta_2^2} \Delta \theta_i^2 + \dots + \frac{\partial^2 f_i(V^k, \theta^k)}{\partial \theta_{n-1}^2} \Delta \theta_i^2 + \frac{\partial^2 f_i(V^k, \theta^k)}{\partial \theta_n^2} \Delta \theta_i^2 \\
& + \frac{\partial^3 f_i(V^k, \theta^k)}{\partial \theta_1^3} \Delta \theta_i^3 + \frac{\partial^3 f_i(V^k, \theta^k)}{\partial \theta_2^3} \Delta \theta_i^3 + \dots + \frac{\partial^3 f_i(V^k, \theta^k)}{\partial \theta_{n-1}^3} \Delta \theta_i^3 + \frac{\partial^3 f_i(V^k, \theta^k)}{\partial \theta_n^3} \Delta \theta_i^3 + \dots
\end{aligned} \tag{3.25}$$

Re-arranging and truncating all terms of second order and above, the following expression emerges:

$$f_i(V^{k+1}, \theta^{k+1}) - f_i(V^k, \theta^k) =$$

$$\begin{aligned}
& \left[ \frac{\partial f_i(V^k, \theta^k)}{\partial \mathcal{V}_1} + \frac{\partial f_i(V^k, \theta^k)}{\partial \mathcal{V}_2} + \dots + \frac{\partial f_i(V^k, \theta^k)}{\partial \mathcal{V}_{n-1}} + \frac{\partial f_i(V^k, \theta^k)}{\partial \mathcal{V}_n} \right] \Delta V_i \\
& + \left[ \frac{\partial f_i(V^k, \theta^k)}{\partial \theta_1} + \frac{\partial f_i(V^k, \theta^k)}{\partial \theta_2} + \dots + \frac{\partial f_i(V^k, \theta^k)}{\partial \theta_{n-1}} + \frac{\partial f_i(V^k, \theta^k)}{\partial \theta_n} \right] \Delta \theta_i.
\end{aligned} \tag{3.26}$$

Applying the same technique to all the nodes in a network gives the following equation set for the real power flow  $f(V, \theta)$  function at each node.

$$\begin{aligned}
& f_1(V^{k+1}, \theta^{k+1}) - f_1(V^k, \theta^k) \\
&= \left[ \frac{\partial f_1(V^k, \theta^k)}{\partial V_1} + \frac{\partial f_1(V^k, \theta^k)}{\partial V_2} + \dots + \frac{\partial f_1(V^k, \theta^k)}{\partial V_{n-1}} + \frac{\partial f_1(V^k, \theta^k)}{\partial V_n} \right] \Delta V_1 \\
&+ \left[ \frac{\partial f_1(V^k, \theta^k)}{\partial \theta_1} + \frac{\partial f_1(V^k, \theta^k)}{\partial \theta_2} + \dots + \frac{\partial f_1(V^k, \theta^k)}{\partial \theta_{n-1}} + \frac{\partial f_1(V^k, \theta^k)}{\partial \theta_n} \right] \Delta \theta_1; \\
& \\
& f_2(V^{k+1}, \theta^{k+1}) - f_2(V^k, \theta^k) \\
&= \left[ \frac{\partial f_2(V^k, \theta^k)}{\partial V_1} + \frac{\partial f_2(V^k, \theta^k)}{\partial V_2} + \dots + \frac{\partial f_2(V^k, \theta^k)}{\partial V_{n-1}} + \frac{\partial f_2(V^k, \theta^k)}{\partial V_n} \right] \Delta V_2 \\
&+ \left[ \frac{\partial f_2(V^k, \theta^k)}{\partial \theta_1} + \frac{\partial f_2(V^k, \theta^k)}{\partial \theta_2} + \dots + \frac{\partial f_2(V^k, \theta^k)}{\partial \theta_{n-1}} + \frac{\partial f_2(V^k, \theta^k)}{\partial \theta_n} \right] \Delta \theta_2; \\
& \\
& \vdots \\
& \\
& f_n(V^{k+1}, \theta^{k+1}) - f_n(V^k, \theta^k) \\
&= \left[ \frac{\partial f_n(V^k, \theta^k)}{\partial V_1} + \frac{\partial f_n(V^k, \theta^k)}{\partial V_2} + \dots + \frac{\partial f_n(V^k, \theta^k)}{\partial V_{n-1}} + \frac{\partial f_n(V^k, \theta^k)}{\partial V_n} \right] \Delta V_n \\
&+ \left[ \frac{\partial f_n(V^k, \theta^k)}{\partial \theta_1} + \frac{\partial f_n(V^k, \theta^k)}{\partial \theta_2} + \dots + \frac{\partial f_n(V^k, \theta^k)}{\partial \theta_{n-1}} + \frac{\partial f_n(V^k, \theta^k)}{\partial \theta_n} \right] \Delta \theta_n.
\end{aligned}$$

An equation set of exactly the same form can be extracted for the reactive power flow function  $g(V, \theta)$ ; the general form of which, for any node  $i$  is

$$\begin{aligned}
& g_i(V^{k+1}, \theta^{k+1}) - g_i(V^k, \theta^k) \\
&= \left[ \frac{\partial g_i(V^k, \theta^k)}{\partial V_1} + \frac{\partial g_i(V^k, \theta^k)}{\partial V_2} + \dots + \frac{\partial g_i(V^k, \theta^k)}{\partial V_{n-1}} + \frac{\partial g_i(V^k, \theta^k)}{\partial V_n} \right] \Delta V_i \\
&+ \left[ \frac{\partial g_i(V^k, \theta^k)}{\partial \theta_1} + \frac{\partial g_i(V^k, \theta^k)}{\partial \theta_2} + \dots + \frac{\partial g_i(V^k, \theta^k)}{\partial \theta_{n-1}} + \frac{\partial g_i(V^k, \theta^k)}{\partial \theta_n} \right] \Delta \theta_i.
\end{aligned} \tag{3.27}$$

As with the expression for real power flow, this equation is applicable to all  $n$  nodes in a network.

Grouping the equations together in matrix form gives the following general expression for an  $n$  node network.

$$\begin{bmatrix} \Delta f_1(V^k, \theta^k) \\ \vdots \\ \Delta f_n(V^k, \theta^k) \\ \Delta g_1(V^k, \theta^k) \\ \vdots \\ \Delta g_n(V^k, \theta^k) \end{bmatrix} = \begin{bmatrix} \frac{\partial f_1(V^k, \theta^k)}{\partial V_1} & \dots & \frac{\partial f_1(V^k, \theta^k)}{\partial V_n} & \frac{\partial f_1(V^k, \theta^k)}{\partial \theta_1} & \dots & \frac{\partial f_1(V^k, \theta^k)}{\partial \theta_n} \\ \vdots & \ddots & \vdots & \vdots & \ddots & \vdots \\ \frac{\partial f_n(V^k, \theta^k)}{\partial V_1} & \dots & \frac{\partial f_n(V^k, \theta^k)}{\partial V_n} & \frac{\partial f_n(V^k, \theta^k)}{\partial \theta_1} & \dots & \frac{\partial f_n(V^k, \theta^k)}{\partial \theta_n} \\ \frac{\partial g_1(V^k, \theta^k)}{\partial V_1} & \dots & \frac{\partial g_1(V^k, \theta^k)}{\partial V_n} & \frac{\partial g_1(V^k, \theta^k)}{\partial \theta_1} & \dots & \frac{\partial g_1(V^k, \theta^k)}{\partial \theta_n} \\ \vdots & \ddots & \vdots & \vdots & \ddots & \vdots \\ \frac{\partial g_n(V^k, \theta^k)}{\partial V_1} & \dots & \frac{\partial g_n(V^k, \theta^k)}{\partial V_n} & \frac{\partial g_n(V^k, \theta^k)}{\partial \theta_1} & \dots & \frac{\partial g_n(V^k, \theta^k)}{\partial \theta_n} \end{bmatrix} \begin{bmatrix} \Delta V_1 \\ \vdots \\ \Delta V_n \\ \Delta \theta_1 \\ \vdots \\ \Delta \theta_n \end{bmatrix} \tag{3.28}$$

In equation 3.28  $\Delta f_i(V^k, \theta^k)$  represents  $\Delta f_i(V^{k+1}, \theta^{k+1}) - \Delta f_i(V^k, \theta^k)$  and likewise  $\Delta g_i(V, \theta)$  represents  $\Delta g_i(V^{k+1}, \theta^{k+1}) - \Delta g_i(V^k, \theta^k)$ . The matrix on the left-hand side of equation 3.28 can be simplified as

the solution of the equation set requires that  $f_i(V^{k+1}, \theta^{k+1}) = 0$  and  $g_i(V^{k+1}, \theta^{k+1}) = 0$  for all nodes in the system. The terms in the left-hand matrix therefore reduce to  $-\Delta f_i(V^k, \theta^k)$  and  $-\Delta g_i(V^k, \theta^k)$ .

$$\begin{bmatrix} -f_1(V^k, \theta^k) \\ \vdots \\ -f_n(V^k, \theta^k) \\ -g_1(V^k, \theta^k) \\ \vdots \\ -g_n(V^k, \theta^k) \end{bmatrix} = \begin{bmatrix} \frac{\partial f_1(V^k, \theta^k)}{\partial V_1} & \dots & \frac{\partial f_1(V^k, \theta^k)}{\partial V_n} & \frac{\partial f_1(V^k, \theta^k)}{\partial \theta_1} & \dots & \frac{\partial f_1(V^k, \theta^k)}{\partial \theta_n} \\ \vdots & \ddots & \vdots & \vdots & \ddots & \vdots \\ \frac{\partial f_n(V^k, \theta^k)}{\partial V_1} & \dots & \frac{\partial f_n(V^k, \theta^k)}{\partial V_n} & \frac{\partial f_n(V^k, \theta^k)}{\partial \theta_1} & \dots & \frac{\partial f_n(V^k, \theta^k)}{\partial \theta_n} \\ \frac{\partial g_1(V^k, \theta^k)}{\partial V_1} & \dots & \frac{\partial g_1(V^k, \theta^k)}{\partial V_n} & \frac{\partial g_1(V^k, \theta^k)}{\partial \theta_1} & \dots & \frac{\partial g_1(V^k, \theta^k)}{\partial \theta_n} \\ \vdots & \ddots & \vdots & \vdots & \ddots & \vdots \\ \frac{\partial g_n(V^k, \theta^k)}{\partial V_1} & \dots & \frac{\partial g_n(V^k, \theta^k)}{\partial V_n} & \frac{\partial g_n(V^k, \theta^k)}{\partial \theta_1} & \dots & \frac{\partial g_n(V^k, \theta^k)}{\partial \theta_n} \end{bmatrix} \begin{bmatrix} \Delta V_1 \\ \vdots \\ \Delta V_2 \\ \Delta \theta_1 \\ \vdots \\ \Delta \theta_2 \end{bmatrix} \quad (3.29)$$

Equation 3.29 can be condensed to the following form

$$\begin{bmatrix} R_p \\ R_Q \end{bmatrix} = \begin{bmatrix} J_{\partial f / \partial V} & J_{\partial f / \partial \theta} \\ J_{\partial g / \partial V} & J_{\partial g / \partial \theta} \end{bmatrix} \begin{bmatrix} \Delta V \\ \Delta \theta \end{bmatrix}. \quad (3.30)$$

$R_p$  represents the column matrix of real power residuals (equivalent to the mass flow residuals in a fluid flow simulation),  $R_Q$  represents the column matrix of reactive power residuals:

$$R_p = \begin{bmatrix} -f_1(V^k, \theta^k) \\ -f_2(V^k, \theta^k) \\ \vdots \\ -f_n(V^k, \theta^k) \end{bmatrix}, R_Q = \begin{bmatrix} -g_1(V^k, \theta^k) \\ -g_2(V^k, \theta^k) \\ \vdots \\ -g_n(V^k, \theta^k) \end{bmatrix}.$$

$\Delta V$  and  $\Delta \theta$  are column matrices representing the difference in the modulus and arguments, respectively, of the known variable set  $(V^k, \theta^k)$  and the unknown variable set  $(V^{k+1}, \theta^{k+1})$  (equivalent to the pressure correction vector in a fluid flow simulation):

$$\Delta V = \begin{bmatrix} \Delta V_1 \\ \Delta V_2 \\ \vdots \\ \Delta V_n \end{bmatrix}, \Delta \theta = \begin{bmatrix} \Delta \theta_1 \\ \Delta \theta_2 \\ \vdots \\ \Delta \theta_n \end{bmatrix}.$$

In equation 3.30 the Jacobian matrix contains four terms which represent four groups, or sub-matrices of partial derivatives present within in it:

$$J_{\frac{\partial f}{\partial V}} = \frac{\bar{\partial} f_i(V, \theta)}{\partial V}, J_{\frac{\partial f}{\partial \theta}} = \frac{\bar{\partial} f_i(V, \theta)}{\partial \theta}, J_{\frac{\partial g}{\partial V}} = \frac{\bar{\partial} g_i(V, \theta)}{\partial V}, J_{\frac{\partial g}{\partial \theta}} = \frac{\bar{\partial} g_i(V, \theta)}{\partial \theta}, i = 1, \dots, n.$$

The coefficients of these groups comprise of eight basic forms: the diagonal terms of each group

$$\frac{\bar{\partial} f_i(V, \theta)}{\partial V_i}, \frac{\bar{\partial} f_i(V, \theta)}{\partial \theta_i}, \frac{\bar{\partial} g_i(V, \theta)}{\partial V_i}, \frac{\bar{\partial} g_i(V, \theta)}{\partial \theta_i} \text{ and the off-diagonal terms}$$

$$\frac{\bar{\partial} f_i(V, \theta)}{\partial V_j}, \frac{\bar{\partial} f_i(V, \theta)}{\partial \theta_j}, \frac{\bar{\partial} g_i(V, \theta)}{\partial V_j}, \frac{\bar{\partial} g_i(V, \theta)}{\partial \theta_j} j = 1 \dots n, j \neq i. \text{ These forms are created from}$$

the partial derivatives of equation 3.23a and 3.23b calculated with a known set of nodal voltages  $\bar{V}^k$ . They are defined as follows [1].

$$\frac{\bar{\partial} f_i(V, \theta)}{\partial V_i} = V_i Y_{ii} \cos(\alpha_{ii}) + \sum_{j=1}^n V_j Y_{i,j} \cos(\theta_i - \theta_j - \alpha_{i,j}); \quad (3.31a)$$

$$\frac{\bar{\partial} f_i(V, \theta)}{\partial \theta_i} = -\sum_{j=1}^n V_i V_j Y_{i,j} \sin(\theta_i - \theta_j - \alpha_{i,j}) j \neq i \quad (3.31b)$$

$$\frac{\bar{\partial} g_i(V, \theta)}{\partial V_i} = -V_i Y_{ii} \sin(\alpha_{ii}) + \sum_{j=1}^n V_j Y_{i,j} \sin(\theta_i - \theta_j - \alpha_{i,j}); \quad (3.31c)$$

$$\frac{\partial g_i(V, \theta)}{\partial \theta_i} = \sum_{j=1}^n V_i V_j Y_{i,j} \cos(\theta_i - \theta_j - \alpha_{i,j}) j \neq i; \quad (3.31d)$$

$$\frac{\partial f_i(V, \theta)}{\partial V_j} = V_i Y_{ij} \cos(\theta_i - \theta_j - \alpha_{i,j}) j \neq i; \quad (3.31e)$$

$$\frac{\partial f_i(V, \theta)}{\partial \theta_j} = V_i V_j Y_{ij} \cos(\theta_i - \theta_j - \alpha_{i,j}) j \neq i; \quad (3.31f)$$

$$\frac{\partial g_i(V, \theta)}{\partial V_j} = V_i Y_{ij} \sin(\theta_i - \theta_j - \alpha_{i,j}) j \neq i; \quad (3.31g)$$

$$\frac{\partial f_i(V, \theta)}{\partial \theta_j} = -V_i V_j Y_{ij} \sin(\theta_i - \theta_j - \alpha_{i,j}) j \neq i; \quad (3.31h)$$

Equation 3.30 forms the basis for the iterative solution of the network characteristic equations. Solution of this equation, for the known set of nodal voltages ( $V^k, \theta^k$ ) by LU decomposition (see section 2.3.4) gives the voltage modulus and argument correction factors. These are added to the known voltages to give the voltage values for the next iteration:

$$\begin{bmatrix} V^{k+1} \\ \theta^{k+1} \end{bmatrix} = \begin{bmatrix} V^k \\ \theta^k \end{bmatrix} + \begin{bmatrix} \Delta V \\ \Delta \theta \end{bmatrix}, \quad (3.32)$$

As equation 3.32 converges on a solution for the nodal voltages, the column matrix of nodal real and reactive power flow residual terms ( $R_p^k$  and  $R_Q^k$ ) will tend towards zero. An ideal solution would give a real and reactive power balance at each node:

$$R_{p_i} = -f_i(V_1, V_2, \dots, V_n, \theta_1, \theta_2, \dots, \theta_n) = -\sum_{p=1}^n V_i V_p Y_{s,p} \cos(\theta_i - \theta_p - \alpha_{i,p}) + \sum_{q=1}^y P_{G_i^q} - \sum_{r=1}^z P_{L_i^r} = 0,$$

and

$$R_{Q_i} = -g_i(V_1, V_2, \dots, V_n, \theta_1, \theta_2, \dots, \theta_n) = -\sum_{p=1}^n V_i V_p Y_{s,p} \sin(\theta_i - \theta_p - \alpha_{i,p}) + \sum_{q=1}^y Q_{G_i^q} - \sum_{r=1}^z Q_{L_i^r} = 0.$$

Consequently, as the solution is approached, the corrections applied to the modulus and arguments of the nodal voltage corrections will also tend towards zero. An approximate solution for the electrical network voltages is obtained if the iterative process is halted when these corrections fall below some user defined convergence value (i.e.  $\Delta V_i < 0.0001 V_i^k$  and  $\Delta \theta_i < 0.0001 \theta_i^k$ ,  $i=1 \dots n$ ).

Once the approximate solutions are obtained for  $V_i$  and  $\theta_i$  at each node  $i$ , the complex nodal voltages can be obtained by substituting these values into equation 3.21a

Summarising: the solution method described here will solve the nodal voltages in an electrical network, which comprises of a coupled set of electrical control volumes. Solution of the power flows in the network requires that two non-linear balance equations are derived for each control volume; these are solved simultaneously using a Newton-Raphson iterative technique. This solution method is the same as that applied within ESP-r to the fluid flow network

It is possible to derive all the other network flow terms: transmitted current and transmitted power, using the solved voltages and the known impedance characteristics of the network. Recall that the current flowing between two control volumes,  $i$  and  $j$ , was given by equation 3.5

$$\bar{I}_{i,j} = \frac{\bar{V}_i - \bar{V}_j}{\bar{Z}_{i,j}}$$

The complex power flowing between the same two volumes is given by the application of equation 3.9:

$$\bar{S}_{i,j} = V_i (\bar{I}_{i,j})' = V_i \left( \frac{\bar{V}_i - \bar{V}_j}{\bar{Z}_{i,j}} \right)' \quad (3.33)$$

### 3.3.1 Requirements for the Network Solution

The basic power balance equations for an the electrical control volumes (3.23a and 3.23b) contain terms relating to the complex nodal voltage, the impedance characteristics of the connections between the nodes and also to the power injected into and drawn from the node by loads and sources respectively. Solution of the equation set dictates that, with  $2n$  network equations, there can be a maximum of  $2n$  unknowns. The previous section showed how the network can be solved with the complex voltage argument  $V$ , and modulus  $\theta$ , as the unknowns. It therefore follows that the other variables in the power flow equations: the impedance characteristics of the network connections and the power drawn from and injected into each node, must be known quantities.

The impedance characteristics of the network are in fact those of the components that connect the various control volumes together. In a typical building these components would be the lines, cables and transformers that make up the distribution system; the modelling of these network constituents, and the derivation of their impedance characteristics is dealt with in chapter 5.

The real and reactive power flow boundary conditions (the power drawn from and injected into each node in the network) are the major linkage points between the thermal model, described in chapter 2, and the electrical network model. It is the task of the thermal element of the building model to provide this power flow information (e.g. electric lighting loads, fan and pump power consumption, electric heating loads, photovoltaic array output, etc.). In order for the building model to provide this array of information a process of integration and model development must be undertaken; this is described in chapters 4 and 5 respectively.

The final pre-requisite for solution of the electrical network is that at least one of the nodal voltages in the network is known: this value acts as a reference for the iterative solution. If no



nodal voltage were known, then an infinite number of network voltage states would satisfy the requirements of a network solution. This situation happens because the nodal power flows are driven by a voltage difference. Hence, as long as the nodal voltage differences are the same, any number of permutations of nodal voltage values would satisfy the requirements for real and reactive power balance at each node. The use of a known value ensures that only one set of nodal voltages gives the correct solution. The known value in the network is usually taken as the point where the main power source connects to the network. That power source can either be a generator or the connection to the local supply grid. The node connected to the power source will then take the voltage of the supplying generator or the connected grid. Note that the known voltage value need not be constant, but can change throughout the simulation (but not during the iterative solution). This opens up the possibility for voltage time series data (i.e. real grid voltage data) to be used as a boundary condition for the network solution.

The starting point for the iterative solution process is some initial set of voltages  $\bar{\mathbf{V}}^k$ . These can be provided through a guess, or more conveniently, the set of voltages from a previously solved system state, which in the context of a building simulation can be the network voltages that were calculated at the previous time step.

### 3.4 Application to Typical Building Electrical Systems

The previous sections have detailed a generic means of describing and solving an electrical system. However, to be useful, this solution method must be flexible enough to be applied to the types of systems found in buildings, these are: three-phase a.c., single-phase a.c. and d.c. systems. The network approach to modelling the electrical system relies on it being modelled as an equivalent circuit, with the circuit state variables described as phasor quantities. Hence, to model any particular electrical system it is necessary to represent it in that particular form. How this is done for the three system types mentioned above is outlined in the following sections.

### 3.4.1 Alternating Current and Phasor System Variables

The most common type of power system found in buildings involve alternating current (a.c.), where both the supplied current and voltage vary sinusoidally with time, with an angular frequency of  $\omega$  radians per second. Under normal operating conditions the frequency is steady and these two quantities can be characterised by the general equation:

$$a(t) = A \cos(\omega t + \varphi) \quad (3.34)$$

Where  $a(t)$  is the sinusoidally varying quantity,  $A$  is its amplitude,  $\omega$  is its angular frequency (radians/s) and  $\varphi$  is the phase angle (radians) in relation to the time domain.

Real and reactive power, which are both derived from voltage and current terms, must therefore also vary sinusoidally. So, for the a.c. power system, all the voltage and power-related quantities used in the various balance equations of sections 3.2.2-3.2.4 can be characterised by this type of function. However, the method of solution outlined in the previous section described the system state variables as phasor quantities. This was done because at solution frequencies of considerably longer than the time period of the sinusoidal oscillation ( $\approx 0.02$ s) the sub-second fluctuations of voltage and current become unimportant. The solution frequency in energy simulations usually ranges from hourly to sub-minutely calculations. Hence, in this case it is acceptable to use the phasor value for the electrical system state variables: a phasor being an entity that captures the time-averaged characteristics of a sinusoidally varying function and is derived as follows.

Equation 3.34 can be re-written in the form:

$$a(t) = A(\text{Re}[\cos(\omega t + \varphi) + i \sin(\omega t + \varphi)]) .$$

Applying De Moivre's theorem and separating the time varying components gives

$$a(t) = A(\text{Re}[(\cos \omega t + i \sin \omega t)(\cos \varphi + i \sin \varphi)]) . \quad (3.35)$$

If  $a(t)$  is analysed at a period longer than  $2\pi/\omega$  (the time period of the sinusoidal oscillation) then the phasor value  $\bar{A}$  is a more appropriate measure of the oscillating quantity. This requires that the time varying component of  $a(t)$  is replaced with its root mean squared (r.m.s.) value (from [4]):

$$\left[ A \int_{t=0}^{t=T} \frac{\text{Re}[\cos \omega t + i \sin \omega t]^2}{T} dt \right]^{1/2} = \frac{A}{\sqrt{2}}. \quad (3.36)$$

The phasor value is defined as:

$$\bar{A} = \frac{A}{\sqrt{2}} (\cos \varphi + i \sin \varphi) = A(\cos \varphi + i \sin \varphi). \quad (3.37)$$

The phasor contains the vital information of the sinusoidal function: the magnitude and the relation to the time domain (the phase angle). Provided the system frequency is known, the original sinusoidal function can be reconstructed from the phasor value:

$$a(t) = \sqrt{2} \text{Re}[(\bar{A})(\cos \omega t + i \sin \omega t)]. \quad (3.38)$$

However, this reverse transformation is not required for the purposes of an energy simulation as the phasor quantity contains all the information necessary for the calculation of the system power flows.

### 3.4.2 Three Phase and Single Phase a.c. Systems

The power supplied to buildings is normally provided by three separate conductors, which supply three separate phases of power. A fourth, grounded conductor, the neutral, acts as a return path for the three-phase currents and as the reference for the other conductor voltages. Note that in the analysis that follows the neutral conductor is not considered, the reasons for this are explained in chapter 5, when the component models of the conductors (the connections between the control volumes) are derived.

In the three conductors, the phase of power is determined by the relationship between the sinusoidal variation of the voltage and current with the time domain; this is represented by the phase angle  $\varphi$ . In three-phase systems the sinusoidal variations of both current and voltage between each conductor are separated by  $2\pi/3$  radians, or  $120^\circ$ ; the phasor representations of these voltages and currents are as follows.

Conductor 1:

$$\bar{V}_1 = V_1 (\cos \alpha_1 + i \sin \alpha_1); \quad (3.39a)$$

$$\bar{I}_1 = I_1 (\cos \beta_1 + i \sin \beta_1); \quad (3.39b)$$

conductor 2:

$$\bar{V}_2 = V_2 (\cos(\alpha_2 + 3\pi / 2) + i \sin(\alpha_2 + 3\pi / 2)); \quad (3.40a)$$

$$\bar{I}_2 = I_2 (\cos(\beta_2 + 3\pi / 2) + i \sin(\beta_2 + 3\pi / 2)); \quad (3.40b)$$

finally, for conductor 3:

$$\bar{V}_3 = V_3 (\cos(\alpha_3 - 3\pi / 2) + i \sin(\alpha_3 - 3\pi / 2)); \quad (3.41a)$$

$$\bar{I}_3 = I_3 (\cos(\beta_3 - 3\pi / 2) + i \sin(\beta_3 - 3\pi / 2)). \quad (3.41b)$$

The three-phase power flow is given by

$$\begin{aligned}
\bar{S}_{3-ph} &= \bar{V}_1 \bar{I}'_1 + \bar{V}_2 \bar{I}'_2 + \bar{V}_3 \bar{I}'_3 \\
&= V_1 I_1 (\cos \alpha_1 + i \sin \alpha_1) (\cos \beta_1 - i \sin \beta_1) \\
&\quad + V_2 I_2 (\cos(\alpha_2 + 3\pi/2) + i \sin(\alpha_2 + 3\pi/2)) (\cos(\beta_2 + 3\pi/2) - i \sin(\beta_2 + 3\pi/2)) \\
&\quad + V_3 I_3 (\cos(\alpha_3 - 3\pi/2) + i \sin(\alpha_3 - 3\pi/2)) (\cos(\beta_3 - 3\pi/2) - i \sin(\beta_3 - 3\pi/2)).
\end{aligned} \tag{3.42}$$

Applying de Moivre's theorem gives

$$\begin{aligned}
\bar{S}_{3-ph} &= V_1 I_1 [\cos(\alpha_1 - \beta_1) + i \sin(\alpha_1 - \beta_1)] \\
&\quad + V_2 I_2 [\cos(\alpha_2 - \beta_2) + i \sin(\alpha_2 - \beta_2)] \\
&\quad + V_3 I_3 [\cos(\alpha_3 - \beta_3) + i \sin(\alpha_3 - \beta_3)].
\end{aligned} \tag{3.43}$$

Note that the three-phase power is a function of the voltage and current magnitudes and the phase angle between them. The  $3\pi/2$  phase differences disappear from the expression.

### 3.4.2.1 A Comprehensive Three-phase Analysis

The most direct means of analysis of a three-phase system involves the explicit representation of each in a comprehensive network model. This task is made easier by the fact that three-phase distribution systems are generally symmetrical, with each point in the network linked by three-phase conductors, or three, separate single phase conductors. Note, three-phase conductors are individual conductors which share a common path (e.g. encapsulated in a single cable) and share a common neutral. The close proximity of the phase conductors creates electromagnetic (mutual) couplings between them, this is explored further in chapter 5, and complicates the analysis of the three-phase system. Separate single-phase conductors are generally not mutually coupled. Both the three-phase and single-phase conductors are shown in figure 3.4. It should be noted that the mutual couplings are the only interactions between the phases, which are essentially three separate, symmetrical, circuits.

Given the inherent symmetry of the three-phase system, and the need to treat the power flows in each phase independently, it is convenient to adapt the nodal schema to suit the nature of the network. Recall that in the previous analyses a node was placed at each point in the system, this can be extended to the three-phase case by placing a three-node array at each point of interest in the system (e.g. conductor junctions), where each node relates to a phase. Considering a point  $i$  in a network, the corresponding three-node array would be  $i_1$ ,  $i_2$  and  $i_3$ ; the subscript denotes the phase of the node. Given the fact that each phase is a separate circuit, a node can only connect to another node in the network if it shares the same subscript (i.e. phase) and consequently, the subscript notation must remain consistent throughout the network. This is shown in figure 3.4.

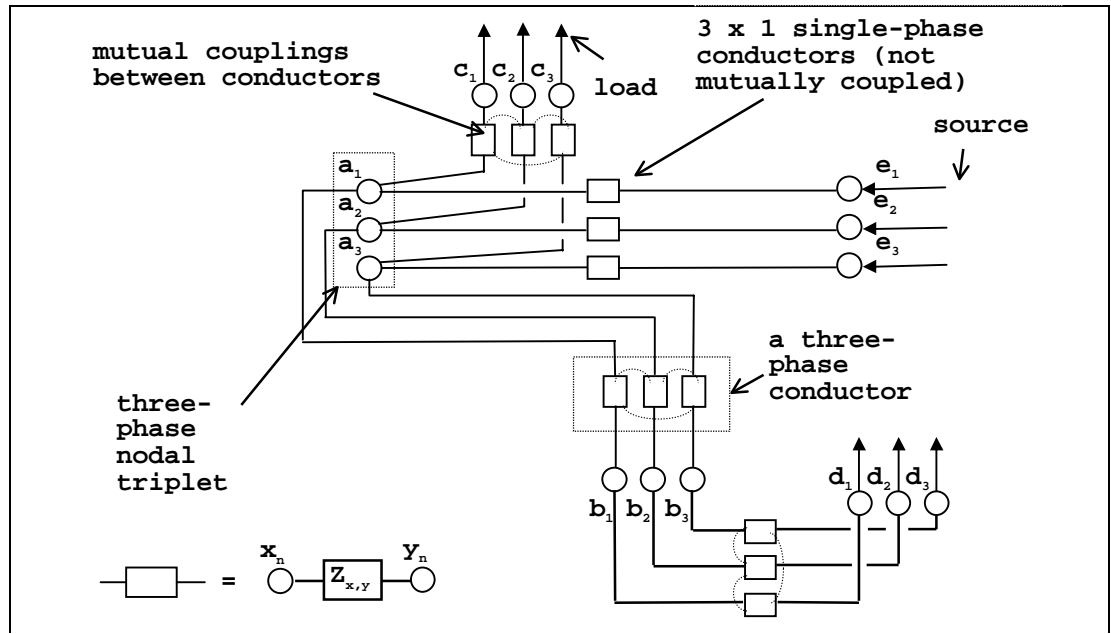


Figure 3.4 A comprehensive three-phase network model.

All the equations derived previously can be applied in the analysis of the comprehensive three-phase network. However, each point will have six energy balance equations (two for each node); it is therefore convenient to express these equations in matrix form. Consider the characteristic energy balances derived previously: in a comprehensive three-phase network their form would be as follows.

$$\sum_{p=1}^n \left[ V_i V_p Y_{i,p} \cos(\theta_i - \theta_p - \alpha_{i,p}) \right]^{23} + \sum_{q=1}^y P_{G_i^q}^{123} - \sum_{r=1}^z P_{L_i^r}^{123} = 0, \quad (3.44a)$$

where  $n$  is the number of three-phase conductors connected to node  $i$ ,  $y$  is the number of connected sources and  $z$  is the number of connected loads.

$$P_{L_i^r}^{123} = \begin{bmatrix} P_{L_{i_1}^r} \\ P_{L_{i_2}^r} \\ P_{L_{i_3}^r} \end{bmatrix} \text{ and } P_{G_i^q}^{123} = \begin{bmatrix} P_{G_{i_1}^q} \\ P_{G_{i_2}^q} \\ P_{G_{i_3}^q} \end{bmatrix}.$$

The bracketed elements of equation 3.44a can be split into two groups: those in which  $i = p$  and those in which  $i \neq p$ . These are defined as follows.

$$\left[ V_i V_p Y_{i,p} \cos(\theta_i - \theta_p - \alpha_{i,p}) \right]^{23} = \begin{bmatrix} V_{i_1} V_{p_1} Y_{i_1,p_1} \cos(\phi_{i_1,p_1}) & 0 & 0 \\ 0 & V_{i_2} V_{p_2} Y_{i_2,p_2} \cos(\phi_{i_2,p_2}) & 0 \\ 0 & 0 & V_{i_3} V_{p_3} Y_{i_3,p_3} \cos(\phi_{i_3,p_3}) \end{bmatrix} p = i, \quad (3.44b)$$

where  $\phi_{i_n,p_n} = \theta_{i_n} - \theta_{p_n} - \alpha_{i_n,p_n}$ ;

and

$$\left[ V_i V_p Y_{i,p} \cos(\theta_i - \theta_p - \alpha_{i,p}) \right]^{23} = \begin{bmatrix} V_{i_1} V_{p_1} Y_{i_1,p_1} \cos(\phi_{i_1,p_1}) & 0 & 0 \\ 0 & V_{i_2} V_{p_2} Y_{i_2,p_2} \cos(\phi_{i_2,p_2}) & 0 \\ 0 & 0 & V_{i_3} V_{p_3} Y_{i_3,p_3} \cos(\phi_{i_3,p_3}) \end{bmatrix} p \neq i. \quad (3.44c)$$

When a three-phase conductor connects the points  $i$  and  $p$ , whose conductors are mutually coupled, the elements of the bracketed term of equation 3.44a change to the following.

$$\left[ V_i V_p Y_{i,p} \cos(\theta_i - \theta_p - \alpha_{i,p}) \right]^{23} =$$

$$\begin{bmatrix} V_{i_1} V_{p_1} Y_{i_1,p_1} \cos(\phi_{i_1,p_1}) & V_{i_1} V_{p_2} Y_{m_{12i,p}} \cos(\phi_{i_2,p_2,m_{12i,p}}) & V_{i_1} V_{p_3} Y_{m_{13i,p}} \cos(\phi_{i_3,p_3,m_{13i,p}}) \\ V_{i_2} V_{p_2} Y_{m_{21i,p}} \cos(\phi_{i_1,p_1,m_{21i,p}}) & V_{i_2} V_{p_2} Y_{i_2,p_2} \cos(\phi_{i_2,p_2}) & V_{i_2} V_{p_3} Y_{m_{23i,p}} \cos(\phi_{i_3,p_3,m_{23i,p}}) \\ V_{i_3} V_{p_3} Y_{m_{31i,p}} \cos(\phi_{i_1,p_1,m_{31i,p}}) & V_{i_3} V_{p_3} Y_{m_{32i,p}} \cos(\phi_{i_2,p_2,m_{32i,p}}) & V_{i_3} V_{p_3} Y_{i_3,p_3} \cos(\phi_{i_3,p_3}) \end{bmatrix}$$

$p = i.$

(3.44d)

Where  $\phi_{i_n,p_n,m_{i_n,p_n}} = \theta_{i_n} - \theta_{p_n} - \alpha_{i_n,p_n}$  and  $Y_{m_{xya,b}}$  is the mutual coupling between phases  $x$  and  $y$  of the conductors linking points  $a$  and  $b$ . Note how the effect of the mutual couplings is to introduce off-diagonal terms into the matrix, which act to couple together the equation set of the three-node array.

The elements where  $p \neq i$  are given by

$$\left[ V_i V_p' Y_{i,p} \cos(\theta_i - \theta_p - \alpha_{i,p}) \right]^{23} =$$

$$\begin{bmatrix} V_{i_1} V_{p_1} Y_{i_1,p_1} \cos(\phi_{i_1,p_1}) & V_{i_1} V_{p_2} Y_{m_{12i,p}} \cos(\phi_{i_2,p_2,m_{12i,p}}) & V_{i_1} V_{p_3} Y_{m_{13i,p}} \cos(\phi_{i_3,p_3,m_{13i,p}}) \\ V_{i_2} V_{p_2} Y_{m_{21i,p}} \cos(\phi_{i_1,p_1,m_{21i,p}}) & V_{i_2} V_{p_2} Y_{i_2,p_2} \cos(\phi_{i_2,p_2}) & V_{i_2} V_{p_3} Y_{m_{23i,p}} \cos(\phi_{i_3,p_3,m_{23i,p}}) \\ V_{i_3} V_{p_3} Y_{m_{31i,p}} \cos(\phi_{i_1,p_1,m_{31i,p}}) & V_{i_3} V_{p_3} Y_{m_{32i,p}} \cos(\phi_{i_2,p_2,m_{32i,p}}) & V_{i_3} V_{p_3} Y_{i_3,p_3} \cos(\phi_{i_3,p_3}) \end{bmatrix} \quad (3.44e)$$

$p \neq i.$

In all the preceding equations  $Y_{i_n,i_n} = \sum_{j=1}^n Y_{i_n,j_n}$  and  $Y_{i_n,i_n} = -Y_{i_n,j_n}$ . Similarly

$$Y_{m_{xyi,i}} = \sum_{j=1}^n Y_{m_{xyi,j}} \text{ and } Y_{m_{xyi,i}} = -Y_{m_{xyi,j}}.$$



Expressions for both the admittance terms of the form  $(Y_{a_n, b_n})$  and mutual admittance terms  $(Y_{m_{xya,b}})$  are given in chapter 5, when the three-phase conductor is discussed.

The equation set for the three-node array's reactive power balance is of a similar form:

$$\sum_{p=1}^n [V_i V_p Y_{i,p} \sin(\theta_i - \theta_p - \alpha_{i,p})]^{123} + \sum_{q=1}^y Q_{G_i^q}^{123} - \sum_{r=1}^z Q_{L_i^r}^{123} = 0 \quad (3.44f)$$

The overall iterative equation for the solution of the three-phase equation set would be derived in exactly the same way as described previously, though reflecting the triplicate nature of the three-phase network model, this is shown over.

95

### 3.4.2.2 The Per-Phase Approach

Fortunately, the nature of three-phase systems often makes the complication of a comprehensive model unnecessary as, in many cases, they operate in a balanced state. In this state the currents, voltages and impedances in the each phase are of equal magnitudes, while the phase angle ( $\alpha - \beta$ ) between voltage and current is the same in all three phases. In balanced conditions equation 3.43 can be re-written as

$$\bar{S}_{3-ph} = 3VI[\cos(\alpha - \beta) + i \sin(\alpha - \beta)], \quad (3.45)$$

where  $VI = V_1I_1 = V_2I_2 = V_3I_3$  and  $(\alpha - \beta) = (\alpha_1 - \beta_1) = (\alpha_2 - \beta_2) = (\alpha_3 - \beta_3)$ .

Equation 3.45 gives an important result: in a balanced state, the equations for power flow in each phase are identical. It is therefore possible to solve for only one phase of the system and apply the results to the other two, i.e. only one node needs to be used at each point of interest.

Equations 3.23a and 3.23b could therefore be used to characterise the energy balance at each node. The balanced power flow boundary conditions can be scaled from three to the single phase using a simple division by 3. As only one equivalent circuit of the balanced system is required, the complexity of the network is greatly reduced. This means of analysis is termed ‘per-phase analysis’.

However, where the three-phase system is not balanced, e.g. where one phase is heavily loaded, the need for a comprehensive model is unavoidable.

### 3.4.2.3 Single Phase Systems

Smaller buildings will usually draw power from only one phase of a power supply, where the power is supplied by only one conductor. In this case, as with the per-phase case, only one node needs to be used at each point of interest in the system, and equations 3.23a and 3.23b would characterise the energy balance at each node.

### 3.4.2.4 Mixed Systems

One final type of system which may be analysed is a mixed system: where small single phase sub-networks draw power from a core three-phase network as shown in figure 3.5. The means of analysing this type of network is to deploy three-node arrays in the core three-phase system and single nodes in the single-phase areas of the network. It is useful to maintain the subscript notation in the single-phase areas of the network, as this indicates from which of the phases the single-phase conductors draw their power. Equations 3.23a and 3.23b would characterise the power balances at the single-phase nodes of the network, while equations 3.44a and 3.44b would be used to characterise the equation sets for the three-node arrays of the three-phase system.

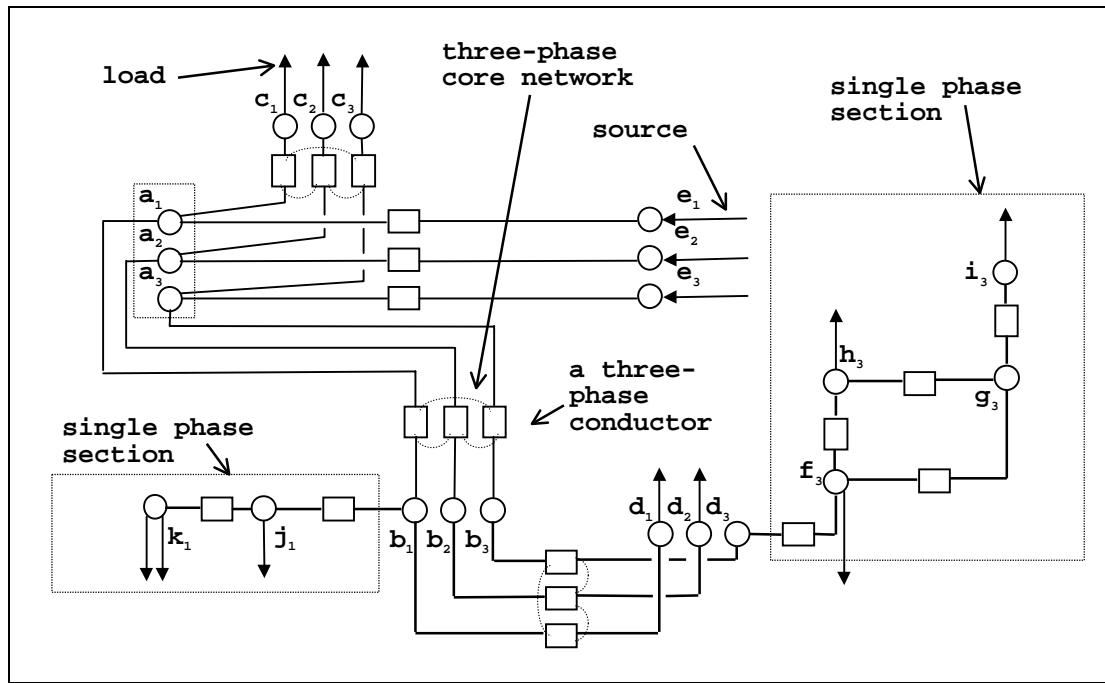


Figure 3.5 A mixed network.

### 3.4.2.5 Per-Unit Analysis

One final technique used in the analysis of a.c. systems is the conversion of the system phasors to per-unit quantities (described in [1]). This is done purely as a convenience and, as will be seen in chapter 5, simplifies the modelling of the power system when transformers are included in the

network. The basis of conversion to per-unit is to choose two base magnitudes of system state variables: usually voltage  $V$  and apparent power  $S$ . Division of these state variables by the corresponding base value will give the per unit quantity. The base value for voltage is chosen so that the resulting per unit value is close to unity. So for a 220V power system, the base value chosen would be 220. At any particular node, where the voltage is  $\bar{V} = V(\cos \theta + i \sin \theta)$ , the per unit voltage is given by

$$\bar{V}_{p.u.} = \frac{V}{V_{base}}(\cos \theta + i \sin \theta). \quad (3.46)$$

The per-unit base values for impedance, admittance, real and reactive power can be easily derived from the two original base values. Note that the per-unit parameters behave in exactly the same way as the originals. Hence all basic circuit theories and equations also hold for per unit parameters.

The other per unit values which are used with the power system are derived as follows.

$$I_{base} = \frac{S_{base}}{V_{base}}, \quad (3.47)$$

$$Z_{base} = \frac{V_{base}}{I_{base}}, \quad (3.48)$$

$$Y_{base} = \frac{1}{Z_{base}}. \quad (3.49)$$

### 3.4.3 d.c. Systems

The key difference between a.c. and d.c. systems is that the circuit state variables do not vary sinusoidally. Hence, it is not necessary to translate the state variables to phasor form; they can be represented by time averaged, real number values. Also not required in the d.c. circuit analysis are any properties relating to reactive power flow. Hence all the imaginary components of the

state variables can be dispensed with. Considering the basic power balance equations 3.23a and 3.23b applied in a d.c. system analysis. Equation 3.23b is not relevant and equation 3.23a can be written as

$$\sum_{p=1}^n V_i V_p C_{i,p} + \sum_{q=1}^y P_{G_i^q} - \sum_{r=1}^z P_{L_i^r} = 0. \quad (3.50)$$

$V_i$  represents a d.c. voltage at some node  $i$  in the system, while  $V_p$  is the d.c. voltage of the connected node  $p$ .  $C_{i,p}$  is a conductance between nodes  $i$  and  $p$  ( $\Omega^{-1}$ ): the conductance is the inverse of this connection's resistance ( $\Omega$ ). The conductance terms of equation 3.50 are constructed in the same way as the admittance terms of equations 3.23a and 3.23b:

$$C_{i,i} = \sum_{p=1}^x C_{i,p} \text{ and } C_{i,p} = -C_{i,p}. \quad (3.51)$$

Finally,  $P_G$  is a real power flow injected into the node from a source, while  $P_L$  is a real power flow drawn from the node by a load. Note that all the variables of the non-linear equations are now real numbers.

Turning to the solution of the d.c. power flow network, the problem has now reduced from  $2n$  equations in  $2n$  unknowns, for the a.c. case, to  $n$  equations of type  $f(V_1, V_2, \dots, V_n)$  in  $n$  unknowns. The unknowns are the d.c. voltage at each node. Hence, for a system of  $n$  nodes, the following set of equations would emerge.

$$f_1(V_1, V_2, \dots, V_n)$$

$$f_2(V_1, V_2, \dots, V_n)$$

$$\vdots$$

$$f_n(V_1, V_2, \dots, V_n)$$

Application of Taylor's series about a known set of network d.c. voltages  $V^k$ , as was done in the a.c. solution, would eventually lead to the following equation:

$$\begin{bmatrix} -f_1(V)^k \\ -f_2(V)^k \\ \vdots \\ -f_n(V)^k \end{bmatrix} = \begin{bmatrix} \frac{\partial f_1(V)^k}{\partial V_1} & \dots & \frac{\partial f_1(V)^k}{\partial V_n} \\ \vdots & \ddots & \vdots \\ \frac{\partial f_n(V)^k}{\partial V_1} & \dots & \frac{\partial f_n(V)^k}{\partial V_n} \end{bmatrix} \begin{bmatrix} \Delta V_1 \\ \Delta V_2 \\ \vdots \\ \Delta V_n \end{bmatrix}. \quad (3.52)$$

Equation 3.52 can be re-written as

$$[R_p^k] = \left[ J_{\frac{\partial}{\partial V}} \right] [\Delta V]. \quad (3.53)$$

$R_p^k$  represents a column matrix of real power residuals; these are determined from the application of equation 3.23a at each node in the network.  $J_{\frac{\partial}{\partial V}}$  is the matrix of partial differentials, while  $\Delta V$

are the corrections to apply to the d.c. voltage at each node to obtain the value at iteration  $k+1$ ; these are obtained by solution of equation 3.52 LU decomposition.

The voltages for the next iteration of the d.c. network solution are therefore given by

$$[V^{k+1}] = [V^k] + [\Delta V]. \quad (3.54)$$

The same requirements for a solution apply to the d.c. network as applied to the a.c. case: all power flow boundary conditions must be known along with at least one nodal voltage.

### **3.5 Application of the Technique to an Exemplar**

The techniques outlined in this chapter for the modelling and solution of electrical systems will now be applied to the simple exemplar introduced in chapter 2, through the addition of a simple electrical system to the building model.



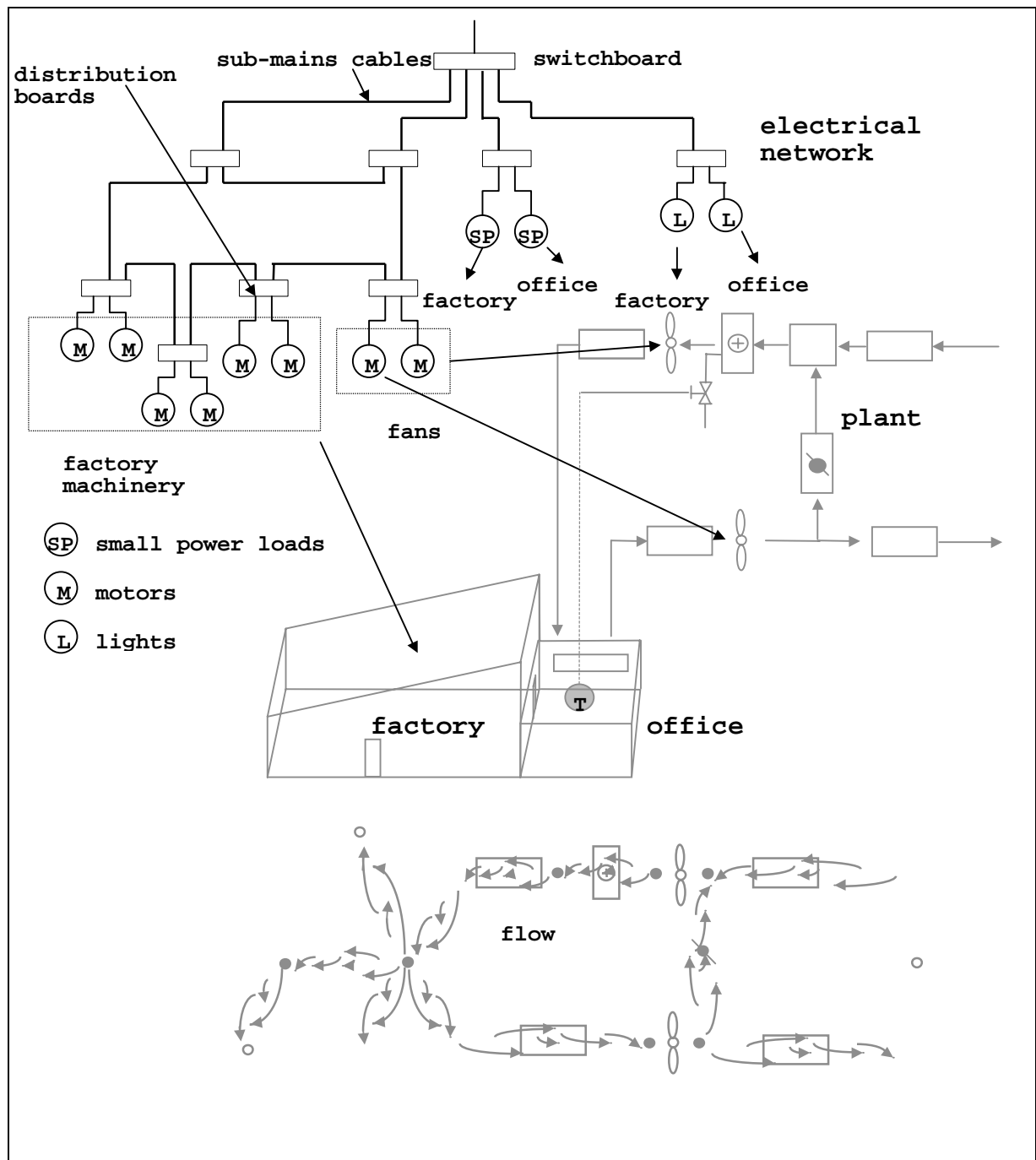


Figure 3.6 An electrical system added to the building model.

Figure 3.6 shows that the electrical network supplies power to several constituents of the model: the fans in the plant networks, electric motors in machinery on the factory floor and the lighting system and small power loads in both zones.

Examining the power system of figure 3.6 in isolation, it can be seen that the building power system is hierarchical: the main supply is brought in via one cable at the switchboard and distributed to the loads by sub-mains cables. The system is three-phase, with power delivered to the building at a line to neutral voltage of  $V_s$ . The motors in the factory and plant network draw power from all three phases of the supply, while each lighting and small power load draws its power from only one phase. The cables which supply power to the lights and small power loads terminate at distribution boards, while the cables which supply the fans and motors terminate in motor control centres: these house all the control and safety apparatus necessary for the proper operation of the connected rotational loads. The smaller, single-phase loads are assumed to be distributed evenly over the three phases, hence the system is assumed to be balanced and a per-phase analysis can be performed on the system.

The network illustrates two different type of power distribution network: the motors being fed by a ring main, while the smaller loads are fed by a radial distribution network. In the ring main, for reasons of security of supply, there are two routes for power to flow to each load. In the radial distribution part of the network, there is only one route for the power to flow to the loads. Also note that details such as switches and fuses have been omitted from the diagram: in an energy simulation they are unimportant. Finally, note that a common element of a power system is missing from the model: transformers. How they are incorporated into a simulation will be dealt with in chapter 5.

### **3.5.1 Developing the Network Model**

The next stage in the modelling process is the representation of one phase of the power system as a network; this is shown in figure 3.7. The control volumes are placed at distribution points and cable junctions, with the cables represented by impedances. The loads in the system are replaced by real and reactive power flows.

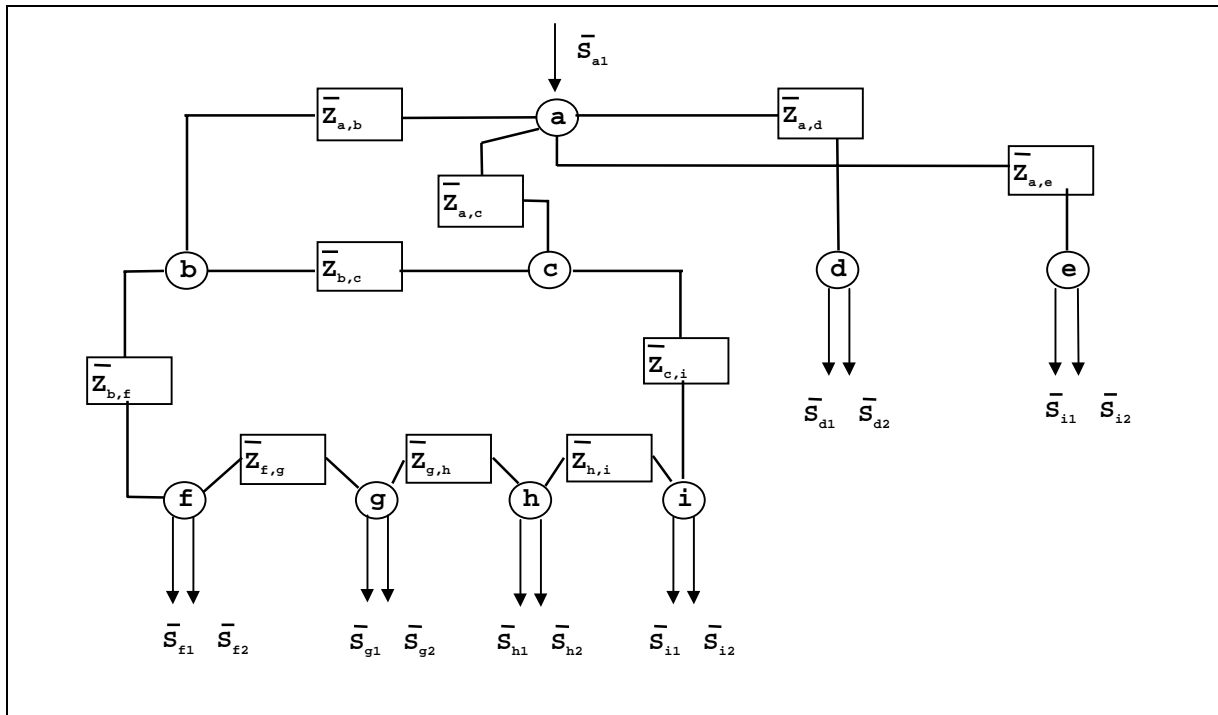


Figure 3.7 The nodal representation of the building power system.

### 3.5.2 Forming the Matrix Equation for the Network

Using equations 2.23a-3.23b to calculate the power flow residuals at each node of figure 3.7 and equations 3.31a-3.31e to calculate the diagonal and off-diagonal terms of each Jacobian group, the following matrix equation can be formulated.



The matrix equation of the previous page forms the basis for the per-phase solution of the power system of figure 3.6. The power flow system state can be determined using the iterative process described in section 3.3 for a particular set of real and reactive power flow boundary conditions. The results for the solved phase of the power system can then be applied to the other two phases and a balanced, three-phase network solution obtained.

### **3.6 Modelling Larger Electrical Systems**

This chapter has described the modelling and solution of the electrical network within a building. However in conceptualising the electrical system as a network the modeller is not limited to the confines of the building. Larger scale electrical systems can be modelled in exactly the same manner; the same modelling method can be applied with equal validity to both a single building and groups of buildings [5]. The possibility therefore exists to expand the scope of integrated thermal and electrical modelling to include such systems as community-wide renewable energy schemes, centralised cogeneration (large scale CHP), remote renewable power generation and distribution [6,7], etc. However, the modelling of these large-scale systems is the subject of another thesis.

### **3.7 Summary**

This chapter has demonstrated how the control volume technique can be applied to the modelling of electrical systems, where the power system is modelled as a network. Characteristic power balance equations were developed for the electrical control volumes in terms of real and reactive power flow. Application of these equations, to each control volume (represented by a node) in the electrical network, allowed a characteristic equation set to be extracted. This equation set was solved for the complex voltage at each control volume using an iterative Newton-Raphson solution technique. The solution required that real and reactive boundary power flows were supplied as boundary conditions to the electrical network. The calculation of these boundary conditions and the integration of the electrical system into the rest of the building model is the subject of the next chapter.

### 3.8 References

1. Gross C A, *Power system analysis 2<sup>nd</sup> Edition*, Wiley, New York, 1986.
2. Stagg G and El-Abiad A H, *Computer methods in power system analysis*, McGraw-Hill, New York, 1968.
3. Sweet M V, *Algebra, geometry and trigonometry in science, engineering and mathematics*, Ellis Horwood Ltd., Chichester, 1984.
4. Boylestad R L, *Introductory circuit analysis 5<sup>th</sup> Edition*, Merrill Publishing, London, 1987.
5. Driver K L, *Experience using a power system analysis program for the simulation of building power system operation*, System Simulation in Buildings, Proceedings of the Fourth International Conference, Liege Belgium, 1994.
6. Clarke J A, Evans M S, Grant A D and Kelly N J, *Simulation tools for the exploitation of renewable energy in the built environment: the EnTrack-GIS System*, Proceedings of Building Simulation '97, Prague, Czech Republic, 1997.
7. Kariniotakis G, Stavrakakis G, Nogaret E and Bordier M, *Advanced modelling and identification of autonomous wind-diesel power systems. Application on the French island Desirade*, Proceedings of the European Community Wind Energy Conference, Lübeck-Travemünde, Germany, 1993.

### 3.9 Bibliography

Arillaga J P, Arnold C P and Harker B J *Computer simulation of power systems*, Wiley, New York 1983.

Boylestad R L, *Introductory circuit analysis*, 5<sup>th</sup> Edition, Merrill Publishing, London, 1987.

Gross C A, *Power system analysis 2<sup>nd</sup> Edition*, Wiley, New York, 1986.

Jay P and Hemsley J, *Electrical services in buildings*, Elsevier Publishing, London 1968.

Stagg G, El-Abiad A H, *Computer methods in power system analysis*, McGraw-Hill, New York, 1968.

Weedy B M, *Electric power systems*, Wiley, New York, 1979.

## **Chapter 4 - Integration of Power Flow Modelling into ESP-r**

### **4. Introduction**

This chapter describes how power flow modelling is integrated into ESP-r. Firstly, the means of augmenting the existing building model with the electrical network is described; this forms the basis of an integrated building model, incorporating fabric, fluid flow, plant and the power system. An integrated model is the necessary prerequisite for the modelling and simulation of building-integrated energy systems; the components for use in such simulations are discussed in the next chapter.

Attention then focuses on how the solution process for the electrical network (the electrical solver) is coupled with ESP-r's existing solvers, enabling a simultaneous solution of the time varying high and low grade energy flows in the integrated building model.

Note that this chapter only deals with the more theoretical aspects of power flow modelling integration within ESP-r. The software development work undertaken during this project (the implementation of power flow modelling into ESP-r and the integration of the CHP and PV models) is not described. This is done for two reasons. Firstly, the continuing and rapid evolution of the ESP-r program means that any description of software and its associated structure would rapidly become obsolete. Secondly, this thesis is intended to be as generic as possible in its description of integrated modelling. Hence, in this context, it is the method of power flow integration, rather than the mechanics of its implementation that is discussed here.

#### **4.1 Coupling the Electrical Network to the Integrated Model**

Once a network representation of the building's electrical system is constructed, as described in the previous chapter, it must be coupled to the other constituents of the integrated building model. The nodes in the electrical network where power is injected by sources or supplied to loads provide the coupling points with the rest of the model. These power flows at these nodes



manifest themselves as the boundary condition terms in the characteristic equations of the electrical control volumes (equations 3.23a and 3.23b). As stated in chapter 3, the provision of the power flow boundary conditions is an essential requirement for the solution of the equation set derived from the electrical network.

The means of supplying the boundary power flows is to connect power consuming or generating components to a node in the electrical network (figure 4.1). The types of power consuming components which can be coupled include lighting loads, small power loads (e.g. computers, printers, photocopiers, etc.), fans, pumps and electric heaters. The sources of power that can be connected include building-integrated energy system components: a combined heat and power unit and photovoltaic materials (PV). The network can also be connected to the grid.

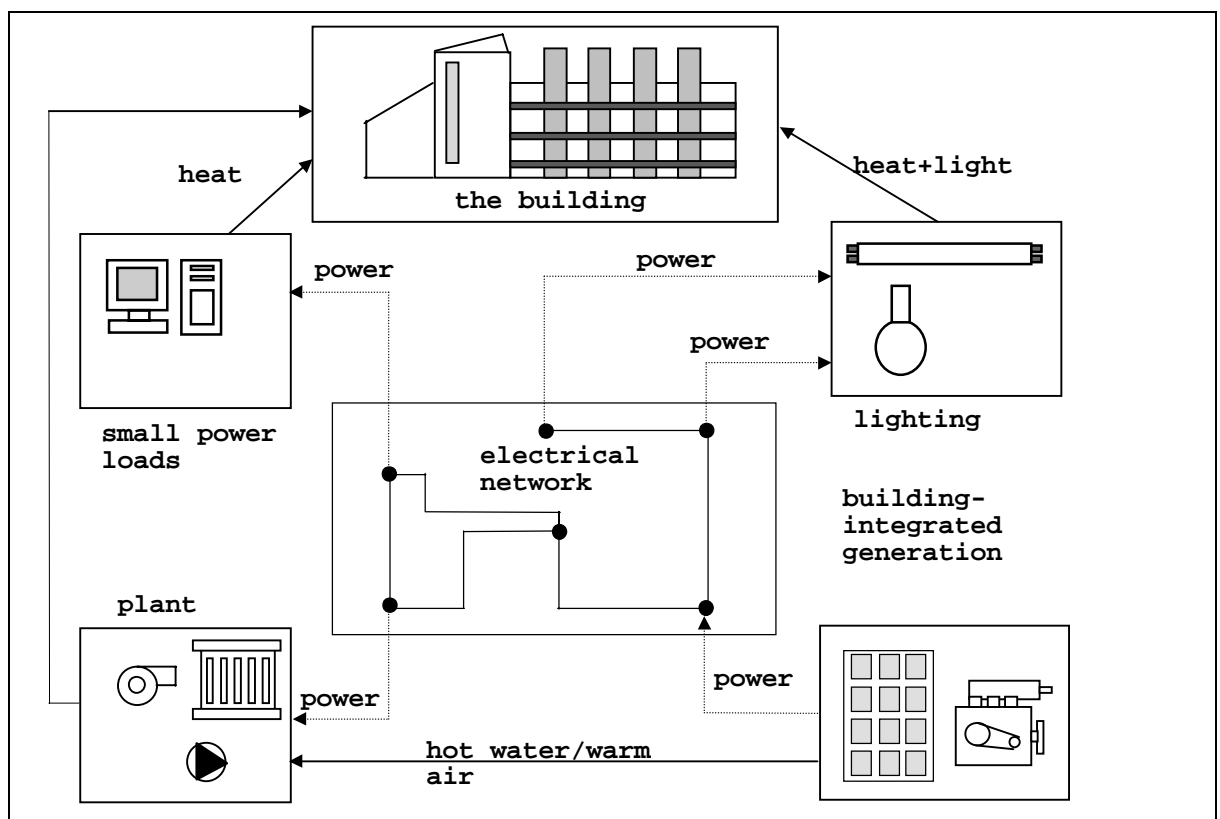


Figure 4.1 Linking hybrid components to the periphery of the electrical network.

The components which supply or draw power from the network also exist as entities in other areas of the building model, typically as components in the plant network (fans, pumps and heaters), elements of the construction (e.g. a PV facade) or in the zones (lighting and small power loads). To provide the required power flow information, these components must perform the task of translation between the thermal and electrical ‘worlds’: acting to convert thermal or fluid flow phenomena into real and reactive power. Examples include: photovoltaic components converting solar radiation falling on the building facade to electrical power, or pumps consuming electrical energy to transport hot water within a heating system. These ‘hybrid’ components [1] simultaneously affect the thermal and electrical constituents of the integrated model. The hybrid components for use in the simulation of building-integrated energy systems are developed and described in detail in chapter 5.

The use of hybrid components to provide the boundary conditions for the solution of the electrical network strongly couples its solution with thermal and flow processes occurring in other parts of the building system. The electrical network therefore needs to be solved simultaneously with the rest of the building model; this necessitates its integration into ESP-r’s modular simultaneous solution process.

## **4.2 Coupling the Electrical Solver into ESP-r’s Integrated Solution Process**

Chapter 2 outlined how the modular simultaneous solution process is already capable of processing, in an integrated fashion, the equation sets from the multi-layered constructions, air volumes, CFD, plant, fluid flow and moisture flow networks. The following section describes how the solution of the electrical network is incorporated.

The modular simultaneous solution process is a means of solving the energy subsystems of the building model by the most appropriate and efficient means. A range of solvers is used to process the different energy subsystem equation sets (discussed in chapter 2). The solvers can be thought of as individual blocks that can be linked together to form a unified solution process for the entire model.

The exact construction of the solution process is variable: different combinations of solvers may be used at any one time. The number and type of solvers used will depend upon the characteristics of a particular model. The constituents the model (fabric, plant, flow, CFD, etc.) will use the relevant solver as required (see figure 4.3).

The framework upon which the ESP-r solution process is built is provided by a governing control algorithm: a simulation controller (this is described by Clarke [2]). The combination of the solvers and the simulation controller forms ESP-r's 'numerical engine', which is able to simultaneously solve all of the subsystems of the building model. This controller determines the structure of the solution process for a particular model, both in terms of the solvers that are used, their interactions and couplings, and in their temporal relationships. This use of both a simulation controller and solvers was designed to be flexible enough to enable such functionality as variable frequency processing of the equation sets, iteration (described in section 2.4.2) and variable time-stepping (implemented by Aasem [3]) within an ESP-r simulation. All these functions are essential for the successful execution of a complex, integrated building simulation.

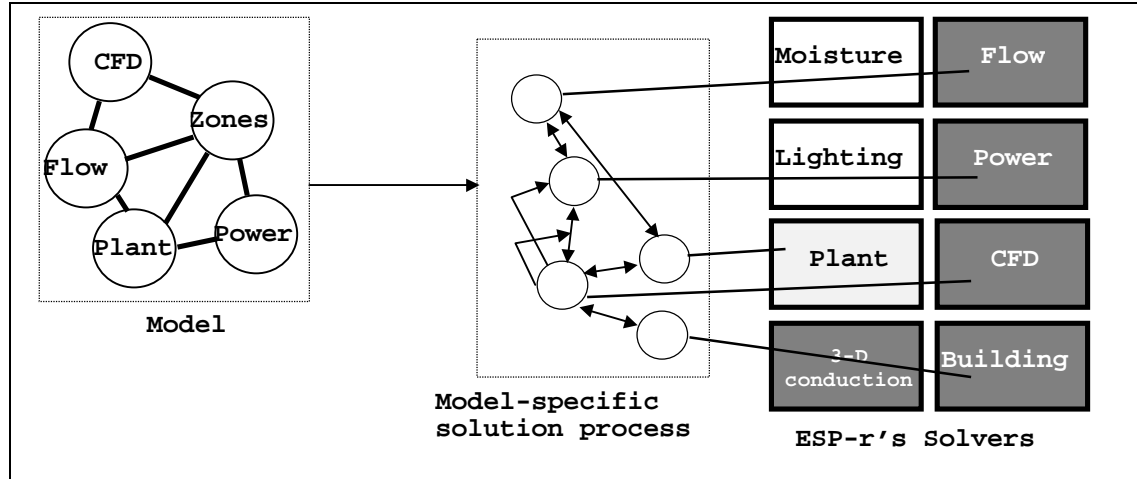


Figure 4.2 ESP-r's flexible simultaneous solution process.

One possible solution process is shown in figure 2.10, where the flow, building-side (i.e. thermal zones)<sup>13</sup> and plant solvers are active. The temporal simulation control is such that the equation sets of the plant and flow networks are solved at a higher frequency than the building-side equation set. The reasons for this have been explained in chapter 2. The flow network is solved first, as the calculated energy flows and temperatures are usually highly sensitive to the fluid flow rates. With the exception of buoyancy driven flows, the fluid flows are relatively insensitive to temperature fluctuations. This order of the flow and energy solutions improves the likelihood of convergence and minimises the amount of iteration required in the simulation.

#### **4.2.1 Positioning of the Electrical Solver in the Solution Process**

Within ESP-r the simulation controller has been modified to enable the integration of the electrical network solver. The positioning of the solver within the overall solution process is dictated by the fact that the power flow boundary conditions must be known before the network solution can proceed. As explained previously, these boundary conditions are calculated using hybrid components, embedded in the plant network and thermal zones. Hence, the electrical network must be solved after the power consumption or generation within these hybrid components has been calculated. The electrical network must therefore be solved after the fluid flow network, plant network and building-side solutions.

The electrical energy equation set must also be solved at a frequency capable of capturing the important effects relating to power flow occurring in other energy subsystems of the building model: the switching on and off of power consuming plant components, control action on lighting systems, variations in solar radiation on PV materials, etc. Therefore, within the context of mixed-frequency equation set processing (section 4.4.2), the solution of the electrical network

---

<sup>13</sup> Note that the representation of the building-side solver within this diagram is a simplification; in ESP-r the building solution may involve the use of more than one solver i.e. CFD, 3-D conduction, etc.

proceeds apace with the most frequently solved subsystem of the building model: usually that of the plant network<sup>14</sup>.

Taking the criteria mentioned above into account, the position of the electrical solver within the overall solution process is after the solution of the flow, building-side and plant equation sets, and within the solution time step of the most frequently solved building constituent: usually the plant network. Note that if an integrated model contains thermal zones and an electrical network (but no plant network), the electrical network will be processed at the same frequency as the zonal energy and air flow equation sets.

As a demonstration of the positioning of the electrical solver, figure 2.20 is modified to include it. This is shown in figure 4.2.

---

<sup>14</sup> Note that this means that the electrical network will usually be processed at a high frequency, resulting in the generation of large quantities of data. The quantity of data produced from elements of a model processed at short time steps becomes unmanageable in long term simulations (i.e. yearly simulations). However ESP-r minimises this problem by allowing results averaging, reducing the quantity (though also the quality) of data produced by the simulation. Usually, simulations employing subsystem processing at short time steps (e.g. a few seconds) would only be performed on short periods of interest (1 to 7 days).

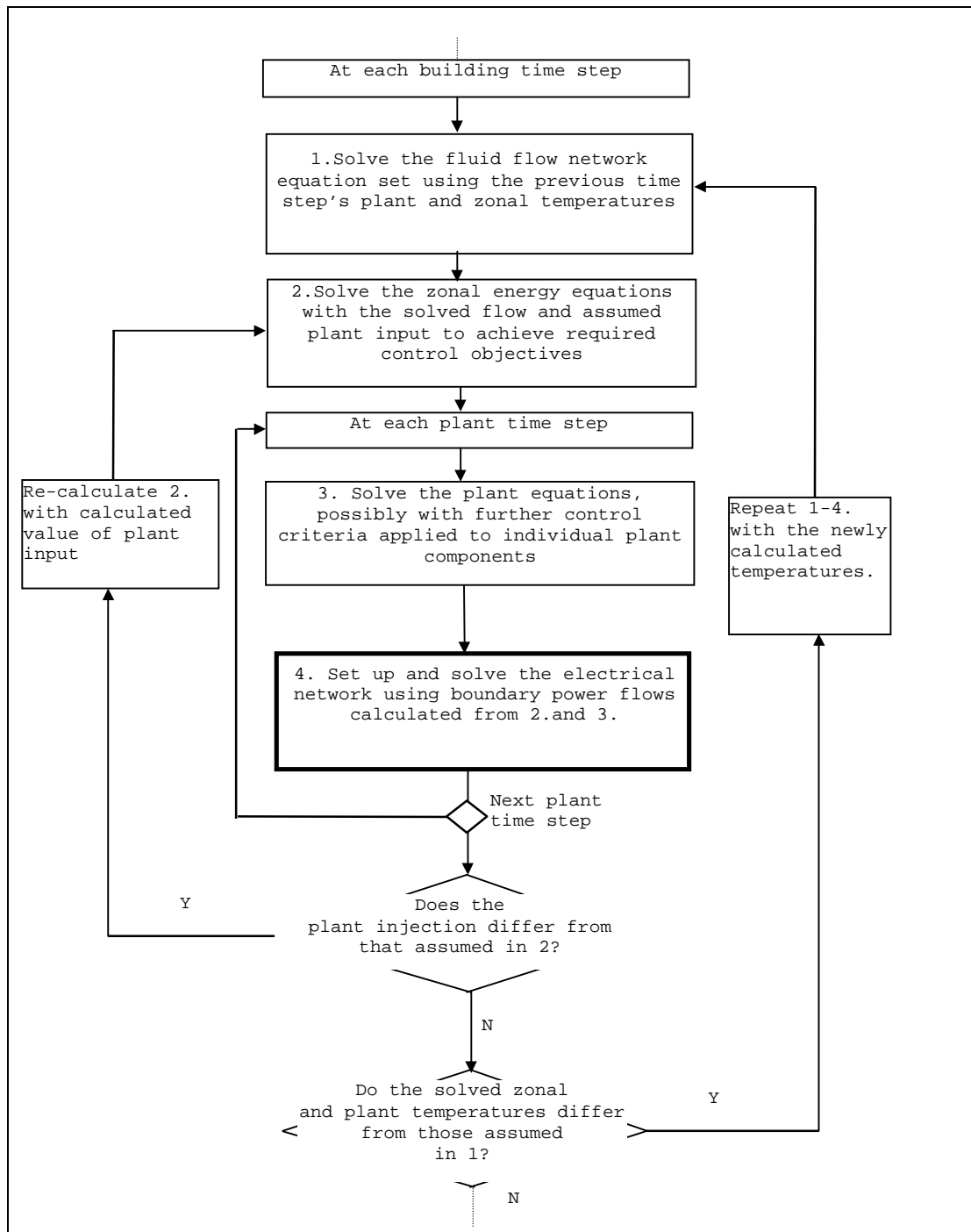


Figure 4.3 The solution process with the electrical solver (adapted from Hensen [4])

### 4.3 The Structure of the Electrical Solver

Figure 4.3 shows the electrical solver as a simple block diagram. However, behind this simple graphical representation is a more complex structure. Chapter 3 outlined the theory behind the electrical network solution, and the diagram below shows the basic structure of the solution algorithm as installed in ESP-r.

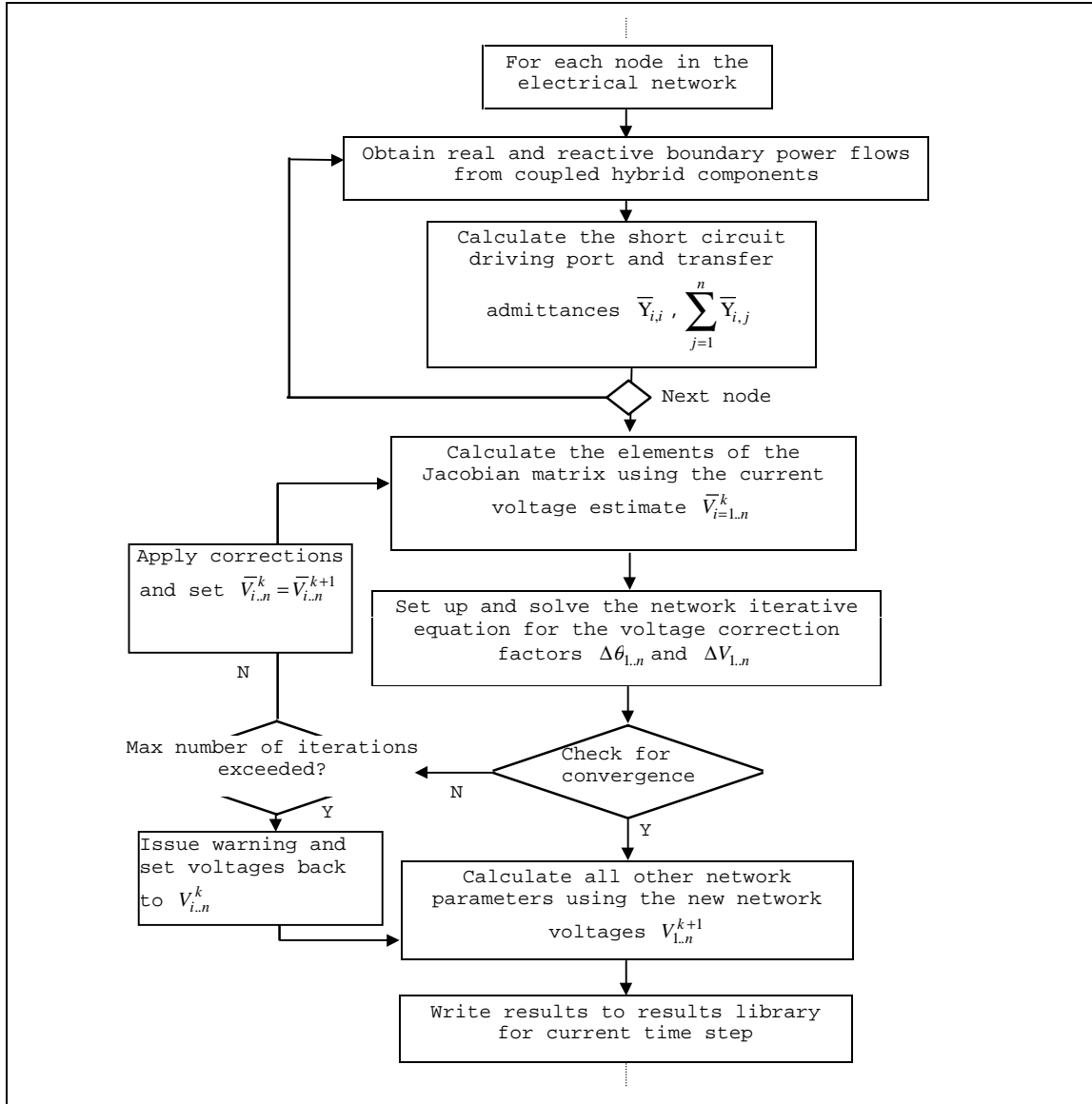


Figure 4.4 The structure of the network solution algorithm.

Note that, for the sake of clarity, figure 4.4 represents the electrical network solution process at a high level of abstraction: each block in the diagram masks a further layer of complexity.

The elements of this diagram, which are peripheral to the network solution, and which were not fully described in chapter 3, are explained below.

#### 4.3.1 Obtaining Initial Values for the Iterative Solution

Like all iterative solution techniques, the solution of the electrical network characteristic equation set requires the provision of initial values of the solved parameters (the set of complex nodal voltages  $\bar{V}_{1..n}^k$ ). These initial values are obtained in one of two ways. At the beginning of the simulation process the nodal values are set to the base voltage values used in the per unit conversion (see section 3.4.2), hence all the nodal voltages begin at a value of  $1.0 + j0$  p.u. Thereafter, the iterative solution uses the nodal voltages calculated at the previous simulation time step as the starting point for the current time step iterative solution.

#### 4.3.2 Forming the Elements of the Jacobian Matrix

The coefficients of the Jacobian matrix are calculated at each iteration using equations 3.31a-3.31h with the current estimates of the nodal voltages  $\bar{V}_i^k$ , the short circuit driving port admittances  $\bar{Y}_{i,i}$  and transfer admittances  $\bar{Y}_{i,j}$  of each node  $i$ . As mentioned in chapter 3, these admittance terms are calculated using the impedance characteristics of the conducting components (lines, cables and transformers) that couple the nodes in the electrical network. The modelling of these coupling components and expressions for the calculation of their impedance and admittance characteristics is described in chapter 5.

Solution proceeds as described in the previous chapter: equation 3.30 is solved for the complex voltage correction factors ( $\Delta V$  and  $\Delta \theta$ ), which are then added to the current estimate of the nodal voltages  $\bar{V}^k$ . The newly calculated voltages are then used as the basis for the calculation of the next estimate of nodal voltages  $\bar{V}^{k+1}$ .



### 4.3.3 Convergence

Convergence of the solution process is determined by comparing the magnitude of the calculated voltage argument  $|V|$  and its modulus  $|\theta|$  against the magnitudes of their respective corrections:  $|\Delta V|$  and  $|\Delta \theta|$ . If all the corrections are less than a user defined value, then the iterative process has converged to a close approximation of the ideal solution. The convergence criteria are met when corrections of less than 0.1% of the present value of the voltage argument and modulus need to be applied to each node in the network. If convergence is not obtained within a defined number of iterations a warning is given to the user and the nodal voltages are reset to default values of  $1.0 + j0.0$  p.u (the starting values for the next time step iterative calculation). The entire simulation then continues on to the next time step, though of course the results obtained for the time step in which the electrical network solution did not converge may be erroneous. The Newton-Raphson technique used in the network solution process is strongly convergent: a solution is normally obtained within 20 iterations.

The convergence of the power flow solution process installed in ESP-r has been improved (compared to the algorithms described by Gross [6] and Weedy [7]) in that control of nodal voltages, to which a power source connects, has been removed from within the iterative solution process. This eliminates a possible source of discontinuity (i.e. a nodal voltage changing its value between iterations) and improves the chances of the iterative solution converging. Nodal voltage control and its implementation within ESP-r is explained and discussed further in section 5.4.3.

At the end of each time step, the network power flows and currents are calculated and written to a results file. The results of the network solution represent an averaged ‘snapshot’ of the network state during the simulation time step. Note that high frequency transient effects (e.g. motor start up power consumption, switching transients, etc.) cannot be captured using phasor state variables. However, for the purposes of an energy simulation it is the phasor values that are important. The effect on energy consumption of higher frequency effects is small, though it should be mentioned that the solution method outlined in chapter 3 can also be applied in the simulation of short time constant, transient electrical phenomena [6,7].

#### 4.4 More Complex Couplings: the ‘Onion’ Approach

The integrated solution algorithm of figure 4.3 shows the electrical network being processed after all the other subsystems of the building model have been solved. Note that there are no iterative couplings between the electrical solution and the other solved subsystems. This type of solution intrinsically assumes that the power system is always able to meet the electrical energy requirements of the other subsystems. In effect, the solutions of the other energy subsystems generate both the supply and demand profiles for the electrical network and no feedback is required. However, there are circumstances where it is desirable or necessary for the electrical network to interact with the rest of the solution process, and have an effect on the other energy subsystems. Situations where this type of interactive coupling is applicable include:

- where the electrical system can only supply a finite amount of energy, e.g. in stand-alone renewable energy or building-integrated energy schemes;
- where limits are imposed in the energy drawn by a building (i.e. to prevent financial penalties being imposed if a maximum demand is exceeded) and these limits are enforced by a supervisory control action in a building energy management system (BEMS);
- or where the electrical capacities of components in the electrical network are exceeded, i.e. overloading of a cable or generator.

In these three cases the electrical network will be unable to meet the electrical demand of the power consuming components in the other energy subsystems and thus their solved state is invalid as it is based on the assumption of a full power supply. The solution of the entire building must therefore be iteratively re-calculated, but with achievable power demands.

One mechanism for instigating this iterative coupling is the use of control action within the simulation. Control can be used to modify the power demands of the power consuming

components in the building's other energy subsystems, such that the power demand of the building model is at a level which can be met by the power system. Examples are given below.

- Shutting off plant and lighting until the power demand can be met by a finite power source or the power demand is below the maximum limit set by a supervisory controller.
- Where components exceed their maximum working ratings the control action would represent the action of switches or fuses: effectively shutting off the supply to power consuming components connected to the overloaded electrical network element.

The form of control action indicated in the preceding paragraphs would require recalculation of the other subsystems, taking into account the power loss to affected energy consuming components. This is illustrated in figure 4.3. The application of control in the modelling of the power system is discussed in more detail in the next chapter.

An iterative coupling between the electrical network solution and the rest of the building solution, i.e. 'iterative handshaking', has been described by Hensen [8] as an 'onion'-type coupling. In this type of iterative mechanism the various coupled solvers used in the simulation are iterated within each simulation time step until an overall solution is achieved. Such a coupling mechanism is already used between the building, plant and flow solvers.

## **4.5 Summary**

This chapter has outlined the means of coupling the electrical network to the rest of the building model using 'hybrid' components that also exist in other energy subsystems of the building model. These hybrid components supply the power flows necessary for the solution of the electrical network.

The integration of the electrical network solver into ESP-r's flexible, modular simultaneous solution process was also described, along with a description of the structure of the electrical

solver. Finally, a control-based means of iterative interaction between the electrical solver and the rest of the building solution process was outlined.

The next chapter describes the hybrid components that connect to the electrical network, the components that make up the network itself and the application of control to both the component models and the whole electrical network solution (including the control-based coupling discussed in this chapter).

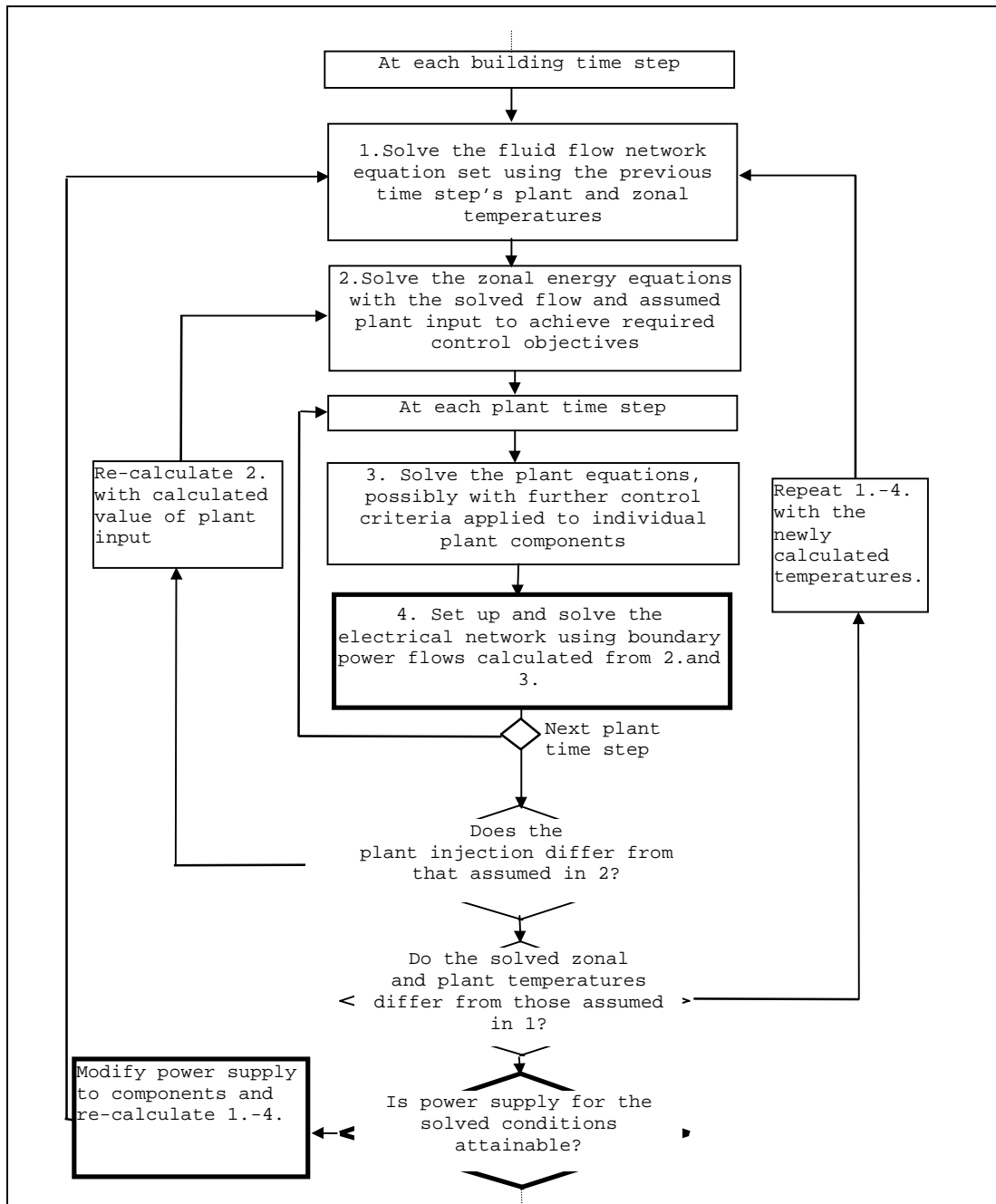


Figure 4.5 A control-based iterative coupling for the electrical network.

## 4.6 References

1. Chandrashekar M and Gupta S, *A unified approach to modelling photovoltaic powered systems*, Solar Energy, Vol. 55, No. 4, Elsevier Science Ltd., 1995.
2. Clarke J A, *Energy Simulation in Building Design*, Adam Hilger, New York, 1985.
3. Aasem E O, *Practical simulation of air conditioning systems in the transient domain*, PhD Thesis, University of Strathclyde, Glasgow, 1993.
4. Hensen J L M, *On the thermal interaction of building structure and heating and ventilating system*, Doctoral Dissertation, Eindhoven University of Technology, 1991.
5. Stagg G and El-Abiad A H, *Computer methods in power system analysis*, McGraw-Hill, New York, 1968.
6. Stangerup P, ESCAP technical reference, Stansim Research, Denmark, 1993.
7. Driver K L, *Experience using a power system analysis program for the simulation of building power system operation*, System Simulation in Buildings, Proceedings of the Fourth International Conference, Liege Belgium, 1994.
8. Hensen J L M, *Modelling coupled heat and airflow: ping-pong vs. onions*, ESRU Paper, 1995.

# **Chapter 5 - Component Models for Building-Integrated Energy Systems Simulation**

## **5. Introduction**

This chapter describes the component models which are required to facilitate the simulation of both the electrical network and, more specifically, building-integrated energy systems. The previous chapters have indicated the types of components needed for this task:

- the conducting elements, which link the nodes in the electrical network;
- loads which draw power from the network;
- and, finally, the building-integrated generation sources that inject power into the network.

This chapter develops and describes these components.

### **5.1 Components of the Electrical Network**

Key elements of the electrical network, described in chapter 3, were the components connecting the electrical control volumes. These were characterised by an impedance, the inverse of which (admittance) was used in the power balance equations for each electrical control volume.

The connecting components represent the elements of the building's distribution system: conductors (cables and transmission lines) and transformers. Their impedance characteristics are derived from an equivalent circuit model. The equivalent circuit is an abstract physical model that captures the electrical attributes of the connecting component. The exact form of the equivalent circuit depends upon the type of system being modelled. Recall that the types of

systems considered in chapter 3 were comprehensive and per-phase three-phase a.c., single-phase a.c. and direct current. For each system, slightly different models are required. The circuit models of both conductors and transformers and their derived impedance characteristics are described in the following sections.

### 5.1.1 Conductors

The equivalent circuit model of an electrical conductor is determined by its basic electrical properties: resistance, capacitance and inductance, each of which is used in the calculation of its impedance characteristics.

#### 5.1.1.1 Three-Phase Conductors

The three-phase conductor is the most important connecting device in the three-phase system and its equivalent circuit is shown in figure 5.1. The model includes four conductors: the neutral and each of the phase conductors. Each conductor has a series resistance and inductance, notice also that the equivalent circuit also contains mutual inductance and capacitance couplings: both of these couplings result from the interaction of the magnetic fields around conductors in close proximity [1].

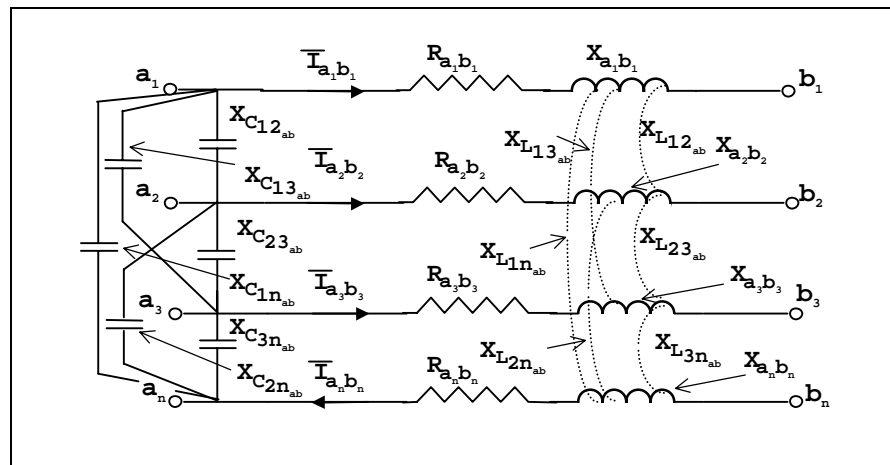


Figure 5.1 The equivalent circuit model of a three phase conductor.



In figure 5.1  $R_{a_k, b_k}$   $k=1...3, n$  is the series resistance of each conductor ( $\Omega$ ),  $X_{L_{a_k, b_k}}$   $k=1...3, n$  is the series inductive reactance ( $\Omega$ ),  $X_{C_{xy_{a,b}}}$  and  $X_{L_{xy_{a,b}}}$  are the capacitive reactance ( $\Omega$ ) and the mutual inductive reactance ( $\Omega$ ) respectively, between conductors  $x$  and  $y$ . The reactance quantities are derived from the basic conductor characteristics (resistance, inductance and capacitance). This is shown in the equations that follow.

Firstly, the series inductive reactance is given by

$$X_{L_{a_k, b_k}} = j\omega L_{a_k, b_k} \quad (5.1)$$

$L_{a_k, b_k}$  is the series inductance of the conductor (H),  $\omega$  is the angular frequency (in radians) of the sinusoidal-varying alternating current (a.c.) travelling along the conductor, where  $\omega = 2\pi f$  and  $f$  is the frequency (Hz) of the sinusoidal variation.

The mutual reactance is defined by

$$X_{L_{xy_{a,b}}} = \omega L_{xy_{a,b}} \quad (5.2)$$

$L_{xy_{a,b}}$  is the mutual inductance of the two conductors  $x$  and  $y$ , which link points  $a$  and  $b$  in the electrical network.

Finally, the capacitive reactance is defined by

$$X_{C_{xy_{a,b}}} = \frac{-1}{\omega C_{xy_{a,b}}} \quad (5.3)$$

$C_{xy_{a,b}}$  is the capacitance (F) between the two conductors  $x$  and  $y$  linking points  $a$  and  $b$ .

According to Weedy [2], in short conductors such as those found in buildings, the effect of capacitance can be neglected. The equivalent circuit of figure 5.1 can therefore be reduced to the following.

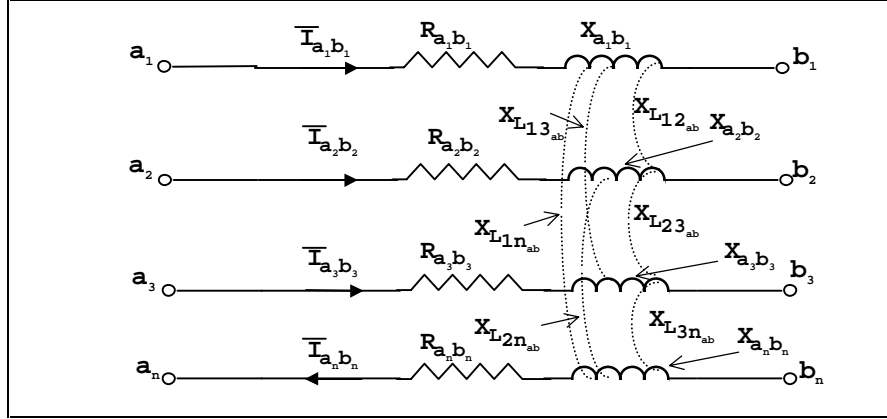


Figure 5.2 The equivalent circuit for a short three phase conductor (from [3]).

The couplings between the control volumes in the electrical network of chapter 3 were defined in terms of impedance. The impedance characteristics of the three-phase conductor model can be derived as follows.

The series impedances between nodes  $a_k$  and  $b_k$  are:

$$\bar{Z}_k = R_{a_k b_k} + X_{a_k b_k} \quad k = 1, 2, 3, n,$$

and the mutual impedances of conductors,  $x$  and  $y$ , linking points  $a$  and  $b$  are given by

$$\bar{Z}_{m_{xy a, b}} = j\omega L_{xy a, b} \quad x = 1, 2, 3, n \quad x \neq y.$$

These impedances can be used in the development of the three-phase conductor equivalent circuit model, the first step of which is the creation of a characteristic equation set: this is created

by application of Kirchhoff's voltage law to the circuit model. This law stipulates that the algebraic sum of the voltages differences around any traced, closed path in a circuit is zero. Three such paths (indicated by the dotted lines) are shown in figure 5.3.

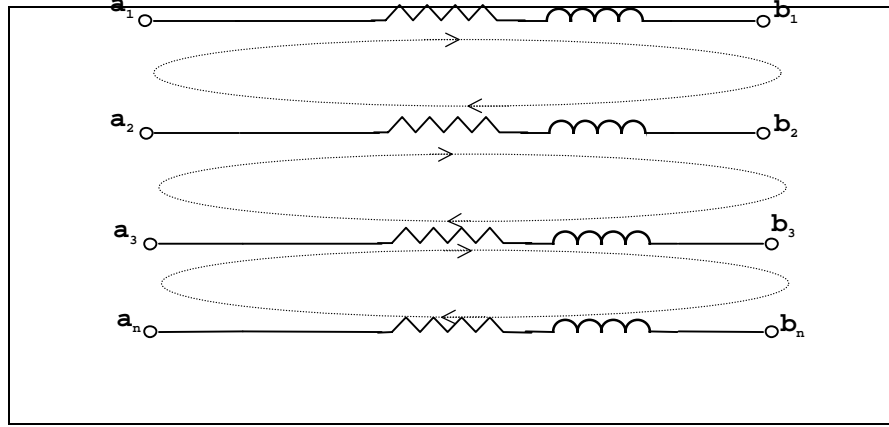


Figure 5.3 The three phase conductors with voltage loops superimposed.

For the loop between the conductors 1 and 2:

$$(\bar{V}_{a_1} - \bar{V}_{b_1}) + (\bar{V}_{b_1} - \bar{V}_{b_2}) + (\bar{V}_{b_2} - \bar{V}_{a_2}) + (\bar{V}_{a_2} - \bar{V}_{a_1}) = 0 ; \quad (5.4)$$

applying Ohm's law and rearranging gives

$$\bar{V}_{a_1} - \bar{V}_{b_1} = \bar{I}_{a_1, b_1} \bar{Z}_{a_1, b_1} + \bar{I}_{a_2, b_2} \bar{Z}_{m_{12a, b}} + \bar{I}_{a_3, b_3} \bar{Z}_{m_{13a, b}} + \bar{I}_{a_n, b_n} \bar{Z}_{m_{1na, b}} \quad (5.5)$$

and

$$\bar{V}_{b_2} - \bar{V}_{a_2} = \bar{I}_{a_1, b_1} \bar{Z}_{m_{21a, b}} + \bar{I}_{a_2, b_2} \bar{Z}_{a_2, b_2} + \bar{I}_{a_3, b_3} \bar{Z}_{m_{23a, b}} + \bar{I}_{a_n, b_n} \bar{Z}_{m_{2na, b}} . \quad (5.6)$$

Substituting equations 5.5 and 5.6 into 5.4 and rearranging gives

$$\begin{aligned}
& \bar{I}_{a_1, b_1} \bar{Z}_{a_1, b_1} + \bar{I}_{a_1, b_1} \bar{Z}_{m_{21a, b}} + \bar{I}_{a_2, b_2} \bar{Z}_{a_2, b_2} + \bar{I}_{a_2, b_2} \bar{Z}_{m_{12a, b}} + \bar{I}_{a_3, b_3} \bar{Z}_{a_3, b_3} + \bar{I}_{a_3, b_3} \bar{Z}_{m_{23a, b}} \\
& + \bar{I}_{a_n, b_n} \bar{Z}_{m_{1na, b}} + \bar{I}_{a_n, b_n} \bar{Z}_{m_{2na, b}} \\
& = (\bar{V}_{a_1} - \bar{V}_{b_1}) + (\bar{V}_{a_2} - \bar{V}_{b_2}).
\end{aligned} \tag{5.7}$$

Similar equations can be derived for the other two loops. All three equations are then used to form the following equation for the three-phase conductor, which expresses the voltage difference across the conductors in terms of the conductor currents, series and mutual impedances.

$$\begin{bmatrix} \bar{Z}_{a_1, b_1} & \bar{Z}_{m_{12a, b}} & \bar{Z}_{m_{13a, b}} & \bar{Z}_{m_{1na, b}} \\ \bar{Z}_{m_{21a, b}} & \bar{Z}_{a_2, b_2} & \bar{Z}_{m_{23a, b}} & \bar{Z}_{m_{2na, b}} \\ \bar{Z}_{m_{31a, b}} & \bar{Z}_{m_{32a, b}} & \bar{Z}_{a_3, b_3} & \bar{Z}_{m_{3na, b}} \\ \bar{Z}_{m_{n1a, b}} & \bar{Z}_{m_{n2a, b}} & \bar{Z}_{m_{n3a, b}} & \bar{Z}_{a_n, b_n} \end{bmatrix} \begin{bmatrix} \bar{I}_{a_1, b_1} \\ \bar{I}_{a_2, b_2} \\ \bar{I}_{a_3, b_3} \\ \bar{I}_{a_n, b_n} \end{bmatrix} = \begin{bmatrix} \bar{V}_{a_1} - \bar{V}_{b_1} \\ \bar{V}_{a_2} - \bar{V}_{b_2} \\ \bar{V}_{a_3} - \bar{V}_{b_3} \\ \bar{V}_{a_n} - \bar{V}_{b_n} \end{bmatrix}. \tag{5.8}$$

It is normal in three-phase systems to reference all the phase voltages to the neutral  $\bar{V}_n$ , giving the line-to-neutral or phase voltage. The neutral acts as a common return path for the current flowing in the other conductors and is earthed at various points. Referencing all the voltages to the neutral simplifies the equation set shown above.

Considering conductor 1, the voltages referenced to the neutral are  $\bar{V}_{a_1} - \bar{V}_{a_n}$  and  $\bar{V}_{b_1} - \bar{V}_{b_n}$ . The voltage difference across the conductor would be given by  $(\bar{V}_{a_1} - \bar{V}_{a_n}) - (\bar{V}_{b_1} - \bar{V}_{b_n})$ . Application of Kirchhoff's voltage law to the loop formed by the first and neutral conductor gives the following.

$$(\bar{V}_{a_1} - \bar{V}_{b_1}) + (\bar{V}_{b_1} - \bar{V}_{b_n}) + (\bar{V}_{b_n} - \bar{V}_{a_n}) + (\bar{V}_{a_n} - \bar{V}_{a_1}) = 0; \tag{5.9}$$

rearranging this equation gives

$$(\bar{V}_{a_1} - \bar{V}_{a_n}) - (\bar{V}_{b_1} - \bar{V}_{b_n}) = (\bar{V}_{a_1} - \bar{V}_{b_1}) - (\bar{V}_{a_n} - \bar{V}_{b_n}). \quad (5.10)$$

A similar expression can be derived to conductors 2 and 3. Now, by inspection, referencing the voltages of conductors 1, 2 and 3 to the neutral voltage requires that the expression for the voltage difference across the neutral conductor is subtracted from each row of matrix equation 5.6. This gives the following equation, with all voltages referenced to the neutral:

$$\begin{bmatrix} \bar{Z}_{a_1, b_1} - \bar{Z}_{m_{1n_a, b}} & \bar{Z}_{m_{12a, b}} - \bar{Z}_{m_{2n_a, b}} & \bar{Z}_{m_{13a, b}} - \bar{Z}_{m_{3n_a, b}} & \bar{Z}_{m_{1n_a, b}} - \bar{Z}_{a_n, b_n} \\ \bar{Z}_{m_{21a, b}} - \bar{Z}_{m_{1n_a, b}} & \bar{Z}_{a_2, b_2} - \bar{Z}_{m_{2n_a, b}} & \bar{Z}_{m_{23a, b}} - \bar{Z}_{m_{3n_a, b}} & \bar{Z}_{m_{2n_a, b}} - \bar{Z}_{a_n, b_n} \\ \bar{Z}_{m_{31a, b}} - \bar{Z}_{m_{1n_a, b}} & \bar{Z}_{m_{32a, b}} - \bar{Z}_{m_{2n_a, b}} & \bar{Z}_{a_3, b_3} - \bar{Z}_{m_{3n_a, b}} & \bar{Z}_{m_{3n_a, b}} - \bar{Z}_{a_n, b_n} \\ 0 & 0 & 0 & 0 \end{bmatrix} \begin{bmatrix} \bar{I}_{a_1, b_1} \\ \bar{I}_{a_2, b_2} \\ \bar{I}_{a_3, b_3} \\ \bar{I}_{a_n, b_n} \end{bmatrix} = \begin{bmatrix} (\bar{V}_{a_1} - \bar{V}_{b_1})_n \\ (\bar{V}_{a_2} - \bar{V}_{b_2})_n \\ (\bar{V}_{a_3} - \bar{V}_{b_3})_n \\ 0 \end{bmatrix} \quad (5.11)$$

Notice that the neutral voltage is removed from the equation. Also, as the neutral acts as a common return path for the three currents, the following equation applies.

$$\bar{I}_{a_n, b_n} = -(\bar{I}_{a_1, b_1} + \bar{I}_{a_2, b_2} + \bar{I}_{a_3, b_3}). \quad (5.12)$$

Now in three phase conductors, the mutual impedances between the conductors are balanced,

hence  $\bar{Z}_{m_{12a, b}} = \bar{Z}_{m_{21a, b}} = \bar{Z}_{m_{13a, b}} = \bar{Z}_{m_{31a, b}} = \bar{Z}_{m_{23a, b}} = \bar{Z}_{m_{32a, b}} = \bar{Z}_{m_{ph_a, b}}$  and

$\bar{Z}_{m_{1n_a, b}} = \bar{Z}_{m_{2n_a, b}} = \bar{Z}_{m_{1n_a, b}} = \bar{Z}_{m_{n_a, b}}$ . Also as the three phase conductors are identical, the three

phase impedances must also be identical, hence  $\bar{Z}_{a_1, b_1} = \bar{Z}_{a_2, b_2} = \bar{Z}_{a_2, b_2} = \bar{Z}_{a_{ph}, b_{ph}}$

Noting the above and substituting 5.12 into equation 5.11 allows the neutral current to be eliminated:

$$\begin{aligned}
& \begin{bmatrix} \bar{Z}_{a_{ph},b_{ph}} + \bar{Z}_{a_n,b_n} - 2\bar{Z}_{m_{n_{a,b}}} & \bar{Z}_{m_{pha,b}} + \bar{Z}_{a_n,b_n} - 2\bar{Z}_{m_{n_{a,b}}} & \bar{Z}_{m_{pha,b}} + \bar{Z}_{a_n,b_n} - 2\bar{Z}_{m_{n_{a,b}}} \\ \bar{Z}_{m_{pha,b}} + \bar{Z}_{a_n,b_n} - 2\bar{Z}_{m_{n_{a,b}}} & \bar{Z}_{a_{ph},b_{ph}} + \bar{Z}_{a_n,b_n} - 2\bar{Z}_{m_{n_{a,b}}} & \bar{Z}_{m_{pha,b}} + \bar{Z}_{a_n,b_n} - 2\bar{Z}_{m_{n_{a,b}}} \\ \bar{Z}_{m_{pha,b}} + \bar{Z}_{a_n,b_n} - 2\bar{Z}_{m_{n_{a,b}}} & \bar{Z}_{m_{pha,b}} + \bar{Z}_{a_n,b_n} - 2\bar{Z}_{m_{n_{a,b}}} & \bar{Z}_{a_3,b_3} + \bar{Z}_{a_n,b_n} - 2\bar{Z}_{m_{n_{a,b}}} \end{bmatrix} \begin{bmatrix} \bar{I}_{a_1,b_1} \\ \bar{I}_{a_2,b_2} \\ \bar{I}_{a_3,b_3} \end{bmatrix} \\
& = \begin{bmatrix} \left( \bar{V}_{a_1} - \bar{V}_{b_1} \right) \\ \left( \bar{V}_{a_2} - \bar{V}_{b_2} \right) \\ \left( \bar{V}_{a_3} - \bar{V}_{b_3} \right) \end{bmatrix}
\end{aligned} \quad (5.13)$$

Notice that the  $n$  subscript is dropped; all voltages can therefore be considered as referenced to the neutral.

Combining terms relating to the neutral conductor such that  $\bar{Z}_{a_n,b_n} - 2\bar{Z}_{m_{n_{x,y}}} = \bar{Z}_n$ , equation 5.13 can therefore be re-written as

$$\begin{bmatrix} \bar{Z}_{a_{ph},b_{ph}} + \bar{Z}_n & \bar{Z}_{m_{pha,b}} + \bar{Z}_n & \bar{Z}_{m_{pha,b}} + \bar{Z}_n \\ \bar{Z}_{m_{pha,b}} + \bar{Z}_n & \bar{Z}_{a_{ph},b_{ph}} + \bar{Z}_n & \bar{Z}_{m_{pha,b}} + \bar{Z}_n \\ \bar{Z}_{m_{pha,b}} + \bar{Z}_n & \bar{Z}_{m_{pha,b}} + \bar{Z}_n & \bar{Z}_{a_{ph},b_{ph}} + \bar{Z}_n \end{bmatrix} \begin{bmatrix} \bar{I}_{a_1,b_1} \\ \bar{I}_{a_2,b_2} \\ \bar{I}_{a_3,b_3} \end{bmatrix} = \begin{bmatrix} \left( \bar{V}_{a_1} - \bar{V}_{b_1} \right) \\ \left( \bar{V}_{a_2} - \bar{V}_{b_2} \right) \\ \left( \bar{V}_{a_3} - \bar{V}_{b_3} \right) \end{bmatrix}. \quad (5.14)$$

#### 5.1.1.1.1 The Three-phase Conductor Model

The equivalent circuit model of the three-phase conductor for use in a comprehensive three-phase electrical network model is as shown in figure 5.4

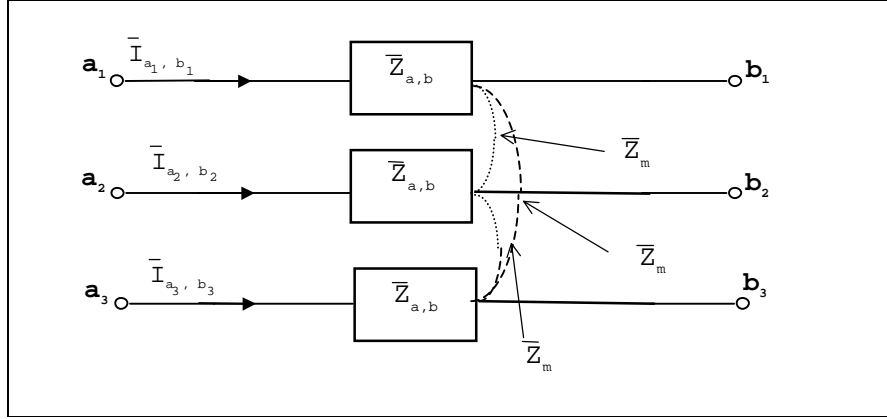


Figure 5.4 The equivalent circuit model of the three-phase conductor

In figure 5.4  $\bar{Z}_{a,b} = \bar{Z}_{a_{ph},b_{ph}} + \bar{Z}_n$  and  $\bar{Z}_m = \bar{Z}_{m_{ph,a,b}} + \bar{Z}_n$ .

Recall that the power balance equations of chapter 3 used the admittance rather than the impedance. The admittance form of equation 5.14 is obtained by multiplying the both sides of the equation by the inverse of the impedance matrix; this gives the following:

$$\begin{bmatrix} \bar{Y}_{a_{ph},b_{ph}} & \bar{Y}_{m_{ph,a,b}} & \bar{Y}_{m_{ph,a,b}} \\ \bar{Y}_{m_{ph,a,b}} & \bar{Y}_{a_{ph},b_{ph}} & \bar{Y}_{m_{ph,a,b}} \\ \bar{Y}_{m_{ph,a,b}} & \bar{Y}_{m_{ph,a,b}} & \bar{Y}_{a_{ph},b_{ph}} \end{bmatrix} \begin{bmatrix} (\bar{V}_{a_1} - \bar{V}_{b_1})_n \\ (\bar{V}_{a_2} - \bar{V}_{b_2})_n \\ (\bar{V}_{a_3} - \bar{V}_{b_3})_n \end{bmatrix} = \begin{bmatrix} \bar{I}_{a_1,b_1} \\ \bar{I}_{a_2,b_2} \\ \bar{I}_{a_3,b_3} \end{bmatrix}. \quad (5.15)$$

The admittance parameters of this expression are defined as follows.

For the diagonal terms:

$$Y_{a_{ph},b_{ph}} = \frac{\bar{Z}_{a,b} + \bar{Z}_m}{(\bar{Z}_{a,b} + 2\bar{Z}_m)(\bar{Z}_{a,b} - \bar{Z}_m)}, \quad (5.16)$$

and for the off-diagonal terms:

$$Y_{m_{pha,b}} = \frac{-\bar{Z}_m}{(\bar{Z}_{a,b} + 2\bar{Z}_m)(\bar{Z}_{a,b} - \bar{Z}_m)}. \quad (5.17)$$

Note that the diagonal and off-diagonal admittance terms of equation 5.15 are of the same value over the three phases. The admittances calculated using equations 5.16 and 5.17 are those that would be used in equations 3.44a-3.44e: the power balances for the three-node array to which the three-phase conductor connects

#### 5.1.1.1.2 The Per-Phase Conductor Model

Chapter 3 described how, in normal balanced operating conditions, the three phases of an electrical network can be analysed by modelling only one phase: so-called ‘per-phase’ analysis. The model of the three-phase conductor can be simplified by the assumption of balanced operating conditions. Applying the equations for the current and voltage in the balanced three-phase situation (3.39a, 3.40a, 3.41a, 3.39a, 3.40a and 3.41a) gives (after some manipulation using de Moivre’s theorem)

$$\begin{bmatrix} \bar{Y}_{a_{ph},b_{ph}} & \bar{Y}_{m_{pha,b}} & \bar{Y}_{m_{pha,b}} \\ \bar{Y}_{m_{pha,b}} & \bar{Y}_{a_{ph},b_{ph}} & \bar{Y}_{m_{pha,b}} \\ \bar{Y}_{m_{pha,b}} & \bar{Y}_{m_{pha,b}} & \bar{Y}_{a_{ph},b_{ph}} \end{bmatrix} \begin{bmatrix} (V_a - V_b)_n (\cos(\theta_a - \theta_b) + i \sin(\theta_a - \theta_b)) \\ \left(-0.5 + i\sqrt{\frac{3}{2}}\right)(V_a - V_b)_n (\cos(\theta_a - \theta_b) + i \sin(\theta_a - \theta_b)) \\ \left(-0.5 - i\sqrt{\frac{3}{2}}\right)(V_a - V_b)_n (\cos(\theta_a - \theta_b) + i \sin(\theta_a - \theta_b)) \end{bmatrix} \quad (5.18)$$

$$= \begin{bmatrix} I(\cos \beta + i \sin \beta) \\ \left(-0.5 + i\sqrt{\frac{3}{2}}\right)I(\cos \beta + i \sin \beta) \\ \left(-0.5 + i\sqrt{\frac{3}{2}}\right)I \cos \beta + i \sin \beta \end{bmatrix}$$



Further algebraic manipulation leads to the following expression

$$\begin{aligned}
& \begin{bmatrix} \bar{Y}_{ph} & 0 & 0 \\ 0 & \bar{Y}_{ph} & 0 \\ 0 & 0 & \bar{Y}_{ph} \end{bmatrix} \begin{bmatrix} (V_a - V_b)_n (\cos(\theta_a - \theta_b) + i \sin(\theta_a - \theta_b)) \\ (V_a - V_b)_n (\cos(\theta_a - \theta_b) + i \sin(\theta_a - \theta_b)) \\ (V_a - V_b)_n (\cos(\theta_a - \theta_b) + i \sin(\theta_a - \theta_b)) \end{bmatrix} \\
&= \begin{bmatrix} I(\cos \beta + i \sin \beta) \\ I(\cos \beta + i \sin \beta) \\ I(\cos \beta + i \sin \beta) \end{bmatrix},
\end{aligned} \tag{5.19}$$

where

$$\bar{Y}_{ph} = \bar{Y}_{a_{ph}, b_{ph}} - \bar{Y}_{m_{pha,b}}. \tag{5.20}$$

Notice that the equations for each phase are identical and completely decoupled. Hence, the three conductors can be analysed using only one phase equation and the results applied to the other two (as was noted in chapter 3).

Substituting equations 5.16 and 5.17 into equation 5.20 gives

$$\begin{aligned}
\bar{Y}_{ph} = & \frac{\bar{Z}_{a,b} + \bar{Z}_m}{(\bar{Z}_{a,b} + 2\bar{Z}_m)(\bar{Z}_{a,b} - \bar{Z}_m)} + \frac{\bar{Z}_m}{(\bar{Z}_{a,b} + 2\bar{Z}_m)(\bar{Z}_{a,b} - \bar{Z}_m)}.
\end{aligned} \tag{5.21}$$

Hence the per-phase admittance for the balanced three-phase conductor, with mutual inductance between the conductors, is

$$\bar{Y}_{ph} = \frac{1}{(\bar{Z}_{a,b} - \bar{Z}_m)}. \tag{5.22}$$

$\bar{Y}_{ph}$  is the admittance value that should be used in equations 3.23a and 3.23b when calculating the transfer and short circuit driving port admittances for a node to which the per-phase conductor connects. The characteristic impedance of the per-phase conductor is therefore

$$\bar{Z}_{ph} = \bar{Z}_{a,b} - \bar{Z}_m. \quad (5.23)$$

The equivalent circuit model of the per phase conductor is as shown in figure 5.5.

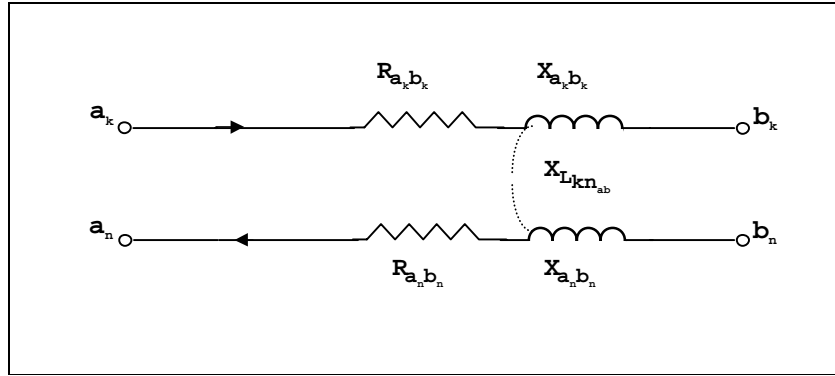


Figure 5.5 The per-phase equivalent circuit model of a three phase conductor.

#### 5.1.1.2 The Single Phase Conductor Model

The equivalent circuit for this is given in figure 5.6

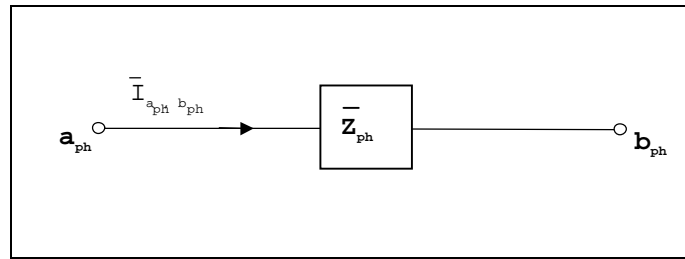


Figure 5.6 The single-phase conductor equivalent circuit model.

The model contains both a phase conductor and a neutral. Performing a similar analysis to that conducted on the three-phase line and referencing all voltage values to the neutral gives the following equation for the voltage drop across the conductor.

$$\bar{Y}_{a_k, b_k} (\bar{V}_{a_k} - \bar{V}_{b_k})_n = \bar{I}_{a_k, b_k}, \quad (5.24)$$

where  $k = 1, 2$ , or  $3$ .  $k$  relates to which phase flows along the single-phase conductor; in a single-phase system this subscript becomes irrelevant. The admittance term in the equation is given by

$$\bar{Y}_{a_k, b_k} = \frac{1}{(\bar{Z}_{a_k, b_k} + \bar{Z}_{a_n, b_n}) - 2\bar{Z}_{m_{ka, b}}} \quad (5.25)$$

$\bar{Y}_{a_k, b_k}$  is the admittance value that should be used in equations 3.23a and 3.23b when calculating the transfer and short circuit driving port admittances for a node to which the single-phase line connects.

The form of the equivalent circuit for the single phase conductor is identical to that of the per phase representation of the three phase conductor (see figure 5.6), however the characteristic impedance of this single phase conductor is

$$\bar{Z}_{a_k, b_k} = (\bar{Z}_{a_k, b_k} + \bar{Z}_{a_n, b_n}) - 2\bar{Z}_{m_{ka, b}}. \quad (5.26)$$

Note that this model can be used in a single phase and a comprehensive three-phase network model: where single-phase loads draw power from the three phase network, i.e. the mixed network case of section 3.4.2.4, or where nodes in the three phase network are connected by conductors with individual neutrals and no mutual couplings.

### 5.1.1.3 The d.c. Conductor Model

In the d.c. line model only resistance is considered, and all quantities are real as opposed to phasor values (see chapter 3). The line equivalent circuit model is given in figure 5.7.

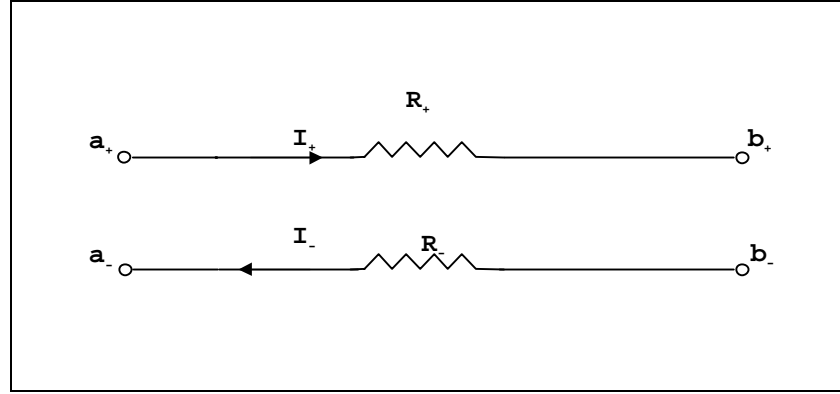


Figure 5.7 The d.c. conductor model.

Kirchhoff's voltage law can again be applied, so referencing all voltages to the negative conductor gives the following equation for the relationship between the current and voltage difference.

$$V_a - V_b = I^+ (R_{a^+,b^+} + R_{b^-,b^-}) . \quad (5.27)$$

The characteristic resistance of the conductor is therefore

$$R = (R_{a^+,b^+} + R_{a^-,b^-}) \quad (5.28)$$

and the general form of the conductance terms that would be used in equation 3.50 is

$$C_{a,b} = \frac{1}{(R_{a^+,b^+} + R_{a^-,b^-})} . \quad (5.29)$$

#### 5.1.1.4 Equivalent Circuit Parameters

Note that many comprehensive references exist, such as [4], which give the equivalent circuit parameters for a wide range of conductors. Oatley [1] and Gross [3] gives details of explicit methods for the calculation of the conductor parameters from first principles.

#### 5.1.1.5 Connection Resistances

Before leaving the subject of conductors, it is worth noting that in many short lengths of conductor the resistance of its end connections may be significant. These connection resistances can be represented on the equivalent circuit models by the addition of an extra series resistance term to the line series resistance as shown below.

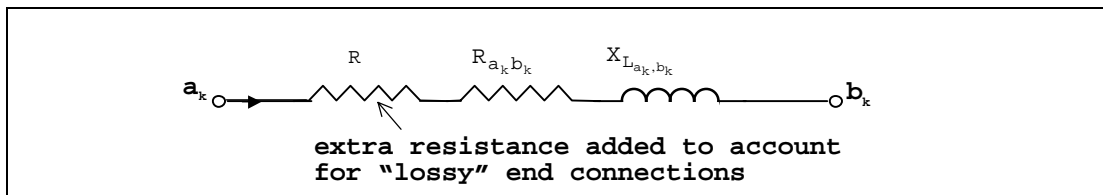


Figure 5.8 A conductor with connection resistances included.

### 5.1.2 Transformers

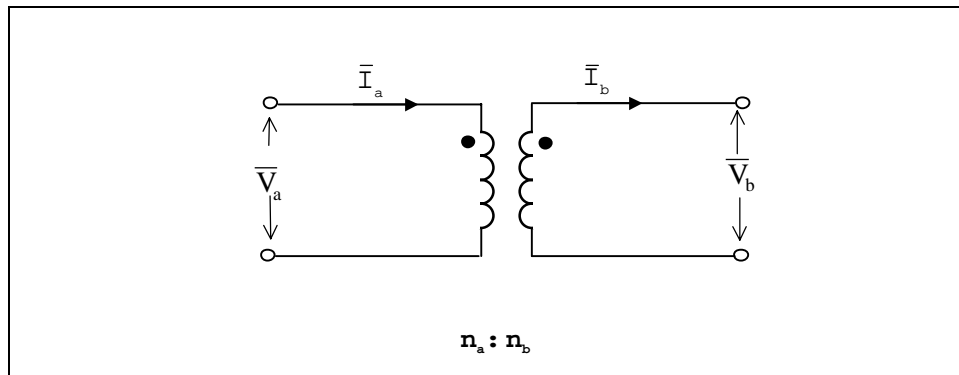
In an a.c. electrical system, the transformer performs two important functions: firstly, the voltage and current magnitudes between the two points it connects are, as the name suggests, transformed, secondly, the transformer convey power between these two points. This section describes the transformer's equivalent circuit model for use in the network representation of the electrical system.

If a transformer connects two points  $a$  and  $b$ , then the voltage at points  $a$  and  $b$  will be dictated by the transformer turns ratio, denoted by  $n_a/n_b$ , such that

$$\bar{V}_a = \frac{n_a}{n_b} \bar{V}_b, \quad (5.30)$$

similarly

$$n_a \bar{I}_a + n_b \bar{I}_b = 0. \quad (5.31)$$



An equivalent circuit model, for an ideal, two-winding<sup>15</sup> transformer is given in figure 5.9.

Figure 5.9 An ideal two-winding ideal transformer from [3].

---

<sup>15</sup> This refers to the construction of the transformer: which consists of a conductor wound round a core material. Note that a transformer may have two or more of windings, however only the very common two winding case is considered here.

Recall that in chapter 3 (section 3.4.2.2), the use of per unit values in the electrical network was said to reduce the complexity of the transformer model. Converting equation 5.30 to per unit form gives

$$\frac{\bar{V}_a}{\bar{V}_{a_{base}}} = \frac{n_a}{n_b} \frac{\bar{V}_b}{\bar{V}_{b_{base}}} . \quad (5.32)$$

As the relationship between base values is exactly the same as the relationships between the phasor values it follows that

$$\bar{V}_{a_{base}} = \frac{n_a}{n_b} \bar{V}_{b_{base}} . \quad (5.33)$$

Substituting this equation into 5.32 gives

$$\frac{\bar{V}_a}{\bar{V}_{a_{base}}} = \frac{n_a}{n_b} \left( \frac{n_b}{n_a} \frac{\bar{V}_b}{\bar{V}_{b_{base}}} \right) ; \quad (5.34)$$

so in per-unit terms

$$\bar{V}_{a_{pu}} = \bar{V}_{b_{pu}} . \quad (5.35)$$

Applying the same principles to the current in the transformer gives

$$\bar{I}_{a_{pu}} + \bar{I}_{b_{pu}} = 0 . \quad (5.36)$$

Hence, if the electrical network is analysed using per unit values, the transformers in the network will disappear. However, the effects of the transformers will still be evident in that the base voltage values change between points connected by them. The change in base values is dictated by the transformer turns ratio. In per-unit terms, the transformer can be thought of as a component which partitions the network into different base voltage sections, where the base

voltages of each section are related to the overall network base voltage by the turns ratios of the intervening transformer(s).

Returning to the equivalent circuit model of the transformer, it was noted that the circuit models of the conductors in the electrical network were dependent upon the nature of the system being modelled; the same is true for the transformer. The equivalent circuit models for different a.c. system types will be considered in the following sections.

#### **5.1.2.1 The Transformer Connected in three-phase**

The equivalent circuit for three, two-winding transformers in a three-phase connection (as would be used in a comprehensive three-phase electrical network) is shown in figure 5.10.



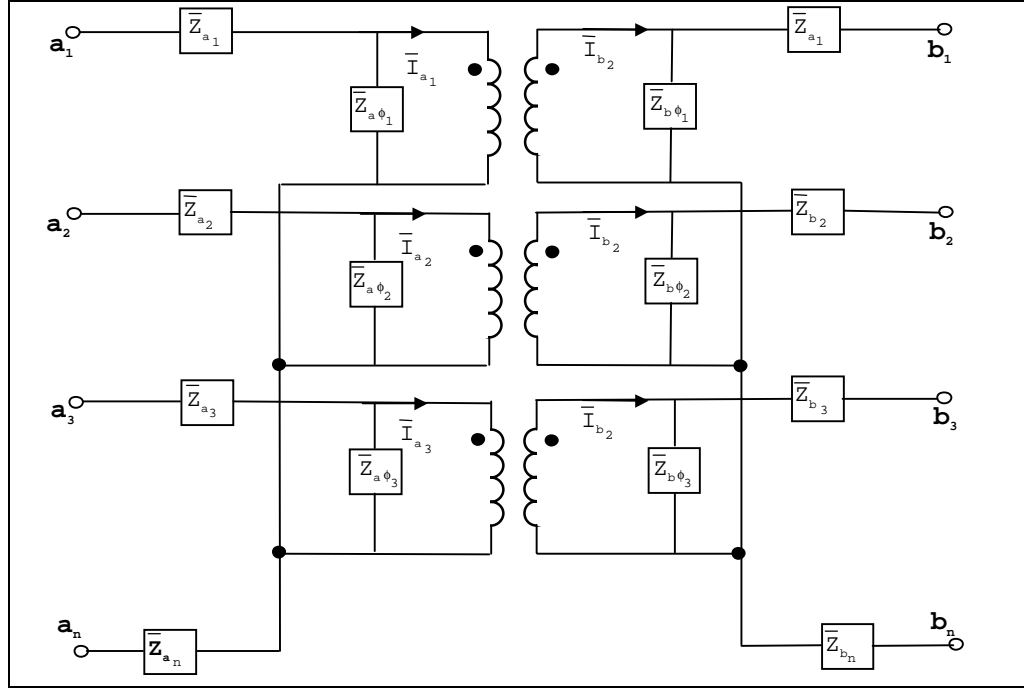


Figure 5.10 Three transformers in a three phase-connection<sup>16</sup> (modified from [3]).

Note that the transformer winding losses are now included: these take the form of the impedances  $\bar{Z}_{x_k}$  connected in series with each phase and the neutral. The parallel connected impedance terms,  $\bar{Z}_{x\phi_k}$ , are inserted into the circuit to represent losses in the core of the transformer. The circuit model can be simplified if the parallel-connected impedances are ignored; in most transformers (but not those used in small-scale embedded systems) the core losses are negligible (<1% [3]).

<sup>16</sup> Note that the circuit model is of two star-connected transformers (\*-\*). It is also possible to have star-delta and delta-delta connections, however these can be transformed to the star-star connection type shown above (for an example of these different connection types refer to Gross[3]).

By performing a similar analysis to that performed for the three-phase conductor, and ignoring the parallel connected impedances, the following matrix equations emerge for the voltages on either side of the transformer. Again, all voltages are referenced to the neutral conductor<sup>17</sup>.

For the left hand side of the circuit model

$$\begin{bmatrix} \bar{Z}_{a_1} + \bar{Z}_{a_n} & \bar{Z}_{a_n} & \bar{Z}_{a_n} \\ \bar{Z}_{a_n} & \bar{Z}_{a_2} + \bar{Z}_{a_n} & \bar{Z}_{a_n} \\ \bar{Z}_{a_n} & \bar{Z}_{a_n, b_n} & \bar{Z}_{a_3} + \bar{Z}_{a_n} \end{bmatrix} \begin{bmatrix} \bar{I}_{a_1} \\ \bar{I}_{a_2} \\ \bar{I}_{a_3} \end{bmatrix} = \begin{bmatrix} \bar{V}_{a_{1,n}} \\ \bar{V}_{a_{2,n}} \\ \bar{V}_{a_{3,n}} \end{bmatrix} \quad (5.37)$$

and for the right hand side of the circuit model

$$\begin{bmatrix} \bar{Z}_{b_1} + \bar{Z}_{b_n} & \bar{Z}_{b_n} & \bar{Z}_{b_n} \\ \bar{Z}_{b_n} & \bar{Z}_{b_2} + \bar{Z}_{b_n} & \bar{Z}_{b_n} \\ \bar{Z}_{b_n} & \bar{Z}_{b_n} & \bar{Z}_{b_3} + \bar{Z}_{b_n} \end{bmatrix} \begin{bmatrix} \bar{I}_{b_1} \\ \bar{I}_{b_2} \\ \bar{I}_{b_3} \end{bmatrix} = \begin{bmatrix} \bar{V}_{b_{1,n}} \\ \bar{V}_{b_{2,n}} \\ \bar{V}_{b_{3,n}} \end{bmatrix}. \quad (5.38)$$

If the equations are converted to per-unit form<sup>18</sup>, then the three, ideal transformer components can be eliminated and equation 5.35 applied to all three phases such that:

$$\bar{I}_{a_1} = -\bar{I}_{b_1}; \quad (5.39a)$$

---

<sup>17</sup> Note that in any transformer if the neutral conductor on one or both sides of the transformer are earthed, then the value of the earthed neutral impedance is zero, i.e.  $\bar{Z}_{n_x} = 0$ .

<sup>18</sup> The pu subscript is omitted for clarity; all circuit state variables from this point on will be in per-unit form.

$$\bar{I}_{a_2} = -\bar{I}_{b_2}; \quad (5.38b)$$

$$\bar{I}_{a_3} = -\bar{I}_{b_3}. \quad (5.38c)$$

Subtracting the per-unit form of equation 5.36 from 5.37 and substituting the equations 5.38a-c eventually gives

$$\begin{bmatrix} \bar{Z}_{a_1} + \bar{Z}_{b_1} + \bar{Z}_{a_n} + \bar{Z}_{b_n} & \bar{Z}_{a_n} + \bar{Z}_{b_n} & \bar{Z}_{a_n} + \bar{Z}_{b_n} \\ \bar{Z}_{a_n} + \bar{Z}_{b_n} & \bar{Z}_{a_2} + \bar{Z}_{b_2} + \bar{Z}_{a_n} + \bar{Z}_{b_n} & \bar{Z}_{a_n} + \bar{Z}_{b_n} \\ \bar{Z}_{a_n} + \bar{Z}_{b_n} & \bar{Z}_{a_n} + \bar{Z}_{b_n} & \bar{Z}_{a_3} + \bar{Z}_{b_3} + \bar{Z}_{a_n} + \bar{Z}_{b_n} \end{bmatrix} \begin{bmatrix} \bar{I}_{a_1} \\ \bar{I}_{a_2} \\ \bar{I}_{a_3} \end{bmatrix} = \begin{bmatrix} (\bar{V}_{a_2} - \bar{V}_{a_2})_n \\ (\bar{V}_{a_2} - \bar{V}_{b_2})_n \\ (\bar{V}_{a_3} - \bar{V}_{c_3})_n \end{bmatrix}. \quad (5.40)$$

This is the basic, characteristic equation for the transformer in a comprehensive three-phase network model, with all values in per unit notation. Note that the neutral impedance terms couple the individual phase equations.

Equation 5.39 can be re-written in admittance form:

$$\begin{bmatrix} \bar{Y}_{a_{ph},b_{ph}} & \bar{Y}_{m_{pha,b}} & \bar{Y}_{m_{pha,b}} \\ \bar{Y}_{m_{pha,b}} & \bar{Y}_{a_{ph},b_{ph}} & \bar{Y}_{m_{pha,b}} \\ \bar{Y}_{m_{pha,b}} & \bar{Y}_{m_{pha,b}} & \bar{Y}_{a_{ph},b_{ph}} \end{bmatrix} \begin{bmatrix} (\bar{V}_{a_1} - \bar{V}_{b_1})_n \\ (\bar{V}_{a_2} - \bar{V}_{b_2})_n \\ (\bar{V}_{a_1} - \bar{V}_{b_2})_n \end{bmatrix} = \begin{bmatrix} \bar{I}_{a_1} \\ \bar{I}_{a_2} \\ \bar{I}_{a_3} \end{bmatrix}. \quad (5.41)$$

The per-unit admittance values are defined as follows.

$$\bar{Y}_{a_{ph},b_{ph}} = \frac{(\bar{Z}_{a_{ph}} + \bar{Z}_{b_{ph}}) + 2(\bar{Z}_{a_n} + \bar{Z}_{b_n})}{\left[ (\bar{Z}_{a_{ph}} + \bar{Z}_{b_{ph}}) + 3(\bar{Z}_{a_n} + \bar{Z}_{b_n}) \right] (\bar{Z}_{a_{ph}} + \bar{Z}_{b_{ph}})}, \quad (5.42)$$

Note, by the symmetry of the transformers in three-phase connection:

$$\bar{Z}_{a_k} = \bar{Z}_{a_{ph}} \text{ and } \bar{Z}_{b_k} = \bar{Z}_{b_{ph}}, k = 1, 2, 3.$$

Also,

$$\bar{Y}_{m_{ph_{a,b}}} = \frac{-(\bar{Z}_{a_n} + \bar{Z}_{b_n})}{\left[ (\bar{Z}_{a_{ph}} + \bar{Z}_{b_{ph}}) + 3(\bar{Z}_{a_n} + \bar{Z}_{b_n}) \right] (\bar{Z}_{a_{ph}} + \bar{Z}_{b_{ph}})}. \quad (5.43)$$

$\bar{Y}_{a_{ph},b_{ph}}$  and  $\bar{Y}_{m_{ph_{a,b}}}$  are the admittance values that would be used to calculate the admittance terms of equations 3.44a and 3.44b: the power balance equations for the three-node arrays to which the transformer equivalent circuit connects.

### 5.1.2.2 The Per-Phase Transformer Model

Applying the equations for current and voltage under balanced operating conditions (3.39 to 3.40) to equation 5.42, gives the following.

$$\begin{bmatrix} \bar{Y}_{ph} & 0 & 0 \\ 0 & \bar{Y}_{ph} & 0 \\ 0 & 0 & \bar{Y}_{ph} \end{bmatrix} \begin{bmatrix} \left( V_{a_1} - V_{b_1} \right)_n (\cos(\theta_a - \theta_b) + i \sin(\theta_a - \theta_b)) \\ \left( V_{a_2} - V_{b_2} \right)_n (\cos(\theta_a - \theta_b) + i \sin(\theta_a - \theta_b)) \\ \left( V_{a_3} - V_{b_3} \right)_n (\cos(\theta_a - \theta_b) + i \sin(\theta_a - \theta_b)) \end{bmatrix} = \begin{bmatrix} I(\cos \beta_{a,b} + i \sin \beta_{a,b}) \\ I(\cos \beta_{a,b} + i \sin \beta_{a,b}) \\ I(\cos \beta_{a,b} + i \sin \beta_{a,b}) \end{bmatrix}. \quad (5.44)$$

As was the case with the three-phase conductor, the equations for each phase of the transformer, in balanced operation, are identical and decoupled. The results of an analysis on one phase of the transformer can therefore be applied to the other three phases.

The diagonal elements in the admittance matrix of equation 5.44 are given by

$$\bar{Y}_{ph} = \bar{Y}_{a_{ph}, b_{ph}} - \bar{Y}_{m_{ph_{a,b}}} . \quad (5.45)$$

Substituting equations 5.42 and 5.43 into this expression gives

$$\bar{Y}_{ph} = \frac{1}{\bar{Z}_{a_{ph}} + \bar{Z}_{b_{ph}}} . \quad (5.46)$$

Equation 5.46 gives the admittance value that should be used in equations 3.23a and 3.23b, when calculating the short-circuit driving port and transfer admittances of nodes (in a balanced three-phase network) to which the transformer connects. The equivalent circuit model is as shown in figure 5.11.

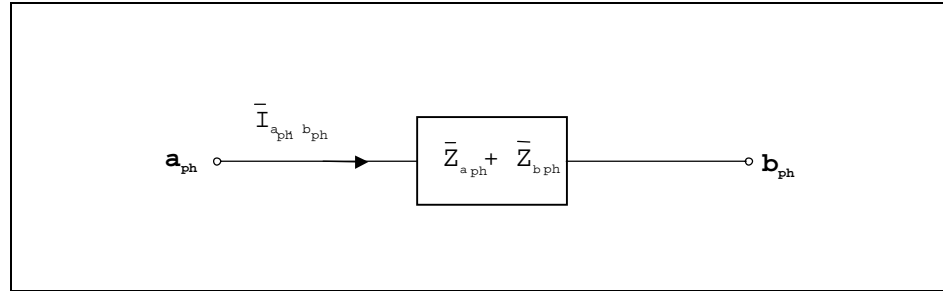


Figure 5.11 The per-phase, per-unit model of the three-phase transformer.

The characteristic impedance of the per phase model is given by

$$Z_{a_{ph}, b_{ph}} = \bar{Z}_{a_{ph}} + \bar{Z}_{b_{ph}} . \quad (5.47)$$

Note, because the voltage base changes between  $a$  and  $b$ , the impedance bases,  $Z_{base\ a}$  and  $Z_{base\ b}$  used in the calculation the  $\bar{Z}_{a_{ph}}$  and  $\bar{Z}_{b_{ph}}$  per-unit values, will also change:  $Z_{base\ a} = \frac{(V_{base\ a})^2}{S_{base}}$  and  $Z_{base\ b} = \frac{(V_{base\ b})^2}{S_{base}}$ .  $S_{base}$  remains the same throughout the system.

### 5.1.2.3 The Basic Two-Winding Transformer Model

The per-unit equivalent circuit for a transformer, connected in single-phase network is shown in figure 5.12

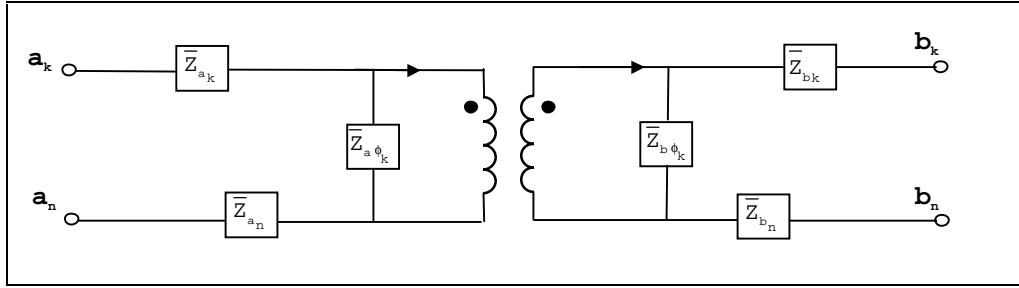


Figure 5.12 The equivalent circuit model of a transformer in a single phase network.

Applying the same analysis techniques as used previously gives the following equation, which relates the per unit voltage drop, current and impedance (again ignoring the parallel connected impedances):

$$\bar{V}_{a_k} - \bar{V}_{b_k} = \bar{I}_{a_k} \left[ (\bar{Z}_{a_k} + \bar{Z}_{b_k}) + (\bar{Z}_{a_n} + \bar{Z}_{b_n}) \right] \quad k = 1, 2 \text{ or } 3. \quad (5.48)$$

The equivalent circuit model of the model is of exactly the same form as the per-phase equivalent circuit model, though note that the characteristic impedance is given by the term in square brackets in equation 5.47.

The admittance that should be used in the calculation of the short-circuit driving port and transfer admittance of the nodes to which the single phase transformer component connects is

$$Y_{a_k, b_k} = \frac{1}{(\bar{Z}_{a_k} + \bar{Z}_{b_k}) + (\bar{Z}_{a_n} + \bar{Z}_{b_n})}. \quad (5.49)$$

Note that the models derived here, for the basic two-winding transformer and transformers in three phase connections, are far from a complete catalogue of all possible transformer types: transformers with off-nominal turns ratios, 3 or more windings and transformers with different permutations of three-phase connections are not considered. Weedy [2], Gross [3] and Stagg and El-Abiad [5] give circuit models and derivations of characteristic equations for various other transformer types.

## 5.2 Hybrid Components

The loads and sources which connect to the electrical network were described in the last chapter as ‘hybrid’ components, as they also exist in other areas of the ESP-r model: the fabric, the plant network, the flow network and the fluid volumes which form the interior space of the building. As mentioned in the last chapter, the function of these hybrid components is to translate the electrically related heat and fluid flow phenomena occurring in the building to the power flows, which act as boundary data for the electrical network. These hybrid components are described in the following sections.

### 5.2.1 Hybrid Load Components

#### 5.2.1.1 Lighting and Small Power Loads

These power loads interact with both the thermal and electrical constituents of an ESP-r model, in that they draw power from the electrical network and also dissipate heat into the thermal zones. Currently, the thermal output from each power load manifests itself in the form of a convective heat gain to the associated fluid volume, and as a radiative gain to the surface layers

of the multi-layered constructions surrounding the fluid volume. Recall, that the characteristic equations which represent both the fluid volume and surface layers contained heat injection terms that could represent the heat gain from internal sources (refer to equations 2.8 and 2.23 respectively). The total heat gain (W) from a power-consuming component  $i$  would be given by

$$q_{i_c} + \sum_{s=1}^n q_{r_s} , \quad (5.50)$$

where  $q_{i_c}$  is the convective heat dissipated to the zone air volume and  $\sum_{s=1}^n q_{r_s}$  is the sum of the radiant heat dissipated to the surrounding surfaces.

In ESP-r, heat gains from equipment, lighting and occupants are defined as generic ‘casual gains’ [6]. Casual gains are time-variant and have radiant and convective portions. The temporal variation of the gain during the simulation is obtained by multiplying a base gain (W) by a time-varying profile, the magnitude of which varies between 0 and 1. Lighting gains can also be subjected to daylight control. The thermal gains to the zone will therefore vary with time and climate-dependent control action. To obtain the power consumption information from these thermal gains it is necessary to hybridise them, i.e. relate their heat emission to their electrical power consumption. The resulting hybrid casual gain and electrical entity is defined as a ‘zone load’ component.

Each piece of power consuming equipment (in the form of a zone load) acts like a resistor, dissipating heat to the environment with 100% efficiency. All real power consumed by the component is assumed to be (eventually) dissipated as heat. The coupling between the heat emission and the power consumption of the electrical load is given by the following trivial equation.

$$q_{i_c} + \sum_{s=1}^n q_{r_s} = P_i . \quad (5.51)$$



However, equation 5.51 provides only half of the information required for the translation of a thermal gain to an electrical load, as the reactive power consumption is still unknown. Provision of this information requires additional information from the modeller in the definition of the zone load component. The basic information required by each casual gain is as follows.

Type	Heat dissipated	Radiant Fraction	Convective Fraction	Time on	Time off
Equipment/ lighting/ occupant	(W)	%	%	(hrs)	(hrs)

Table 5.1 Information provided for a casual gain.

This information was augmented with the electrical data given in the following table.

Operating Voltage	Power factor (pf)	Load type	Base power consumption (=base heat load)	Connected phase	Connected electrical network node
(V)	(0 - 1)	capacitive, resistive, reactive	(W)	(1,2,3 or all)	(-)

Table 5.2 Additional information for a zone load.

The information allows all the relevant power flow information to be deduced from the thermal heat dissipation of the casual gain. The reactive power consumption is given by

$$Q_i = P \left( \frac{1}{pf_i} - 1 \right)^{0.5} \quad 0 < pf \leq 1 \quad (5.52)$$

The power factor,  $pf$ , is defined as the ratio of the real power consumption of the component divided by the magnitude of the apparent power consumption:

$$pf_i = \frac{P_i}{\left( P_i^2 + Q_i^2 \right)^{0.5}} \quad (5.53)$$

Note that the nature of the load determines the characteristics of its reactive power consumption. If the load is inductive, then the reactive power consumption is assigned a positive value:  $+jQ$  . If the load is capacitive, then the reactive power consumption is assigned a negative value:  $-jQ$  ; reactive and capacitive power are diametrically opposed.

The real power consumptions of or many types of small power loads are given in [7], though this reference contains no information on small load power factors. Information on lighting and rotational load power consumptions and power factors is given in [8] and [9] respectively.

The other electrical information determines where the electrical load draws power from the electrical network. In a balanced system, the load is assumed to draw power evenly from all three phases of the power system. If the three-phase system is modelled comprehensively, the connected node and phase data would be used to identify which node of a three-node array the load would draw power from. Three-phase loads such as fans and pumps would power from all three nodes. The voltage information can be used to check the operating voltage of the load component against the predicted voltage of the connected electrical load; if the two differ significantly, the zone load may be switched off by a control law (see section 5.5.1).

Note that the zone load component inherits all the characteristics of the associated casual gain, and so the electrical load drawn from the network by each particular component will vary (as was stated in section 5.2.1.1) both temporally and with climate influenced control.

As an example to illustrate the function of the zone load, consider the case of daylight responsive luminaires. These will be controlled based on lighting levels inside a zone (calculated by ESP-r or perhaps RADIANCE<sup>19</sup> running in tandem with ESP-r), with the lighting control altering the light output of the luminaires to maintain a constant illumination level. The control of light output will affect the heat dissipated by the lights into to the zone and also their electrical

---

<sup>19</sup> A lighting simulation tool produced by Lawrence Berkeley Laboratories

power consumption. The lighting hybrid component will therefore provide a time-varying power flow boundary condition to the electrical network, while also providing a related time-varying heat input to the lit zone. This hybrid component therefore acts as a coupling mechanism between the thermal and electrical energy flows associated with the zone. The temporal variation of these energy flows is primarily affected by the characteristics of the daylight control and the prevailing climatic conditions. The concept of the hybrid component is shown schematically in figure 5.

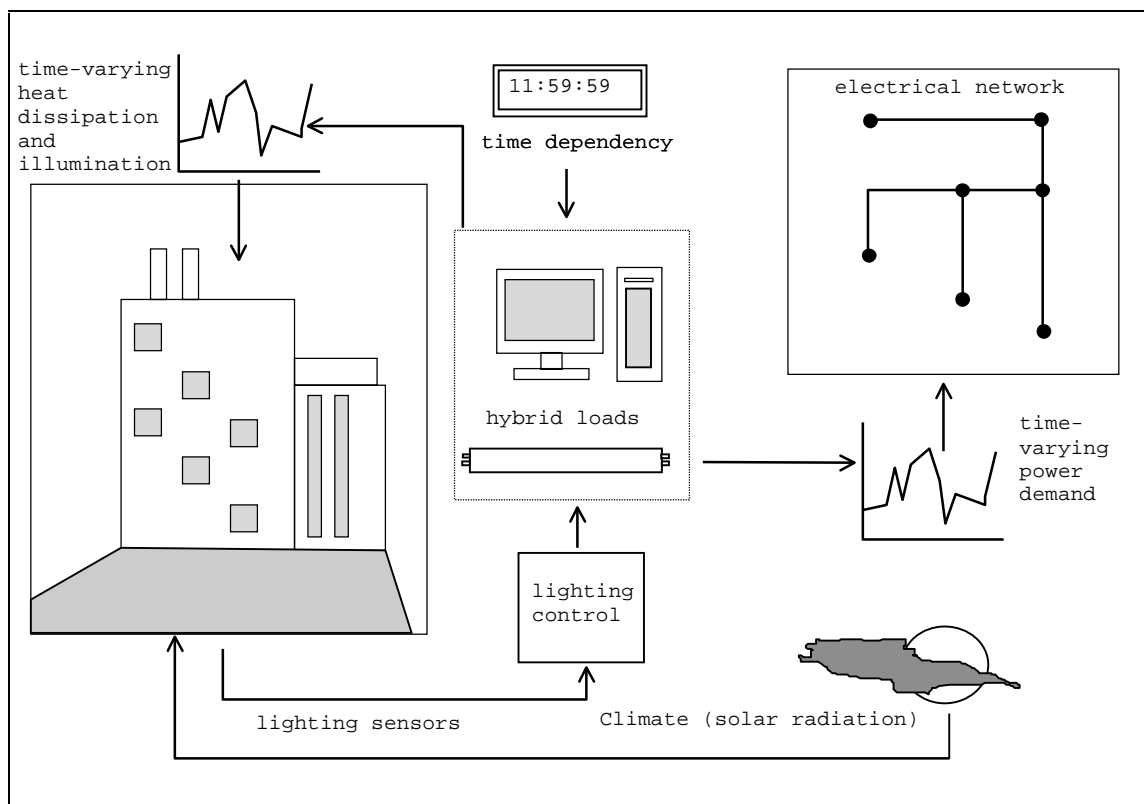


Figure 5.13 The schematic definition of a zone load.

### 5.2.2 Fans and Pumps

In ESP-r both fans and pumps can be labelled with the generic term ‘flow-inducing components’, and exist in both the plant and fluid flow networks. Hence, in an integrated ESP-r

model, the flow inducing entities can be constructed using both a plant and fluid flow component model; the fluid flow component calculates the pressure and flow characteristics, while the plant component deals with the energy balance. The descriptions of both the plant and fluid flow components for fans and pumps are given in [10] and [11].

To determine the power consumption of the fan or pump it is necessary to hybridise the plant component model by the addition of an extra energy balance equation; this relates the component flow characteristics to its power consumption. The foundation for this relation is an equivalence of electrical and mechanical power, for which it is necessary to express the mechanical power consumption,  $P_m$  (W), of the component in terms of the induced flow. This relationship is given by the following equation.

$$P_m = \frac{\dot{m}\Delta P}{\eta_m} \quad (5.54)$$

$\dot{m}$  is the induced mass flow rate (kg/s) resulting from the pressure rise,  $\Delta P$  (Pa), across the component and  $\eta_m$  is the mechanical efficiency of the flow-inducing component.

The following cubic polynomial relationship is given in [11] and relates the pressure rise and flow rate in ESP-r's flow inducing components (both pumps and fans).

$$\Delta P = a_o + a_1 \left[ \frac{\dot{m}}{\rho} \right] + a_2 \left[ \frac{\dot{m}}{\rho} \right]^2 + a_3 \left[ \frac{\dot{m}}{\rho} \right]^3 \quad (5.55)$$

$a_{i=1..3}$  are empirically obtained coefficients which fit equation 5.54 to the flow component's performance curve: this is usually supplied by the manufacturer;  $\rho$  is the working fluid density (kg/m<sup>3</sup>).

The mechanical power required by the component is given by the substitution of equation 5.55 into equation 5.54:

$$P_m = \frac{\dot{m}}{\eta_m} \left( a_o + a_1 \left[ \frac{\dot{m}}{\rho} \right] + a_2 \left[ \frac{\dot{m}}{\rho} \right]^2 + a_3 \left[ \frac{\dot{m}}{\rho} \right]^3 \right). \quad (5.56)$$

The mechanical power to the flow inducing component will be provided by an electrical motor, the performance of which can be characterised by a conversion efficiency; this relates the electrical power consumption of the motor to the mechanical power consumed inducing the flow of working fluid. The relation is as follows.

$$P_m = \eta_e P_e. \quad (5.57)$$

Substituting this expression into equation 5.56 gives the relationship between the induced flow rate in the fan or pump and electrical power consumption of the electrical motor that would be required to produce it.

$$P_e = \frac{\dot{m}}{\eta_m \eta_e} \left( a_o + a_1 \left[ \frac{\dot{m}}{\rho} \right] + a_2 \left[ \frac{\dot{m}}{\rho} \right]^2 + a_3 \left[ \frac{\dot{m}}{\rho} \right]^3 \right). \quad (5.58)$$

Note that as with the casual gain coupling equation (5.51), this equation only determines the real power consumption of the fan or pump. To determine the reactive power consumption, additional information must be used with the plant component. This additional information is similar to that which augmented the casual gains.

Operating Voltage	Power factor (pf)	Load type	Efficiency of electric motor	Connected phase	Connected electrical node
(V)	(0 - 1)	capacitive, reactive	(0 - 1)	(1,2,3 or all)	(-)

Table 5.3 Additional information required for a power consuming plant component.

The reactive power consumption is calculated using equation 5.52, and assigned a positive or negative value according to the load type.

Flow inducing components can be subject to control action, with the possibility of the flow rate of each being varied according to temperature, pressure, humidity or some other sensed property somewhere in the building model. Note also, that the thermophysical and fluid flow property terms, used in the equation to calculate the power consumption, will vary as the pressure and temperatures of the plant and flow networks change with time. As a consequence, the power consumption of the plant component, like those of the casual gains, will also change with time according to control action, thermal and flow conditions, providing a fluctuating power flow boundary condition to the electrical network.

## 5.3 Hybrid Electrical Power Generation Components

### 5.3.1 Small-Scale Combined Heat and Power (CHP)

A small scale combined heat and power system consists of two basic physical elements: an engine and generator unit and a heat recovery system. The engine and generator provide power to the electrical network, while the heat recovered (in the form of hot water) from the engine jacket cooling water and exhaust gas can be used in the plant network.

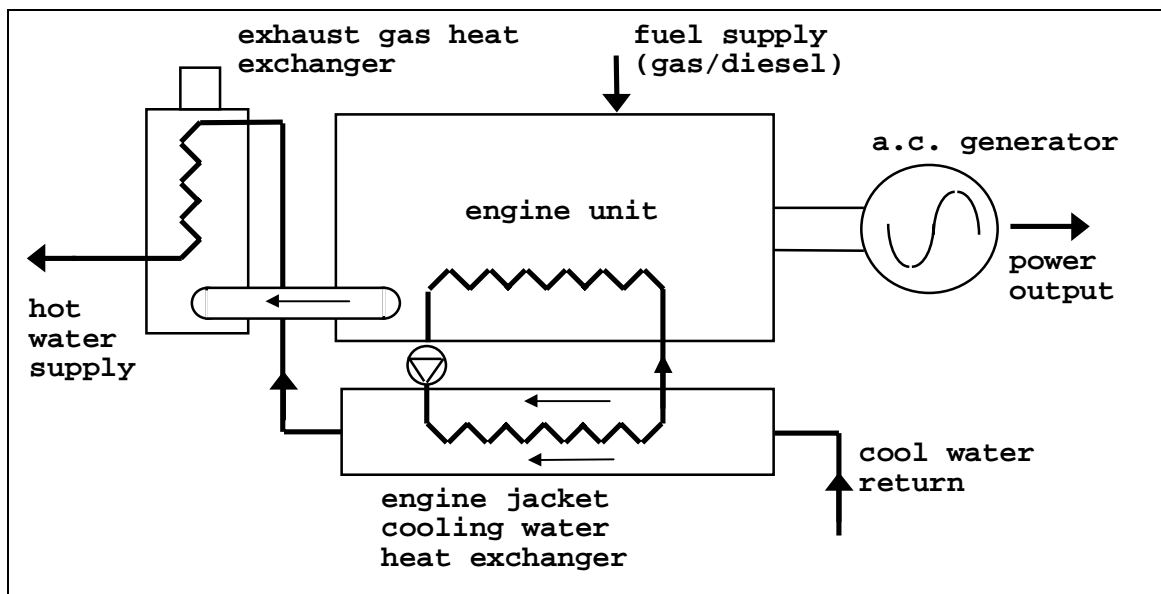


Figure 5.14 A small-scale combined heat and power unit (from [12]).

Small scale combined heat and power systems, as shown in figure 5.14, are an integral part of a building's electrical and hot water services; the ESP-r model of the CHP unit was developed with this in mind and can be integrated into both the plant and electrical network. The model is constructed from a number of plant components. Each is modelled using control volumes:

- an engine and generator unit (a hybrid thermal electrical component);
- a cooling water heat exchanger (a purely thermal component);
- a gas - air heat exchanger (another purely thermal plant component).

The following sections describe these component models which, when combined with an ESP-r plant network, form a model of a CHP system integrated into a building's hot water services. The plant network can, in turn, be integrated with the rest of the ESP-r building model, including a coupling to the electrical network, forming a complete model of the CHP building-integrated energy system. A system model of this type is shown in the exemplar of chapter 7.

#### **5.3.1.1 The Engine and Generator Unit**

The basis for the description of the engine and generator unit, as with all the other plant components in ESP-r is the control volume. The Engine unit shown in figure 5.14 can be represented by three control volumes:

- a combustion gas control volume;
- a solid engine block control volume;
- a coolant control volume.

The three-node model is a depiction of the basic thermodynamic processes occurring inside the CHP unit. The combustion gas node represents the hot gas/fuel mixture contained in the engine cylinders. This transfers heat to the engine block, which loses heat to the environment and circulating cooling water, which is represented by the coolant control volume.

This three-node model is used as it can be easily integrated into an ESP-r model. The hot water node can be coupled directly to ESP-r heating system components in a plant network (i.e. heat exchangers, piping, pumps, etc.). The combustion chamber node can induce air from and exhaust to a gas node representing atmospheric air. The connection of the model into an ESP-r plant network is shown in chapter 7.

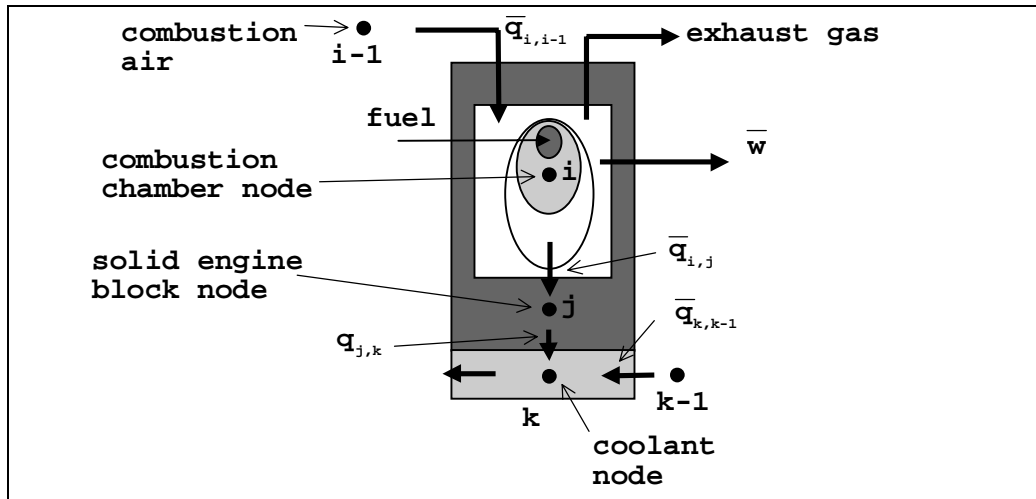


Figure 5.15 The three node model of the CHP engine unit.

The model is clearly an abstraction of the real engine and should be seen as a compromise between a purely “black box” input/output model and more complex (though usually partial) models such as that detailed by McCrorie et al. [13]. These are generally unsuitable for integration into energy simulation tools as, for reasons of numerical stability, they require processing with very small time steps ( $<0.0000001$ s). The form of the model is shown in figure 5.15



#### 5.3.1.1.1 The Combustion Gas Control Volume

The four-stroke cycle of the engine unit, consisting of an induction, compression, power and exhaust stroke, can be considered as a continual, cycle-averaged thermodynamic process, if the period of analysis is much greater than the time period of the individual strokes. This is generally the case in an energy simulation. Further, if the cycle is averaged, then all the cylinders can be lumped into the one control volume, because at any time  $t$  they will be at the same, averaged state. Application of the first law of thermodynamics to the lumped control volume, gives rise to the following one-dimensional, energy balance equation for the cycle-averaged combustion process:

$$\bar{q}_c = \bar{q}_{i-1,i} + \bar{q}_{i,j} + \bar{w}_i . \quad (5.59)$$

A barred variable represents a quantity averaged over all the phases of the four stroke-cycle.  $\bar{q}_c$  is the heat release rate from fuel combustion (W),  $\bar{q}_{i-1,i}$  is the energy loss due to the intake of cool combustion air into the cylinders (W),  $\bar{q}_{i,j}$  is the heat loss to the cylinder walls and  $\bar{w}_i$  is the net mechanical work output from the combustion process (W).

The heat release from combustion can be calculated from

$$\bar{q}_c = \eta_c \dot{m}_f CV , \quad (5.60)$$

where  $\eta_c$  is the efficiency of combustion in the engine cylinders,  $\dot{m}_f$  is the fuel mass flow rate (kg/s) and  $CV$  is its calorific value (J/kg).

The heat transfer due to the induction of air for the combustion process is given by

$$\bar{q}_{i,i-1} = \dot{m}_{i-1} c_{i-1} (\theta_{i-1} - \bar{\theta}_i) . \quad (5.61)$$

$\dot{m}_{i-1}$  is the mass flow rate of combustion air, and  $c_{i-1}$  is its specific heat (J/kgK).  $\theta_{i-1}$  is the temperature of the gas leaving control volume  $i$ .

The heat transfer with the cylinder walls is calculated from the following equation.

$$q_{i,j} = \bar{h}_{cy} \bar{A}_{cy} (\theta_j - \bar{\theta}_i) \quad (5.62)$$

$\theta_j$  is the temperature of the neighbouring engine block node  $\bar{h}_{cy}$  is the cycle-averaged heat transfer coefficient (W/m<sup>2</sup>K) at the cylinder walls and  $A_{cy}$  is the cycle averaged cylinder heat transfer surface area (m<sup>2</sup>).  $\bar{h}_{cy}$  can be calculated by the time-averaged version of the empirical equation given by Woschini [14]. Alternatively engine test data can be used to calculate the overall cylinder wall conductance ( $\bar{h}_{cy} \bar{A}_{cy}$ ) for the cycle-averaged combustion process; this is discussed further in the next chapter.

Finally, the work output of the cylinder is the work of the engine unit after frictional losses have been accounted for. Frictional losses are considered to be a heat gain in the cylinder and are therefore lumped together with the heat release term  $q_c$ .

Combining equations 5.59-5.62 gives the following fully explicit, characteristic equation for the gas control volume at some time  $t$  (the effect of any thermal capacitance of the cylinder gases is neglected).

$$-(\dot{m}_{i-1}^t c_{i-1} + \bar{h}_{cy}^t A_{cy}) \bar{\theta}_i^t + \dot{m}_{i-1}^t c_{i-1} T_{i-1}^t + \bar{h}_{cy}^t A_{cy} T_j^t = \bar{w}^t. \quad (5.63)$$

The calculated temperature  $\bar{\theta}_i$  is the exhaust temperature of the combustion process, as all the heat transfers, energy losses and transformations (i.e. heat to work) are accounted for in equation 5.63.

The work term  $\overline{w}^t$  is important as this is the link with the electrical output of the CHP unit and enables the engine component to be made hybrid. The term represents the shaft power to the rotor of the electrical generator, attached to the engine unit. The electrical power output of the generator (W), which is fed into the electrical network, is calculated by

$$P_e = \eta_e \overline{w}^t, \quad (5.64)$$

where  $\eta_e$  is the electrical conversion efficiency of the generator attached to the CHP unit. The reactive power output of the generator can be a controllable quantity<sup>20</sup> and is discussed in section 5.3.2.1. Note it is also possible to explicitly model the generator attached to the CHP unit. Generator equivalent circuits are given in appendix 2.

#### 5.3.1.1.2 The Engine Block Control Volume

The basic form of the energy balance for the engine block node  $j$  is as follows

$$M_j c_j \frac{\partial \theta_j}{\partial t} = q_{j,i} + q_{j,k} + q_{j,\infty}. \quad (5.65)$$

The left hand side of equation 5.65 represents the thermal capacitance of the engine block;  $M_j$  is its mass (kg),  $C_j$  its volume-weighted, average specific heat (J/kgK). The terms on the right hand side are the basic energy exchanges associated with the engine block.

$q_{j,\infty}$  is the heat loss from the engine block to the environment, which is given by

---

<sup>20</sup> This is possible with synchronous generators, but *not* with asynchronous generators, which always absorb reactive power (see appendix 2).

$$q_{j,\infty} = K_{j,\infty}(\theta_\infty - \theta_j), \quad (5.66)$$

where  $K_{j,\infty}$  is the heat loss modulus from the engine exterior to the surroundings (W/K) and  $\theta_\infty$  is the environmental temperature of the surroundings.

$\bar{q}_{j,i}$  is the heat transfer from the walls of the cylinders, given by negative form of equation 5.62:

$$\bar{q}_{j,i} = \bar{h}_{cy} \bar{A}_{cy} (\bar{\theta}_i - \theta_j). \quad (5.67)$$

$\bar{q}_{j,k}$  is the heat transferred to the cooling water flowing through the engine block, this is given by:

$$q_{j,k} = h_{j,k} A_c (\theta_k - \theta_j). \quad (5.68)$$

$A_c$  is the heat transfer surface area between the engine block and the cooling water, which has a temperature  $\theta_k$ .  $h_{j,k}$  is the heat transfer coefficient between the cooling water and the engine block. If the cooling water flows through the engine in enclosed channels, the following equation (from [15]) can be used to determine the heat transfer coefficient, assuming fully turbulent flow predominates:

$$\text{Nu} = 0.023 \text{Re}^{0.8} \text{Pr}^n. \quad (5.69)$$

The dimensionless groupings of equation 5.69 are defined as follows.

The Reynolds number is given by  $\text{Re} = \frac{\rho V D_h}{\mu}$ , where  $\rho$  is the coolant density ( $\text{kg/m}^3$ ),  $V$  is its velocity ( $\text{ms}^{-1}$ ) and  $\mu$  is the fluid viscosity ( $\text{kg/ms}$ ).  $D_h$  is the hydraulic radius (m) of the enclosed channel, given by  $D_h = \frac{4 \times \text{flow area}}{\text{wetted perimeter}}$ .

The Nusselt number is given by  $Nu = \frac{h_c D_h}{k}$ , where  $h_c$  is the heat transfer coefficient between the coolant and the channel wall and  $k$  is the conductivity of the coolant (W/mK).

The Prandtl number is given by  $Pr = \frac{c_p \mu}{k}$ ,  $c_p$  is the specific heat of the coolant.

All the fluid parameters are evaluated at the mean temperature of the coolant and enclosed channel walls, i.e.  $(\theta_j^t + \theta_k^t) / 2$ .

As with the cylinder wall heat transfer equations, an alternative to the explicit calculation of the coolant circuit heat transfer coefficient is to use test data to calculate the overall thermal conductance ( $h_{j,k} A_c$ ) between the engine jacket and cooling water. This is discussed when model calibration is considered in the next chapter.

Combining equations 5.65 to 5.68 and replacing the partial derivative with a backward difference expression, gives the following explicit equation for the engine block temperature  $\theta_j^{t+\Delta t}$ .

$$M_j^t c_j^t \left( \frac{\theta_j^{t+\Delta t} - \theta_j^t}{\Delta t} \right) = \bar{h}_{cy}^t \bar{A}_{cy} (\bar{\theta}_i^t - \theta_j^t) + h_{j,k}^t A_c (\theta_k^t - \theta_j^t) + h_\infty^t A_e (\theta_\infty^t - \theta_j^t) \quad (5.70)$$

Combining this explicit expression with its implicit counterpart creates the following familiar form of characteristic equation for the engine block control volume:

$$\begin{aligned}
& \left[ \frac{2M_j^{t+\Delta t} c_j^{t+\Delta t}}{\Delta t} + h_{cy}^{t+\Delta t} A_{cy} + h_{j,k}^{t+\Delta t} A_c \right] \theta_j^{t+\Delta t} \\
& - h_{cy}^{t+\Delta t} A_{cy} \bar{\theta}_i^{t+\Delta t} - h_{j,k}^{t+\Delta t} A_c \theta_k^{t+\Delta t} - h_{\infty}^{t+\Delta t} A_e \theta_{\infty}^{t+\Delta t} \\
& = \left[ \frac{2M_j^t c_j^t}{\Delta t} + h_{cy}^t A_{cy} + h_{j,k}^t A_c \right] \theta_j^t + h_{cy}^t A_{cy} \bar{\theta}_i^t + h_{j,k}^t A_c \theta_k^t + h_{\infty}^t A_e \theta_{\infty}^t.
\end{aligned} \tag{5.71}$$

#### 5.3.1.1.3 The Cooling Water Control Volume

The basic energy balance equation for the cooling water control volume is

$$M_k c_k \frac{\partial \theta_k}{\partial t} = q_{k,k-1} + q_{k,j}. \tag{5.72}$$

The left-hand side of the equation represents the thermal capacity of the cooling fluid encapsulated by the control volume (i.e. contained in the enclosed channels of the engine block);  $M_k$  is its mass and  $C_k$  is its specific heat. The  $q_{k,k-1}$  term is the heat exchange caused by coolant entering the control volume from a connected node ( $k-1$ ) in the plant network:

$$q_{k,k-1} = \dot{m}_{k-1} c_{k-1} (T_{k-1} - T_k). \tag{5.73}$$

The  $q_{k,j}$  term is the negative of the heat exchange with the engine block, which was defined in equation 5.68.

Following the same process as was used with the engine block node, the following characteristic equation emerges for the cooling water control volume:

$$\begin{aligned}
& \left[ \frac{2M_k^{t+\Delta t} c_{p_k}^{t+\Delta t}}{\Delta t} + \dot{m}_{k-1}^{t+\Delta t} c_{p_{k-1}}^{t+\Delta t} + h_{k,j}^{t+\Delta t} A_c \right] \theta_k^{t+\Delta t} \\
& - \dot{m}_{k-1}^{t+\Delta t} c_{p_{k-1}}^{t+\Delta t} \bar{\theta}_{k-1}^{t+\Delta t} - h_{k,j}^{t+\Delta t} A_c \theta_j^{t+\Delta t} \\
& = \left[ \frac{2M_k^t c_{p_k}^t}{\Delta t} + \dot{m}_{k-1}^t c_{p_{k-1}}^t + h_{k,j}^t A_c \right] \theta_k^t + \dot{m}_{k-1}^t c_{p_{k-1}}^t \bar{\theta}_{k-1}^t + h_{k,j}^t A_c \theta_j^t.
\end{aligned} \tag{5.74}$$

### 5.3.1.2 The Cooling Water Heat Exchanger

This component is constructed from two, mixed-property control volumes, which represent the hot and cold side of the heat exchanger, as shown in figure 5.16. The properties of the solid casing of the heat exchanger are assumed to be evenly distributed between these two nodes.

#### 5.3.1.2.1 The Hot-Side Control Volume

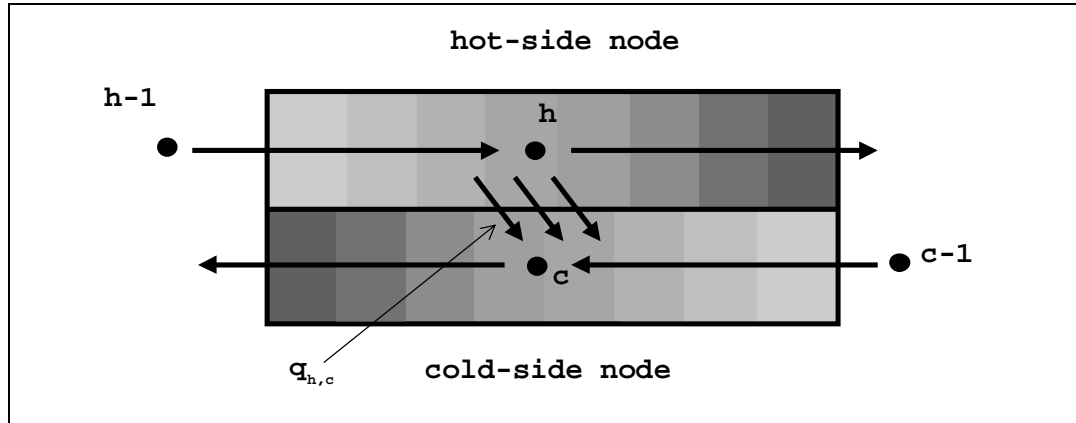


Figure 5.16 The control volume representation of the heat exchanger.

Applying the same process as was used in the derivation of the engine unit's characteristic equations gives the following expression for the hot side of the heat exchanger.

$$\begin{aligned} & \left[ \frac{2M_h^{t+\Delta t} c_h^{t+\Delta t}}{\Delta t} + \dot{m}_{h-1}^{t+\Delta t} c_{h-1}^{t+\Delta t} \right] \theta_h^{t+\Delta t} - \dot{m}_{h-1}^{t+\Delta t} c_{h-1}^{t+\Delta t} \theta_{h-1}^{t+\Delta t} - \phi_{h,c}^{t+\Delta t} \\ &= \left[ \frac{2M_h^t c_h^t}{\Delta t} + \dot{m}_{h-1}^t c_{h-1}^t \right] \theta_h^t + \dot{m}_{h-1}^t c_{h-1}^t \theta_{h-1}^t + \phi_{h,c}^t. \end{aligned} \quad (5.75)$$

$M_h$  is the mass of the casing and encapsulated fluid on the hot side of the heat exchanger and  $c_h$  is their volume weighted, average specific heat.  $\dot{m}_{h-1}$  is the mass flow rate of hot fluid (engine cooling water) into the heat exchanger with a specific heat  $c_{h-1}$ . The heat flux between the hot and cold side of the heat exchanger  $\phi_{h,c}$ , at some time  $t$ , is calculated from

$$\phi_{h,c}^t = \eta_{eff} \left[ C_{\min} (\theta_{h-1}^t - \theta_{c-1}^t) \right]. \quad (5.76)$$

The bracketed term represents the maximum possible heat exchange between the hot and cold side of the heat exchanger. The two temperatures are the inlet temperatures to the hot and cold side of the heat exchanger respectively. The  $C_{\min}^t$  term is the minimum  $\dot{m}_c^t c_{p_c}^t$  or  $\dot{m}_h^t c_{p_h}^t$ .  $\eta_{eff}$  is the effectiveness of the heat exchanger, which varies according to the type of heat exchanger. The well-known number of transfer units (NTU) method [16] is used to calculate this term. As an example, consider a plate heat exchanger in counter flow; the equation for  $\eta_{eff}$  is

$$\eta_{eff} = \frac{1 + e^{-NTU(1-\beta)}}{1 - \beta e^{-NTU(1-\beta)}} \quad (5.77)$$



where  $\beta$  is the ratio  $C_{min}^t/C_{max}^t$ , The  $C_{max}^t$  term is the maximum of  $\dot{m}_c^t c_{p_c}^t$  or  $\dot{m}_h^t c_{p_h}^t$ . Effectiveness equations for different configurations of heat exchanger are given by Kays et al. [16]. The NTU term is given by

$$NTU = \frac{K^t}{C_{min}^t}, \quad (5.78)$$

$K$  is the overall heat transfer modulus (W/K) between the hot and cold side of the heat exchanger: this is defined later.

#### 5.3.1.2.2 The Cold-Side Control Volume

An almost identical control volume characteristic equation to that of the hot-side can be derived for the cold-side of the heat exchanger:

$$\begin{aligned} & \left[ \frac{2M_c^{t+\Delta t} c_c^{t+\Delta t}}{\Delta t} + \dot{m}_{c-1}^{t+\Delta t} c_{p_{c-1}}^{t+\Delta t} \right] \theta_c^{t+\Delta t} - \dot{m}_{c-1}^{t+\Delta t} c_c^{t+\Delta t} \bar{\theta}_{c-1}^{t+\Delta t} - \phi_{c,h}^{t+\Delta t} \\ & = \left[ \frac{2M_h^t c_c^t}{\Delta t} + \dot{m}_{c-1}^t c_{p_{c-1}}^t \right] \theta_c^t + \dot{m}_{c-1}^t c_c^t \bar{\theta}_{c-1}^t + \phi_{c,h}^t. \end{aligned} \quad (5.79)$$

The terms of equation 5.79 have the same meaning as those of equation 5.75, the subscript  $c$  refers to the cold side of the heat exchanger.  $\phi_{c,h}$  is the negative of the flux exchange expression in the hot side characteristic equation.

The calculation of the effectiveness, which in turn is used to calculate the flux exchange between the hot and cold sides of the heat exchanger, requires the calculation of the heat exchange modulus  $K$ . This can be expressed as

$$K^t = \left( \frac{1}{h_c^t A_c} + R_f + \frac{1}{h_h^t A_h} \right)^{-1}. \quad (5.80)$$

$h_h$  and  $h_c$  are the heat transfer coefficients of the hot and cold sides of the heat exchanger respectively, while  $A_h$  and  $A_c$  respectively, are the heat transfer surface areas of the hot and cold sides.  $R_f$  is a resistance term introduced to account for any heat exchanger fouling, typical figures for which are given by Kays et al. [16]. The small thermal resistance of the metallic material between the hot and cold streams is ignored.

If the assumption is made that a plate heat exchanger in counter flow approximates to both fluids flowing in opposite directions along many small channels, separated by thin metallic walls, equation 5.69 can be used to calculate the heat transfer coefficients for both the hot and cold sides.

### 5.3.1.3 The Exhaust Gas Heat Exchanger

The heat exchanger for the engine exhaust gases is modelled in a similar fashion to the cooling water heat exchanger, with a hot-side and cold-side control volumes; the characteristic equations for these control volumes are identical to equations 5.75 and equation 5.79 respectively.

The flow configuration of this heat exchanger is different as, in this particular example the gas and cooling water are in cross-flow rather than counter flow. The equation for the effectiveness with this configuration is given by

$$\eta_{eff} = 1 - e^{\left[ \frac{1 - e^{-C(NTU)^{1.22}}}{C(NTU)^{0.22}} \right]}. \quad (5.81)$$

Assuming the water flow rate inside the heat exchanger is fully turbulent and high enough to prevent localised boiling inside the tube walls, equation 5.69 can be used to calculate the cold-side heat transfer coefficient.

The following equation (given in [17]) can be used to calculate the heat exchange coefficient from the combustion gas as it flows over the tubes containing the cooling water:

$$Nu = 0.33\lambda Re^{0.6} Pr^{0.3}. \quad (5.82)$$

$\lambda$  is an empirical constant, dependent upon the tube bundle geometry. Note that the thermophysical properties of the hot combustion gas are slightly different from those of air; combustion gas property tables [18] can be used to determine them. However, for the stoichiometric combustion of natural gas (used in most CHP units), 96% of the combustion gas is air [19] hence the use of the thermophysical properties of air should not lead to a large discrepancy. Note that the mean temperature of the tube wall (assumed to be close to the cooling water temperature) and adjacent combustion gas is used in the calculation of equation 5.82.

#### 5.3.1.3.1 The Complete CHP Unit

The components of the CHP unit connect together as in figure 5.17.

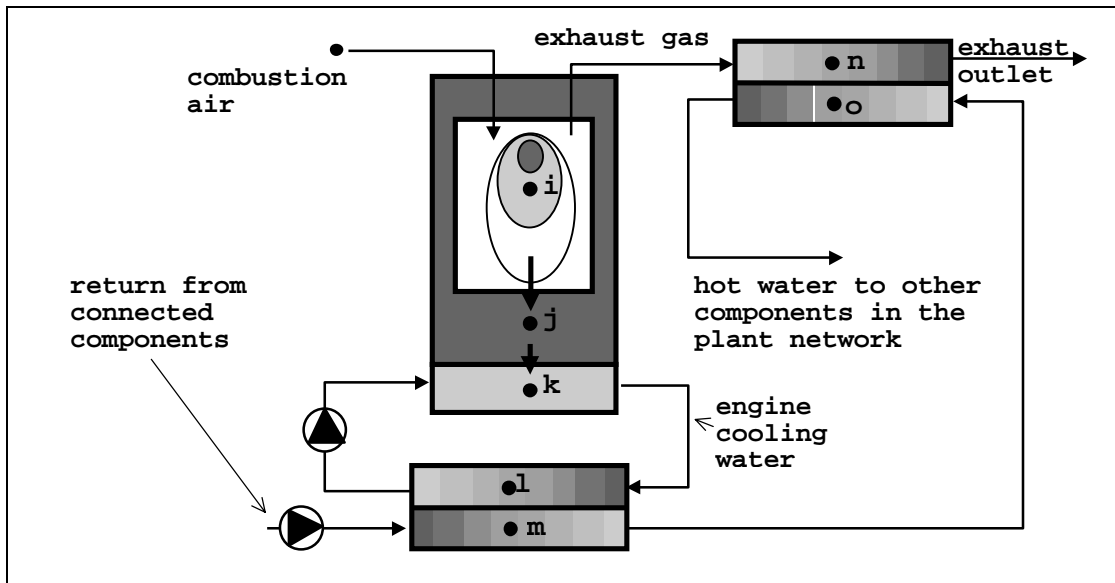


Figure 5.17 The complete CHP unit model.

CHP is discussed further in the technology review of appendix 2.

### 5.3.2 Photovoltaics

To enable the modelling of photovoltaic (PV) components in ESP-r, the concept of the ‘special material’ was introduced [20]<sup>21</sup>. This allows PV elements of the building facade to be treated in the same way as all other solid elements of the building fabric, while accounting for the special power producing nature of these materials.

Building-integrated PV components are constructed of several elements: the PV material, conductors, a binder and a casing. The PV material is the power producing element, the conductors carry away the material’s power output, while the casing encloses the PV material and the conducting elements, providing both protection and rigidity. The binding material glues the whole construction together. At a fundamental level, the facade-integrated PV component can be represented as an ESP-r multi-layered construction (see section 2.2.4): the PV material forming one layer of this construction. It is the PV layer that is designated as a ‘special material’.

Consider the case of a photovoltaic facade element as shown in figure 5.18. This element, a PV panel, consists of four layers of material: inner and outer glazing, a PV material layer and a resin binder. Note that the PV layer in the panel consists of a number of solar cells, which incorporate both the PV material and conducting elements. The individual solar cells, connected together, are considered to be a layer of homogeneous PV material. Solar cells are described in more detail in appendix 1.

---

<sup>21</sup> Note that the special material concept is not only used in the modelling of photovoltaic materials, it has also been applied in the modelling of special glazing elements [18].

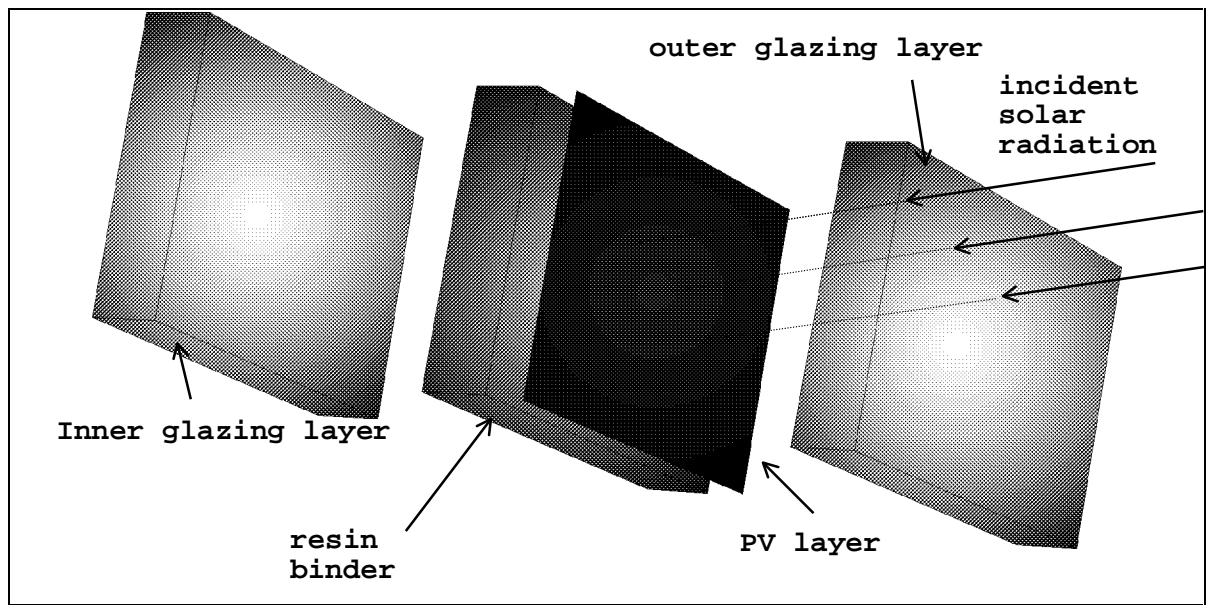


Figure 5.18 A Multi-layered construction incorporating a photovoltaic material.

Focusing on the layer of PV material, this is an internal element of the construction (see section 2.2.4), which can be represented by 3 control volumes: a homogeneous layer and two mixed-property layers (see figure 5.18).

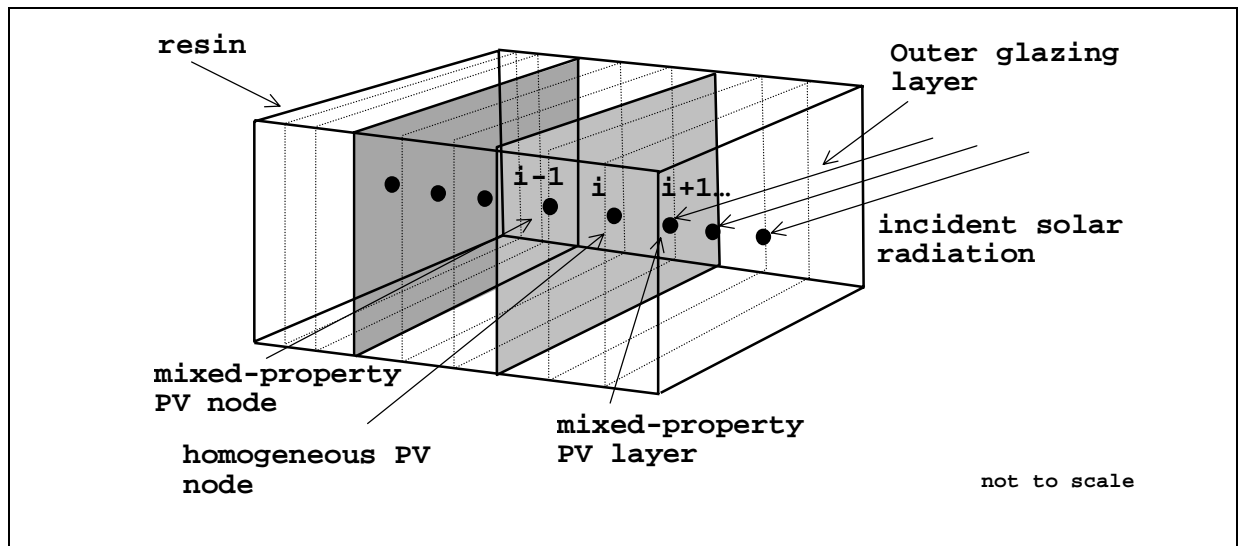


Figure 5.19 PV material control volumes

Recall from chapter 2 that the characteristic equations for these control volumes were as follows.

For the internal homogeneous element (node  $i$ ):

$$\begin{aligned} & \left( \frac{2\rho_i c_i}{\Delta t} + \frac{k_{i,i+1} + k_{i,i-1}}{\Delta x_i^2} \right) \theta_i^{t+\Delta t} - \frac{k_{i,i+1}}{\Delta x_i^2} \theta_{i+1}^{t+\Delta t} - \frac{k_{i,i-1}}{\Delta x_i^2} \theta_{i-1}^{t+\Delta t} - \frac{q_{i_e}^{t+\Delta t}}{(\Delta x \Delta y \Delta z)_i} \\ &= \left( \frac{2\rho_i c_i}{\Delta t} + \frac{k_{i,i+1} + k_{i,i-1}}{\Delta x_i^2} \right) \theta_i^t + \frac{k_{i,i+1}}{\Delta x_i^2} \theta_{i+1}^t + \frac{k_{i,i-1}}{\Delta x_i^2} \theta_{i-1}^t + \frac{q_{i_e}^t}{(\Delta x \Delta y \Delta z)_i}. \end{aligned}$$

The thermophysical properties of this control volume would be those of the PV material.

For the mixed-property layers, the characteristic equation of (node  $i-1$ ) is given by

$$\begin{aligned} & \left( \frac{2\rho_{i-1} c_{i-1}}{\Delta t} + \frac{k_{i,i-1} R + 2\Delta x_{i-1}}{\Delta x_{i-1} (\Delta x_{i,i-1} + \Delta x_{i-2,i-1}) R} + \frac{k_{i-2,i-1} R + 2\Delta x_{i-1}}{\Delta x_{i-1} (\Delta x_{i,i-1} + \Delta x_{i-2,i-1}) R} \right) \theta_{i-1}^{t+\Delta t} - \\ & \left( \frac{k_{i,i-1} R + 2\Delta x_{i-1}}{\Delta x_{i-1} (\Delta x_{i,i-1} + \Delta x_{i-2,i-1}) R} \right) \theta_i^{t+\Delta t} - \left( \frac{k_{i-2,i-1} R + 2\Delta x_{i-1}}{\Delta x_{i-1} (\Delta x_{i,i-1} + \Delta x_{i-2,i-1}) R} \right) \theta_{i-2}^{t+\Delta t} - \frac{q_{i-1_e}^{t+\Delta t}}{(\Delta x \Delta y \Delta z)_{i-1}} \\ &= \left( \frac{2\rho_{i-1} c_{i-1}}{\Delta t} + \frac{k_{i,i-1} R + 2\Delta x_{i-1}}{\Delta x_{i-1} (\Delta x_{i,i-1} + \Delta x_{i-2,i-1}) R} + \frac{k_{i-2,i-1} R + 2\Delta x_{i-1}}{\Delta x_{i-1} (\Delta x_{i,i-1} + \Delta x_{i-2,i-1}) R} \right) \theta_{i-1}^t + \\ & \left( \frac{k_{i,i-1} R + 2\Delta x_{i-1}}{\Delta x_{i-1} (\Delta x_{i,i-1} + \Delta x_{i-2,i-1}) R} \right) \theta_i^t + \left( \frac{k_{i-2,i-1} R + 2\Delta x_{i-1}}{\Delta x_{i-1} (\Delta x_{i,i-1} + \Delta x_{i-2,i-1}) R} \right) \theta_{i-2}^t + \frac{q_{i-1_e}^t}{(\Delta x \Delta y \Delta z)_{i-1}}. \end{aligned}$$

For node  $i+1$ :

$$\begin{aligned}
& \left( \frac{2\rho_{i+1}c_{i+1}}{\Delta t} + \frac{k_{i,i+1}R + 2\Delta x_{i+1}}{\Delta x_{i+1}(\Delta x_{i,i+1} + \Delta x_{i+2,i+1})R} + \frac{k_{i+2,i+1}R + 2\Delta x_{i+1}}{\Delta x_{i+1}(\Delta x_{i,i+1} + \Delta x_{i+2,i+1})R} \right) \theta_{i+1}^{t+\Delta t} - \\
& \left( \frac{k_{i,i+1}R + 2\Delta x_{i+1}}{\Delta x_{i+1}(\Delta x_{i,i+1} + \Delta x_{i+2,i+1})R} \right) \theta_i^{t+\Delta t} - \left( \frac{k_{i+2,i+1}R + 2\Delta x_{i+1}}{\Delta x_{i+1}(\Delta x_{i,i+1} + \Delta x_{i+2,i+1})R} \right) \theta_{i+2}^{t+\Delta t} - \frac{q_{i+1}^{t+\Delta t}}{(\Delta x \Delta y \Delta z)_{i+1}} \\
& = \left( \frac{2\rho_{i+1}c_{i+1}}{\Delta t} + \frac{k_{i,i+1}R + 2\Delta x_{i+1}}{\Delta x_{i+1}(\Delta x_{i,i+1} + \Delta x_{i+2,i+1})R} + \frac{k_{i+2,i+1}R + 2\Delta x_{i+1}}{\Delta x_{i+1}(\Delta x_{i,i+1} + \Delta x_{i+2,i+1})R} \right) \theta_{i+1}^t + \\
& \left( \frac{k_{i,i+1}R + 2\Delta x_{i+1}}{\Delta x_{i+1}(\Delta x_{i,i+1} + \Delta x_{i+2,i+1})R} \right) \theta_i^t + \left( \frac{k_{i+2,i+1}R + 2\Delta x_{i+1}}{\Delta x_{i+1}(\Delta x_{i,i+1} + \Delta x_{i+2,i+1})R} \right) \theta_{i+2}^t + \frac{q_{i+1}^t}{(\Delta x \Delta y \Delta z)_{i+1}}.
\end{aligned}$$

The thermophysical properties of the two mixed-property volumes would be the mass weighted averages of the PV material and resin binder (node  $i-1$ ), or the PV material and the outer glass cover sheet (node  $i+1$ ).

In the construction of figure 5.18, solar radiation is transmitted to the surface of the PV layer through the glass cover material. The calculation of the intensity of solar radiation incident on the glass surface is handled by ESP-r's solar processing algorithms. The incident radiation is a function of the surface geometry, site location (latitude and longitude), shading and the temporal characteristics of the climatic data at the simulation time step. Refer to Clarke [10] for more details.

In most other construction materials (excluding phase change materials), the absorption of solar radiation would result in a temperature rise, through the conversion of the absorbed solar radiation to heat. The absorption of this radiation at the surface of the PV material, node  $i+1$ , is represented by the  $q_{i+1}$  heat injection term in its characteristic equation. However, a PV material is regarded as a 'special material' in ESP-r, as not all the absorbed solar is converted to heat: a proportion is converted to electrical energy, and transported away as electrical current in the conducting elements. The characteristic equation of the PV material control volumes must

therefore be altered to take account of this fact, by the addition of an extra term to account for the production of electrical energy (e.g. for node  $i+1$ ).

$$\begin{aligned}
& \left( \frac{2\rho_{i+1}c_{p,i+1}}{\Delta t} + \frac{k_{i,j+1}R + 2\Delta x_{i+1}}{\Delta x_{i+1}(\Delta x_{i,j+1} + \Delta x_{i+2,j+1})R} + \frac{k_{i+2,j+1}R + 2\Delta x_{i+1}}{\Delta x_{i+1}(\Delta x_{i,j+1} + \Delta x_{i+2,j+1})R} \right) \theta_{i+1}^{t+\Delta t} - \\
& \left( \frac{k_{i,j+1}R + 2\Delta x_{i+1}}{\Delta x_{i+1}(\Delta x_{i,j+1} + \Delta x_{i+2,j+1})R} \right) \theta_i^{t+\Delta t} - \left( \frac{k_{i+2,j+1}R + 2\Delta x_{i+1}}{\Delta x_{i+1}(\Delta x_{i,j+1} + \Delta x_{i+2,j+1})R} \right) \theta_{i+2}^{t+\Delta t} - \frac{q_{i+1,e}^{t+\Delta t} - q_{i+1,p}^{t+\Delta t}}{(\Delta x \Delta y \Delta z)_{i+1}} \\
& = \left( \frac{2\rho_{i+1}c_{p,i+1}}{\Delta t} + \frac{k_{i,j+1}R + 2\Delta x_{i+1}}{\Delta x_{i+1}(\Delta x_{i,j+1} + \Delta x_{i+2,j+1})R} + \frac{k_{i+2,j+1}R + 2\Delta x_{i+1}}{\Delta x_{i+1}(\Delta x_{i,j+1} + \Delta x_{i+2,j+1})R} \right) \theta_{i+1}^t + \\
& \left( \frac{k_{i,j+1}R + 2\Delta x_{i+1}}{\Delta x_{i+1}(\Delta x_{i,j+1} + \Delta x_{i+2,j+1})R} \right) \theta_i^t + \left( \frac{k_{i+2,j+1}R + 2\Delta x_{i+1}}{\Delta x_{i+1}(\Delta x_{i,j+1} + \Delta x_{i+2,j+1})R} \right) \theta_{i+2}^t + \frac{q_{i+1,e}^t - q_{i+1,p}^t}{(\Delta x \Delta y \Delta z)_{i+1}}
\end{aligned}$$

The  $\frac{q_{i+1,p}^t}{(\Delta x \Delta y \Delta z)_i}$  term represents the electrical power (W) produced by the PV layer per unit

volume at some time  $t$ . Note that the term is of the opposite sign to the heat injection term.

Hence, when producing electrical power, the temperature of the PV layer would be cooler than would occur in the situation where no power was produced.

Note that the PV component can either be transparent or opaque<sup>22</sup>. Radiation will be absorbed in all three nodes of the transparent material. It is assumed that all power production in a transparent PV material occurs at the centre node of the layer (node  $i$ ). The heat injection term would be altered in the same manner as that of node  $i+1$ . In an opaque PV material all the solar energy is absorbed in the first (mixed) layer of material. Again power production is assumed to occur at the homogeneous node in the PV material. Note that the PV layer is thin compared to

---

<sup>22</sup> The fundamentals of PV materials are discussed in appendix 1.



the other layers in the construction and so the relative positions of solar absorption and power production within the layer are thermodynamically unimportant.

The previous paragraphs have shown how a PV panel can be modelled thermophysically in ESP-r by its definition as a multi-layered construction. This allows the temperature, and more importantly the intensity of solar radiation absorbed in the solar cell to be calculated. As will be shown below, these quantities are required in the calculation of the power generated by the PV element, which in turn is a quantity required by the characteristic equations of the PV material control volumes. The temperature, solar incident radiation and PV power output are therefore coupling variables between the thermal and electrical equations of the PV material.

To calculate the power produced by the PV material, its central, homogeneous thermal control volume must be augmented with electrical control volumes; one for each solar cell in the layer. The PV material therefore becomes a hybrid thermal/electrical component. Each electrical control volume consists of an equivalent circuit model, which encapsulates the electrical characteristics of the solar cell. This is shown in figure 5.20.

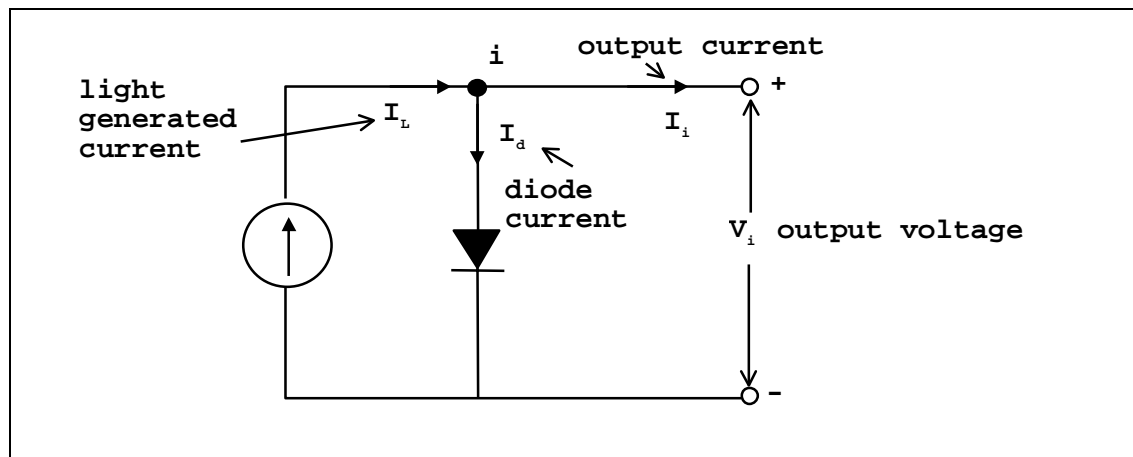


Figure 5.20 The equivalent circuit of the solar cell.

The circuit model shown above is based on that described by Buresch [21] and many others. The current source represents the current generated by absorption of solar radiation in the cell: the

light generated current. The diode is included to provide a flow path for a diode current, which opposes the flow of light generated current. As with the electrical control volumes of chapter 3, a characteristic equation can be constructed for equivalent circuit by the application of Kirchhoff's current law. The current balance equation about the electrical node  $i$  is

$$I_i = I_d - I_L. \quad (5.83)$$

$I_i$  is the current flowing from node  $i$ ,  $I_d$  is the diode current and  $I_L$  is the light generated current. The equation for the diode current is given by

$$I_d = I_g \left( 1 - \exp \left[ \frac{eV_i}{\lambda k T_i} \right] \right). \quad (5.84)$$

$I_d$  is the current (A) which flows in the solar cell when no light is present,  $V_i$  is the voltage of node  $i$ ,  $e$  is the charge on an electron:  $1.6 \times 10^{-19}$  (C) and  $k$  is the Boltzmann constant:  $1.38 \times 10^{-23}$ . Notice that the diode current is a function of the absolute nodal temperature  $T_i$  (K), hence temperature is a coupling variable, which links the thermal and electrical control volumes. The  $\lambda$  term in the equation is added to account for losses caused by imperfections in the PV material and is termed the cell 'ideality factor' [22].

The light generated current can be described by a linear function of the solar radiation absorbed in the solar cell.

$$I_{L_i} = \frac{q_{i_{sw}}}{a}. \quad (5.85)$$

$a$  is quantity derived from test data (explained later) and is a ratio of the solar radiation absorbed in the PV material at test conditions and the radiation absorbed at the current simulation time step. Notice that the absorbed solar radiation is another coupling variable between the thermal and electrical control volumes as the term also appears in the equations for the PV thermal control volumes.

Substituting the equations for  $I_d$  and  $I_L$  into the current balance equation gives

$$I_i = I_g \left( 1 - \exp \left[ \frac{eV_i}{\lambda k T_i} \right] \right) - \frac{q_{i\,sw}}{a}. \quad (5.86)$$

The d.c. power output from the solar cell (W) is given by

$$P_i = V_i I_i = V_i I_g \left( 1 - \exp \left[ \frac{eV_i}{\lambda k T_i} \right] \right) - \frac{V_i q_{i\,sw}}{a}. \quad (5.87)$$

The output for the entire PV layer in the multi-layered construction is calculated by multiplying the individual cell output by the number of cells in the layer:

$$P_{layer} = n \times \left\{ V_i I_g \left( 1 - \exp \left[ \frac{eV_i}{\lambda k T_i} \right] \right) - \frac{V_i q_{i\,sw}}{a} \right\}. \quad (5.88)$$

Notice that the equation for the power output from the PV layer contains numerous unknowns:  $V_i$ ,  $a$ ,  $\lambda$  and  $I_g$ , hence the solution of this equation requires that these unknowns are defined.

The unknown terms can be calculated if test data is available for the PV panel component: the open circuit voltage  $V_{ocp}$ , the short circuit current  $I_{scp}$ , the optimum operating voltage  $V_{mpp}$  and the optimum operating current  $I_{mpp}$ . All the properties are measured at a reference temperature of  $T_{ref}$  (K) and absorbed solar radiation flux<sup>23</sup>,  $q_{i\,sw\,ref}^\perp$  (W).

---

<sup>23</sup> Note that in most cases the given test value for PV components is the radiation incident on the outer cover of the panel at an incidence angle of 0°. For equation 5.81 the radiation absorbed by the PV material at these reference conditions is required. This can be calculated from test value of incident solar radiation if the angular dependent optical properties of the PV material and glass cover sheet are known.

Note that the previously defined equations were derived in terms of cell characteristics and not panel characteristics. The test data must therefore be converted to cell values. This is a straightforward process: for a panel with  $x$  branches of cells connected in parallel, and  $y$  cells connected in series in each branch (the total number of cells is  $n = x \times y$ ). The values to use in the cell equations are as follows.

$$I_{sc} = \frac{I_{sc_p}}{x}, I_{mp} = \frac{I_{mp_p}}{x} \text{ and } V_{oc} = \frac{V_{oc_p}}{y}, V_{mp} = \frac{V_{mp_p}}{y}.$$

The extra  $p$  subscript denotes a quantity relating to the entire panel.

The test data can then be used as boundary condition information for the derived equations, enabling the calculation of the unknown terms as follows.

For the equivalent circuit of the PV material (figure 5.20), in the open circuit conditions,  $V_i = V_{oc}$  and  $I_i = 0$ . Substituting these values into equation 5.86 gives

$$I_L = I_g \left( \exp \left[ \frac{eV_{oc}}{\lambda k T_{ref}} \right] \right) \text{ at } q_i^{\perp}{}_{sw_{ref}}. \quad (5.89)$$

In the short circuit condition  $I_i = I_{sc}$ ,  $V_i = 0$  and  $I_d = 0$ , therefore

$$I_L = -I_{sc} \text{ at } q_i^{\perp}{}_{sw_{ref}}, T_{ref}. \quad (5.90)$$

Combining these two equations and re-arranging gives an expression for the unknown current,  $I_g$ , in terms of measured test quantities  $V_{oc}$ ,  $I_{sc}$  and  $T_{ref}$ :

$$I_g = \frac{-I_{sc}}{\left( \exp \left[ \frac{eV_{oc}}{\lambda k T_{ref}} \right] - 1 \right)}. \quad (5.91)$$

$I_g$  also varies with the temperature of the PV material (i.e. the temperature of the nodes in the PV material). The following equation (given in [23]) describes the change in  $I_g$  with temperature, in relation to the reference temperature  $T_{ref}$ .

$$I_{g(T_i)} = 2^{\left( \frac{T_i - T_{ref}}{\sigma} \right)} \left[ I_{g(T_{ref})} \right]. \quad (5.92)$$

Substituting into equation 5.91 gives

$$I_g = - \frac{2^{\left( \frac{T_i - T_{ref}}{\sigma} \right)} I_{sc}}{\left( \exp \left[ \frac{eV_{oc}}{\lambda k T} \right] - 1 \right)}. \quad (5.93)$$

Note that the variable  $\sigma$  is an empirical constant, whose value varies with the characteristics of the PV material. Buresch uses a value of  $\sigma = 10$ , while a value of  $\sigma = 15$  was found by experimentation in [24]. The derivation of this value is discussed in the next chapter.

The ideality factor  $\lambda$  is calculated from the following equation

$$\lambda = \frac{\left( \frac{e}{k T_{ref}} \right) (V_{mp} - V_{oc})}{\ln \left( \frac{I_{sc} - I_{mp}}{I_{sc}} \right)}. \quad (5.94)$$

Finally, the variable  $a$  is calculated from

$$a = \frac{\alpha_i^{\perp sw_{ref}}}{\alpha_i}, \quad (5.95)$$

where  $\alpha_i$  is the absorbed solar radiation ( $\text{W/m}^3$ ) in the photovoltaic material layer at the current simulation time step (already calculated by ESP-r).  $\alpha_i^{\perp sw_{ref}}$  is the solar radiation absorbed at test conditions ( $\text{W/m}^3$ ).

The power output for the panel (equation 5.88) can now be solved if  $V_i$  is known. Very often the power output from a PV component is controlled such that it always operates at the optimum power producing conditions: the ‘maximum power point’ (see appendix 1). At this condition

$\frac{\partial P_i}{\partial V_i} = 0$ . Taking the derivative of equation 5.88 with respect to  $V_i$  gives the following

transcendental equation for the voltage  $V_i$  at the maximum power point:

$$1 + \frac{I_L}{I_g} = \exp\left(\frac{eV_i}{\lambda k T_i}\right) \left[ 1 + \frac{eV_i}{\lambda k T_i} \right]. \quad (5.96)$$

The iterative solution of this equation for  $V_i$  and its substitution into equation 5.88 allows the power output from the PV element to be calculated. This can then be inserted into the control volume characteristic equations (described previously) for the calculation of the PV element temperature. In crystalline PV materials, the thermal and electrical equations are closely coupled: the electrical output of the PV panel is a function of the PV layer temperature, which is affected by the power output of the PV material. Note that the power output of the PV element is d.c. and so before it can be injected into an a.c. electrical network it must undergo an inversion process; this is discussed, along with an examination of solar cell physics, in appendix 1.

## **5.4 Control in Integrated Simulations**

So far this chapter has described the components necessary for the modelling and simulation of electrical and building-integrated energy systems. However, one other vital constituent of the simulation model has yet to be discussed: control.

Control plays an important part in both the simulation of the electrical network and in the simulation of the overall integrated model. The basis of control in ESP-r, the control loop [10], was described in chapter 2. The control loop imposes a user-defined control action on individual zones, plant or flow components. The operation of each control loop is dictated by a control law. An additional layer of control, ‘global control’ (MacQueen [25]), has been added to ESP-r, which is active at the highest level within the integrated simulation. Global control supervises the activity of the lower level control loops, based on a high-level global control strategy.

The two levels of control form a control hierarchy and enable ESP-r to simulate many types of building control including building energy management systems [25]. Both of these levels of control affect the simulation of electrical power flow, as will be described in the following sections.

### **5.4.1 The Action of the Control Loop on the Electrical Network**

Control loops play an important part in the electrical simulation, as they regulate the power demand of many of the hybrid components attached to the electrical network. Fans, pumps and lighting can all be affected by control action. As mentioned in chapter 2, a control action operates to bring about a user defined control objective. This is achieved by altering the state of a controlled entity (e.g. a plant component) based on the interaction of a sensed property (time, temperature, pressure, wind speed, daylight, etc.) and a control law. When control is used in the regulation of the hybrid components, which supply the power flow boundary conditions to the electrical network, it implicitly couples these boundary conditions to sensed environmental conditions in all other constituent parts of the building model, e.g. temperatures in the zones, plant component states, flow rates, etc.

### **5.4.2 The Addition of an Electrical Control Loop**

The concept of the control loop has been extended to operate within the electrical network itself, in the form of an electrical control loop, the principles of which are exactly the same as all other control loops in ESP-r. The electrical control loop senses a state variable at a point in the electrical network (voltage, current, real or reactive power). Based on the state of the sensed variable, an electrical control law acts to bring about a user-defined control objective, through the actuation of another electrical state variable at another point in the network. Note that the explicit modelling of the electrical network is particularly important in this case as it is the means by which the voltage variables necessary for the input to the control algorithm can be calculated.

### **5.4.3 A Generator Voltage Control Law**

As an example of electrical control, recall that the reactive power output from the CHP unit, fitted with a synchronous generator, was a controllable quantity; this controllability is used for voltage regulation in power systems and a controller of this type has been installed in ESP-r. The basis of the voltage regulation is to maintain a user-defined constant voltage at the generator terminals (the node in the electrical network to which the generator is attached) by varying its reactive power output to exactly meet the demands of the coupled electrical system. However, there are limits to the reactive power output of the generator; once these limits are reached, the voltage across the generator terminals can no longer be fixed and will float. The form of the control law is shown in figure 5.21.



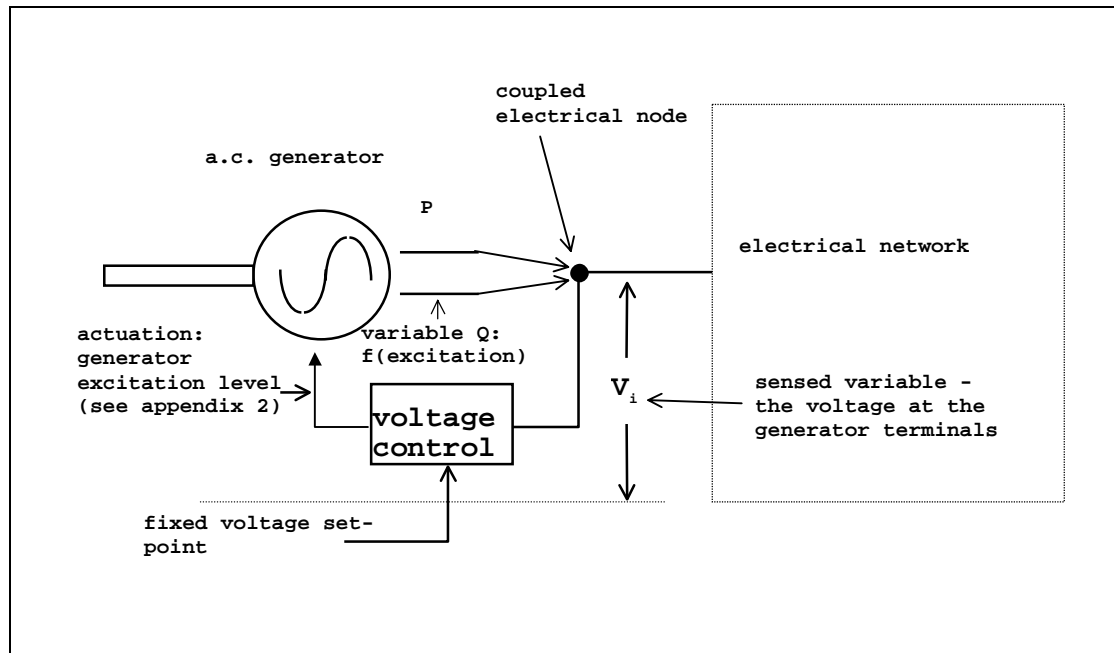


Figure 5.21 Synchronous generator voltage control.

#### 5.4.4 Global Control

The use of control to iteratively couple the electrical network solver into the overall solution process was discussed in section 4.4. One control scenario discussed was where the electrical network could only supply a finite amount of energy to the building: either because of tariff limitations or because of a finite generating capacity, e.g. where the building operates a stand-alone electrical energy generation system. When the limits of electrical power supply are reached, the global controller would act to reduce the demand of the building by shutting off power consuming components thereby explicitly affecting the building environmental conditions based on set electrical energy limits. This requires the re-calculation of the building, plant and flow network environmental states based on the new power supply conditions.

The foundations to achieve this coupling between the electrical network and the building environmental conditions already exist, in the form of high-level level global control. One such controller, the ‘global capacity controller’ [25], is ideally suited to the task of electrical energy management.

At each simulation time step, the global capacity controller supervises the state of the plant and control loops based on user defined capacity limits; these limits can be thermophysical such as heat output or fluid flow. The controller monitors the level of the thermophysical property and, if the capacity limit is exceeded, acts to sequentially close down selected components (e.g. lights or items of plant) to bring the level of the relevant property back within set limits.

In an electrical context, capacity limiting would work as follows. The system power consumption would be determined from the power imported via the reference node of the electrical network. If the user defined power consumption capacity limit is exceeded, the global control would act to sequentially zero the output of selected control loops, shutting down the component to which they are connected, until the monitored power consumption falls back below the capacity limit. The overall solution for the building, at the affected time step, would then be re-calculated based on the new control state. This global control action is represented schematically in figure 5.22

It should be noted that the addition of the electrical network and power producing components opens up a range of possibilities for the development of new ESP-r control strategies, using the range of controllable quantities (electrical power flows and state variables) calculated in the electrical network. This short section has only discussed a very few of these new control possibilities, more are discussed in chapter 8.

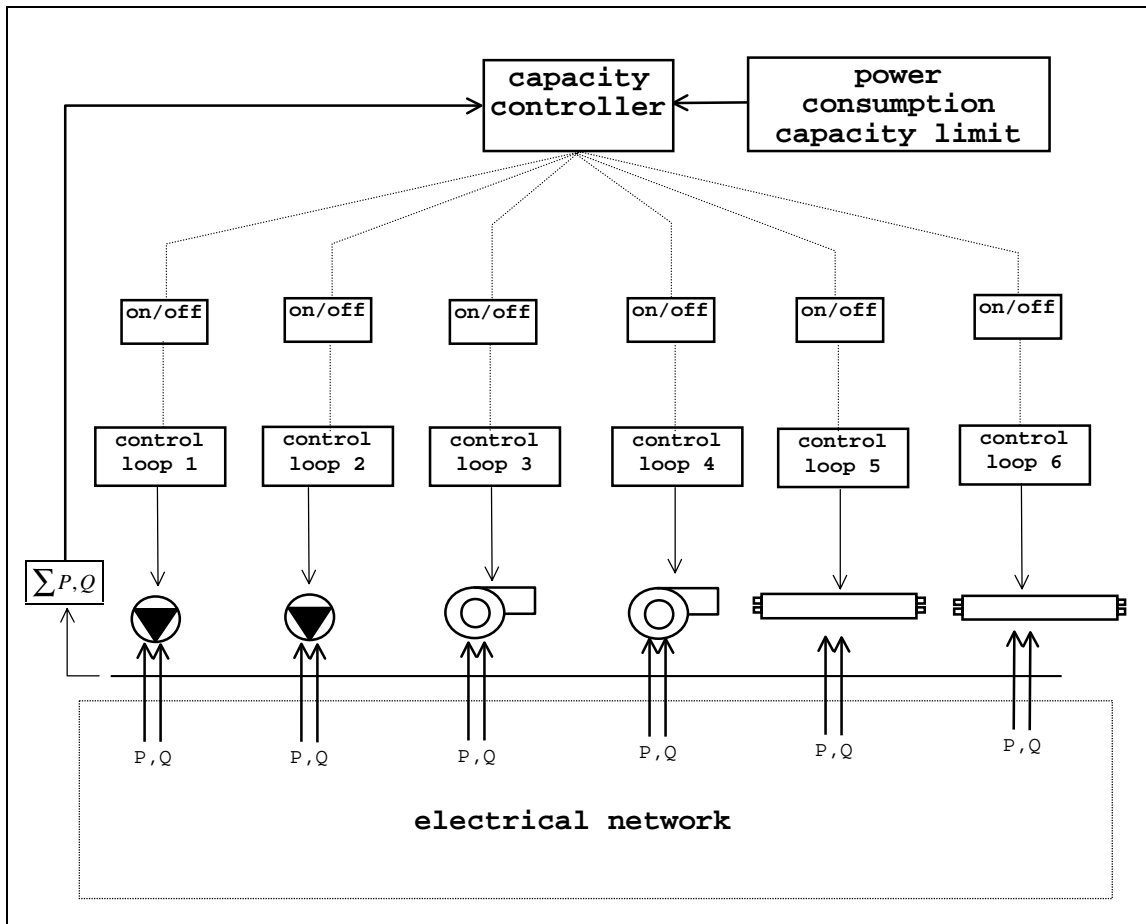


Figure 5.22 The global capacity controller, applied in an electrical context.

## 5.5 Summary

This chapter has described the various component types that have been added to ESP-r for use in the integrated simulation of the electrical network and building-integrated energy systems:

- the electrical conductors and transformers which couple the control volumes in the electrical network;

- the hybrid load and plant components which draw power from the electrical network, while simultaneously affecting thermophysical conditions in other parts of the building network;
- the hybrid and plant components can be used in the modelling of building-integrated energy systems.

The use of these component models within the context of an integrated simulation is demonstrated in chapter 7. However before this is done the next chapter describes the techniques used to validate both the developed models and the electrical network solver described in chapter 3.

## 5.6 References

1. Oateley C, *Electric and magnetic fields - an introduction*, Cambridge University Press, 1980.
2. Weedy B M, *Electric Power Systems*, Wiley, New York, 1979
3. Gross C A, *Power System Analysis*, Wiley, New York, 1986.
4. BICC, *Electric Cables Handbook*, Blackwell, 1990.
5. Stagg G W and El-Abiad, *Computer Methods in Power System Analysis*, McGraw-Hill, New York, 1968.
6. *ESP-r user's guide*, Energy Simulation Research Unit, Glasgow, 1998.
7. Parsloe C and Hejab M, *Small power loads*, Building Services Research and Information Association Technical Note TN8/92.
8. Chapman D F, Slater A I, Isaacs A L, *Energy limiters - their place in lighting control*, BRE Report 114/3/4, 1986.
9. Capehart B L, Slack K D, *Power factor benefits of high efficiency motors*, Energy Engineering, Vol. 93, No. 3, 1996.
10. Clarke J A, *Energy simulation in building design*, Adam Hilger, Bristol 1985.

11. Hensen J L M, *On the thermal interaction of building structure and heating and ventilating system*, Doctoral Dissertation, Eindhoven University of Technology, 1991.
12. The Energy Efficiency Office, *Guidance notes for the implementation of small scale packaged combined heat and power*, Energy Efficiency Office Best Practice Program, Good Practice Guide 1, 1989
13. McCrorie KAB, Underwood W B, le Feuvre R F, *Small-scale combined heat and power simulations: development of a dynamic spark-ignition engine model*, Building Services Engineering Research and Technology, Vol 17, No. 3, 1996.
14. Woschini G, *A universally applicable equation for the instantaneous heat transfer coefficient in the internal combustion engine*, Society of Automotive Engineers International, Paper 670931.
15. Welty J R, Wicks C E and Wilson, R E, *Fundamentals of momentum, heat, and mass transfer*, 3<sup>rd</sup> Edition, Wiley, New York, 1984.
16. Kays W M and London A L, *Compact heat exchangers*, McGraw-Hill, New York, 1964.
17. Grimson E D, *Correlation and utilisation of new data on flow resistance and heat transfer for cross flow of gasses over tube banks*, Transactions of the American Society of Mechanical Engineers, 1937.
18. Keenan J H K, *Gas tables, thermodynamic properties of air, products of combustion and component gases, compressible flow functions*, 1948
19. Private communication with Scottish Gas, 1997.

20. Evans M S and Kelly N J, *Modelling active building elements using special materials*, ESRU Technical Report 95/18, University of Strathclyde Glasgow, 1995.
21. Buresch M, *Photovoltaic energy systems - design and installation*, McGraw-Hill, New York, 1983.
22. Twidell J and Weir T, *Renewable energy resources*, E & FN Spon, London, 1986.
23. Millman J and Grabel A, *Microelectronics*, McGraw-Hill, New York, 1987.
24. Clarke J A, Johnstone C M, Hand J W, Kelly N J, Strachan P A, *The Characterisation of photovoltaic-integrated building facades under realistic operating conditions*, Proc. 4<sup>th</sup> European Conference on Solar Energy in Architecture and Urban Planning, Berlin, March 1996.
25. MacQueen J, *The modelling and simulation of energy management control systems*, PhD Thesis, University of Strathclyde, Glasgow, 1997.

# **Chapter 6 - Verification of the Electrical Network Solver and Hybrid Model Calibration**

## **6. Introduction**

Before integration into the ESP-r environment, both the electrical solver and the component models underwent testing and calibration respectively. The purpose of the testing process was to verify that the solver installed in ESP-r functioned properly and gave correct results. The calibration of the component models involved tuning their parameters so that their output matched that measured in experiments. Note that unlike the testing process, calibration does not verify the correctness of the model. This chapter provides an overview of these two processes.

### **6.1 Verification of the Electrical Solver**

Judkoff et al.[1] recommend a three part testing process consisting of analytical tests, empirical validation and inter-model comparison. Unfortunately, in most circumstances such a comprehensive approach to testing is not practical, due to either a lack of empirical data sets, comparable models or suitable analytical tests.

In the case of electrical systems modelling the most useful means of verification is achieved through analytical testing and inter-model comparisons. Analytical tests can easily be devised for the electrical solver, while other software tools are available against which to compare its performance. However, an exhaustive testing exercise such that proposed in [1] above must wait until data, time and finances become available for the task.

The basic aim of the verification exercise described in this chapter was to develop confidence in the output from the electrical solver. The electrical conductor component models, described in chapter 5, are an integral part of the electrical system, and so verification of the network model



and solver also implicitly validates these component models. The verification tests adopted for the solver are shown in table 6.1.

Verification Method		
Analytical Tests	Inter-model Comparison	Empirical Comparison
Simple analytical tests were undertaken during the development process.	The model was tested against predictions from other power flow modelling programmes	This was not undertaken due to lack of available data sets.

Table 6.1 Methods of verification used on the solver and component models.

### 6.1.1 Testing for Robustness

As the electrical network solver was to be used in a simulation environment that would subject it to time-varying boundary conditions, a series of ‘stress tests’ were also conducted in parallel with the verification tests. The purpose of these tests was to check the numerical robustness of the solver to time-varying inputs, as would occur in a dynamic simulation.

### 6.1.2 The Verification Process

Testing of the electrical network solver was done in two stages. Firstly, during the development process the solver was tested against simple d.c. and a.c. electrical network problems for which a hand calculated solution was achievable. For example, consider the d.c. network of figure 6.1. The series and parallel resistances are combined to give a single resistance of  $16.33\Omega$ .

Application of a power balance to node y indicates that the real power transmitted from node x must balance the real power (W) drawn from the node:

$$P_{x,y} = P_{L^y} = 100 . \quad (6.1)$$

The power flow (W) between  $x$  and  $y$  is calculated by

$$P_{x,y} = V_y I_{x,y} = V_y \frac{(V_x - V_y)}{Z_{x,y}} , \quad (6.2)$$

therefore combining equations 6.2 and 6.3 gives

$$V_y \frac{(V_x - V_y)}{Z_{x,y}} = 100 . \quad (6.3)$$

solving equation 6.3 gives a voltage of 232.99V for node  $y$ . Analysis of the network using the ESP-r electrical network solver gave an identical answer.

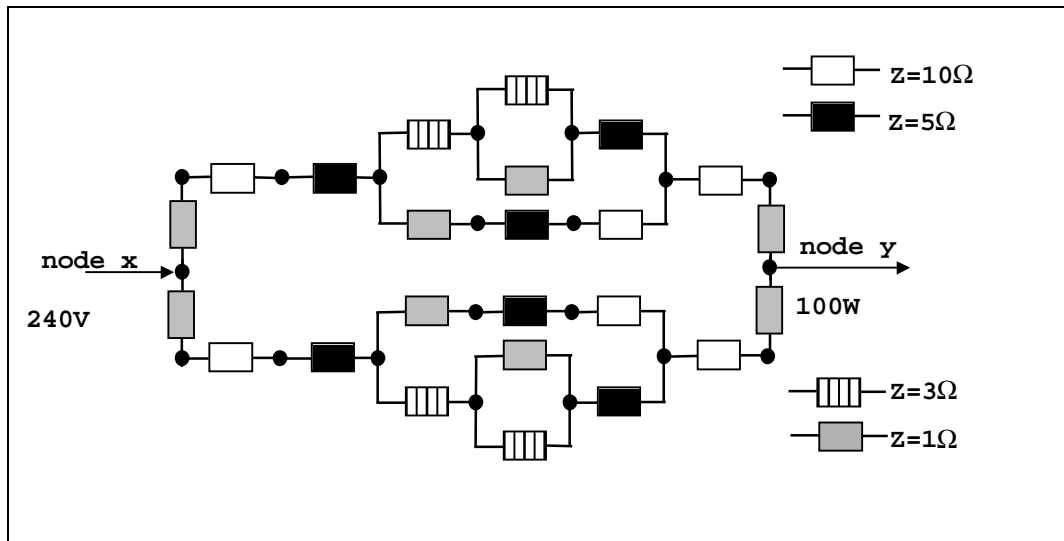


Figure 6.1 An example of a simple test network used for analytical verification.

### **6.1.3 Inter-model Comparison**

The most practical means of validating the completed network solver involved a series of comparative tests against another power flow solver. In this case the solver used for comparison was the validated, PC-based program, FLOW, developed by the University of Strathclyde's Centre for Electrical Power Engineering (CEPE). The FLOW simulation tool uses a solver based on the Gauss-Siedel iterative method, as opposed to ESP-r's Newton-Raphson-based solver. The Gauss-Seidel electrical network solution method is described by both Weedy [1] and Gross [2].

The test procedure adopted involved comparing the predictions of voltage states from the two solvers for three different electrical networks. The three network configurations (shown in figure 6.1) represent a range of distribution system layouts and complexity, and were tested using a range of boundary condition power flows.

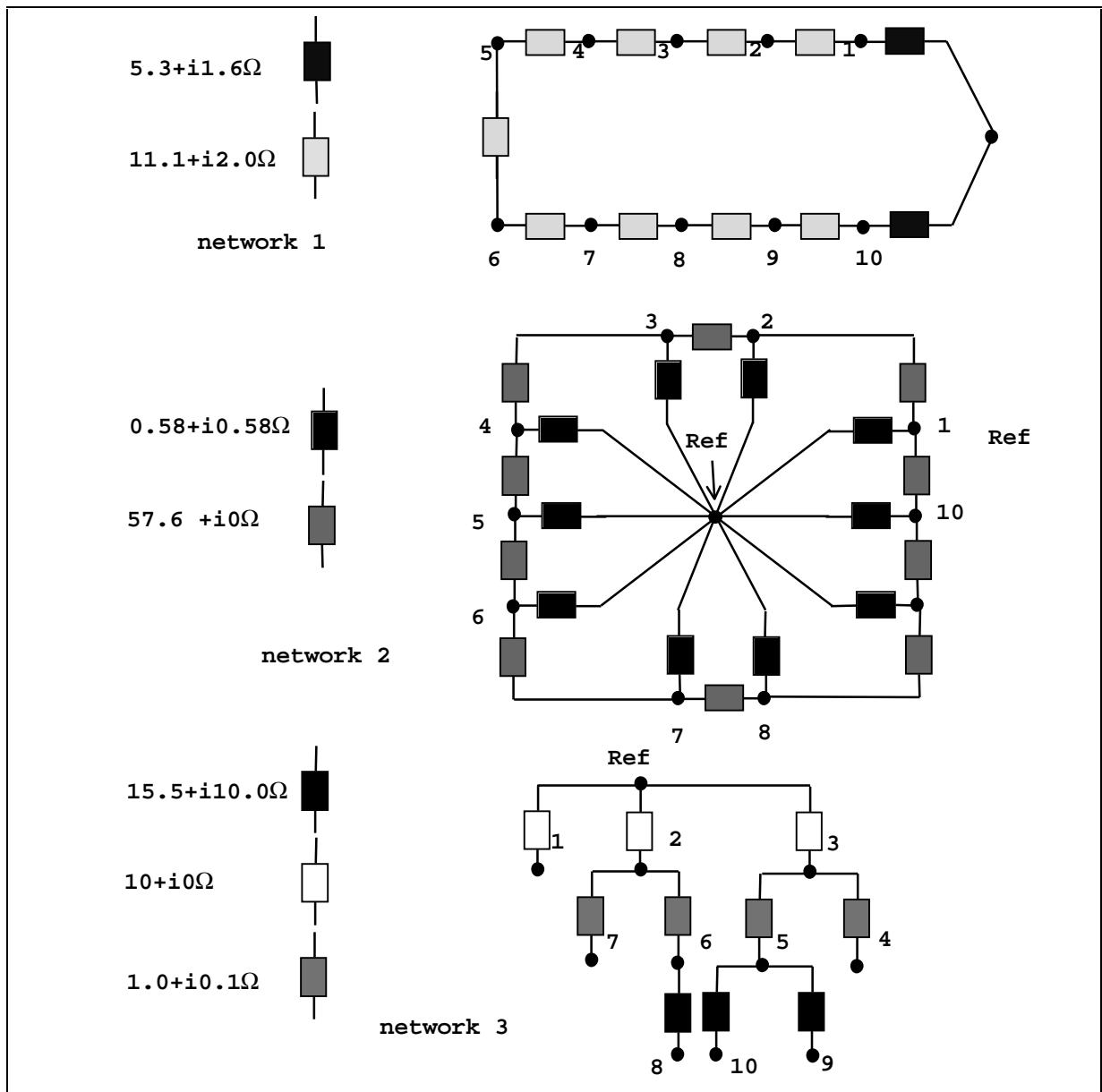


Figure 6.2 The power flow networks against which the two solvers were tested.

Examples of the results from the inter-model comparisons (for system 1) are shown in figure 6.3.

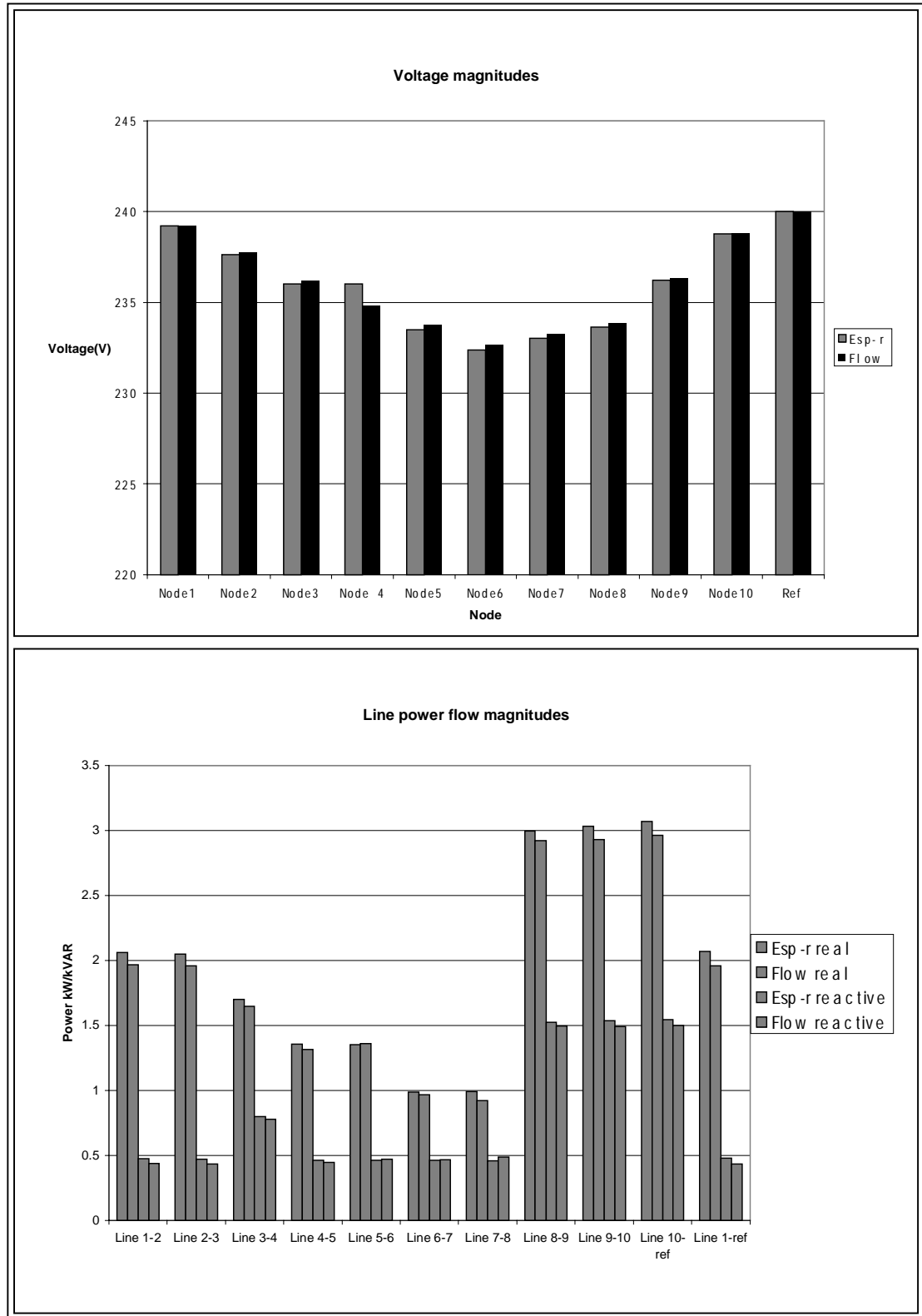


Figure 6.3 Sample results from the comparison exercise.

Overall, the ESP-r solver's results were in very close agreement with those predicted by the FLOW program, with voltage magnitudes and phase angles at each node varying by less than 1%.

#### 6.1.4 Inter-algorithmic Comparison and Testing for Robustness

The inter-model comparison checked the ESP-r electrical solver's ability to correctly predict the network voltage state for both different electrical network types and a range of power flow boundary condition scenarios. However, the FLOW solver is not configured to operate with time-varying boundary conditions, so the ESP-r solver's ability to predict the network state with changing boundary conditions was not tested, though this would occur in a normal simulation. Hence, further tests were conducted on the electrical solver, which took the form of an inter-algorithmic comparison with time-varying boundary conditions. A form of the FLOW program's Gauss-Siedel solver was implemented in ESP-r, and its output compared against that of the standard Newton-Raphson solution algorithm. This test is an important check on the stability of the ESP-r solution algorithm, as the starting point for the electrical network solution, at any simulation time step, is the solved voltage state from the last time step. The solved voltage network state will therefore have a direct bearing on the next time-step solution.

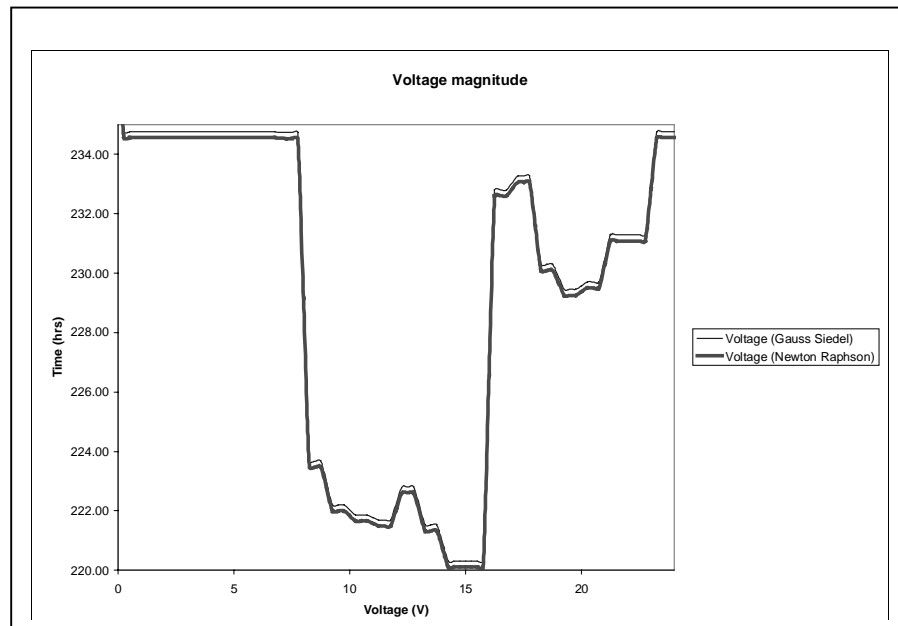


Figure 6.4 Example of predicted nodal voltages with time varying boundary conditions.

The tests described in the preceding paragraphs indicated that the solver predicts network state correctly for different network configurations, steady and time-varying boundary conditions. However the most rigorous test for the solver will occur during a real simulation process; the use of the solver in integrated simulations is described in the next chapter.

## **6.2 Calibration of the Hybrid Power Generating Component Models**

The testing of these models involved comparing their output against data collected in experimental tests of the real component. This form of testing is generally termed as model calibration. The calibration of the combined heat and power (CHP), heat exchanger and photovoltaic (PV) component models was effectively a tuning process, where the model parameters were iteratively adjusted until the output of the model matched that of the test data from the real component. Similar, though more rigorous component calibration exercises are described by many other authors, e.g. Bourdhouxhe et al [4].

As was mentioned previously, while the calibration of the model enables its output to closely match that of the measured output, the process does not validate the correctness (or otherwise) of the model. A well-tuned, though poor physical model will give correct results (within the limits of the calibration data) though the parameters obtained from the calibration process may bear no relation to physical reality.

### **6.2.1 Calibration of the CHP Engine Model with Test Data**

The test data [5] used in the calibration of the CHP engine model gave the important thermodynamic and electrical outputs of the component at various levels of loading (mechanical work output). The tuning process used an iterative search algorithm to adjust the engine cylinder and cooling circuit heat transfer moduli (see equations 5.62 and 5.67) until the cooling water output temperature and the exhaust gas temperature closely matched those given in the test data. Using simple curve fitting techniques, both heat transfer moduli were then expressed in the engine model as a function of the loading, the engine work output. This is shown in figure 6.5.

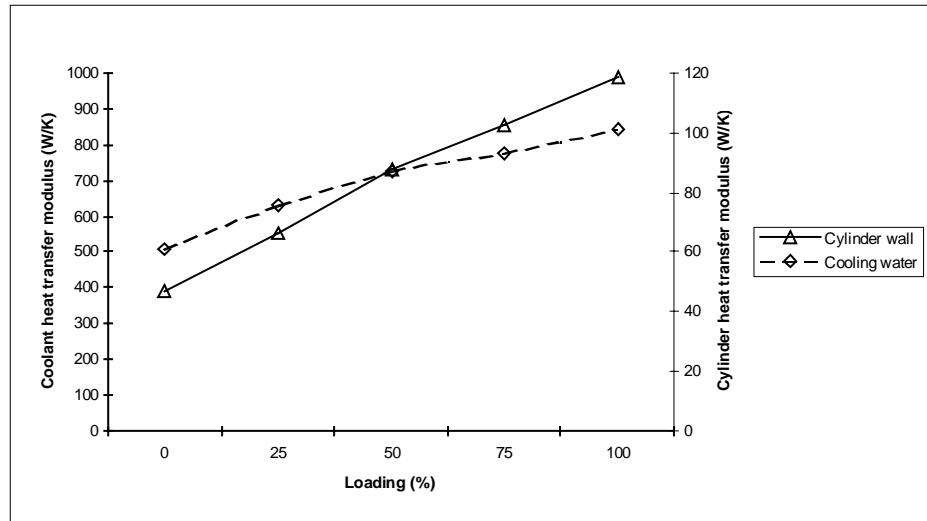


Figure 6.5 Heat transfer moduli derived from calibration of the CHP engine model.

The following tables show the data used to calibrate the model and the model outputs in terms of temperatures, exhaust gas heat flow rate and primary cooling water heat recovery rate.

Electrical power output (kWe)	Primary cooling water temperatures (°C)	Simulated outlet temperature (°C)	Water flow rate (kg/s) (lab and simulation)	Inlet temperature (°C) (lab and simulation)	Measured Heat recovery rate (kW)	Simulated Heat recovery rate (kW)
0 (idling)	87.80	87.80	2.44	85.88	19.58	19.58
25	88.76	88.70	2.46	86.00	28.38	27.76
50	88.70	88.60	2.45	85.10	36.86	35.85
75	89.05	89.10	2.49	84.83	43.92	44.44
100	89.49	89.50	2.49	84.49	52.04	52.14

Table 6.2 a Primary cooling water calibration data

Electrical power output (kWe)	Exhaust gas outlet temperature (°C)	Simulated outlet temperature (°C)	Gas flow rate (kg/s) (lab and simulation)	Calculated gas heat flow rate from lab tests (kW)	Calculated gas heat flow rate in simulation (kW)
0 (idling)	428.6	432.1	0.0247	12.71	12.81
25	472.6	472.1	0.0297	16.87	16.85
50	525.7	527.0	0.0350	22.08	22.13
75	579.3	578.2	0.0413	28.73	28.67
100	603.6	606.0	0.0480	34.76	34.89

Table 6.2 b Exhaust gas calibration data.



The model calibration process described previously is useful if there is a limited quantity of component data available. However, its major disadvantage is that the derived component model parameters are not generic and must be re-calibrated for different primary cooling circuit flow rates differ or another engine type requires simulation.

Analytical expressions for the calculation of both the cylinder wall and cooling water heat transfer coefficients could have been used, however this would have required access to more detailed engine performance information than was made available in the test data (i.e. cylinder pressures, cooling circuit configuration, etc.).

Figure 6.6 shows the tuned engine unit model output against the test data for the most important thermal parameters: exhaust gas temperature and cooling water outlet temperatures, both are plotted against the engine work output.

### **6.2.2 Calibration of the PV model**

One of the key features of the PV model, discussed in chapter 5, is the relationship between the power output and temperature of the PV material, with the power output (in crystalline silicon PV materials) generally decreasing with increasing material temperature. Recall that in chapter 5 a variable,  $\sigma$ , was used in the model of the PV material (equation 5.92).  $\sigma$  affects the power output of the PV material through its influence on the calculation of the diode current (which directly opposes the light generated current) and therefore influences the characteristics of the power output. This variable must be obtained from laboratory testing of the PV material and calibration of the parameter  $\sigma$  against the resulting test data.

The tuning method involved iteratively changing the value of  $\sigma$  until the slope of the PV module power output against temperature (at constant incident radiation intensity) matched that achieved in laboratory tests.

The laboratory tests on the PV modules were done using a solar simulator, consisting of an array of tungsten lamps, which gave an irradiance level of  $600\text{W/m}^2$ . The modules were fitted to a ventilated test rig from which temperatures, power output and heat recovery were measured. Outputs from the tests included the combined efficiency of the PV module (i.e. the power output plus recovered heat, the heat to power ratio and the power output to temperature characteristics. More details of the tests and testing procedure are given in [11].

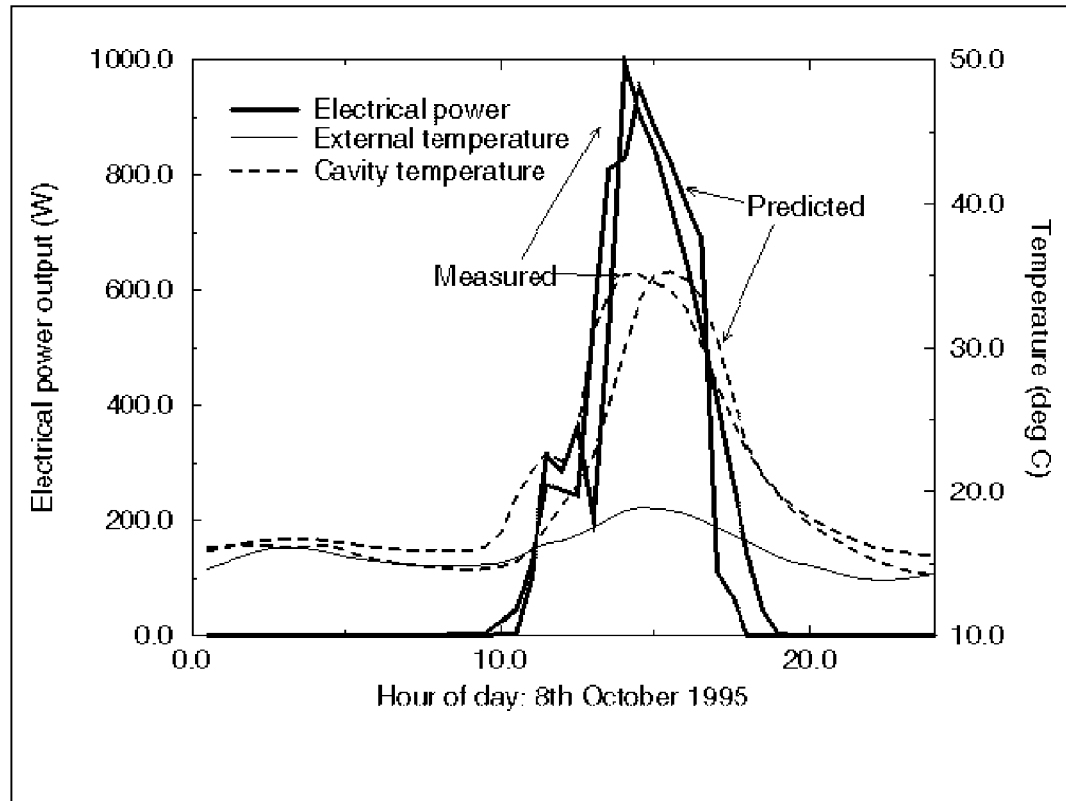


Figure 6.6 Some results from ESP-r's simulations of PV panels against field trial data.

The other PV model parameters are obtained from manufacturer's test data. Note this data is measured at only one temperature, and so is of no use in determining temperature dependent characteristics such as  $\sigma$ .

The photovoltaic special material model has been calibrated against numerous photovoltaic module (panel) types, which incorporated both amorphous<sup>24</sup> and crystalline solar cells, this is reported on by Strachan [9, 10] and Clarke et al. [11] (refer to appendix 1 for a definition of crystalline and amorphous photovoltaic materials).

The calibrated PV material models have also been integrated into ESP-r models of full scale, outdoor PV facade test facilities [11, 12]. The output of the model was then compared to real thermal and electrical data collected from experiments conducted using the test facilities. The results from these field trial comparisons indicate that the predicted electrical output from the calibrated PV component models agreed well with the collected data (see figure 6.7). The equally important thermal performance of the ESP-r PV model also agreed well with the experimental data. Note that figure 6.7 shows an apparent discrepancy between the time of the measured and simulated values. This is probably caused by an unintentional time shift in the simulation output data, which has gone uncorrected<sup>25</sup>.

### **6.2.3 Calibration of the Heat Exchanger Components**

The cooling and gas water heat exchanger models were calibrated against manufacturer's data. However, this data covered the heat exchanger performance in limited steady state conditions and therefore provided no test for the dynamic characteristics of the model. There is a general lack of suitable data for use in plant component modelling verification, especially usable dynamic data sets, against which plant component model transient performance can be tested.

---

<sup>24</sup> In amorphous silicon materials the power output tends to remain constant with temperature. A best fit with the laboratory data was achieved by setting  $\sigma$  to a high value (100), giving a flat power output to temperature characteristic.

<sup>25</sup> The phase shift is possibly due to the measurements being made in British summer time (BST), while simulations are always conducted in Greenwich Mean Time (GMT).

Testing of each model's transient performance was restricted to comparisons against simple dynamic situations, and some inter-model comparisons. For the purposes of verification, Aasem [6] has installed a facility within ESP-r that allows plant components to be subjected to simple excitations such as step inputs in temperature and flow, ramp inputs in temperature and flow, sinusoidally varying temperatures and flow, etc. The output from the excited component can then be compared to an analytical solution of the dynamic process or the output from another model of the component. One such model is shown in figure 6.8: this shows the representation of the liquid-liquid heat exchanger, when modelled using the SIMULINK® simulation tool.

A series of analytical tests were carried out on the heat exchanger components and are reported on in [7] and [8]. These tests also allowed errors and numerical instabilities in the components to be identified and rectified.

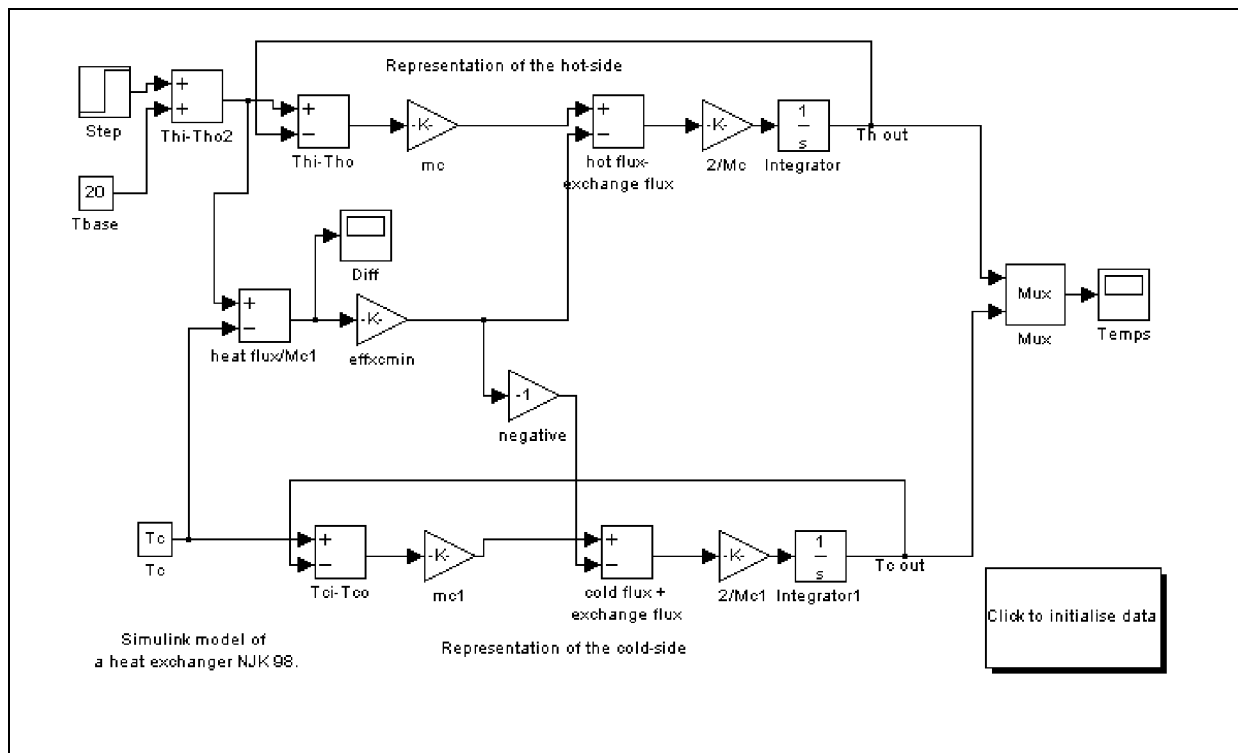


Figure 6.7 The SIMULINK model of the liquid-liquid heat exchanger.

Figure 6.9 shows the ESP-r and SIMULINK<sup>®</sup> model's predictions of the temperature of the heat exchanger cold-side node in response to a sudden step input in the hot -side temperature from 20-80°C.

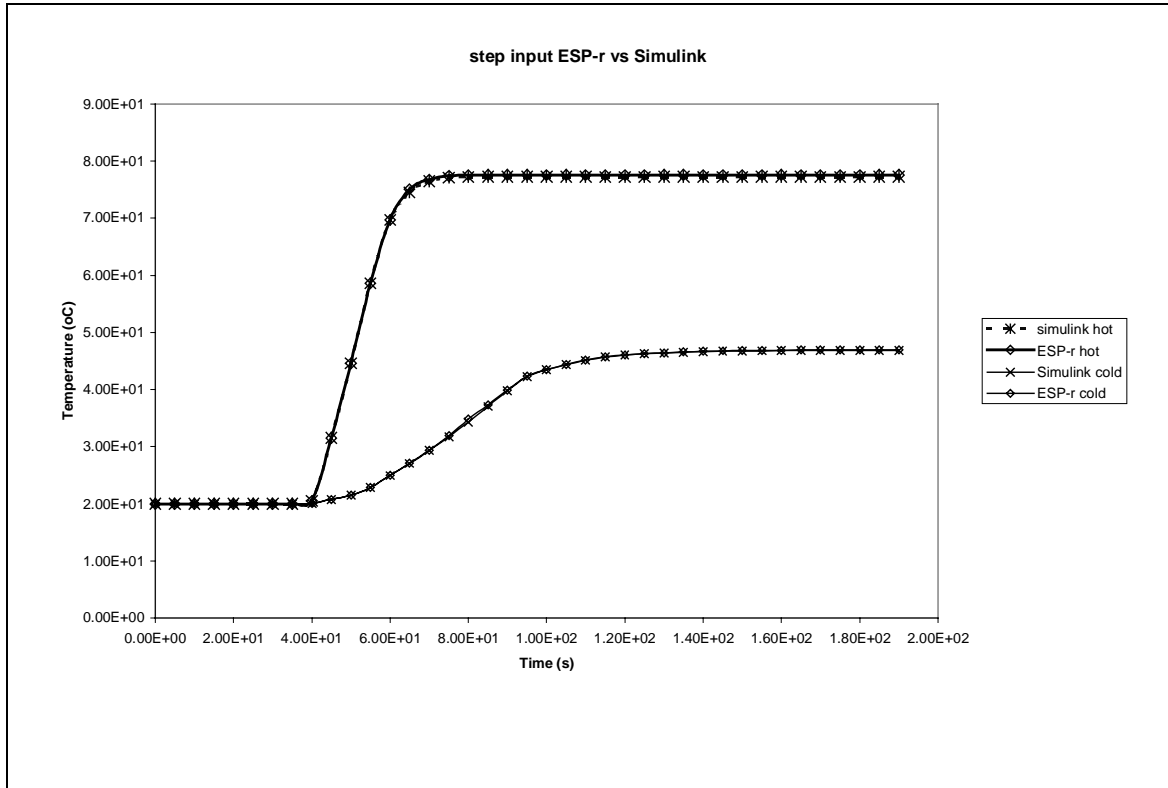


Figure 6.9 The response of the ESP-r and SIMULINK heat exchanger models to a step change in hot water supply temperature.

### 6.3 Summary

This chapter has described the methods used in the verification of ESP-r's electrical network solver, and has shown that the predictions of the solver agree with those of a similar tool. The verification tests also showed excellent agreement between the Newton-Raphson-based solution algorithm (described in chapter 3) and a simpler Gauss-Siedel-based solver, when predicting the nodal voltages in a network subjected to time varying power flow boundary conditions.

This chapter has also described the calibration of the CHP and PV, building-integrated energy system component models. The calibration process involved the tuning of component parameters against experimental data, so that the output of the models approximated that of measured reality. The PV component model was further tested against experimental field trial data, with encouraging results.

Both the solver and component models can therefore be used, with some confidence, in full-scale, integrated models of building-integrated energy systems. The modelling of two such systems is the subject of the next chapter.

## 6.4 References

1. Judkoff R, Wortman R, O'Docherty and Burch D, *A methodology for validating building energy analysis simulations*, Report TR-254-1508, Solar Energy Research Institute, Colorado, USA.
2. Gross C A, *Power systems analysis, 1<sup>st</sup> Edition*, Wiley, New York, 1979.
3. Weedy B M, *Electric power systems*, Wiley New York, 1979.
4. Bourdouxhe P, Grodent M, Lebrun J, Saavendra C, *Cooling tower model developed in toolkit for primary HVAC system Energy Calculation - part 1: model description and validation using catalogue data*, Proc. 4<sup>th</sup> International Conference, System Simulation in Buildings, University of Liege, 1994.
5. CHP engine unit data from the Korean Institute of Energy Research (KIER).
6. Aasem E O, *Practical simulation of air conditioning system in the transient domain*, PhD Thesis, University of Strathclyde, 1994.
7. Smith A C, *Validation of a cooling coil model*, BEng Thesis, University of Strathclyde, 1996.
8. Granger G, *Evaluation of HVAC component models for energy simulation*, BEng Thesis, University of Strathclyde, 1996.
9. Strachan P A, *Calibration of RMS95 modules using data from ITW Stuttgart*, Preliminary Energy Systems Research Unit Report, University of Strathclyde, 1997.

10. Strachan P A, *Calibration with PST semi-transparent PV modules*, Energy Systems Research Unit Report, 1998.
11. Clarke J A, Hand JW, Johnstone CM, Kelly N J, Strachan P A, *The Characterisation of photovoltaic-integrated building facades under realistic operating conditions*, Proc. 4<sup>th</sup> European Conference on Solar Energy in Architecture and Urban Planning, Berlin, March 1996.
12. Clarke J A, Johnstone C, Strachan P and Bloem JJ, Ossenbrink HA, *Thermal and power modelling of the Photovoltaic facade on the ELSA building ISPRA*, 13<sup>th</sup> Photovoltaic Solar Energy Conference, Nice, 1995.



# **Chapter 7 - Modelling and Simulation of Building-Integrated Energy Systems: Examples**

## **7. Introduction**

This chapter describes how the theory and model development of the previous chapters is brought together to facilitate the key objective of this thesis: the simulation of the thermal and electrical aspects of building performance, specifically the simulation of building-integrated energy systems. Two exemplars are presented in this chapter, which demonstrate the capabilities of an ESP-r model, augmented with a power flow network, in the analysis of such integrated thermal/electrical systems. These exemplars are:

- a small sports centre incorporating a combined heat and power unit, supplying both the electrical system and the hot water services;
- a factory building with a photovoltaic facade which supplies power to the building and from which heat is recovered.

It must be emphasised at this point that the models and simulations presented in this chapter are not intended to portray a design exercise: the current electrical modelling capability installed within ESP-r is as yet prototypical and is not suitable for this function. The main functions of these exemplars are to demonstrate how a model incorporating the thermal and electrical domains is constructed and to illustrate the capabilities of an integrated simulation.

### **7.1 Modelling Integrated Systems in ESP-r**

The building-integrated energy systems described in this chapter are some of the more complicated models that can be defined in ESP-r: they incorporate various energy subsystems, with very different time-constants. The modelling of such varied and stiff systems (i.e. with

elements of varying time constants) is perfectly suited to ESP-r's flexible, modular approach to both model definition and simulation.

### 7.1.1 The Definition of Integrated Models in ESP-r

Chapter 2 described how, in ESP-r, the complete building is modelled using a number of integrated constituents: attributed polyhedral zones, which describe the form and fabric of the building, and a series of superimposed networks, which describe the building's energy subsystems. In a dynamic simulation both the zones and networks are combined with real climate data, time-varying internal thermal gains and detailed control information, forming a single mathematical description of the building and its environment.

Each constituent of the building model can be thought of as a 'layer', with each layer adding functionality and detail. The requirements of a particular simulation will dictate the form and complexity of the model, with extra layers being added by the modeller as need requires. For example, the most basic energy simulation would involve only one layer in a model, e.g. the geometry and fabric of the building. If more functionality were required, this layer would be augmented with air flow, CFD, plant and electrical networks, etc. The following table describes the functionality added by the various constituents of an ESP-r model.

Model Constituent	Functionality	Typical Uses
the essential model "core": building fabric, climate, occupancy, idealised ventilation and infiltration	basic fabric thermal energy flows, air, surface and fabric temperatures, 'free floating' environmental conditions driven by climatic and internal excitations, daylight factor calculations, solar distribution	overheating and summer comfort analysis, basic lighting studies

+ zone based control	logically and temporally controlled heating and cooling input to the zones and fabric	control strategy testing, heating/cooling loads, plant sizing, lighting control, heated/cooled floor and ceiling models
+ shading and insulation, blind/shutter control	solar gains control, external and internal solar shading	passive solar studies, location of thermal mass, external shading device studies, more detailed overheating analysis
+ more detailed fabric modelling: 3-D conduction, non-linear material properties, special materials	three dimensional conduction, detailed fabric thermal and non thermal (i.e. electrical energy) flows, advanced materials	thermal bridging, detailed floor heat flows, phase change materials, photovoltaics, advanced glazing studies
+ air flow network	pressure driven air flow and ventilation, inter-zonal air flow and moisture transport, detailed fan models	natural and forced ventilation studies, detailed overheating analysis, passive/ambient cooling strategies, e.g. night flushing
+ CFD	air velocities and momentum, temperature distributions, air/surface boundary layer information	detailed forced and natural ventilation studies, convective heat transfer coefficient calculations, displacement ventilation modelling, detailed heating/cooling studies, atria airflow patterns, etc.
+ moisture flow	fabric moisture transport, surface moisture absorption/evaporation,	interstitial condensation analysis, mould growth prediction and

	moisture storage	analysis, rain water penetration, desiccant material studies
+ plant	detailed, component-based plant descriptions, component temperatures and energy flows	basic, uncontrolled plant operation
+ component level control	local component-based control loops, logically and temporally-based component operation	detailed air conditioning systems modelling, control strategy analysis, etc.
+ hot water flow network	pressure driven hot water flows, detailed pump models	detailed hot water services modelling
+ hybrid components	power generation component models, lighting and small power load electrical details	basic electrical energy flows and demand calculations, basic supply and demand analysis
+ electrical network	real and reactive power flows electrical energy flows, losses, grid connection, power factors, electrical transmission, system voltages and current flows	detailed supply and demand analysis, power systems modelling, building-integrated energy systems modelling, renewable energy systems modelling, grid import/export
+ global control strategies	supervisory-level control, control hierarchy, simulation-based control	modelling of BEMS, global control strategy modelling: peak heat and power demand management, controls systems conflict resolution, etc.

Table 7.1 The added functionality from different layers of an ESP-r model.

Depending upon the requirements for a simulation, modellers have the choice of which of the constituents listed in table 7.1 to use in their model, this allows great flexibility in both the types of system that can be modelled and the level of detail to which they are defined. The modeller can describe a building and its systems abstractly and then add more detailed layers as required.

It should be kept in mind that the larger and more detailed the model, the greater is the data input requirement on the modeller. It is also worth noting is that as more detailed layers that are added to the model the more expert knowledge is required from the modeller (i.e. knowledge of plant modelling and HVAC systems or knowledge of power systems for power flow modelling). Hence two important limiting factors on the eventual form of a model are the information available to the modeller and the expertise of the modeller or design team.

However using a layered, modular problem description somewhat alleviates the problems described above as the simulation model can evolve with a design, with the model gradually acquiring more details as they become available (reducing the data input burden). Also, certain elements of the model may be defined in more or less detail, depending on whether expert knowledge is or is not available. This flexible approach to the problem definition is made possible by the consistent application of the control volume in the description of every constituent of the building model. Hence, while the model can be constructed from many different and diverse layers (e.g. moisture flow, electrical networks, air flow networks, etc.) each layer is based on the same elemental components: control volumes. Therefore, when the constituents of the building model are connected together, they form a consistent mathematical description of the building, no matter what the systems describe or the variation in the level of detail throughout the model.

### **7.1.2 Simulation of Integrated Models**

ESP-r's modular simultaneous solution method is perfectly suited to complement the program's flexible approach to model description; it can be tailored to suit the constituents of any particular model. As mentioned in chapter 4, the solution of the integrated system is achieved using a unified simultaneous solution process. This is constructed from several coupled solvers, each of

which processes a particular energy subsystem of the model in an efficient manner and at a frequency suited to the time constant of that particular element of the model. For example, the plant, flow and electrical networks are usually processed at a high frequency, to suit their rapid fluctuations in state, while the building fabric, with a longer time constant and more gradual changes of state, can be processed at a more appropriate low frequency.

The examples that follow demonstrate the layer based modelling approach and the subsequent use of the modular simultaneous solution process in the simulation of the integrated model.

## **7.2 Example 1: Combined Heat and Power in a Sport Centre**

In this example, the modelling of a small sport centre is described. The building itself consists of five main areas: a reception, changing rooms, a gym, the main sports hall and a plant room at the rear of the building. Heat and power are provided by a small-scale combined heat and power unit (CHP) integrated into the electrical services and the hot water services.

The loads that the hot water services feed include a heating coil in a mechanical ventilation system, which heats the supply air to various zones in the centre, and a hot water calorifier, which links to the domestic hot water services. The plant system is controlled so that the combined heat and power unit will run as a lead boiler, supplying the base heating load of the building during its opening hours. The major electrical loads in the building are the lighting system, which is subject to daylight control, and the rotational loads (fans and pumps) in the plant system. The electrical system of the building is three-phase a.c. and draws power from both the CHP unit and a grid connection.

### **7.2.1 The Form and Function of the Model**

In the modelling of this CHP-based energy system, the primary objective is to examine the interactions between the energy supply from the CHP unit and the demand in the building. It is therefore necessary to model both the CHP system and the building, particularly its heat and

power loads, in detail. The elements of the model required to do this are described in the following paragraphs.

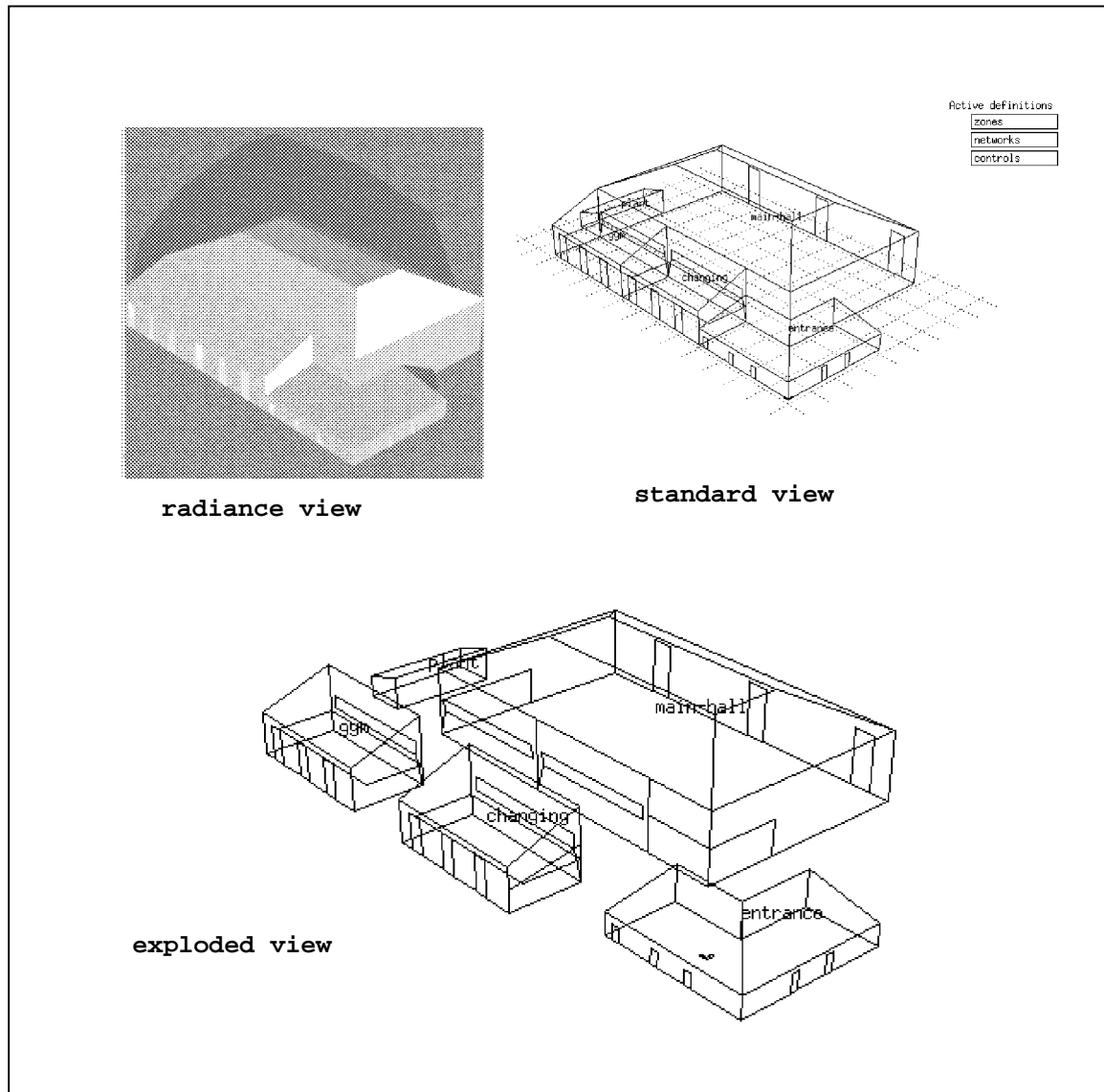


Figure 7.1 The ESP-r model of the sport centre.

### 7.2.1.1 The Building Geometry and Fabric

Five thermal zones are used to model the geometry and fabric of the building (figure 7.1), which has a total floor area of  $2520\text{m}^2$  and an internal volume of  $23,500\text{m}^3$ . The building is steel framed with an inner layer of block work, insulation and an outer layer of facing brick. The roof is constructed from aluminium sheeting, backed with an insulating layer. The fabric of the building is modelled using multi-layered constructions. Note that the definition of the building geometry also allows the calculation of the daylight factors necessary for the simulation of the lighting control system.

The lighting system is modelled as a hybrid load in each zone, with both the electrical and thermal characteristics being described. The total thermal and real power load for the lighting system is taken as  $12\text{W}/\text{m}^2$ . The lights in the building are an inductive load and are therefore modelled with the lagging power factor of 0.95. The lighting control in the building assumes the lighting in each zone (except the reception where lighting is uncontrolled) is arranged in three banks running parallel to the glazed exterior sections of the building envelope. Each bank of lights has its own daylighting sensor as shown in figure 7.2. When the sensed daylighting level rises above a user defined lux set point, the lighting controlled by the sensor is dimmed or switched off. Note, the form of daylight calculation and control used in these simulations is idealised, Clarke and Janak [2] describe more complex lighting simulations which utilise both ESP-r and the RADIANCE<sup>26</sup> lighting analysis program.

The thermal loading from occupants inside the building is modelled using a time varying sensible and latent heat gain to each zone.

---

<sup>26</sup> Developed by Lawrence Berkeley Laboratories, California.



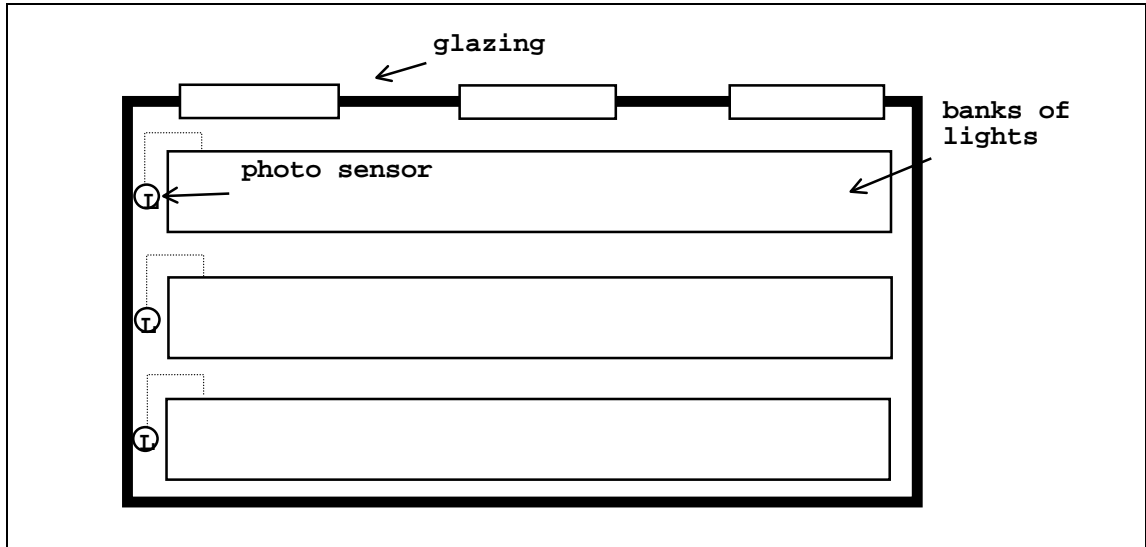


Figure 7.2 The lighting control layout in the main hall.

#### 7.2.1.2 The Plant and Fluid Flow Networks

The plant network for the building describes both the hot water services and the mechanical ventilation system. The hot water services comprise three 35kW boiler units feeding a hot water calorifier and the air-heating coil of the ventilation system. A CHP hybrid thermal/electrical component (described in the previous chapter) is connected in parallel with the boiler units, this has a total heat output of 75kW at full load, and real electrical power output of 36kW at a lagging power factor of 0.9.

The plant network is augmented with two separate flow networks, which describe the air flow in the mechanical ventilation system and the hot water flow in the hot water services. Infiltration and ventilation in the thermal zones are also modelled with the air flow network. The flow inducing components, fans and pumps, are modelled in both the plant and fluid flow networks. The flow components are augmented with electrical data; all are three-phase inductive loads with a lagging power factor of between 0.75 and 0.8.

The plant network associated with the building model is shown in figure 7.3.

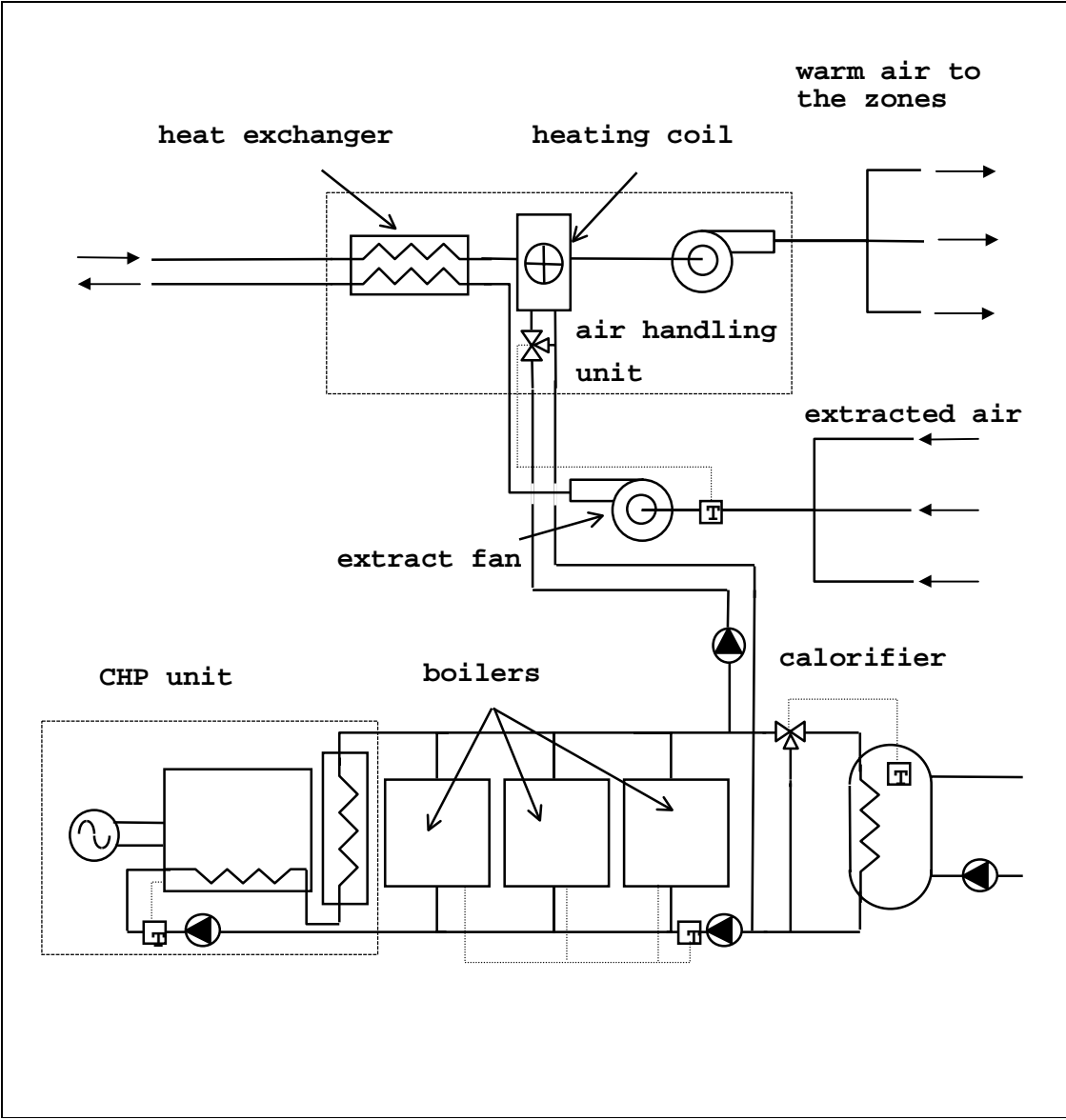


Figure 7.3 The sport centre's plant network incorporating the CHP unit.

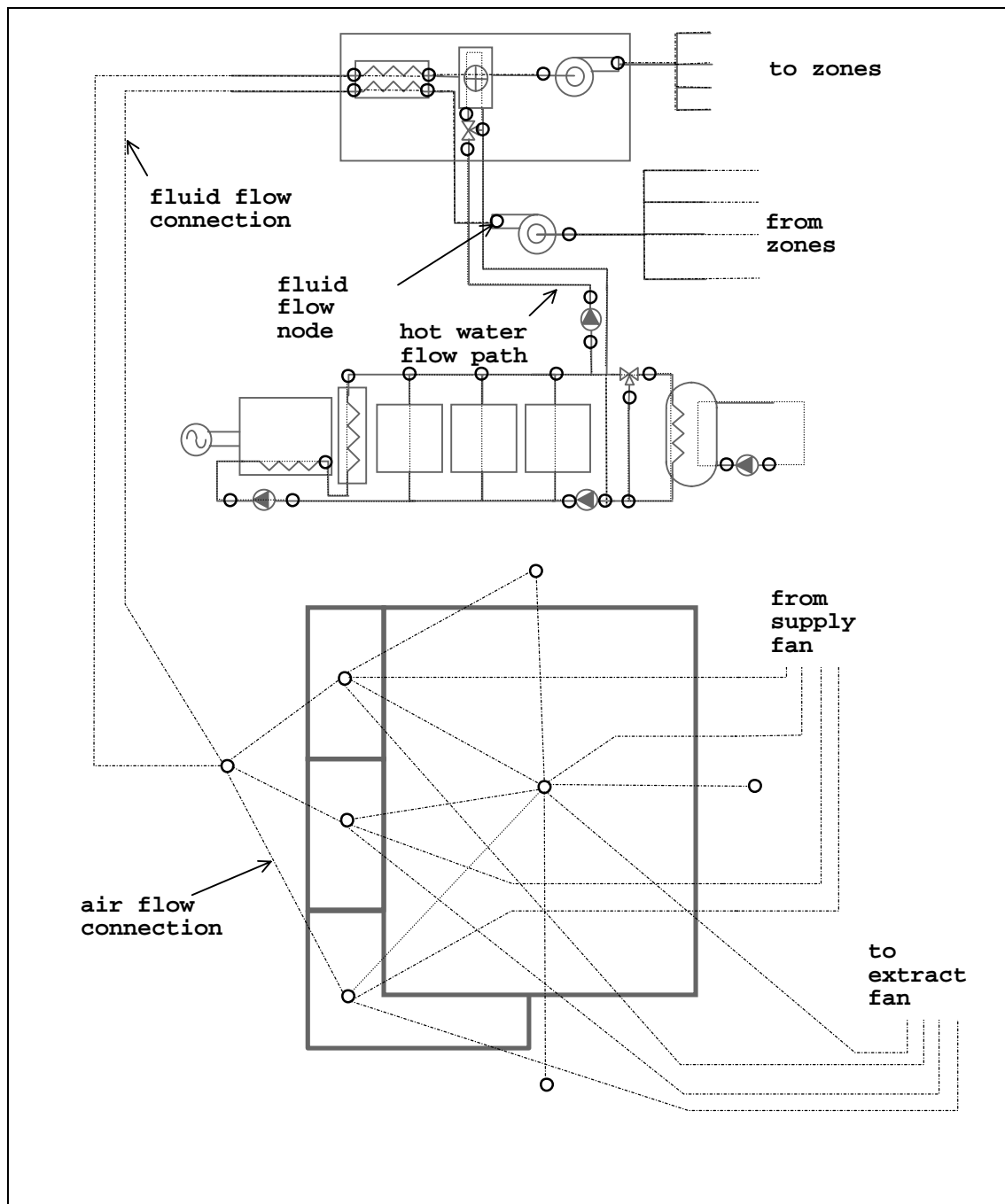


Figure 7.4 The fluid flow networks.

### **7.2.1.3 Control**

The majority of the control associated with the model is contained in the plant network. Firstly, the boilers and CHP network are controlled on the hot water return temperature (as described in [3]) using a series of on/off control loops. The set points are arranged in such a way that the CHP unit operates as the lead boiler, with the three boiler units acting, incrementally, as backup when required. The CHP unit shuts off when the return temperature rises above 90°C or according to time control. The air temperature in the sports centre is maintained between 19°C and 23°C by proportionally varying the flow rate of hot water through the heating coil using a 3-port diverting valve. Similarly, the hot water supply temperature from the calorifier is maintained at between 50-60°C by varying the supply flow-rate from the CHP and boilers, again using a diverting valve. The plant system is time-controlled such that it operates during the centre opening hours and a pre-heat period: this corresponds to an on period between 6.00 a.m. and 11.00 p.m., with an unconditional off period outside these hours. The described control loops are superimposed upon the plant network of figure 7.3

### **7.2.1.4 The Electrical Network**

As has been indicated throughout this thesis, the electrical network is a critical constituent of the building model, linking both the loads and CHP unit together and also linking the building to the outside electricity grid. The electrical network of the model describes the building's three-phase distribution system and transports the power produced by the CHP unit to the lighting, small power and rotational loads distributed throughout the thermal zones, plant and flow networks. The link to the external grid is used as the reference node in the solution of the electrical network (see section 3.3.1). The grid connection is bi-directional, when the loads in the building exceed the generated output of the CHP unit power is drawn from the grid. However, when surplus power is generated by the CHP unit, it is exported to the grid, which acts as an infinite source or sink for electrical power. The electrical network for the sports centre is shown in figure 7.5. The connections between the nodes in the network are three-phase cables, the nodes in the network represent cable junctions or distribution points for electrical power.

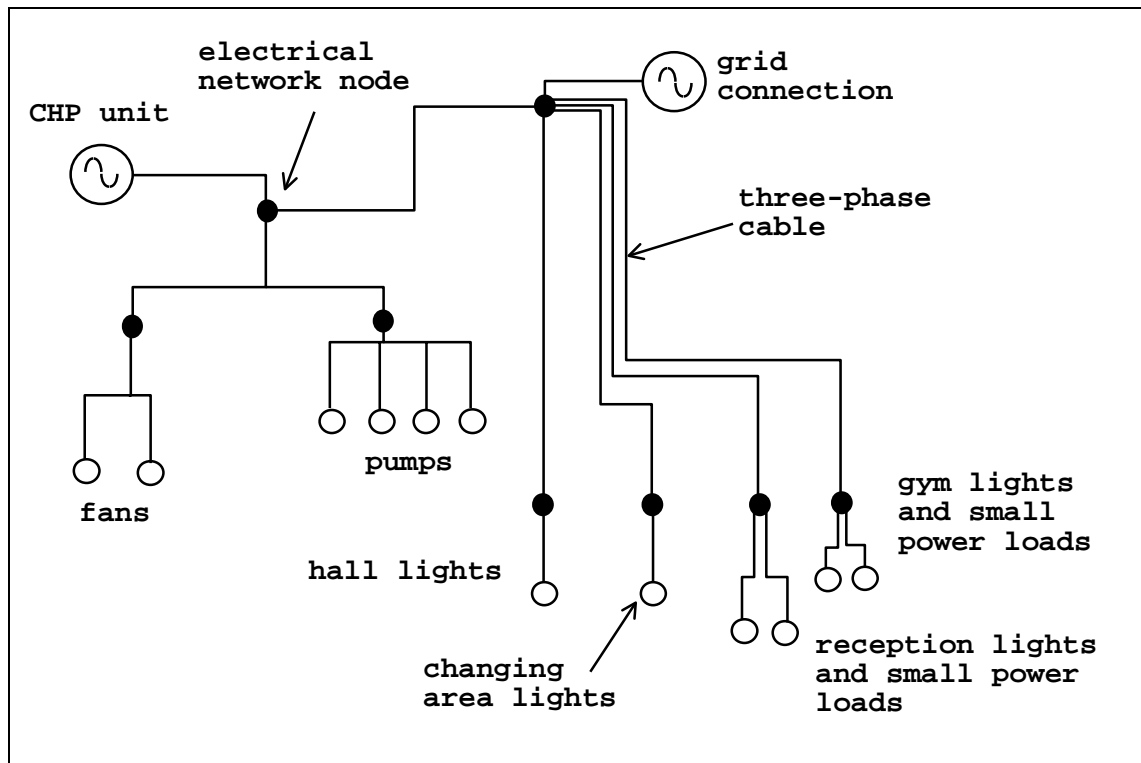


Figure 7.5 The electrical network for the sports centre.

### 7.2.2 Simulations with the Model

An example simulation with the integrated model is conducted over the course of a winter design week, 9-15th of January, using climate data from the Kew 1967 standard data set, considered typical of climate conditions in the United Kingdom.

The modelling of the sports centre requires the use of several of ESP-r's solvers: the building solver, the plant solver, the fluid flow solver and the electrical network solver. These are used to process systems of differing time constants. In this case the plant and electrical networks will change their states rapidly, in the course of a few seconds. The air and surface layers of the thermal zones will have a time constant of a few minutes, while the deeper fabric layers will change their temperature over the space of a few hours. To cope with the stiffness of this problem, variable frequency processing is employed, with the building zones solved every 15 minutes time and the plant, flow and electrical networks solved every 15 seconds. The high

frequency of processing on the plant and flow networks is necessary to capture the dynamics of the changes in the state of the plant system and its associated effects on the plant control loops. The electrical network must be processed at the same frequency, as any change in the state of power consuming components in the plant network will have an effect on the electrical system state. Processing at the same frequency allows these power consumption fluctuations to be captured in the power system solution.

### **7.2.3 Typical Output from the Simulation**

The following collage shows the spectrum of results data that can be recovered from the simulation of the integrated system. It should again be stressed that these results are intended to be indicative of the capabilities of an integrated simulation and are not the outcome of a design exercise.

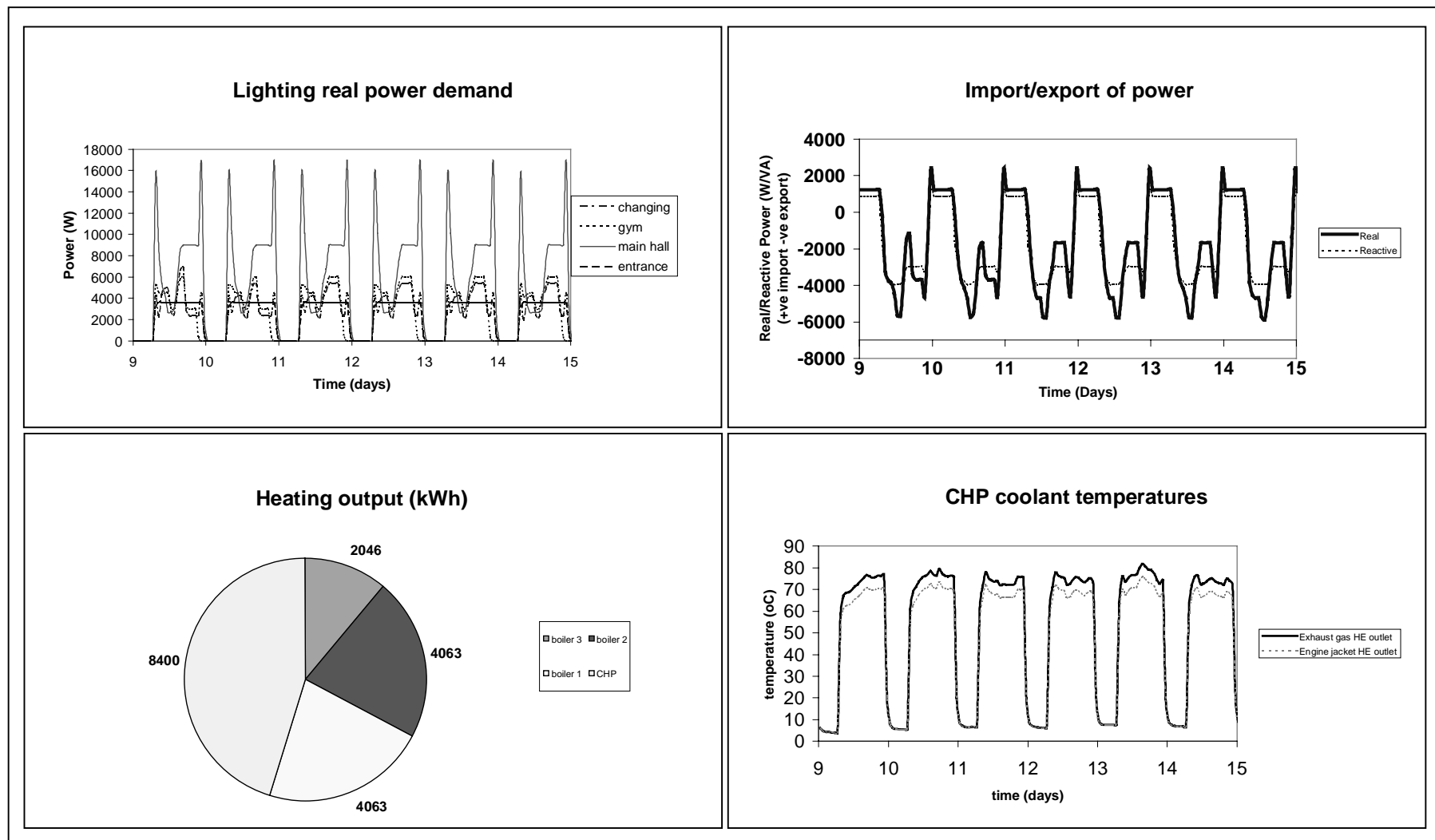


Figure 7.6 Samples of results obtained from the integrated CHP simulation

Analysis of the results from this illustrative simulation showed that the total heating energy supplied by the CHP unit was 8280kWh. The heating system maintained an average daytime temperature of 19.7°C in the main hall. The total real power consumption of the building was approximately 3129kWh, supplied at a lagging power factor of 0.89. Some 47kWh of this power was required to make up resistive losses in the distribution system. The power output of the CHP unit was 4033kWh, delivered at a lagging power factor of 0.9. Around 904kWh of real power was supplied to the grid. Note that the first two graphs of figure 7.6 show the interaction between the lighting control and the import/export of electricity; during the middle of the day lighting power demand is drastically reduced, allowing the export of surplus power.

The paragraph above describes only a small quantity of the data that can be obtained from such a complex simulation. Details of more information that could be extracted from integrated simulations and its possible uses are given in the next chapter.

### **7.3 A Photovoltaic Facade on a Factory Building**

This example looks at a photovoltaic facade integrated into the fabric of a factory building. The facade feeds power into the building's electrical system, while heat is recovered from air warmed as it is drawn through the facade cavity. The model is loosely based on the ELSA building at the EC's research centre in Ispra, Italy [4].

The building itself consists of two main areas: a factory and an adjacent office area. Both sections of the building are served by a mechanical ventilation system; this heats the incoming air to the offices and factory, attempting to maintain a temperature of 20°C in both areas. The warm air from the facade is passed into a heat exchanger, which heats the inlet air to the mechanical ventilation system.

The electrical loads inside the building consist of rotational motor loads on the factory floor and in the plant system, and also lighting loads in the factory and office zones.



### **7.3.1 The Form and Function of the Model**

The main purpose of a integrated façade simulation is to quantify the useful recoverable heat and power from the facade. The components of an integrated model required to do this are described in the following sections. Again, as with the CHP exemplar, the function of the exemplar is illustrative rather than a design exercise.

#### **7.3.1.1 The Building Geometry and Fabric**

The main sections of the building, the office and factory area are modelled using three thermal zones. The total floor area of these zones is  $1600\text{m}^2$  and they enclose a volume of  $12500\text{m}^3$ . The building fabric is modelled using multi-layered constructions, and mainly consists of pre-fabricated, insulated cladding.

The lighting and small power loads are modelled using zone load hybrid components, however unlike the previous exemplar, the lighting in both the offices and the factory space is not controlled and is switched on and off according to a time-schedule. Small power loads and thermal gains from equipment and occupants are calculated using time-varying profiles.

The photovoltaic facade of the building is modelled in detail, using several thermal zones to represent the facade construction: this consists of a ventilated photovoltaic module, mounted on top of the insulated cladding of the building facade. In total, the facade is fitted with 420 photovoltaic panels, which are modelled using multi-layered constructions consisting of an outer and inner glazing layer, a resin binder layer and an amorphous silicon PV special material layer. The zones in the facade model represent the air gap behind the PV modules and allow the explicit modelling of the important energy exchanges occurring inside and at the surface of the facade: short-wave absorption, convective exchange, long-wave radiant exchange, conduction, etc. The stacking of the facade zones (shown in figure 7.7) allows the modelling of the temperature gradient as the air passes up through the facade.

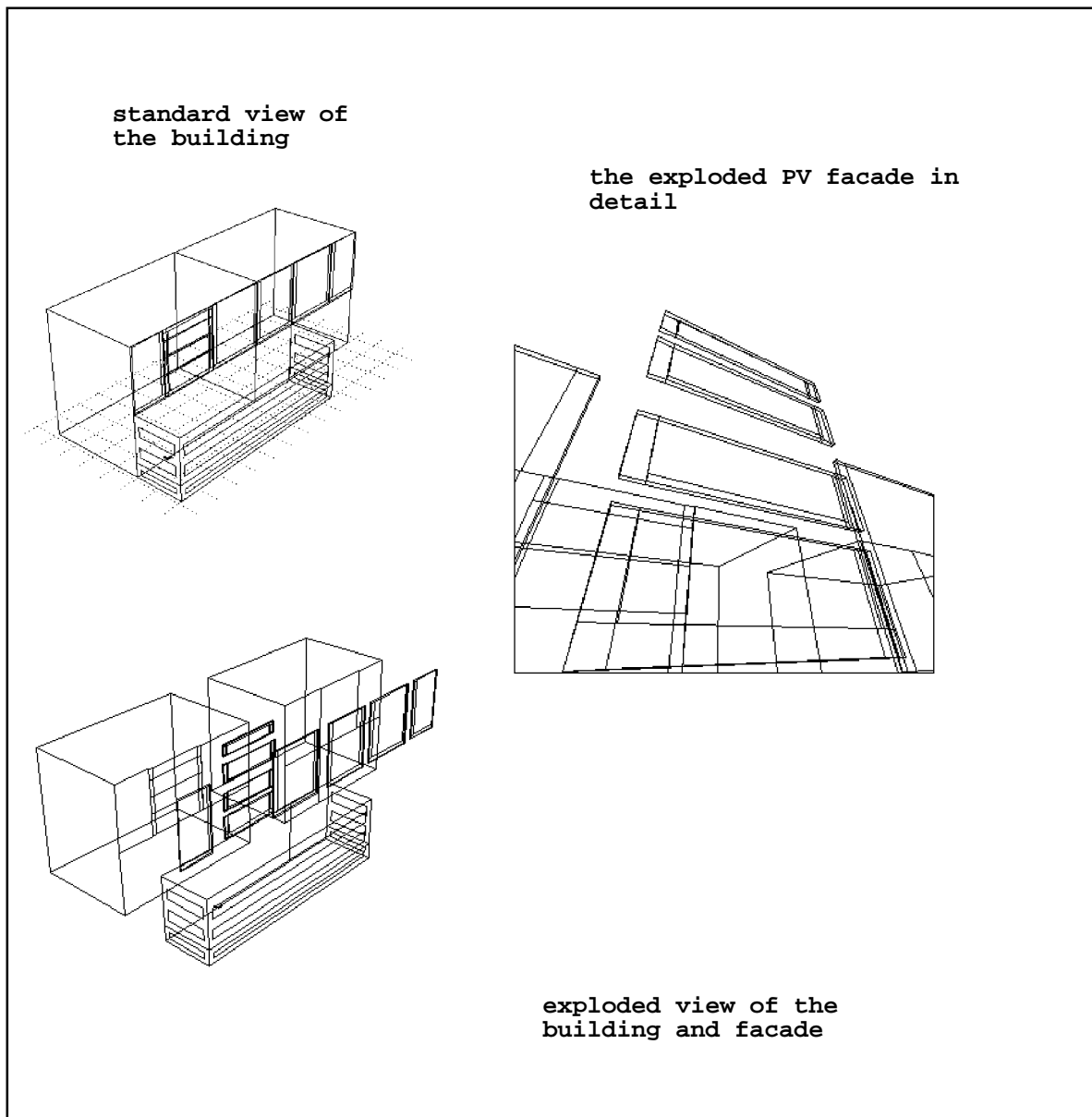


Figure 7.7 The building and detailed facade model.

### 7.3.1.2 The Plant and Air Flow Networks

The basic building model is augmented with a plant network that describes the mechanical ventilation system connected to the building. This heats the incoming supply air, such that comfort conditions in both the offices and factory area are maintained. The heating and cooling coil inside the ventilation system are supplied from hot water and chilled water systems respectively (these are not modelled explicitly in this example). The plant network is also used to

describe the heat recovery system from the photovoltaic facade: warm air from the facade is passed into a heat exchanger and used to pre-heat the filtered air entering the ventilation system. This is shown in figure 7.8. The fans in the plant system are modelled using hybrid components, incorporating both electrical and thermal information.

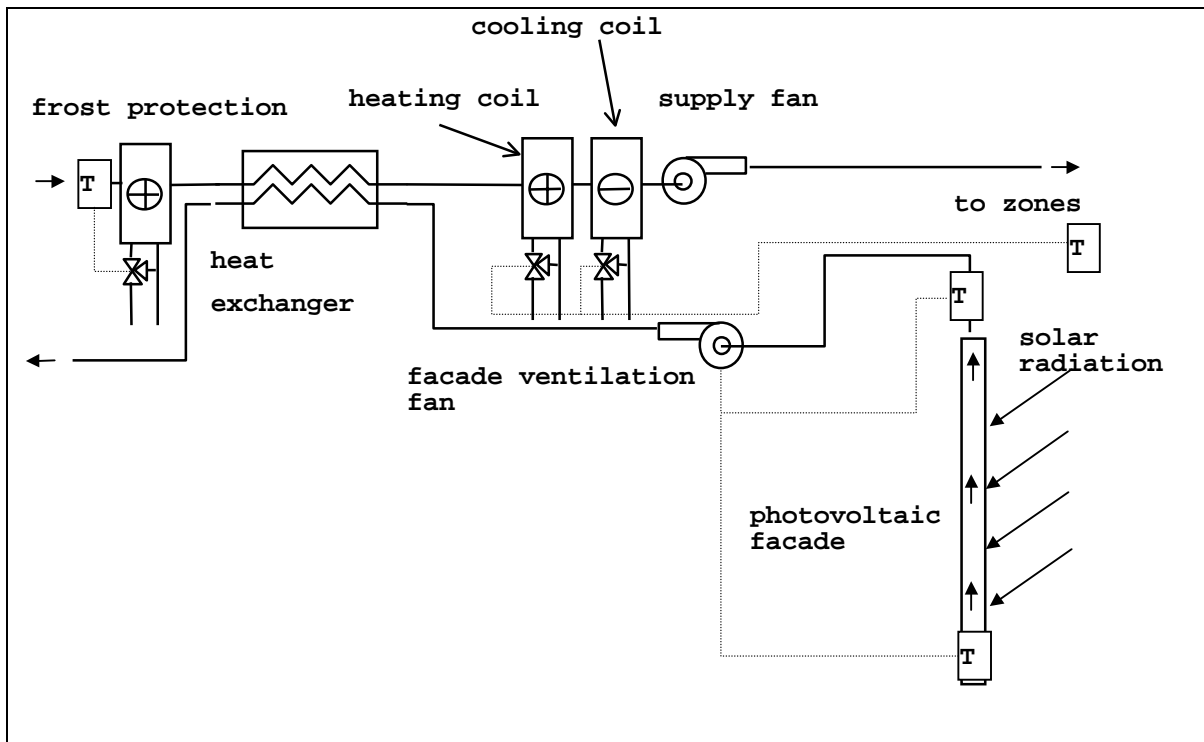


Figure 7.8 The plant network.

The basic building fabric model is augmented with an air flow network, which has the primary function of modelling the ventilation air flows at the rear of the photovoltaic facade. The network is also used to calculate the infiltration into the thermal zones and the air flow through the mechanical ventilation system. The air flow network is shown in figure 7.9.

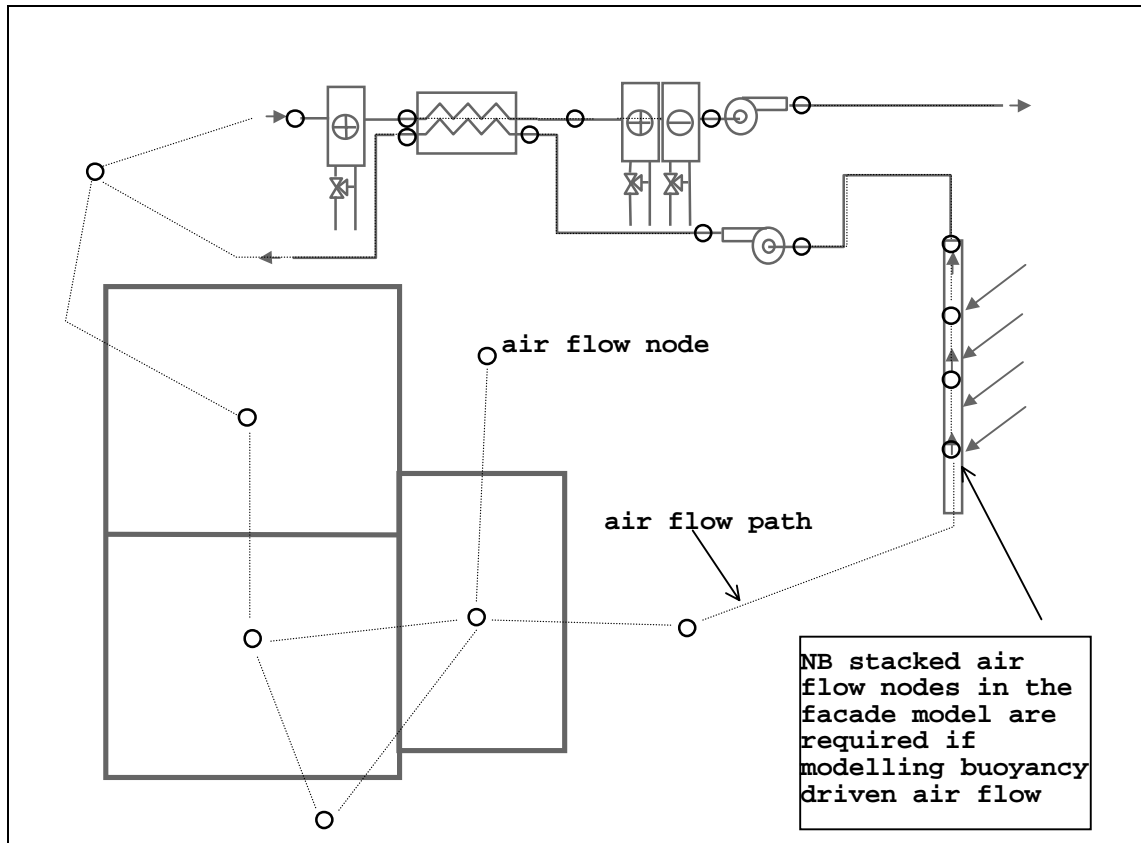


Figure 7.9 The air flow network

### 7.3.1.3 Control

Control in the building is associated with the heating coil and fan components in the plant network. The hot water flow rates through the heating and cooling coils are adjusted using a three-port diverting valve such that the air temperature in the offices and factory are maintained above 19°C. The control on the supply fan is time-based such that it provides fresh air to the factory and offices between 8a.m and 5p.m. The fan drawing air from the PV facade is programmed to operate when the temperature of the air emerging from the facade is 5°C warmer than the ambient air temperature. This creates a reasonable energy flow across the heat exchanger and between the two air streams. The component control loops are superimposed upon the plant network of figure 7.9

#### 7.3.1.4 The Electrical Network

As with the previous exemplar, the electrical network is used to model the three-phase distribution system of the building and includes a connection to the grid, which is used as the reference node. Power from the photovoltaic facade is fed into the electrical network, after inversion. All the lighting and small power loads in the zones and the fan loads of the plant system are connected to the network. This is shown in figure 7.10

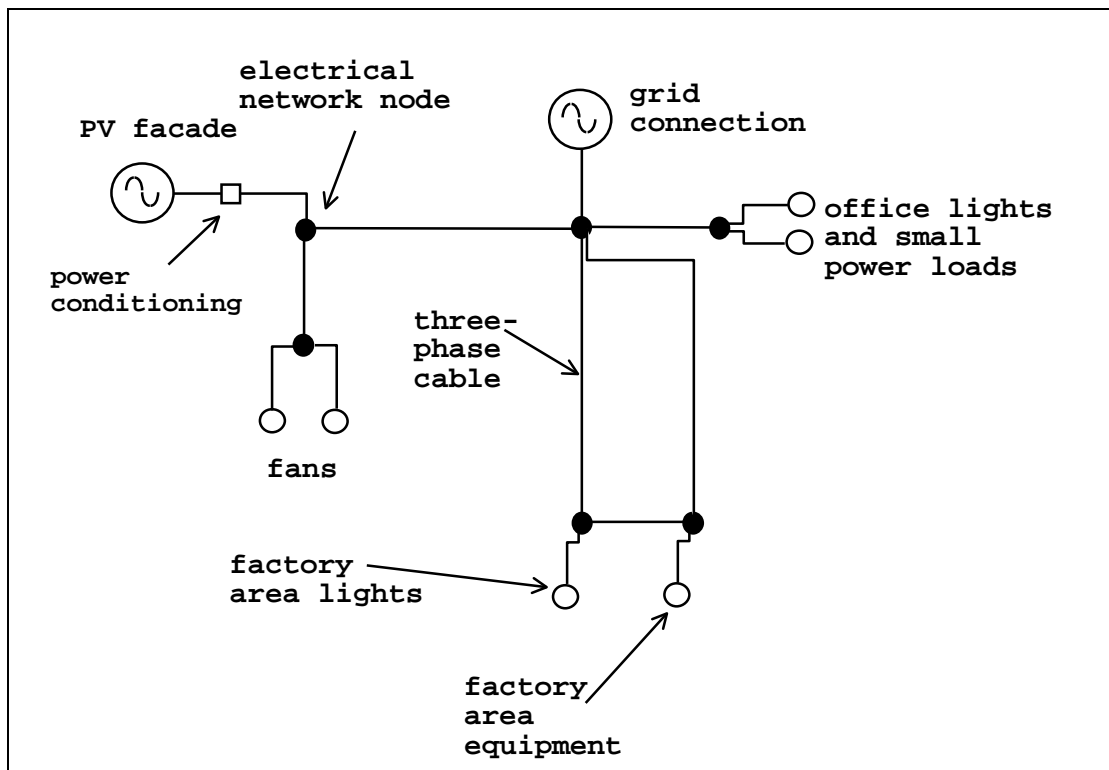


Figure 7.10 The electrical network with input from the PV facade.

#### 7.3.2 Simulation

A simulation can now be run to determine the recoverable heat and power from the facade when subjected to a UK climate. The simulation is run for a spring week from 3-9th March, using the standard Kew climate set. As with the sports centre, the different elements of the building are

processed at suitable frequencies, with the plant, airflow and electrical networks solved at 15-second time intervals and the building processed at 10-minute time intervals.

### **7.3.3 Typical Results Output from the Simulation**

Sample output from the simulation is shown in the results collage of figure 7.11.

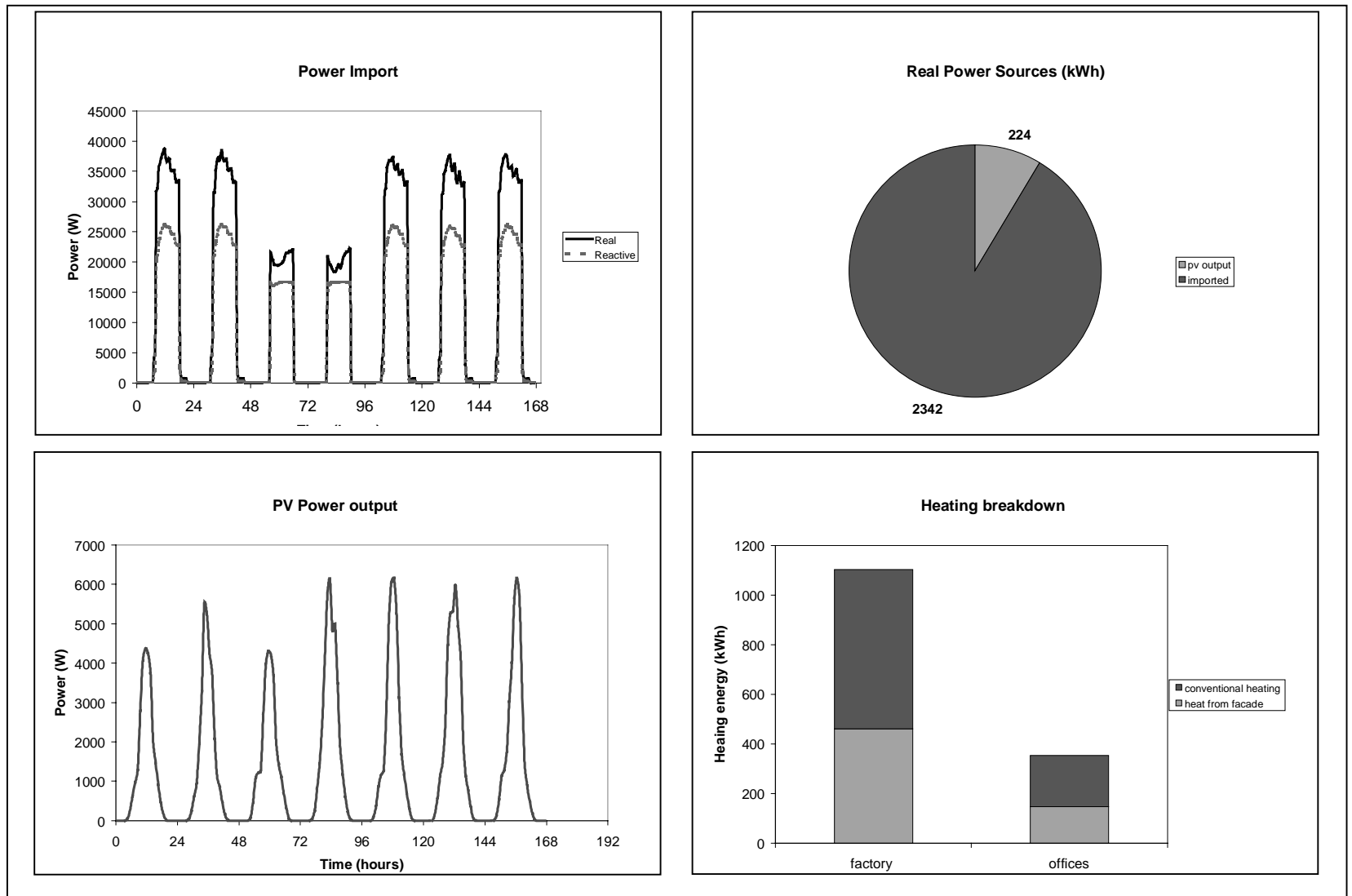


Figure 7.11 Sample of results obtained from the integrated PV facade

Over the simulation period the power produced by the facade totalled 224 kWh, while the useful heat recovered totalled 608 kWh. The combined efficiency of the facade was 31%, the total heating energy consumption of the building was 1455 kWh, while 2342.4 kWh of electrical energy was consumed in the office and factory areas. This was supplied at a lagging power factor of 0.88. 9.4% of the real power demand was supplied by the facade with the remainder drawn from the grid.

Again, the information given in the preceding paragraphs is only a small fraction of that available from the integrated simulation.

## **7.4 Summary**

This chapter has described the modelling of two buildings using ESP-r, both of which incorporate a building-integrated energy system. Using the components and electrical solver developed in this thesis, both the thermal and electrical systems of the buildings were modelled and simulated. Some sample results from these simulations were presented. These two exemplars have been installed for use on the ESP-r system for training purposes in the modelling of integrated systems.

The building-integrated energy systems models described in this chapter are but one use of the capabilities of the ESP-r system augmented with an electrical network and hybrid thermal/electrical modelling components. More potential uses are discussed in the next chapter.



## 7.5 References

1. Clarke J A, *Energy simulation in building design*, Adam Hilger, Bristol, 1985.
2. Clarke J A and Janak M, article in IBPSA News, Spring 1998.
3. Energy Efficiency Office Best Practice Program, *Guidance notes for the implementation of small scale packaged combined heat and power*, HMSO, 1989.
4. Clarke J A, Johnstone C, Strachan P, Bloem J J and Ossensbrink H A, *Thermal and power modelling of the Photovoltaic facade on the ELSA building Ispra*, 13<sup>th</sup> Photovoltaic Solar Energy Conference, Nice, 1995.

## 7.6 Bibliography

Santamouris M, Asimakopoulous D N (editors), *Energy conservation strategies for sports centres*, vol 2: case studies, European Commission Directorate General for Energy Save Programme, 1996.

Energy Efficiency Office Best Practice Program Report, *Remote monitoring of second generation small-scale CHP units*, New Practice Report No. 41, 1992.

Energy Efficiency Office Best Practice Program Report, *CHP in a medium sized hotel*, New Practice Report NP/30, 1991

Energy Efficiency Office Demonstration Scheme Report, *Combined heat and power in a University Hall of Residence*, Final Report, ED/206/228, 1988.

## **Chapter 8 - Review and Conclusions**

### **8. Introduction**

This chapter reviews what has been achieved in this thesis and also looks ahead to how the work undertaken may be improved upon. Further research opportunities in the field of integrated thermal and electrical modelling are discussed.

#### **8.1 Review**

This thesis has described a means of simulating the building's electrical energy flows as part of an integrated analysis of the entire building energy system.

The need for the integration of electrical energy flows into building energy simulation was brought about by a desire to model building-integrated energy systems and also by a general realisation that electrical power flows had been overlooked in building simulation. Thinking in terms of the building as an energy system, electrical energy flows is equally as important as their heat energy equivalent; therefore any complete model of the building must include them.

While a means to model the electrical energy flows is a useful addition for many aspects of building simulation (i.e. BEMS modelling, lighting studies, etc.), this thesis has concentrated on electrical power flow modelling within the context of the modelling of building-integrated energy systems. These systems produce high-grade electrical and low-grade heat energy for the building; thus the modelling of electrical energy flows is required. The two examples of such systems described in this thesis were small-scale combined heat and power and photovoltaic building facades. Both of these technologies are cleaner (and in the case of CHP more efficient) sources of heat and power than the alternative of local hot water boilers coupled with electricity supplied via the grid.

The design and analysis of building-integrated energy systems is complicated because interactions with the building must be taken into account: the thermal interaction with the building fabric, electrical demand and supply profiles, the influence of occupants, climate, plant and control, and capacity limits imposed by components. It was stated previously that an appropriate means of evaluating and designing such a system was through the use of a computer simulation tool that could adequately simulate all the aforementioned thermal and electrical interactions. This can be achieved by modelling the electrical power generation and distribution systems with the rest of the building in a unified and integrated fashion.

Therefore, the objective defined for this thesis was to develop a prototype of such a tool, which would enable the modelling and simulation of building-integrated energy systems through the conflation of electrical systems modelling with building energy simulation. The program chosen as the vehicle for this task was ESP-r [1].

At the commencement of the thesis, the ESP-r program could already model the complex thermal interactions occurring between the building, the external environment, occupant interactions, plant and control systems. The addition of a means to model the electrical energy flows would allow the program to model both the thermal and electrical aspects of building performance in an integrated fashion, whilst also laying the foundations of a tool for the evaluation and design of building-integrated energy systems.

The steps required to achieve the objective of simulating the building's electrical energy flows and building-integrated energy systems modelling were defined as follows.

- The development of a means to describe and model the electrical energy system within the building and a means of solving the electrical energy flows associated with it.
- The integration of this model of the electrical system into the ESP-r simulation program, enabling the simulation of the electrical energy flows in the context of an integrated, whole building simulation.

- The development of component models for use in the simulation of electrical and building-integrated energy systems.
- The testing of the component models and electrical network solution technique.
- The development of exemplar applications to illustrate the use and capabilities of the thermal modelling program augmented with an electrical modelling capacity.

The following sections summarise how the steps outlined above have been implemented.

## **8.2 The Integration of Electrical Power Flow Modelling into ESP-r**

### **8.2.1 Description of the Electrical System**

Chapter 2 described how, in ESP-r, the fundamental means of modelling the entire building involves describing the building and its HVAC systems as a collection of connected control volumes. Chapter 3 extended the concept of the control volume to encompass the modelling of the building's electrical system. This was described using a network, consisting of a set of electrical control volumes coupled together by electrical conductors. The description of the electrical system as a network was consistent with the means of describing other energy subsystems in ESP-r, such as plant, air and moisture flows.

The concept of an electrical network proved amenable to the description of different types of electrical systems; application of the network approach to three-phase and single-phase alternating current, direct current and mixed systems was outlined in chapter 3.

### **8.2.2 Solution of the Electrical Power Flows**

Solution of the electrical energy flows in the network was achieved by deriving, for each control volume, two non-linear power flow balance equations for the real and reactive power flows. The

simultaneous solution of the resulting set of balance equations allowed the calculation of the electrical network's state variables (such as voltage) and the electrical power flows. A Newton-Raphson iterative solver was developed to perform this task. The network solution requires that boundary conditions, in the form of power drawn from and injected into the electrical network, were known.

### **8.2.3 Integration into ESP-r**

The power flow boundary conditions provided the means to integrate both the electrical network and the solver into ESP-r, as they are calculated using the building model's electrically driven components (e.g. fans and pumps) and any building-integrated power generation (e.g. façade-integrated photovoltaic components). These constituents of the building are also associated with thermal phenomena (e.g. fluid flow) and so serve as a means to couple the electrical and thermal networks.

The integration of the electrical solver into ESP-r's modular simultaneous solution approach for the whole building model was detailed in chapter 4; this enabled the electrical network to be solved simultaneously with the other constituents of the building model.

### **8.2.4 Electrical Conductor Component Models**

The component models of electrical conductors, which link the control volumes of the electrical network together, were developed in chapter 5. Models of three phase and single-phase electrical conductors and transformers were described. The impedance characteristics of these component models were used in the formulation of the power flow balance equations for the electrical network.

### **8.2.5 'Hybrid' Component Model Development**

The concept of the 'hybrid' component was introduced in chapter 4 and related models were derived in chapter 5. These provided the means of translating the electrically driven thermal

phenomena occurring in the building model to the power flows required for the solution of the electrical network. For example, a hybrid fan component, driving air around an HVAC network model would draw the energy required to induce that flow from the electrical network.

Hybrid components were also developed for the modelling of building-integrated energy system components: a combined heat and power unit and a ‘special material’, which could be used to model both amorphous and crystalline photovoltaic components.

### **8.2.6 Verification**

Chapter 6 described how the electrical network solver has been subjected to a series of verification tests. In these tests the performance of ESP-r’s electrical solver was compared to that of another power flow solution program. Both were used to model various test networks and gave almost identical results.

Chapter 6 also described how the parameters of the CHP and photovoltaic special materials were calibrated using laboratory data. Two heat exchanger models, developed for use with the CHP model, were subjected to simple thermal excitations and their output compared against analytically derived solutions and against other models; there was close agreement between all of the models and the analytical solutions. Further tests of the photovoltaic model showed that its predictions agreed well with experimental data taken from field trials.

### **8.2.7 Demonstration**

Finally, two detailed exemplar applications were described in chapter 7. These were developed with the aim of demonstrating the extended capabilities of ESP-r with respect to the modelling and simulation of thermal and electrical energy systems in buildings, particularly building-integrated energy systems. Both models are available on-line within ESP-r for use in the training of users.

### **8.3 Suggestions for Future Work**

The work undertaken in this thesis represents only the first step in the integration of electrical systems modelling within building simulation. The electrical modelling capability integrated into ESP-r as part of this thesis is only a prototype, which can be improved and expanded upon. Some suggestions for this and possible further uses for integrated thermal/electrical modelling are described in the following paragraphs.

#### **8.3.1 Improvements to ESP-r and the Power Flow Solver**

##### **8.3.1.1 Three-phase Unbalanced and Mixed-Phase Systems**

The capability of the electrical power flow solver currently installed in ESP-r is limited to the modelling of balanced three-phase, single-phase and direct current power systems. The ability to model unbalanced three-phase and mixed phase systems, as described in chapter 3, remains to be implemented.

##### **8.3.1.2 Improved Solver Integration Using Control**

With the addition of global control strategies and electrical systems modelling into ESP-r [2], there now exists the possibility for the development of electrical demand management control in ESP-r. Recall that electrical demand management was discussed in chapter 4 as a means of further coupling the electrical solver into ESP-r's modular simultaneous solution method.

##### **8.3.1.3 Load Models**

ESP-r is currently equipped with hybrid component models of most of the major electrical loads in the building: fans, pumps, small power loads and lighting. However this list is not yet complete. Components such as compressors in refrigeration plant, vertical transportation loads (i.e. lifts) and cooling towers must be added to ESP-r's databases.

#### **8.3.1.4 Detailed Rotational Load and Generator Models**

The current hybrid rotational load models, described in chapter 5, are somewhat simplistic in that both the rotational dynamics and a detailed equivalent circuit model of the electric motor are not included. The addition of these two elements into more detailed fan, pump and generator models would allow the modelling of transient, electro-mechanical effects such as power surges and voltage drops during motor start-up and supply frequency variation.

#### **8.3.1.5 More Realistic Representation of Small Power Loads**

The representation of small heat and power loads (e.g. computers, faxes, televisions, etc.) in simulation programs requires further investigation. Currently, the temporal variation of these loads is represented by simplified, time-dependent profiles. There is a need for the development of stochastic methods for the calculation and generation of more realistic electrical demand (and thermal loading) profiles, particularly for larger buildings, which have large populations of these small loads.

### **8.3.2 Uses for Integrated Thermal/Electrical Modelling**

This thesis has described the application of electrical power flow modelling in the context of the modelling of building-integrated energy systems. However, the network-based approach used to model these systems is applicable to any type of electrical system, not just localised power generation. Hence, the scope for modelling combined thermal and electrical systems is large. Situations where the modelling of both the building's thermal and electrical systems could be beneficially deployed are outlined below.

#### **8.3.2.1 Control**

Perhaps the richest area for exploitation using integrated thermal and electrical modelling lies in the field of control. The addition of electrical power flow modelling adds a new range of



variables (voltage, power flow, current, etc.) around which new control laws can be developed. The example of a generator voltage controller has already been given in chapter 5.

Another example of where control could be applied in the power generation process is in optimising the efficiency of inversion from a PV façade. If multiple inverters are used in this process the number of active inverters can be controlled so that each operates at high loading and high efficiency: inverters can be switched on or off, using a controller, as the power output from the façade rises and falls with time.

As mentioned in chapter 4, control can be used to represent electrical safety devices such as fuses and switches, which act to cut off the electrical supply to overloaded system conductors. Also, if minimum and maximum operating voltages are incorporated into the hybrid components attached to the electrical network, control could be used to model the effect of these component's safety devices, shutting them down if the operating limits are exceeded.

Further developments in interaction between energy pricing (especially electricity pricing), demand, increasing flexibility in the electricity market and controls may play an increasingly important role in the energy supply to buildings. For example, one system already operational in France [3], uses the price of electricity to affect the control and electrical energy consumption of domestic heating systems. The temperature set point of the system is reduced at times of high electricity prices, which also coincides with periods of peak demands. Such tariff-responsive building controls may well become reality in the UK commercial and domestic sectors. Building simulation tools equipped with an electrical modelling capability may be used in the simulation of this form of energy demand management.

Finally, returning to building-integrated energy systems, integrated simulation could be used in the testing and development of advanced control algorithms, which match the demand of the building to the supply of the integrated generation system. Such a system would be responsible for making most efficient use of heat and power, minimising energy usage conflicts (e.g. between lighting, daylighting and cooling), scheduling energy storage, limiting energy demand

and controlling energy supply. In effect, the control described here would be a global energy management system, managing both the supply and demand of energy in a building.

If the advanced control systems mentioned above are to be designed correctly, it will be necessary to model the interactions between the building's electrical system and its energy and environmental performance. The explicit representation of the electrical system in an integrated model is therefore vital.

#### **8.3.2.2 Autonomous Renewable Energy Systems**

Integrated thermal and electrical modelling can be extended to the simulation of all scales of energy systems, including larger-sized systems, which consist of more than one building and power generation source; an autonomous renewable energy system is one such example. The use of a building simulation tool in the modelling of renewable energy schemes is discussed in [4] and power flow modelling is applied to the modelling of a wind energy conversion scheme in [5]. Note that in most large-scale renewable energy simulations, the electrical demand is modelled as a simple profile. The advantage of including the building in a renewable energy system model is that the heat and power demands are explicitly calculated, and will vary as functions of time, climate, control and user interactions. For this size of model, the electrical network describing the building distribution system would become part of a larger network.

The generator voltage controller, discussed in chapter 5, would play an important part in the simulation of autonomous energy systems. This control algorithm would be required to maintain the voltage levels throughout the system as the supply from the connected renewable sources and power demand vary with time and environmental conditions. Note that voltage control is only possible if the electrical network of the system is modelled explicitly. This form of control could also be used in the regulation of back-up generators, with the back-up capacity being switched on as supply voltage drops with increasing load.

### **8.3.2.3 Electrical Systems Design**

Currently, building simulation programs are used in the design and evaluation of the fabric and environmental systems in buildings. The inclusion of a model of the electrical system opens up possibilities for some aspects of electrical systems design to be accomplished within the context of a building simulation. Examples include estimating the loading on cables, the balancing of phase loading in larger buildings and the sizing of capacitor banks for power factor correction. Note that if more detailed, dynamic electro-mechanical models of electrical equipment are integrated into ESP-r (see section 8.3.1.4), the sizing of cables, fuses and switches could also be undertaken within an integrated energy simulation, through the calculation of peak transient loads in the relevant network elements.

## **8.4 Perspective**

With the addition of electrical systems modelling into a building energy simulation tool, the modeller now has the ability to perform a total evaluation of the energy and environmental performance of a building, encompassing all the important energy flows: high grade electrical and low grade thermal. Total building energy analysis will become increasingly important as buildings increase in complexity, incorporating more advanced materials, technologies and control and, as more stringent environmental performance criteria force designers to improve the performance of their creations. This improvement in performance will be required both in terms of energy consumption and occupant comfort.

Part of the solution towards improving the performance of the complex entities that are buildings is through the increasing use of technology in their design. One of the problems in the building design process has been a reluctance and fear on the part of designers and engineers to explore and encourage modern design techniques such as simulation. This conservatism has maintained a somewhat primitive approach to the design of what is a complex energy system and has contributed to the poor performance of many of the buildings in existence today.

However, simulation too, must evolve to improve the accuracy and realism of modelling, and also to take advantage of the ongoing advances in computing technology and applications. To an extent this has happened, with simulation entering areas that were, until recently, untouched or regarded as too complex to explore. For example, the capabilities of the ESP-r tool have been expanded in recent years to include such diverse functionality as microscopic thermofluid simulation [7,8], fabric moisture flow [9] and mould growth prediction [10].

While many areas of simulation remain to be fully developed and explored, it is hoped that the work undertaken in this thesis is a small step in the continuing evolution of building simulation.

## 8.5 References

1. Clarke J A, *Energy Simulation in Building Design*, Adam Hilger, 1985
2. MacQueen J, *The modelling and simulation of energy management control systems*, PhD Thesis, University of Strathclyde, Glasgow, 1997
3. Private communication with Giles Guyon, Électricité de France, 1998
4. Clarke J A, Evans M E, Grant A D and Kelly N J, *Simulation tools for the exploitation of renewable energy in the built environment: the EnTrack-GIS System*, Proceedings of Building Simulation '97, Prague, Czech Republic, 1997.
5. Kariniotakis G, Stavrakakis G, Nogaret E and Bordier M, *Advanced modelling and identification of autonomous wind-diesel power systems. Application on the French island Desirade*, Proceedings of the European Community Wind Energy Conference, Lübeck-Travemünde, Germany, 1993.
6. Evans M S, Kelly N J, *Modelling active building elements using special materials*, Energy Sysyems Research Unit Technical Report 95/18, University of Strathclyde, Glasgow.
7. Negrao C O R, *Conflation of computational fluid dynamics and building thermal simulation*, PhD Thesis, ESRU, University of Strathclyde, Glasgow.
8. Clarke J A, Dempster W M and Negrao C O R, *Predicting indoor air flow by combining network approach, CFD and thermal simulation*, Proceedings 16<sup>th</sup> AIVC Conference, 1995.
9. Nakhi A E, *Adaptive construction modelling within whole-building dynamic simulation*, PhD Thesis, University of Strathclyde, Glasgow 1995.

10. Clarke J A, Johnstone C M, Kelly N J, McLean R C, Nakhi A E, *Development of a simulation tool for mould growth prediction in buildings*, Proceedings Building Simulation, Prague, 1996.

# Appendix 1 - Photovoltaic Technology Review

## A. Introduction

Photovoltaic materials produce electrical power from sunlight. The basic component of photovoltaic power conversion is the solar cell. The amount of electrical energy produced is dependent on the intrinsic properties of the solar cell and the availability and intensity of solar radiation.

### A.1 Solar Cells

Solar cells are most commonly fabricated from silicon, however other materials such as cadmium and gallium may also be used. Silicon is a semiconductor material that is tetravalent, i.e. group IV of the periodic table. If silicon is doped with ions from a group III material it becomes an acceptor (*p*-type), when doped with a group V material it becomes a donor (*n*-type). The *p*-type material is said to have a surplus of holes (rather than a deficit of electrons).

The most common solar cell is basically a *p-n* junction, where the *p*-type (positive) and *n*-type (negative) materials are doped semiconductor(s). The *p-n* junction is a boundary in a semiconductor material where a region of electron depletion neighbours a region of electron surplus. A region of opposing charge is present in the areas of *p* and *n*-type materials (see figure A.1) which are adjacent to the junction. This is known as the depletion region. In a state of thermal equilibrium an electrostatic potential exists in the depletion region, which prevents electrons diffusing from the *n*-type to the *p*-type material.

Four types of silicon semiconductor device are in use: monocrystalline, polycrystalline, thin film polycrystalline and amorphous. Monocrystalline silicon has a highly ordered atomic structure and cells made from it have the highest photovoltaic conversion efficiencies (18%). Polycrystalline silicon consists of many crystalline grains; the conversion efficiency of a solar cell manufactured from polycrystalline silicon is around 13%. Thin film polycrystalline devices

have a lower efficiency (11%). Amorphous silicon has a random atomic structure and solar cells constructed from this form of silicon have a conversion efficiency of around 6-8%. The conversion efficiency of amorphous PV materials tends to decay over time.

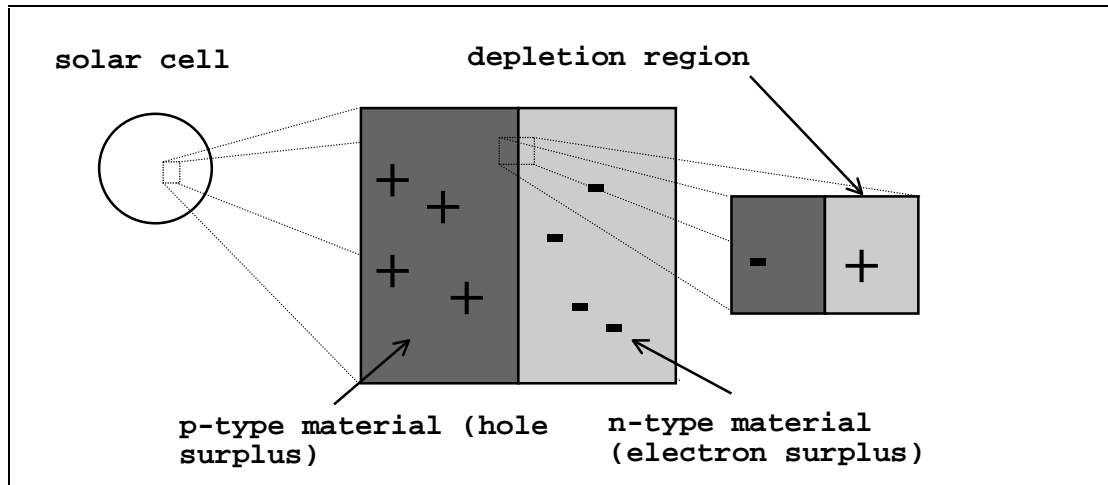


Figure A.1 A  $p$ - $n$  junction

A standard solar cell is typically cut from a large ingot of monocrystalline or polycrystalline silicon and is typically between 200 and 400 microns thick. The thickness of the wafer is largely determined by the manufacturing process, however a minimum thickness of around 100 $\mu$ m is required to ensure that the majority of the incident above-band-gap photons (defined in section A.1.2.3) are absorbed. The wafer has metallic grids deposited on each side, which act as electrical contacts and allow current liberated by sunlight to flow away from the cell.

Thin film amorphous silicon cells are created using an amorphous, silicon-hydrogen (Si-H) alloy, which has a much greater ability to absorb photons than crystalline silicon. The semiconductor material used in the cell can therefore be much thinner (e.g. 1 $\mu$ m). The normal process of production is sputtering of the Si-H alloy onto a substrate. Common substrates include glass and metals. The Si-H alloy is doped with phosphorous and boron to create  $n$  and  $p$ -type materials respectively.



Thin film crystalline silicon is created by precipitating the growth of a thin silicon layer on top of molten, saturated solution of tin and silicon. This is done through controlled cooling. The resulting layer is 2-3  $\mu\text{m}$  thick. Texturing of the surfaces of a cell constructed using thin-film silicon ensures that the path length of light through the cell is up to 20 times the cell thickness (due to multiple reflections), thus ensuring that most of the incident photons are absorbed.

### A.1.1 Solar Cell Physics

The following section provides a condensed review of solar cell physics and also explains the basis for the characteristic equations of the photovoltaic special material of chapter 5. For a comprehensive view of solar cell operation and photovoltaic systems the reader is referred to standard texts such as [1]. Note this section only deals with simple  $p$ - $n$  junctions in a single layer of semiconductor (homojunction). Heterojunction cells (i.e. junctions of two different semiconductor materials) are not discussed. Multijunction cells are discussed in section A.1.2.3.

In order for a current to flow in the semiconductor material, electrons in the valence orbitals (which form the bonds between the atoms) must be promoted to a higher energy level so that they are capable of conduction. The energy required for this is achieved by the absorption of photons of light. The amount of energy required for a valence electron to jump to this higher energy level is known as the band gap energy,  $E_g$ . This is an intrinsic property of the material (e.g. crystalline silicon has a band gap energy of 1.12 eV, while that of amorphous silicon is around 1.75 eV). Liberation of the electron involves the transition of the electron from a ground state to an excited state (capable of conduction).

Electrons at or around the ground state energy level are said to be in the valence band (the energy level associated with valence electrons), while electrons at excited energy level are in the conduction band. These energy levels are denoted by  $E_v$  and  $E_c$ , respectively. The band gap energy is given by the difference between them.

$$E_g = E_c - E_v . \quad (\text{A.1})$$

The liberation of an electron can be also be achieved by thermal excitation.

The liberation of an electron creates a corresponding vacancy in the valence band known as a hole. Electrons and holes are the charge carriers in the semiconductor material (i.e. the source of electrical current). In *p*-type materials the holes are the majority carriers, while in *n*-type materials electrons are the majority carriers.

### A.1.2 The p-n Junction

The following section describes and explores the properties of the *p-n* junction in a semiconductor material, firstly in a state of equilibrium, then exposed to an external potential and finally acting as a solar cell (when exposed to a light source).

#### A.1.2.1 The Unilluminated p-n Junction

In a state of thermal equilibrium, the fraction of electrons in the conduction band is given by equation A.2

$$n_c = \int_{E_c}^{E_v} n'(E) f(E) dE \quad (\text{A.2})$$

$n'(E)$  is the number of quantum states per unit volume of material, and is given by the expression

$$n'(E) = 4\pi h^{-3} (2m)^{1.5} E^{0.5}, \quad (\text{A.3})$$

where  $h$  is Planck's constant ( $6.62 \times 10^{-34}$  Js) and  $m$  is the mass of an electron ( $9.11 \times 10^{-31}$  kg),  $E$  is the energy level (eV).

$f(E)$  is a function giving the probability distribution of electrons entering the conduction band (and holes entering the valence band), which is described by the following expression.

$$f(E) = \exp\left(\frac{-E_c - \mu}{kT}\right). \quad (\text{A.4})$$

$\mu$  represents the Fermi energy (J), the apparent energy level from which the majority carriers in a  $p$  or  $n$ -type material are excited into the valence or conduction bands respectively (see figure A.2);  $k$  is the Boltzmann constant ( $1.38 \times 10^{-23}$  J/K), while  $T$  is the temperature of the PV material (K).

Substituting equations A.3 and A.4 into equation A.2 gives

$$n_c = \int_{E_c}^{E_v} 4\pi h^{-3} (2m)^{1.5} E^{0.5} \exp\left(\frac{-E_c - \mu}{kT}\right) dE. \quad (\text{A.5})$$

Evaluation of the integral in equation A.5 gives the following expression for  $n_c$ .

$$n_c = N_c \exp\left(\frac{-E_c(p) - \mu(p)}{kT}\right) \quad (\text{A.6})$$

$N_c$  is a temperature dependant property called the conduction band effective density of state [1].

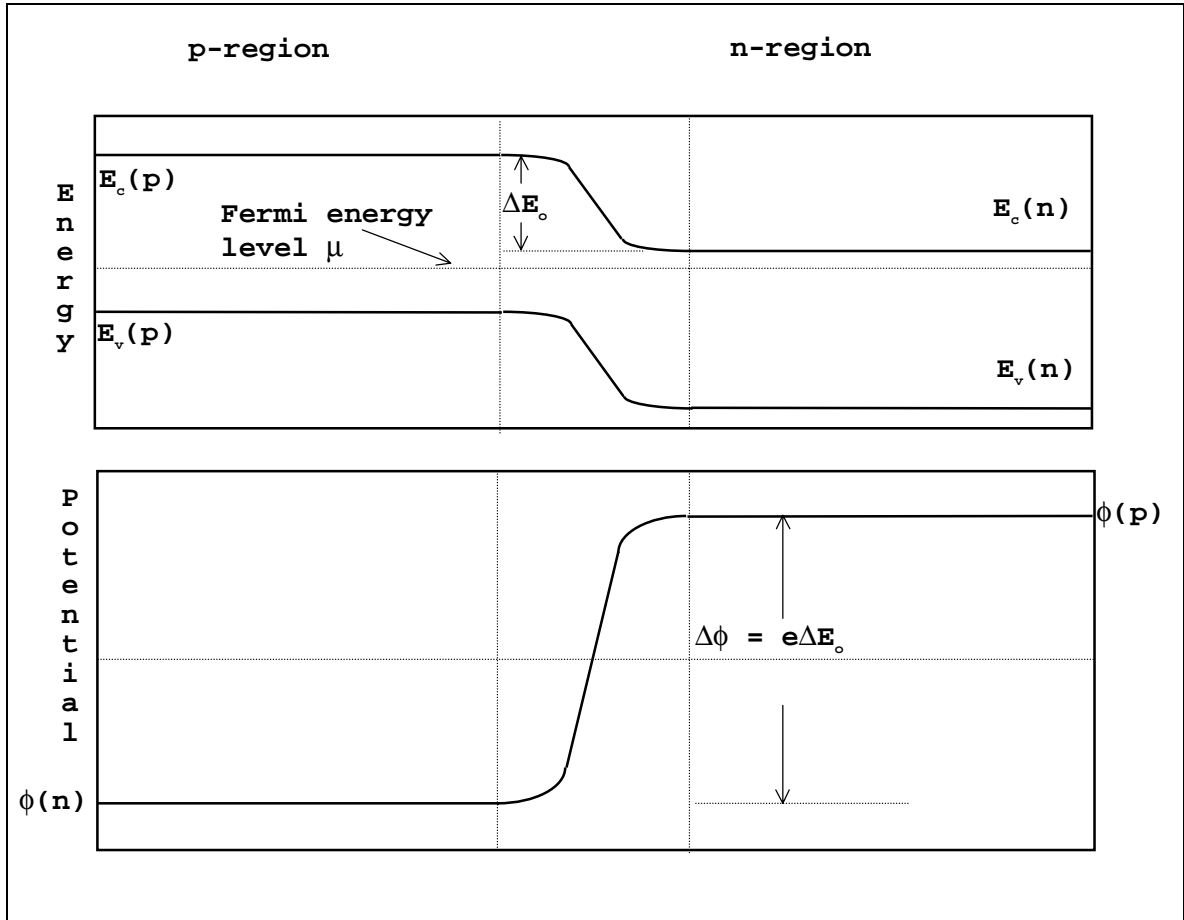


Figure A.2 The electrostatic properties of a p-n junction.

Electrons thermally excited into the conduction band of the p-type material can flow freely into the n-type material. The size of this current,  $I_o^-(p)$  (A), is proportional to the number of electrons in the conduction band of the p-type material, the constant of proportionality,  $\alpha$ , the value of which is dependent on the electron mobility and the gradient of the electrostatic potential.

The generation current is given by

$$I_o^-(p) = \alpha N_c \exp\left(\frac{-E_c(p) - \mu(p)}{kT}\right). \quad (\text{A.7})$$

In the  $n$ -type material, electrons in the conduction band must overcome the electrostatic energy barrier  $\Delta E_o$  (J). The fraction of electrons capable of surmounting this barrier is given by the following equation.

$$n_c(n) = N_c \exp\left(\frac{-E_c(n) - \mu(n) - \Delta E_o}{kT}\right). \quad (\text{A.8})$$

Looking at figure A.2, the electrostatic potential barrier,  $\Delta E_o$ , can be substituted with  $E_c(p) - E_c(n)$ . The expression for the current flow from the electrons excited into the conduction region of the  $n$ -type material can therefore be expressed in the following form.

$$I_o^-(n) = \alpha' N_c \exp\left(\frac{-E_c(p) - \mu(n)}{kT}\right). \quad (\text{A.9})$$

This current is known as the recombination current and flows in the opposite direction to the generation current. Under conditions of thermal equilibrium  $\alpha = \alpha'$ . The net electron current in the system is given by the addition of the  $p$ -type and  $n$ -type currents.

$$I^- = I_o^-(p) + I_o^-(n). \quad (\text{A.10})$$

#### A.1.2.2 The $p$ - $n$ Junction Subjected to an External Potential

Under isolated conditions there can be no imbalance of currents in the depletion zone and the sum of the generation current and recombination current is zero. However, when a potential energy barrier  $E_{ext}$  is applied across the junction (caused by the parallel connection of an external voltage) it is no longer in equilibrium and the generated and recombination currents no

longer equate. For a negative  $E_{ext}$ , the potential barrier that the electrons in the  $n$ -region must overcome is increased and the current  $I_o^-(n)$  decreases exponentially. In this case the net current  $I^-$  approaches  $I_o^-(p)$ . For a positive  $E_{ext}$  the current  $I_o^-(n)$  increases exponentially with the external potential. In both cases  $I_o^-(p)$  remains unchanged, it being dependant upon the small number of electrons thermally excited into the conduction band in the  $p$ -material. This current is temperature dependent.

The Fermi energies within the  $p$ - $n$  material change when the external potential is applied such that they are no longer in equilibrium; the following equation applies.

$$\mu(p) - \mu(n) = -\Delta E_{ext} . \quad (A.11)$$

Re-arranging equation A.11 to an expression for  $\mu(n)$  and substituting into equation A.9 gives the following expression for  $I_o^-(n)$ .

$$I_o^-(n) = -\alpha N_c \exp\left(\frac{-E_c(p) - \Delta E_{ext} + \mu(p)}{kT}\right). \quad (A.12)$$

Substituting equation A.7, this can be simplified to,

$$I_o^-(n) = -I_o^-(p) \exp\left(\frac{\Delta E_{ext}}{kT}\right). \quad (A.13)$$

Substituting equation A.13 into equation A.10, the net electron current in the conduction band, per unit volume of PV material, can now be expressed (for the non-equilibrium state):

$$I_o^- = -I_o^-(p) \left( \exp\left(\frac{\Delta E_{ext}}{kT}\right) - 1 \right). \quad (A.14)$$

For any  $p$ - $n$  junction the flow of electrons is only possible if there is a corresponding flow of holes. The excitation of an electron into the conduction band in both the  $p$  and  $n$  materials creates corresponding holes. These hole currents,  $I_o^+(p)$  and  $I_o^+(n)$ , can be expressed by a similar set of equations as were derived for electron currents. Therefore, the total current  $I$  across the  $p$ - $n$  junction is a summation of the electron and hole currents:

$$I = I_o^- + I_o^+ . \quad (\text{A.15})$$

The total current  $I$ , in a unit volume of PV material, is given by

$$I = -I(p) \left( \exp \left( \frac{\Delta E_{ext}}{kT} \right) - 1 \right) . \quad (\text{A.16})$$

This is called the Shockley equation and characterises the  $p$ - $n$  junction under unilluminated conditions. The unilluminated current flow in the  $p$ - $n$  junction is referred to as the diode current.

### A.1.2.3 The $p$ - $n$ Junction Exposed to Light

As stated earlier, liberation of an electron from the valence band can be achieved by the interaction of a photon with the electron. The jump from the ground state to the excited state liberates one (and only one) electron-hole pair and requires the absorbed photon to have an energy of

$$h\nu > E_g , \quad (\text{A.17})$$

where  $h$  is Planck's constant:  $6.626 \times 10^{-34}$  Js and  $\nu$  is the frequency (Hz). If a photon has an energy greater than  $E_g$ , it creates an electron-hole pair with an energy of greater than  $E_g$ , however the excess energy is soon dissipated as heat. Obviously, photons with a frequency less than  $E_g/h$  will not liberate an electron-hole pair. This creates a fundamental efficiency limitation in all photovoltaic conversion devices: only a fraction of the photons absorbed in the

photovoltaic material will have a frequency greater than  $E_g/h$  (so-called above-band-gap photons) and much of the energy from the above-band-gap photons is wasted as heat.

Note, stacking two or more different layers of thin film layers, each with different band gap semiconductors, can increase the efficiency of photovoltaic conversion. Usually the top film is a high band gap material, while the subsequent layers have sequentially lower band gap energies. With this type of cell a greater proportion of the incident photons are captured. Also, photon capture occurs in layers with appropriate band gaps; with high energy photons captured the upper layer and the lower layers capturing the non-absorbed, lower energy photons which pass through the preceding layer. This reduces the thermal losses from the capture of photons with energy levels greater than the band gap.

Exposure of the  $p$ - $n$  junction to light ends the state of equilibrium in the junction as a large number of electron hole pairs are created as well as increasing the number of thermally generated pairs. The photo-induced current,  $I_s$ , flows in the opposite direction to the current defined by equation A.16. The total current flow in a unit volume of PV material exposed to light, across an external potential drop, is given by

$$I = I_s - I(p) \left( \exp \left( \frac{\Delta E_{ext}}{kT} \right) - 1 \right). \quad (A.18)$$

The  $p$ - $n$  junction exposed to light is in a ‘forward-biased’ condition, where the vast majority of the electrons-hole pairs will be created through photon absorption so that

$$I_s + I(p) \gg I(n).$$

The value of  $I_s$  is dependent upon the proportion of the incident light that has a frequency capable of exciting electrons into the conduction band  $F(\lambda)$ . Other factors which affect the level of light current generation include the fraction of light, of wavelength  $\lambda$ , absorbed by the PV material,  $1-R(\lambda)$  (where  $R(\lambda)$  is the quantity reflected), the radiation intensity,  $q(\text{W/m}^2)$ , and the



intrinsic semiconductor material properties.  $I_s$  can be expressed in terms of the spectral response of the solar cell:

$$I_s = \int_{\lambda=0}^{\lambda=\infty} qF(\lambda)[1 - R(\lambda)]SR(\lambda)d\lambda. \quad (\text{A.19})$$

The spectral response of the cell at a particular wavelength  $\lambda$  of incident light is defined as

$$SR(\lambda) = \frac{I_{sc}(\lambda)}{qF(\lambda)[1 - R(\lambda)]}, \quad (\text{A.20})$$

where  $I_{sc}$  is the measured current produced by the solar cell when exposed to light of wavelength  $\lambda$  and intensity  $q$ . The spectral response is defined as the ratio of the number of liberated carriers leaving the solar cell to the number of photons entering.

### A.1.3 Cell Characteristics

The output of a solar cell depends upon several factors: the properties of the semi-conductor material, the cell temperature (in the case of crystalline silicon cells), ‘light soaking’ effects (in amorphous silicon cells) and the nature of the external loads the cell supplies. The combination of these factors gives rise to the characteristic operating curves, of generated current against the output voltage for the solar cell. Typical examples are shown in figure A.4.

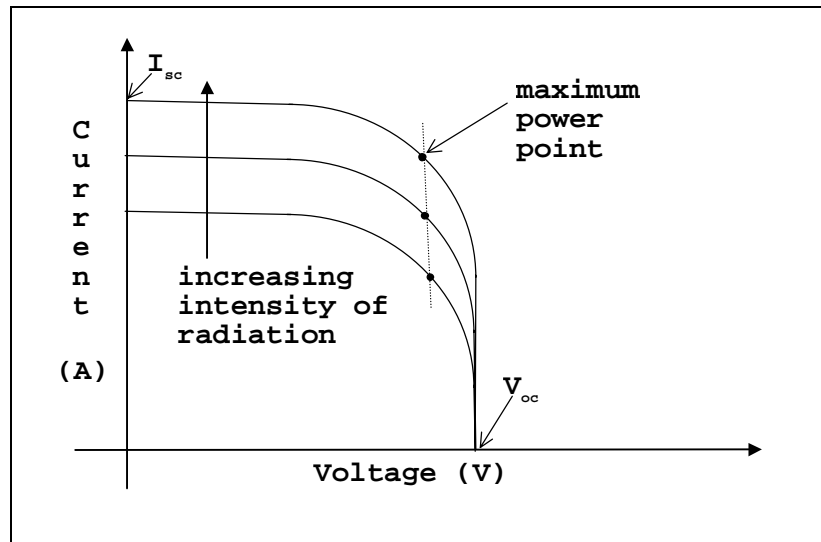


Figure A.4 Characteristic I-V curves for a solar cell.

## A.2 Photovoltaic Panels

The photovoltaic panel consists of a number of solar cells connected in a series and parallel configuration. The cells are encapsulated in a tough rigid structure containing the electrical contacts and circuitry required to remove the liberated electrons to an external circuit. The current output of the panel is dictated by the number of parallel connected cell branches, while the panel output voltage is determined by the number of cells connected in series.

The output of the PV panel is direct current (d.c.). As outlined in the previous sections, the current magnitude is dependent upon many factors including radiation intensity, cell configuration and connected load. The maximum power output of the cell occurs at the knee of their characteristic I-V curve (figure A.4).

### **A.2.1 Power Conditioning**

To ensure that the panel operates at the maximum power point, and hence efficiency, the maximum power point must be tracked, this is done by a dithering technique, where once every few seconds the current from the cells is increased or reduced until the maximum power output point is attained. The technique is known as maximum power point tracking. The maximum power point tracker effectively acts as a pseudo load for the solar panel, the characteristics of which are adjusted so that the cells in the panel operate at their maximum efficiency.

The d.c. power output of the PV panel or array of panels is suitable for such purposes as battery charging or supplying a resistive load. However, if a.c. electrical components are to be supplied with power and/or the PV system is connected to the grid (see section A.3.1), the power output of the PV source must be inverted. Inversion involves the conversion of the d.c. output to a.c.

A device called an inverter is used to convert the d.c. output of the photovoltaic array to an alternating waveform. Three types of inverter are in use: variable frequency inverters (used for stand-alone pumping applications), self-commutating, fixed frequency inverters and line-commutated fixed frequency inverters. Only the latter two types are suitable for use in building-integrated PV systems.

Self-commutating inverters require paralleling control equipment to maintain a synthetic output a.c. waveform at a frequency suitable for connection to the grid. Line commutated inverters (e.g. a switch-mode, pulse-width-modulated inverter) use the grid current waveform as a reference against which to invert the PV output current. Clearly, line-commutated inverters cannot be used in stand-alone systems, as they cannot operate without a grid connection.

### A.3 The Integration of PV into Buildings

#### A.3.1 Integration into the Building Fabric

European Commission and the UK Energy Technology Support Unit (ETSU) studies [2, 3] have identified the integration of PV materials into the building structure as one of the most cost effective means of utilising this form of renewable energy. The reasons for this are that capital costs are reduced, due to fact that the PV is an integral part of the structure and hence the cost of cladding and displaced materials is saved, while land and support structure cost are avoided and transmission losses are minimised.

There are several methods of PV integration into the building structure, these are outlined in figure A.4 and table A.1

Installation type	Advantages	Disadvantages
Stand-off mount	good panel cooling	support structure is required, penetration through structure for cable access, heavy wind loading possible
Direct mount	building structure is array support, cables not exposed, panels displace facade materials	cooling problems, poor access to terminals, corrosion problems in wet climates
Integral mount	panel forms an integral part of the structure, panels can be mounted into structure in the same way as glazing, free access to wiring and terminals	provision of necessary internal air-circulation for cooling purposes
Under-glass mount	cheap and easy to install, easy access and good cooling performance	reflection losses, support structure shading effects

Table A.1 Summary of the advantages and disadvantages of different PV panel mountings.

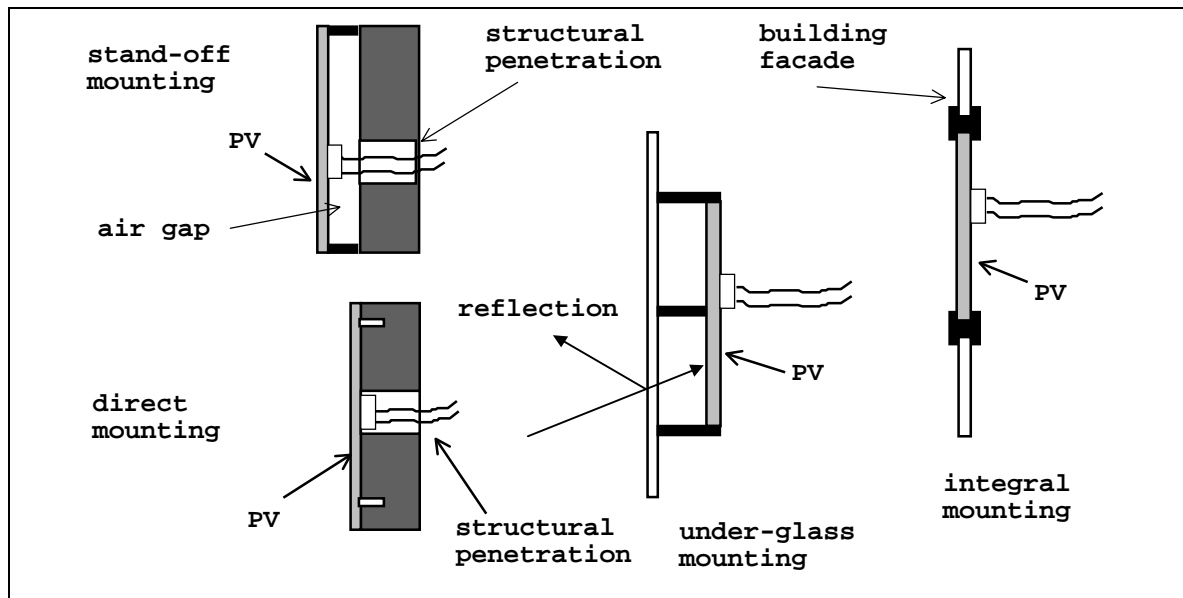


Figure A.4 Photovoltaic panel mountings for building integration.

The most common and suitable type of mounting for new-build is the integral mounting. Here the PV panel forms part of the facade, with the PV panels having the same dimensions as the facade glazing elements. Modern building-facade compatible PV panels are constructed of a glass-resin-glass sandwich with the PV cells set between the outer glass layer and the resin. The glass used in the panel is usually low iron, to cut down on absorption of the incident solar radiation. The solar cells may also be treated with an anti-reflective coating, maximising the amount of solar radiation absorbed by them.

### A.3.2 Grid Connection of Building-Integrated PV

As was mentioned in Chapter 1, one of the attractions of building-integrated energy systems is the possibility of exporting power to the grid. This section looks at the options for the grid connection of PV facades and the export of (suitably conditioned) a.c. power. Note that the discussion here is also applicable to CHP systems.

A key issue in grid-connected buildings is that of metering, as it effects both the mode of operation and the economic feasibility of a PV (or CHP) system. Note, issues relating to power quality and safety are out-with the scope of this thesis. Two metering scenarios are possible: bi-directional metering or single-metering. With bi-directional metering, power exported to the grid will cause the meter to run backwards. Therefore, with this type of meter, the financial value of electricity generated by the building-integrated system is the same as imported electricity. However, this situation does not occur in the UK, where single metering is required: one for exported power and one for imported power. The price paid for the exported power is less than that charged for imported power (typically exported power has 1/3 the value of imported power [4]). In this situation it is therefore economic to use all generated power within the building to offset imported power. This results in most UK building-integrated PV systems being designed to meet only internal building loads.

### **A.3.3 Heat Recovery from PV Facades**

One of the problems with the integration of PV materials into the building structure is the low-efficiency and high cost of the photovoltaic elements. Seasonal efficiencies of 12% have been calculated for crystalline silicon panels (compared to flash test efficiencies of over 18% in some cases). It is obvious that the operational efficiency falls short of that obtained in the laboratory [5]. This lower efficiency results from several factors. Incident radiation intensities are usually lower than the test values of  $1000 \text{ W/m}^2$  as atmospheric absorption of the solar spectrum reduces the available solar radiation below this value. Also, the incident radiation is often not perpendicular to the plane of the façade containing the PV arrays, further reducing the intensity on the cells. Cell temperatures are often higher than the laboratory test values of  $25^\circ\text{C}$ , so that the diode current, which opposes the light generated current, is higher than in test conditions, reducing the output current.

The result of the lower operational efficiencies of PV arrays is that their payback period becomes longer and they become less financially attractive to building owners and designers. One method of boosting the operational efficiency of the PV facade is to recover heated air from the rear of the panels. This boosts the efficiency of the facade in two ways. Firstly, recovered

heat can be fed into the building during the heating season (effectively the facade acts as a solar combined heat and power system) secondly, the cell temperature is reduced, increasing the electrical efficiency of the array.

The effect of the recovery of heated air from the rear of the facade is to greatly increase the efficiency of the PV facade. Simulations have indicated combined efficiencies of up to 44% are possible during the heating season in some climates [5]. The efficiency of the facade system will be greatest when all the heat can be of use in ventilation pre-heat, or direct heating. The temperature of the air recovered from the back of the panels can be as high as 60°C.

The direct displacement of building heating energy consumption due to façade heat recovery and the resulting (slight) increase in electrical output act to improve the economic viability of building-integrated PV.

#### **A.4 References**

1. Buresch M, *Photovoltaic Energy Systems*, McGraw-Hill, New York, 1983.
2. Taylor E H, *Review of Photovoltaic Power Technology*, ETSU, HMSO, London, 1990.
3. *Photovoltaic Technologies and their Future Potential*, Thermie OPET Publication, CEC DG XVII, 1993.
4. Simons A, *Building-Integrated Photovoltaic Systems, Session 2: Technical Aspects of BIPV*, CREST Technical Paper, Loughborough University, 1998.
5. Clarke J A, Hand J W, Johnstone C M, Kelly N J and Strachan P A, *The Characterisation of photovoltaic-integrated building facades under realistic operating conditions*, Proc. 4<sup>th</sup> European Conference on Solar Energy in Architecture and Urban Planning, Berlin, March 1996.

#### **A.5 Bibliography**

Fonash S J, *Solar Cell Device Physics*, Academic Press, New York, 1981.

Hu C and White R M, *Solar Cells - From Basic to Advanced Systems*, McGraw-Hill, New York, 1983.

Markvart T (editor), *Solar Electricity*, John Wiley, Chichester, 1998.

Mohan N, Udehand T M and Robins W P, *Power Electronics: Converters, Application and Design*, John Wiley and Sons, New York 1989.



Palz W, Vianello V, Bonalberti E and Riedel D (editors), *First E.C. Conference on Solar Collectors in Architecture - Integration of Photovoltaic and Thermal Collectors in New and Old Building Structures*, Proceedings of the First International Conference, Venice, Italy 3-5 March 1983.

Partain L D (editor), *Solar cells and their applications*, John Wiley and Sons, New York, 1995.

Sorensen B, *Renewable Energy*, Academic Press, London, 1979.

Twidell J and Weir T, *Renewable Energy Resources*, E & F N Spon Ltd., London, 1986.

## Appendix B - Small-Scale Combined Heat and Power Technology Review

### B. Introduction

Small-scale Combined Heat and Power (CHP) is a well-established technology in the UK and world-wide. The engine drives a generator, which produces power for the building electrical loads, while waste heat from the engine is recovered to produce hot water for use in the building services. CHP units vary in size from 18kWe (electrical output) to over 1 MWe and usual heat-to-power ratios are in the region 1.75:1. The overall efficiency of a packaged CHP unit is in the order of 80%. Typically, about 30% of the fuel energy is converted to mechanical work output, while around 50% of the remaining fuel energy is recovered as hot water. The energy flows associated with a combustion engine small-scale CHP unit are shown in figure B.1

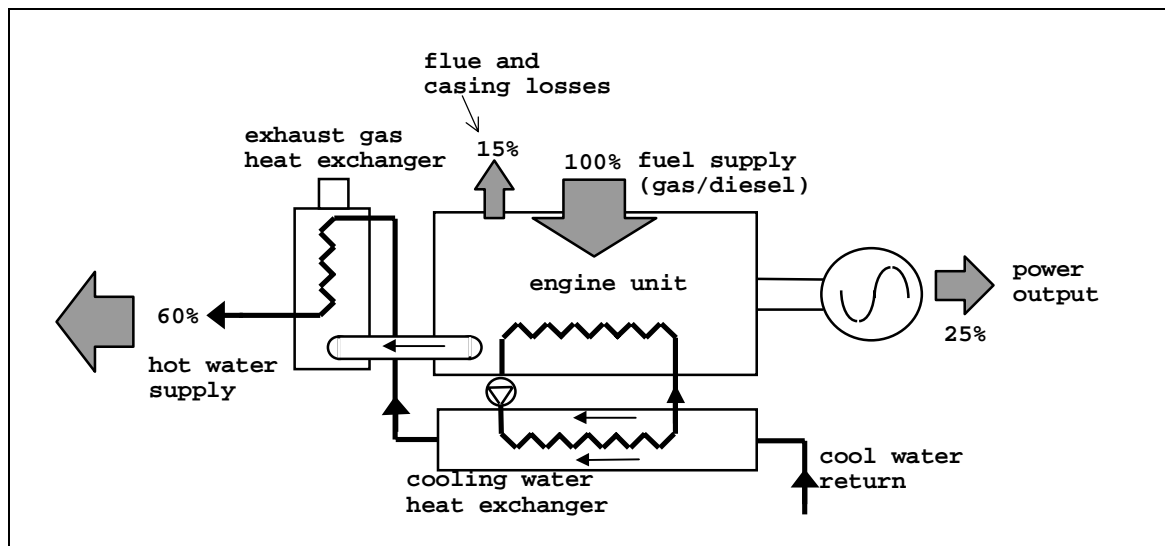


Figure B.1 CHP unit energy flow paths.

By the end of 1993 nearly 1000 units were operational in the UK producing 3000MWe [1]. The current UK government strategy is to encourage a further 2000MWe of new CHP capacity over the period 1995-2000.

## **B.1 The Components of a CHP System**

The main components of a small-scale CHP system are as follows.

- the engine;
- the generator;
- the heat recovery system (cooling water and exhaust gas heat exchangers).

### **B.1.1 The Engine**

The engines used in packaged CHP are usually spark-ignition gas or dual fuel engines, derived from industrial or mass-produced automotive models. Larger CHP units may use a gas turbine, but the principles of CHP operation remain the same. The most common fuels are biogas or natural gas. Diesel is usually only an attractive fuel option if already used on site: it produces appreciable quantities of particulate that tend to foul the exhaust gas heat exchanger.

Engine sizes for small-scale CHP systems can vary from around 25kWe output to very large diesel or gas turbine units >500kWe. Generally, the engines run at a multiple of the grid frequency (50Hz), e.g. 1500 rpm.

A typical internal combustion engine unit engine will run with a jacket temperature of 120°C and an exhaust gas temperature of 650°C. The majority of heat is recovered from the exhaust gases. The temperature at which the engine runs is dependent upon a number of factors including engine speed and the fuel type.

The engine is required to supply a torque,  $T_m$  (Nm), to the generator. Under steady state conditions (the conditions prevailing for the vast majority of the time) this torque is balanced by an electrical counter torque,  $T_e$ . With a constant engine speed the fuel consumption will vary linearly with the torque requirement.

### **B.1.2 The Generator**

The basic components of the generator are the rotor and the stator. The rotor is the component driven by the mechanical torque from the prime mover, (i.e. the engine). The stator is a stationary component that houses the field windings out of which the generated current flows.

The generators in packaged CHP units generally have a 3-phase alternating current output at 415V (line-line voltage), with a power output typically in the range 15kW and upwards. Two types of generators can be used on CHP units: synchronous and asynchronous.

Synchronous generators are self-exciting, i.e. they do not rely on an external power source to energise the stator field windings. The magnetic field necessary for the induction of the current flow in the stator windings is induced by supplying a d.c. excitation current to the rotor, this is supplied via slip rings or brushes. The generated frequency is dependent upon the speed of rotation of the rotor,  $\omega$ , and  $N$  the number of magnetic poles on the rotor. The generated frequency is given by the following expression.

$$f = \frac{\omega N}{4\pi}. \quad (\text{B.1})$$

The output of the synchronous generator is a complex power with a real and reactive component.

Asynchronous (or induction) generators can operate either as motors or generators and require an external source (typically the grid) to provide reactive power for the creation of a rotating magnetic field in the stator windings<sup>27</sup>. If the speed of the rotor is less than the speed of this rotating field in the stator, i.e.  $\omega < \omega_{field}$ , then the machine operates as a motor and real and reactive power are absorbed. If an external force is applied to the rotor, causing it to rotate faster than the rotating stator field such that  $\omega > \omega_{field}$ , then the current flow in the stator windings is reversed and real power flows out of the stator terminals. The induction generator still absorbs reactive power to maintain the rotating stator field. The difference between the rotor speed and the stator field speed is known as the slip. The rotor in an asynchronous generator will always rotate at a greater speed than the synchronous speed when generating power. The amount of power generated from the asynchronous generator is a function of the slip, this is discussed further when control of the generator power output is considered.

### **B.1.3 Heat Recovery System**

All CHP units recover heat from two main areas: the engine coolant water and the exhaust gases. Heat outputs for small-scale CHP units range from 39kW to 1,200kW and are typically twice the electrical output. The maximum operating water temperatures are roughly similar to low temperature hot water (LTHW) systems at approximately 75-90°C.

Two types of heat exchanger are required on the CHP system: the jacket cooling water heat exchanger and an exhaust gas heat exchanger. The cooling water heat exchanger is usually of the shell and tube or plate variety, while the exhaust gas heat exchanger consists of banks of finned tubes, containing the cooling water over which the exhaust gas flows at a temperature of 500-

---

<sup>27</sup> Note that in synchronous generators the field rotates with the rotor, in asynchronous machines the field rotates on the stationary stator as the currents in the stator windings change direction.

650°C. Around 60% of the heat transferred to the cooling water is recovered from the engine jacket, with 40% recovered from the exhaust gas heat exchanger.

## **B.2 Control of CHP Systems**

### **B.2.1 Temperature Control**

Control of a CHP unit is applicable in two areas: control of the thermal output of the unit and control of the electrical output of the generator. Of the two, the control of the thermal operation of the unit is more common and is crucial to the CHP unit's efficient operation.

Thermal control of the unit is based on the heat demand with or without reference to electricity demand and is similar to the control of a conventional boiler (temperature based). The normal control strategy is to run the unit at full load for as long a period as possible, with the CHP unit effectively running as a lead boiler in preference to the back-up boilers in the building's heating system. This ensures that the CHP unit runs for as many hours as possible during the day.

It is common to control the CHP on the hot water return temperature with the supply temperature allowed to float, enabling the CHP unit to supply the maximum quantity of heat to the circulating cooling water.

### **B.2.2 Control of Power Output**

It is also possible to control the electrical output of the generator unit in relation to variation in electrical demand. Control of the electrical output of both synchronous and asynchronous generators is discussed below.

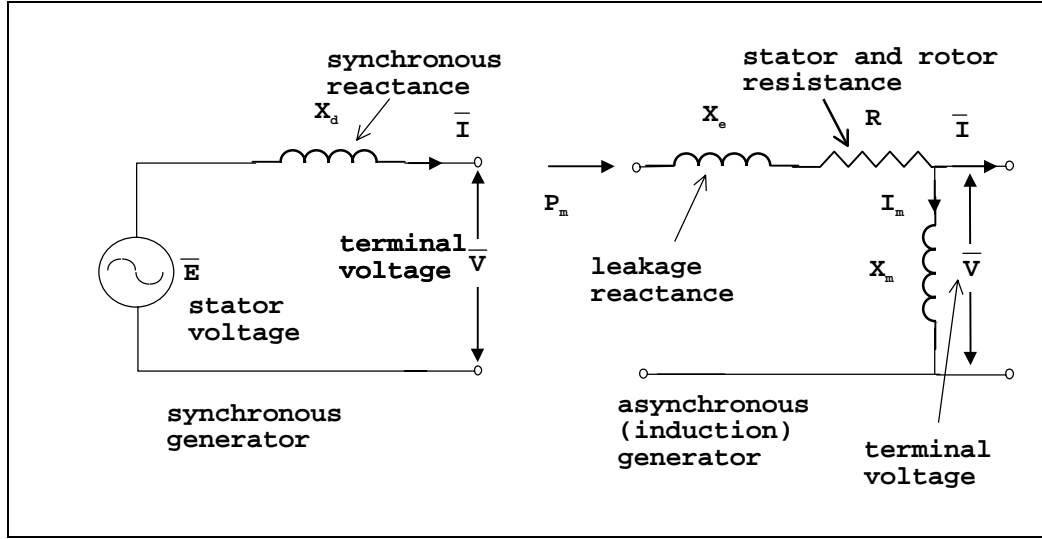


Figure B.2 Per-phase equivalent circuits of synchronous and asynchronous generators

Referring to the per-phase equivalent circuit of the synchronous generator (assuming balanced operation), the complex power (VA) supplied to the system by the generator is

$$\bar{S} = \bar{V} \bar{I}' . \quad (\text{B.2})$$

Apply Ohm's law and replacing  $I$  in equation A2.2 gives

$$\bar{S} = \bar{V} \left( \frac{\bar{E} - \bar{V}}{\bar{X}_d} \right)' . \quad (\text{B.3})$$

Noting that the terminal voltage  $\bar{V} = V$ , the excitation voltage  $E = E(\cos \delta + j \sin \delta)$  and the synchronous reactance  $\bar{X}_d = jX_d (\Omega)$ .  $\bar{S}$  can be expressed as

$$\bar{S} = \frac{VE}{X_d} \sin \delta + j \left[ \frac{VE}{X_d} \cos \delta - \frac{V^2}{X_d} \right] , \quad (\text{B.4})$$

where the real power output of the generator (equal to the mechanical power  $P_m$  supplied by the CHP engine unit) is

$$P = \frac{VE}{X_d} \sin \delta, \quad (\text{B.5})$$

and the reactive power output is given by

$$Q = \frac{VE}{X_d} \cos \delta - \frac{V^2}{X_d}. \quad (\text{B.6})$$

It is possible to control both the real and reactive power output of the generator through two separate control actions. Increasing the mechanical power,  $P_m$  (W), while keeping the rotational speed of the shaft constant, will cause the real electrical power output,  $P$  (W), to increase, with a small decrease in  $Q$  (VAR) and an increase in  $\delta$  (rads). Increasing the magnitude of the excitation voltage  $E$  will leave  $P$  unaffected, while increasing  $Q$  and decreasing  $\delta$ .

In the asynchronous generator, changing the slip angle can control the output of real power. This is achieved by increasing or decreasing the torque from the engine unit. Referring to the equivalent circuit of the induction generator, the relationship between the mechanical power output of the engine and the slip  $s$  is given by

$$P_m = \frac{sKE_o R}{R^2 + sX_o}. \quad (\text{B.7})$$

Here  $K$  is a characteristic term for the generator, given in manufacturer's data, as are  $E_o$ , which is the terminal voltage at standstill.  $X_o$  is the magnetising reactance ( $\Omega$ ) at rotor standstill. The reactive power consumption can be altered using a capacitor bank.



### B.3 Connecting the CHP system into the Building Services

Two methods exist for connection of the CHP unit into the services, these being a series or a parallel configuration. The series connection is the most often used when the CHP unit is retrofitted to an existing installation. This is due to the fact that a series connection creates the minimum disruption to the existing services. However a bypass must be installed to ensure that flow from the CHP unit circulates when the boilers are closed down (i.e. in summer conditions). The parallel connection is used when the entire boiler and CHP package is installed as new. Note that the higher hydraulic resistance of the CHP unit means that it must be equipped with its own pump. The parallel connection configuration is used in the CHP exemplar of chapter 5.

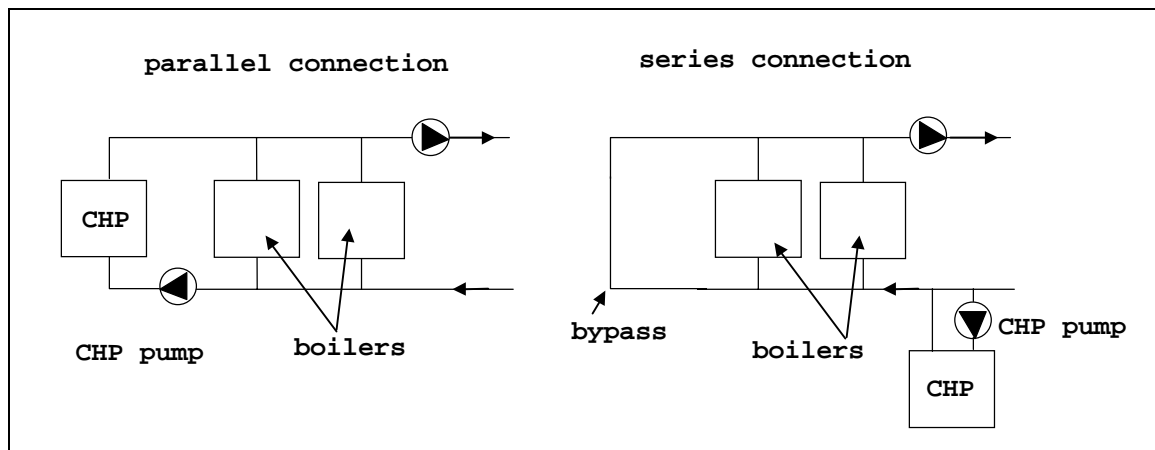


Figure B.3 Connection of a CHP unit to the hot water services.

### B.4 The Viability of CHP

To assess the suitability of small-scale CHP at a given site, a detailed assessment of the site energy demand must be undertaken. If the available heat load is not sufficient to allow the CHP unit to operate for more than 4500 hrs/year it is unlikely that the scheme will prove financially viable [2].

To achieve the required running time, the site must have a demand for hot water all year round. Examples of this type of site include hospitals, offices, hotels and swimming pools. In addition to these sites, research has indicated there are over 3,000 group housing sites, flats, old peoples homes, hostels and sheltered accommodation which could benefit from CHP.

Generally the CHP unit is sized to meet the summer hot water requirement, plus a proportion of the winter heating demand. The boilers supply the additional hot water requirement in winter.

#### **B.4.1 Efficiency and Savings**

This section discusses means of evaluating the efficiency and savings from CHP systems (this can also apply to savings from photovoltaic facades), which can be used in the evaluation of simulations such as the exemplars given in chapter 7.

#### **B.4.2 Measures of Efficiency**

There are many methods of gauging the efficiency of CHP plant, the most simple is the energy utilisation factor (EUF), which is given by

$$EUF = \frac{W + Q_u}{F_c} . \quad (B.8)$$

This is the ratio of useful power and heat output to fuel input. The fuel consumption  $F_c$  can be further defined as

$$F_c = \frac{Q_c}{\eta_c} + IHR_c E_c \quad (B.9)$$

The fuel consumption in the above equation can be broken down into two components: the fuel used for heating purposes and the fuel used for electricity production. The  $IHR_c$  term is the amount of fuel used (kW) per kW of power production. Substituting this back into equation B.8

gives another expression for the EUF in terms of the electrical output, heat output, combustion efficiency and the incremental heat rate.

$$EUF = \frac{1 + \frac{E_c}{Q_c}}{\frac{1}{\eta_c} + \frac{IHR_c E_c}{Q_c}} \quad (B.10)$$

Another measure of efficiency is the fuel energy savings ratio (FESR). This is the ratio of the fuel used by the CHP unit to the fuel that would have been used by a boiler and traditional generating plant to produce the same amount of heat and power:

$$FESR = \frac{F_s - F_c}{F_s} . \quad (B.11)$$

$F_s$  is the parallel generation fuel consumption (i.e. boiler plus power plant) and  $F_c$  is the fuel consumption of the CHP unit. The fuel energy savings ratio is useful when determining the CO<sub>2</sub> savings of CHP installation.

### B.4.3 Financial Savings from CHP

The financial savings associated with CHP come in two possible forms. The first is the saving in imported electricity while the second is the possibility of exporting generated electricity to the grid. The unit value of electricity produced by the CHP system can be written in terms of any sales or displaced purchases:

$$K_{ej} = \frac{E_{cs} K_{esj} + E_{cd} K_{edj}}{E_c} \quad (B.12)$$

$E_{cs}$  is the electricity produced by the CHP unit (kW) and exported to the grid at rate  $K_{esj}$  (£/kW).  $E_{cd}$  (kW) is the displaced electricity at rate  $K_{edj}$  (£/kW). Note that  $E_{cs} + E_{cd} = E_c$  (the total amount

of electricity generated by the unit). The savings accrued from the CHP system are dependent on the value of  $K_{ej}$  and  $K_{edj}$ .

The general case is that  $K_{edj} > K_{esj}$  and connection to the grid for export purposes also carries a charge. Hence, most UK CHP units supply electricity for displacement purposes only.

## **B.5 References**

1. Combined Heat and Power Association, *CHPA yearbook*, CHPA publication, 1995.
2. Evans R D, *Environmental and economic implications of small-scale CHP*, ETSU, 1990.

## **B.6 Bibliography**

Energy Efficiency Office, *Good practice guide 1 - guidance notes for the implementation of small-scale packaged combined heat and power*, HMSO 1993.

Energy Efficiency Office, *Good practice guide 3 - introduction to small scale combined heat and power*, HMSO 1990.

Emanuel P, *Motors, generators, transformers and energy*, Prentice-Hall, New Jersey, 1985.

Gross C A, *Power systems analysis* (1<sup>st</sup> Edition), John Wiley and Sons, New York, 1979.

Horlock J H, *Cogeneration: Combined heat and power*, Pergammon Press, Oxford, 1987.

Porter R W, Manstaniah K, *Thermal-economic analysis of heat matched industrial cogeneration systems*, Energy, Vol. 7, No 2, 1982.